PROCEEDINGS OF
GEOMORPHOMETRY 2009

31 August 2009 – 2 September 2009

Ross Purves · Stephan Gruber
Tomislav Hengl · Ralph Straumann
(Eds.)

Hosted by
Department of Geography
University of Zurich, Switzerland

http://2009.geomorphometry.org

Editors

Ross Purves, Stephan Gruber, Ralph Straumann
Department of Geography
University of Zurich
Winterthurerstrasse 190
CH-8057 Zurich
Switzerland

ross.purves | stephan.gruber | ralph.straumann @geo.uzh.ch
http://www.geo.uzh.ch

Tomislav Hengl
Institute for Biodiversity and Ecosystem Dynamics
University of Amsterdam
Nieuwe Achtergracht 166
1018 WV Amsterdam
The Netherlands

t.hengl@uva.nl
http://www.science.uva.nl/ibed

Organising Committee

Ross Purves
Stephan Gruber
Tomislav Hengl
Ralph Straumann

Programme Committee

Katherine Arrell, University of Leeds, UK
Alexander Brenning, University of Waterloo, Canada
Jürgen Böhner, University of Hamburg, Germany
Olaf Conrad, University of Hamburg, Germany
Lucian Dragut, University of Salzburg, Austria
Ian Evans, Durham University, UK
Peter Fisher, University of Leicester, UK
John Gallant, CSIRO, Australia
Paul Gessler, University of Idaho, USA
Stephan Gruber, University of Zurich, Switzerland
Peter L. Guth, US Naval Academy, USA
Tomislav Hengl, University of Amsterdam, Netherlands
Oliver Korup, WSL, Switzerland
John Lindsay, University of Guelph, Canada
Helena Mitasova, North Carolina State University, USA
Peter Molnar, ETH Zurich, Switzerland
Scott Peckham, Rivix, USA
Ross Purves, University of Zurich, Switzerland
Hannes I. Reuter, GISxperts, Germany
Jochen Schmidt, NIWA, New Zealand
Ralph Straumann, University of Zurich, Switzerland
Andy Turner, Leeds University, UK
Robert Weibel, University of Zurich, Switzerland
John P. Wilson, University of Southern California, USA
Jo Wood, City University London, UK
Qiming Zhou, Hong Kong Baptist University, Hong Kong

Table of Contents

Keynotes

From Ontologies to Software

Methodological Developments

Extracting Landscape Elements

Soil Mapping and Properties

Global-Scale Geomorphometry

Multiscale Methods

Data Considerations

Geomorphological Applications

Extraterrestrial Geomorphometry

Extracting Hydrological Networks

Glaciological Applications

Foreword

On behalf of the organisers we would like to extend a warm welcome to all participants of Geomorphometry 2009 in Zurich. The Geomorphometry 2009 conference continues a series initiated by the Terrain Analysis and Digital Terrain Modelling conference hosted by Nanjing Normal University in November 2006.

Geomorphometry 2009 brings together researchers to present and discuss developments in the field of quantitative modelling and analysis of elevation data. Geomorphometry is the science of quantitative land-surface analysis and description at diverse spatial scales. It draws upon mathematical, statistical and image-processing techniques and interfaces with many disciplines including hydrology, geology, computational geometry, geomorphology, remote sensing, geographic information science and geography.

For the conference, a total of 53 extended abstracts, with authors from 21 countries were submitted for review by the programme committee. Of these, a total of 37 were accepted for presentation at the conference. We believe that the conference programme offers a rich and varied insight into the key themes in geomorphometry today, with a mix of leading researchers in the field presenting methodological advances and young researchers presenting high quality reviewed work to an international audience.

The conference also hosts three keynote speakers. We are delighted that Professor David Mark, SUNY Distinguished Professor in the Department of Geography at the State University of New York at Buffalo and Dr Jo Wood, Reader in GIScience at the Department for Information Science at City University, London will both give presentations on how they have seen development progressing in Geomorphometry during their extensive experience of the field. Furthermore, Stephan Landtwing of BSF Swissphoto, a key producer of LIDAR and other remotely sensed data in Switzerland, will give an industrial keynote – an excellent opportunity for the conference attendees to interface with data producers and better understand issues related to key data sources in geomorphometry.

The conference also hosted two workshops with very different themes, entitled *Automated analysis of elevation data in R+ILWIS/SAGA* and *Back to reality – Reconciling geomorphometry and geomorphology in the field* respectively, providing attendees with the opportunity to get their hands dirty figuratively at the computer screen, and literally in the field!

Finally, we would like to thank all of those who make events such as this a success. Our programme committee, who on time and carefully reviewed a large number of papers, our keynote speakers, the workshop organisers, and all those who helped in the local organisation, especially Dagmar Brandova who dealt with registration, as well as the University of Zurich for providing the conference facilities. Finally, and most importantly, we would like to thank the conference participants – without your work and participation there would be no conference. We hope your stay in Zurich will be an enjoyable and stimulating one.

Ross Purves, Stephan Gruber, Tomislav Hengl and Ralph Straumann
August 15th, 2009

Visualizing Geomorphometry: Lessons from Information Visualization

Jo Wood
the giCentre, Department of Information Science, City University London,, EC1V 0HB, United Kingdom
Telephone: +44 20 7040 0146
Fax: +44 20 7040 8584
Email: jwo@soi.city.ac.uk

1. Introduction

Has geomorphometry really changed in the last 30 years? As someone who mainly researches in the field of information visualization and GI Science, I ask myself this question whenever my research takes me back into the realm of digital elevation model analysis where I started my career 20 years ago.

In the 1970s Ian Evans was proposing the use of quadratic interpolation of DEMs for the systematic measurement of the first and second derivatives of elevation for general geomorphometry (Evans, 1972, 1979, 1980). Modern geomorphometry still uses the techniques and approaches he proposed for slope and curvature measurements over 30 years later. At about the same time David Mark was advocating the systematic use of gridded elevation models and computer based parameterisation of those models as the bases for geomorphometric analysis (Mark, 1975a,b). Again, this forms the basis for modern geomorphometry, albeit with larger DEMs at finer resolutions.

It can be argued that modern hydrological geomorphometry is equally based on the approaches established in the 1980s, such as flow accumulation, channel delineation and watershed partition (e.g. Jenson, 1985; Band 1986; Hutchinson, 1989). Little appears to have changed since then other than the use larger datasets or minor modifications to algorithms such as moving from ***D8*** to $\boldsymbol{D\infty}$ flow models.

Reviewing Hengl and Reuter's text *Geomorphometry*: Concepts, Software and Applications (2008), it is clear that one aspect of geomorphometry has changed in the last 30 years or so, almost beyond recognition. The visual presentation of geomorphometric analysis has evolved from monochrome low resolution overplotting of line printer output to multi-megapixel full colour output. Yet if we think of graphical output as solely a mechanism for presentation, geomorphometry will fail to exploit the true power of recent development in visualization.

In parallel with the development of graphical techniques has been the emergence of *information visualisation* and *visual analytics* – research disciplines that focus on the use of graphics as an intrinsic part of the data analysis process. The speed at which graphical output can be created, along with graphical interaction means that visualization of data can be used as part of the analytical process, feeding back to the way we handle our data and draw conclusions from it. This paper will argue how we can learn from the developments in information visualization and visual analytics in order to enhance the way in which we undertake geomorphometry.

2. Information Visualization and Visual Analytics

Information visualisation as a discipline emerged during the 1990s from the need to formalise the approaches used to handle the increasingly large and diverse digital datasets becoming available. Building on traditions of scientific visualization, statistical graphics, computer science, human computer interaction and cartography, the discipline has overseen the development of new graphical tools, new styles of graphical interaction, empirical evaluation of usability and new theory. More recently, the emerging field of visual analytics has focussed on the integration of visual tools and analysis through graphical interaction. While not exclusively geographical, there are a number of developments in these fields that may benefit geomorphometry.

2.1 Techniques for representing data

Most geomorphometric graphical output tends to be map-orientated, usually with some form of raster mapping with a possible vector overlay. While undoubtedly an effective approach, especially when assessing spatial relationships, there is scope to consider the wider range of techniques used in information visualisation. For example, a large branch of information visualization is concerned with representing tree and graph structures, and in particular providing representations that can handle many thousands or millions of nodes and edges (e.g. VisualComplexity.com, 2009; Holten and van Wijk, 2009). The importance of channel and feature networks in geomorphometry means that the discipline could benefit from many of the network visualisation solutions that have been proposed.

2.2 Scalability

Thomas and Cook (2004) in their influential book *Illuminating the Path*, identified the grand challenges for Visual Analytics. Repeatedly, the notion of *scalability* was identified as being one of the most significant challenges. This encompasses *information scalability* which in a geomorphometry context suggests that we need to be able to develop systems that can handle very large datasets both at a fine spatial and temporal resolution. Geomorphometry would benefit from techniques for tiling, caching and filtering very large datasets used commonly in visual analytics. *Visual scalability* addresses the need to show visually many millions of items simultaneously. There are many techniques in information visualization that try to address this need including reprojection, dynamic filtering and aggregation. Display scalability identifies the need to be able to display graphical representations at a range of output scales from mobile devices in the field to mult-panel wall displays. Perhaps one of the most interesting developments in information visualisation is that which addresses *human scalability* – the ability for many people to interact and contribute simultaneously to the visual analysis of a geomorphometric dataset. An interesting example is provided by Microsoft's *Photosynth* software (Microsoft, 2009) allowing multiply sourced photographic images to be integrated and projected into a common space for exploration.

2.3 Embedding Interaction

One of the key approaches to addressing issues of scalability is to allow filtering of data in order to reduce data and visual complexity. Filtering is often achieved successfully via interactive selection of subsets or aggregations of a dataset. Embedding this interaction as part of the process of query refinement is central to information visualization, encompassed by Shneiderman's 'visual information seeking mantra' - o*verview first, zoom and filter, then details-on-demand* (Shneiderman, 1996), but frequently not applied in geomorphometric analysis.

A second context in which interaction is frequently used in information visualisation is in animated transitions between reprojections of datasets (e.g. Heer and Robertson, 2007). This is particularly important when more abstract projections of data are involved where spatial context can become lost. In geomorphometry, transitions between spatial and thematic projections of data offer potential for new insights for geomorphological insight.

2.4 Integration of graphical presentation, query and analysis

Finally, one of the lessons of successful information visualisation is that visual interaction and presentation is most effective when it is integrated in the hypothesis generation – testing cycle. In other words visual representation of data is used as much in the generation of ideas and analysis of results as it is in summarising findings. This requires a reconsideration of the design of software we use for performing geomorphometry as well as the way in which we use it. It requires true graphical interaction, integration with numerical analytical techniques and quick interactive rendering.

3. Conclusions

Geomorphometry has seen a gradual evolution over the last few decades. Based on established principles of DEM analysis, it has experienced little radical change over the years. Datasets have become larger, analysis quicker, but the approach taken to using geomorphometry software has varied little over the decades. Yet, with a huge proliferation of relevant digital data, and massive increases in computing power, we have the scope to radically change the way we perform geomorphometry. In this paper, it is argued that the way in which that might be successfully achieved is to incorporate modern ideas from the fields of information visualisation and visual analytics. Emerging from disciplines where dataset sizes are increasing by many orders of magnitude, and where there is increasing need to perform analysis and filtering of data, there are many lessons to be learned from these fields of study. Considering how scalability, interaction and analytical integration can be incorporated into visual geomorphometry offers scope for radical development in the tools we use to understand the landscape.

References

Band, L. (1986). Topographic partition of watersheds with digital elevation models. *Water Resources Research* 22(1), 15-24.

Evans, I. (1972). General geomorphometry, derivatives of altitude, and descriptive statistics. in Chorley, R. J. *ed. Spatial Analysis in Geomorphology*, Methuen, London. 17-90.

Evans, I. (1979) An integrated system of terrain analysis and slope mapping. *Final report on grant DA-ERO-591-73-G0040*, University of Durham, England

Evans, I. (1980) An integrated system of terrain analysis and slope mapping. *Zeitschrift fur Geomorphologie, Suppl-Bd* 36, 274-295

Heer, J. and Robertson, G. (2007) Animated transitions in statistical data graphics, *IEEE Transactions on Visualization and Computer Graphics,* 13(6) 1240-1247

Hengl, T. and Reuter, H. (eds.) (2008) *Geomorphometry: Concepts, Software and Applications*, London: Elsevier, ISBN 978 0 12 374345 9

Holten, D. and van Wijk, J. (2009) Force-directed edge bundling for graph visualization, *IEEE-VGTC Symposium on Visualization*, 28(3).

Hutchinson, M. (1989). A new procedure for gridding elevation and stream line data with automatic removal of spurious pits. *Journal of Hydrology* 106, pp.211-232

Jenson, S. (1985). Automated detection of hydrologic basin characteristics from digital elevation model data. *Digital Representation of Spatial Knowledge, Auto-Carto 7.,* American society of Photogrammetry and the American Congress on Surveying and Mapping. 301-310.

Mark, D. (1975a) Geomorphometric parameters: a review and classification, *Geografiska Annaler* 57 A, 165-177.

Mark, D. (1975b) Computer analysis of topography: a comparison of terrain storage methods, *Geografiska Annaler* 57 A, 179-188.

Microsoft (2009) *Photosynth*: http://photosynth.net

Shneiderman, B. (1996) The eyes have it: A task by data type taxonomy for information visualizations, *Proceedings of the IEEE Symposium on Visual Languages,* 336-343

Thomas, J. and Cook, K. (eds.) (2005) *Illuminating the Path: The Research and Development Agenda for Visual Analytics*, National Visualization and Analytics Center, ISBN 0769523234

VisualComplexity.com (2009) http://www.visualcomplexity.com/vc

From Land Form to Landforms: Bridging the Quantitative-Qualitative Gap in a Multilingual Context

D. M. Mark[1]

[1]NCGIA & Department of Geography, University at Buffalo, Buffalo, NY 14261 USA
Telephone: (1) 716 645 0505
Fax: (1) 716 645 5957
Email: dmark@buffalo.edu

1. Introduction

Since the 1960s, geomorphometry has emphasized geometric calculations based on local operators applied to digital elevation data (Evans, 1972; Mark, 1975). Digital elevation data represent discrete approximations to fields of elevations that represent the objective, measurable form of land surfaces.

With the emergence of the World Wide Web and the Semantic Web, there has been increased need for methods to conversion of elevation fields into cognitively meaningful landforms. Some of the research has approached the problem in a 'bottom-up' way, classifying form at a local level. However, in a somewhat counter-intuitive development, improving quality and resolution of digital elevation has had the effect of broadening the conceptual and computational gap between local geometry and meaningful landforms. The issue of automated feature extraction and classification is further complicated by the fact that people from different cultures, speaking different landscapes, group landforms into categories in different ways. Procedures for the automated detection, delimitation, and classification of landforms from elevation data may themselves need to be different for different languages, and at the very least will need to have different parameters.

This paper expands on the issues outlined above, and then present evidence for cultural and linguistic differences in the classification of landforms. Then some aspects of the solutions will be presented.

2. Ontology and Feature Extraction

2.1 Ontology of Landforms

A comprehensive ontology of landforms appears to consist of several distinct components. One part would be an ontology of fields (Peuquet et al., 1998). Mathematically, the shape of the Earth's solid surface can be approximated by a single-valued field (Mark and Smith, 2004). Then, various discrete representations of altitude, such as elevation matrices and TINs, can be considered to be discrete approximations to this field.

Next, we have the question on the ontological nature of landforms themselves. Strictly speaking, landforms are parts of the Earth's surface. But not arbitrary parts. To be a landform, a part of the Earth's surface must have some coherence of form (shape) or process or both (Smith and Mark, 2003). In the DOLCE ontology, landforms are probably best considered to be *features* of a planetary surface. "Typical examples of features are 'parasitic entities' such as holes, boundaries, surfaces, or stains, which are generically constantly dependent on physical objects (their hosts)" (Masolo et al., 2003, p. 29). They go on to mention that "some features may be relevant parts of their host, like a bump or an edge, or places like a hole in a piece of cheese … which are not parts of their host." Development of this ontology will provide elements of the Upper Level or Foundational Ontology for the geographic domain.

A third component of ontology of landforms is the taxonomy of types or kinds. What kinds of landforms are recognized, and how do the kinds relate to each other? For one thing, do landforms constitute a single domain of reality, or of the perceived human environment? If so, what are the main subdivisions? Convex and concave come to mind, but many parts of the Earth's surface are approximately planar. Do horizontal planar regions constitute a top-level class of landforms? Are vertical planar regions (cliffs in English) forms in their own rights, or parts of concave or convex landforms, or both? Voegelin and Voegelin (1957, p. 13) recognized "the Domain of Topography" as a top-level domain, and divided topography into three sub domains: eminences in the landscape; longitudinal depressions in the landscape; and oval or round openings in the earth. Eminences are regions that are higher than their surroundings. (A convex landform could protrude from the side of a hill while not being an eminence, but large examples of this are rare.) The main types of eminences in English are mountains and hills, but the English language also includes terms such as ridge, range, plateau, mesa, butte, pinnacle, tor, and others, which also denote types of eminences. Research into semantic similarity is needed to determine whether these basic-level categories are arranged in a hierarchical fashion, or whether all of these are simply types of eminence. A similar situation exists for longitudinal depressions in the landscape.

Lastly, the ontology of fields must be integrated with the taxonomy of landform types, all within an Upper Level ontology such as DOLCE—not an easy task!

2.2 Cultural Differences

Given the ontological situation outlined above, it is clear that there is room for different human cultures and speech communities to 'parse' the same landscape into different features, and also to group those features into named categories in different ways. Recently, Mark, Turk, and colleagues have presented empirical evidence of this, based on ethnographic studies with the Yindjibarndi and Navajo people (Mark and Turk, 2003; Mark et al., 2007). One does not, however, need to study Indigenous languages to find examples. For example, Mark (1993) presented an example of different categories for water bodies in English and French.

In the Yindjibarndi language, spoken mainly around Roebourne, Western Australia, there is a single term, ***marnda***, that refers to entities that in English would be called rock (the material), hills, mountains, ridges, ranges, etc. (Turk and Mark, 2008). ***Marnda*** appears to be used to refer to almost any eminence. Rather than having separate terms for large or small or flat-topped eminences, Yindjibarndi speakers combine the term ***marnda*** with general adjectives that denote size or shape of the feature. The Yindjibarndi language does have a few other terms that refer to convex features of the landscape (Turk and Mark, 2008). ***Burbaa*** apparently refers to a relatively small ***marnda*** that has a smooth, rounded shape. ***Bargu*** can refer to a small ***marnda*** with a rough or irregular profile, or to a rough rock outcrop protruding from the side of a hill (not an eminence). Lastly, a ***bantha*** is material piled up by a person or animal, and ***munggu*** refers to a termite mound. The distinctions between these categories do not line up well with distinctions among types of eminences made by English speakers.

Preliminary results for the Navajo language, not yet published, indicate that Navajo speakers have terms for eminences that differ in meaning from both the Yindjibarndi terms and the English terms (Mark, Stea, Topaha, and Turk, unpublished). For example, the Navajo language has two terms, ***dził*** and ***yílk'id***, which have meanings that fairly closely parallel the meanings of *mountain* and *hill*, respectively in English. However, the Navajo term ***dził*** is applied to large features covered with pine forest, even if these are called plateau or mesa in English. For features composed of exposed bedrock, the Navajo language uses neither ***dził*** and ***yílk'id***, but employs compound terms starting with ***tsé***, the Navajo term for rock, followed by terms for shape or posture, such as standing, sitting, or lying.

We have similar data for other landscape domains, and again find that the details of the categories are different for the different languages. We also have data for other languages that confirm that categories for landscape features and components do not 'line up' across languages.

2.3 Landform Extraction

As noted above, digital elevation models (DEMs) are discrete approximations to elevation fields. Landforms such as hills or valleys, on the other hand, are regions or parts of the Earth's surface that have a coherence of shape, earth surface processes, or other factors not directly represented in the DEM (Mark and Sinha, 2006). There is interplay between feature extraction and delimitation, quantitative description of the features, and classification of the features into meaningful categories. There is circularity here: one can only compute the size and shape of topography within some region, yet the detection and delimitation of a form depends on the computed size and shape. It is likely that this issue can only be overcome by iterative solutions. Detect a candidate feature, then delimit it, then determine its shape, then classify it, and then use the characteristics of the category to make a better determination of boundaries, re-parameterize, re-classify, until there is a stable solution. The phase where we "use the characteristics of the category" likely will be different for different languages. Sinha's (2007) dissertation provides a good start on the problem for eminences and for terms in English.

3. Summary

Intelligent multilingual landform extraction and classification presents a number of interesting research challenges. Bottom-up DEM-based measures of local form may be useful in some situations, but more global or top-down approaches are likely needed if the goal is to detect, delimit, and classify landforms that correspond to the categories used by earth scientists or by the general information-retrieving public.

Acknowledgements

This work is being done in collaboration with Gaurav Sinha (Ohio University), Andrew Turk (Murdoch University, Perth, Australia), David Stea (Texas State, San Marcos), the Yindjibarndi people (Roebourne, Australia), and the Navajo Nation and people. Discussions with Boyan Broderic and Werner Kuhn have been valuable. The research is supported in part by NSF Grants BCS-0423075 and BCS-0423023 and by an award from Microsoft Research.

References

Evans, I. S., 1972. General geomorphometry, derivatives of altitude, and descriptive statistics. In: R.J. Chorley, Editor, Spatial Analysis in Geomorphology, Methuen, London, pp. 17–90.

Mark, D. M., 1975. Geomorphometric parameters: a review and evaluation. Geografiska Annaler, 57A, 165-77.

Mark, D. M., 1993. Toward a Theoretical Framework for Geographic Entity Types. In Frank, A. U., and Campari, I, editors, Spatial Information Theory: A Theoretical Basis for GIS, Berlin: Springer-Verlag, Lecture Notes in Computer Sciences No. 716, pp. 270-283.

Mark, D. M., and Sinha, G., 2006. Ontology of Landforms: Delimitation and Classification of Topographic Eminences. In M. Raubal, H. Miller, A. Frank, and M. Goodchild, Eds. Geographic Information Science - Fourth International Conference, GIScience 2006, Münster, Germany, September 2006, Extended Abstracts. IfGI prints 28. Verlag Natur & Wissenschaft, Solingen, Germany, pp. 129-132.

Mark D. M., and Smith, B., 2004. A Science of Topography: From Qualitative Ontology to Digital representations. Chapter 3 in Michael P. Bishop and John F. Shroder, editors Geographic Information Science and Mountain Geomorphology Chichester, England: Springer-Praxis, pp. 75-100.

Mark, D. M., and Turk, A. G., 2003. Landscape Categories in Yindjibarndi: Ontology, Environment, and Language. In Kuhn, W., Worboys, M., and Timpf, S., Editors, Spatial Information Theory: Foundations of Geographic Information Science, Berlin: Springer-Verlag, Lecture Notes in Computer Science No. 2825, pp. 31-49.

Mark, D. M., Turk, A. G., and Stea, D., 2007. Progress on Yindjibarndi Ethnophysiography. In Winter, S., Duckham, M., Kulik, L., Kuipers, A., (editors) Spatial Information Theory. Lecture Notes in Computer Science No. 4736, pp. 1-19.

Masolo, C., Borgo, S., Gangemi, A., Guarino, N., and Oltramari, A., 2003. WonderWeb DeliverableD18, Ontology Library (final). Laboratory For Applied Ontology, http://www.loa-cnr.it/Papers/D18.pdf.

Peuquet, D.M., Smith, B. and Brogaard, B., 1998. The Ontology of Fields. Varenius Project Technical Report, (Santa Barbara, CA: National Center for Geographic Information and Analysis (NCGIA).

Sinha, G., 2007. Delineation, Characterization and Classification of Topographic Eminences. Unpublished Ph.D. dissertation, Department of Geography, University at Buffalo.

Sinha, G., and Mark, D. M., 2010. Extraction and Database Modeling of Topographic Eminences. Cartographica, under consideration.

Smith, B., and Mark, D. M., 2003. Do mountains exist? Towards an ontology of landforms. Environment and Planning B: Planning and Design, 30(3), 411-427.

Turk, A. G., and Mark, D. M., 2008. Illustrated Dictionary of Yindjibarndi Landscape Terms. Informal publication, Murdoch Univerity (Australia), October 2008.

Voegelin, C. F., and Voegelin, F. M., 1957. Hopi Domains: A Lexical Approach to the Problem of Selection. Memoir 14 of the International Journal of American Linguistics. Baltimore: Waverly Press, Inc.

Proceedings of Geomorphometry 2009. Zurich, Switzerland, 31 August - 2 September, 2009

Experiences in Developing Landform Ontologies

R. K. Straumann

Department of Geography, University of Zurich, Winterthurerstrasse 190, CH-8057 Zurich, Switzerland
Telephone: +41 44 635 51 98
Fax: +41 44 635 68 48
Email: ralph.straumann@geo.uzh.ch

1. Landforms – Ontologies and Extraction

The aim of this paper is to briefly review some of the work in landform-related research, to highlight the need for a sound ontological basis to such efforts and to present and discuss an approach for gathering domain knowledge and the problems encountered.

There is a considerable volume of geomorphometric literature centred on topographic eminences, specifically publications regarding the delineation or extraction of hills or mountains; e.g. Fisher et al. (2004), Chaudhry and Mackaness (2007) and (less spatially) Greatbatch et al. (2007). However, many of the approaches to landform delineation/extraction start to rapidly delineate crisply or extract fuzzily the desired objects. The authors rely to a certain degree on some common knowledge about what a mountain, a hill or a range is and, to a certain degree, assume that these concepts match what they extract. But there is fundamental work which acknowledges that these and similar landform concepts are not clear at all and that research into concepts and their formalisation is needed (e.g. Brändli 1996, Schmidt and Dikau 1999). A strain of research tries on a fundamental level to elucidate the ontology of geographic objects and with these, of landforms (e.g. Smith and Mark (2001, 2003), Smith and Varzi 2000, Mark and Smith 2004, Mark and Sinha 2006). Furthermore Mark et al. (2007) set out clearly why conceptualisations of landforms are not alike for people of different cultures or language groups.

In Geographic Information Science and geomorphometry there are a range of researchers who have developed methods to describe earth surface forms from digital elevation models (DEMs). Some of this interest has turned away from the mere description of predefined areas of land through DEM derivatives such as hypsometry, gradient or aspect to semantically richer characterisations of surface form. There is a huge breadth of publications related to the extraction of units that are homogeneous in relation to some surface properties. These units are termed (among others) “landform elements”. Besides these landform elements, there has been growing interest in recent years concerning landforms, i.e. larger regions of similar form character.

Besides, geographic information science has seen some effort to render geographic information systems more usable for lay-persons (e.g. Mennis et al. 2000). This has spawned a considerable amount of work on fuzzy spatial relations, such as something “being near” something else (e.g. Robinson 2000). Given this background, we think a similar case can be made that in the long run it would be valuable to enable GISs to make sense of landform terms such as “valley” or “mountain”.

We thus argue that – although there are already many extraction and classification algorithms especially for what are termed landform elements – there is a need to further strengthen the ontological basis such approaches implicitly rely upon. It might be insightful to review the breadth of landforms, to characterise their properties and interrelationships before pondering about ways to extract them from DEMs. We feel such an endeavour may serve well in order to strengthen efforts towards their automatic extraction, specifically, and towards landscape characterisation from DEMs in general.

2. Candidate Sources of Landform Description Catalogues

To elucidate the landform-related domain knowledge of geomorphology we drew on a number of sources. The reference works used range from standards dealing with (among others) landforms to more ontological sources. To build a collection of landform terms that represent important concepts in the domain knowledge, the listed data sources need to be scanned for landform-related categories.

WordNet (2006) is a lexical database of the English language held at the Princeton University. Word types are grouped into synsets. Synsets represent cognitive synonyms and each synset stands for a distinct concept. Different synsets are interlinked by various relations such as hypernymy (superordination), hyponymy (subordination), holonymy (whole-to-part relation) and meronymy (part-to-whole relation). In WordNet most landforms seem to be hyponyms of the synset „geological formation, formation".

SDTS (Spatial Data Transfer Standard; USGS 2007) has been devised as a means of transferring spatial data between computer systems. It is made up of base specifications and profiles. SDTS was ratified by the American National Standards Institute (ANSI) in 1998. We investigated SDTS mainly along the lines of Mark and Smith (2004: 82) who singled out 26 landform categories appearing "to fall under the broad superordinate category of 'landform'".

DIGEST (Digital Geographic Information Exchange Standard; DGIWG s.a.). The Digital Geospatial Information Working Group (DGIWG) was established in 1983 in order to develop standards for the exchange of geographical information among NATO members. DIGEST as developed by DGIWG has become a NATO Standardization Agreement. Landform categories are primarily contained in the section "D-Physiography – DB-Physiography-Landforms" of the Feature and Attribute Coding Catalogue.

Alexandria Digital Library (ADL) Feature Type Thesaurus (Alexandria Digital Library Project 2004). The ADL Feature Type Thesaurus has been developed for typing entries in the ADL Gazetteer and as a means to foster gazetteer interoperability. It contains a hierarchical listing of terms in the administrative, hydrographic, land parcels, man-made, physiographic and regional places domains. Landform-related categories can be found in the domains "Physiographic features" and "Hydrographic features".

SUMO (Suggested Upper Merged Ontology; SUMO 2009, Niles and Pease 2001) is an upper (or top-level, foundation) ontology, i.e. an ontology of very general concepts that are shared among all domains. It is a candidate ontology for the Standard Upper Ontology (IEEE SUO Working Group 2003). The whole SUMO consists of the core SUMO itself, the Mid-Level Ontology (MILO) and several domain ontologies among which there is also one for geography. For our investigation we exploited all concepts that are subclasses of the concept "LandForm" in this geography ontology.

3. Problems in Building a Taxonomy/Ontology

In distilling domain knowledge about landforms and a hierarchy of landforms from the afore-mentioned works and supported by geomorphological literature we found several difficulties. Among others, obvious difficulties arose with ambiguities in definitions or contradictions between definitions. There are also certain categories which suffer from under-specification. In the remainder of this paper we will detail some of these issues.

3.1. Ambiguities Regarding Form and Levels of Granularity

In most reference works the coverage of (sand) dunes is relatively shallow, i.e. they often contain only reference to a category “dune” or “sand dune”. This leaves much room for ambiguity regarding the form of such features. However, for the “dune” category this seems inherent since it is (at least at that general level) mainly characterised by material (sand or granular material) and process (wind-blown), but not form. Both the reference works and other geomorphologic literature heavily stress these aspects. This situation is in some respect similar to that of moraines which are also predominantly defined by material (boulders, stones, debris) and process (transport and deposition by a glacier) but show a large variety of forms.

However, a definition for dunes as “ridges or hills of sand” (DIGEST) is of limited use for devising a delineation/extraction method since it allows for much ambiguity regarding form. In such cases we suggest the enrichment of the vocabulary provided by the reference works to obtain a representation at a sufficient granularity – e.g. through inclusion of categories such as “transverse dune”, “longitudinal dune”, “barchan dune” etc. which are more specific regarding form (and context). These can be grouped in somewhat artificial categories such as “ridge-shaped dunes” or “hill-shaped dunes”.

3.2 Under-specification

Under-specification in the sense of lacking indications as to e.g. the typical size of instances of some category is common. However, in what follows we want to discuss an under-specification which while failing to account for a threshold size or differentiating property at least provides an ordinal measure for distinguishing two categories. While this situation is better than general under-specification, it still has adverse implications for work on delimitation/extraction of such features.

The two probably most popular examples of topographic eminences are “mountain” and “hill”. However, there is an obvious conceptual uncertainty, since the dichotomy between the two is unclear or underdeveloped. In reference works mountains are often described as being “higher than a hill”, whereas hills are described as being “smaller” or “shorter” than mountains (e.g. WordNet, DIGEST, SUMO). However, the uncertainty regarding their semantic delimitation does not seem to make people feel uncomfortable using the two terms. On contrary, the two terms are very popular with non-experts (cf. e.g. Battig and Montague 1969 as cited in Smith and Mark 2001, Smith and Mark 2001).

The conceptual uncertainty regarding hills and mountains is probably due to the (relative to “hill”) late introduction of “mountain” into the English language. According to the Oxford English Dictionary (OED; Oxford University Press s.a.), “hill” was formerly the all-encompassing term “including what are now called mountains”. After the introduction of “mountain”, however, “hill” was “gradually restricted to heights of less elevation”. During the 18th century “mountain” was still used to designate objects of moderate altitude (OED lists a quotation referring to St. Germain near Paris being situated on a mountain).

Derungs and Purves (2007) empirically investigated the conception of mountains of Swiss citizens. Terms often associated with mountains were e.g. “high”, “rock”, “snow”, “steep”. The question regarding minimum altitude of a feature to be called a mountain resulted in a very broad distribution of the answers (1364(±713)metres) hinting indeed that altitude is not a useful criterion.

The solution to this problem of delimitation could be for geomorphometric delineation/extraction tasks to resort to a superordinate category (e.g. “topographic eminence”) and leave the differentiation between hill and mountain to the user (e.g. via a user-adaptable thresholding process) or for later when more research into the differentiation (e.g. using other attributes such as ruggedness or landcover) has been done.

4. Reflections

This paper has touched upon some of the issues encountered with gathering and reconciling geomorphologic knowledge. We are convinced that making such knowledge more explicit before devising geomorphometric methods to extract features of interest could improve present approaches to surface form characterisation. Such knowledge can be used to probably first extract ‘cores’ of landforms (e.g. valley floors for valleys (Straumann and Purves 2008) or peaks and ridges for mountains (Mark and Sinha 2006)). Adopting such an approach subsequently needs methods to be found in order to sensibly ‘spread’ conceptual cores for finding the extent of a landform.

References

Alexandria Digital Library Project, 2004, ADL Gazetteer. http://www.alexandria.ucsb.edu/gazetteer.

Battig WF and Montague WE, 1969, Category norms for verbal items in 56 categories: a replication and extension of the Connecticut Norms. *Journal of Experimental Psychology Monograph*, 80(3), Part 2: 1-46.

Brändli M, 1996, Hierarchical models for the definition and extraction of terrain features. In: Burrough PA and Frank AU (eds), *Geographic Objects With Indeterminate Boundaries*, *GISDATA II*, Taylor & Francis, London, UK, 257-270.

Chaudhry O and Mackaness W, 2007, Automatic identification of hills and ranges using morphometric analysis. *Proceedings of GISRUK 2007*, Maynooth, Ireland, 333-342.

Derungs C and Purves RS, 2007, Empirical experiments on the nature of Swiss mountains. In: Winstanley AC (ed), *Proceedings of GISRUK 2007*, Maynooth, Ireland, 348-352.

DGIWG, s.a., Digital Geographic Information Exchange Standard (DIGEST). http://www.dgiwg.org/digest.

Fisher P, Wood J and Cheng T, 2004, Where is Helvellyn? Fuzziness of multi-scale landscape morphometry. *Transactions of the Institute of British Geographers*, 29(1): 106-128.

Greatbatch I, Wood J and Fisher P, 2007, A comparison of morphometric and web prominence of moun tain features. *Proceedings of GISRUK 2007*, Maynooth, Ireland, 312-317.

IEEE SUO Working Group, 2003, Standard Upper Ontology Working Group (SUO WG) Home Page. http://suo.ieee.org/index.html.

Mark D and Sinha G, 2006, Ontology of landforms: Delimitation and classification of topographic eminences. In: Raubal M, Miller HJ, Frank AU and Goodchild MF (eds), *Proceedings of GIScience 2006*, Muenster, Germany, 129-132.

Mark DM and Smith B, 2004, A science of topography: From qualitative ontology to digital representations. In: Bishop MP and Shroder Jr JF (eds), *Geographic Information Science and Mountain Geomorphology*, Springer, Berlin, Germany, 75-100.

Mark DM, Turk AG and Stea D, 2007, Progress on Yindjibarndi Ethnophysiography. In: Winter S, Duckham M, Kulik L and Kuipers B (eds), *Proceedings of COSIT 2007*, LNCS, 4736, 1-19.

Mennis JL, Peuquet DJ and Qian L, 2000, A conceptual framework for incorporating cognitive principles into geographical database representation. *International Journal of Geographical Information Science*, 14(6): 501-520.

Niles I and Pease A, 2001, Towards a Standard Upper Ontology. In: Welty C and Smith B (eds), *Proceedings of the 2^nd^ International Conference on Formal Ontology in Information Systems, FOIS 2001*, Ogunquit, USA, 2-9.

Oxford University Press, s.a., Oxford English Dictionary (OED) Online. http://dictionary.oed.com.

Robinson VB, 2000, Individual and multipersonal fuzzy spatial relations acquired using human-machine interaction. *Fuzzy Sets and Systems*, 113(1): 133-145.

Schmidt J and Dikau R, 1999, Extracting geomorphometric attributes and objects from digital elevation models – semantics, methods, future needs. In: Dikau R and Saurer H (eds), *GIS For Earth Surface Systems*. Gebrüder Borntraeger, Berlin, Germany, 153-173.

Smith B and Mark DM, 2001, Geographical categories: An ontological investigation. *International Journal of Geographical Information Science*, 15(7): 591-612.

Smith B and Mark DM, 2003, Do mountains exist? Towards an ontology of landforms. *Environment and Planning B: Planning and Design*, 30(3): 411-427.

Smith B and Varzi AC, 2000, Fiat and bona fide boundaries. *Philosophy and Phenomenological Research*, 60(2): 401-420.

Straumann RK and Purves RS, 2008, Delineation of valleys and valley floors. In: Cova TJ, Miller HJ, Beard K, Frank AU and Goodchild MF (eds), *Proceedings of GIScience 2008*, LNCS, 5266, Park City, USA, 320-336.

SUMO, 2009, The Suggested Upper Merged Ontology (SUMO), Ontology Portal. http://www.ontologyportal.org.

USGS, 2007, Spatial Data Transfer Standard Home Page. http://mcmcweb.er.usgs.gov/sdts.

WordNet, 2006, WordNet 2.1 for Windows. A lexical database for the English language. http://wordnet.princeton.edu.

SAGA vs GRASS: A Comparative Analysis of the Two Open Source Desktop GIS for the Automated Analysis of Elevation Data

T. Hengl[1], C. H. Grohmann[2], R. S. Bivand[3], O. Conrad[4], and A. Lobo[5]

[1]IBED University of Amsterdam, UvA B2.34, Nieuwe Achtergracht 166, 1018 WV Amsterdam, The Netherlands
Telephone: +31-(0)20-525-7379
Email: T.Hengl@uva.nl

[2]Institute of Geosciences, University of São Paulo, Rua do Lago, 562, Cidade Universitária 05508-080 São Paulo – SP, Brazil
Email: guano@usp.br

[3]Norwegian School of Economics and Business Administration, Helleveien 30, 5045 Bergen, Norway
Email: Roger.Bivand@nhh.no

[4]University of Hamburg, Institute for Geography, Bundesstraße 55, Raum 810, 20146 Hamburg, Germany
Email: conrad@geowiss.uni-hamburg.de

[5]Institut de Ciències de la Terra “Jaume Almera” (CSIC), Solé Sabarís s/n E–08028 Barcelona, Spain
Email: Agustin.Lobo@ija.csic.es

1. Introduction

Two of the most used open source desktop GIS software for the analysis of DEMs are SAGA[1] (System for Automated Geoscientific Analyses) GIS and GRASS[2] (Geographic Resources Analysis Support System) GIS (Wood, 2008; Steiniger and Bocher, 2009). SAGA has been under development since 2001 at the University of Göttingen (the SAGA development team, has since moved to University of Hamburg), Germany, with aim of simplifying the implementation of new algorithms for spatial data analysis. In 2004, most of SAGA’s source code was published using an Open Source Software license. The functionality of SAGA is described in Böhner et al. (2002) and Böhner et al. (2008); the software design, methods, and usage are explained in detail in Conrad (2007).

GRASS GIS, now one of the eight initial Software Projects of the Open Source Geospatial Foundation (OSGeo), is probably the most known open source GIS software in the world. Its functionality and usage are described in detail in Neteler and Mitasova (2008). GRASS itself is a collection of modules (they vary from version to version). Although originally a Linux-based project, the most recent version of GRASS (6.3; development version) is now also available for MS Windows machines.

GRASS is a much larger project than SAGA considering the number of developers/institutions involved, although their functionality considering the DEM analysis is about similar. Both SAGA and GRASS are increasingly rich considering the functionality they offer: the latest version of SAGA (2.0.3.) contains 48 libraries with 300 modules; GRASS 6.3 contains over 350 routines. Both in fact provide more functionality for the analysis of DEMs than proprietary low-end products such as the basic installation of ArcGIS 9.2. By linking SAGA/GRASS with R environment for statistical computing, a powerful combination is created that allows fusion of GIS and statistical functionality in the same code (Grohmann, 2004; Brenning, 2008).

---

[1] http://www.saga-gis.org

[2] http://grass.osgeo.org

In this article we present the results of a comparative analysis of performances of the two GIS software for the analysis of elevation data. We focus on DEM generation, extraction of hydrological features (stream networks), and extraction of gridded DEM derivatives. We will base our comparison on objective and subjective criteria: measures of accuracy, processing speed, but then also on the user's satisfaction following questionnaires. Our intention is not really to name the winner, but to see what the basic differences are, and to suggest ways to combine the strengths of the two packages.

2. Methods and Materials

In order to make this software comparison objective, we will use reproducible methods and pre-defined technical criteria of principal interest to the users: accuracy, speed, ease of use. Guides and defined criteria to compare GIS software do not really exist. In order to be able to compare two packages, they need to at least overlap considering the functionality they offer. In fact, in order for a comparison to be fair, the software packages should implement the same mathematical models; if this is not the case, they should at least indicate the same type of service: e.g. DEM generation, extraction of hydrological network etc. In the case of SAGA/GRASS, a significant overlap in functionality exists. For each case study we run analysis using sampled elevation data, and then validate the outputs generated using SAGA and GRASS versus the ground truth data. The case study and the processing steps shown in this article are available from the http://geomorphometry.org website (R script).

2.1 Case Studies

We use three standard elevation datasets common for contemporary geomorphometry applications: point-sampled elevations (LiDAR), contours lines digitized from a topo map, and a raster of elevations sampled using a remote sensing system. All three datasets (lidar.shp, contours.shp and DEMSRTM1.shp) refer to the same geographical area — a 1×2 km case study *fishcamp* located in the eastern part of California.

The point-dataset (LiDAR ground reflections) consists of 273,028 densely sampled points. The original LiDAR dataset consist in fact of over 5 million of points, which were sub-sampled to speed up the processing. A very fine resolution (2.5 m) DEM derived from LiDAR measurements was used as a ground truth layer for validation purposes. For the raster-dataset we use the SRTM 1 arcsec (25 m) Shuttle Radar Topography Mission (SRTM) DEM. The complete dataset was obtained from the USGS National Map seamless server[3].

2.2 Comparative Criteria

We have decided to base our comparison on four criteria: (1) absolute accuracy of the DEMs (surface) generated using default settings; (2) spatial accuracy of hydrological features extracted using default settings; (3) processing speed; (4) extendibility i.e. ease of implementation of new algorithms (from mathematical model to a new routine).

The accuracy of generated elevations was assessed versus the most accurate DEM available for the study area of interest (LiDAR-based DEM) using standard accuracy measures (RMSE, MSE). To assess the spatial accuracy of the derived hydrological (stream) networks we used the mean distance from the point line sets that can be derived by overlaying the predicted stream network over the buffer map generated using

---

[3] http://seamless.usgs.gov

the actual stream network. Processing speed was measured using the "system.time" method in R.

3. Results

3.1 DEM Generation Accuracy

We have generated DEM surfaces from contours.shp using spline interpolation, which has been recommended by both SAGA and GRASS developers as the most suited DEM gridding technique for contour data (Conrad, 2007; Neteler and Mitasova, 2008). This looks for closest 10 points in a local search radius and fits the Thin Plate Spline over a 25 m grid. This initial DEM can be hydrologically adjusted using the deepen drainage route. The resulting DEM surface can be seen in Fig. 1.

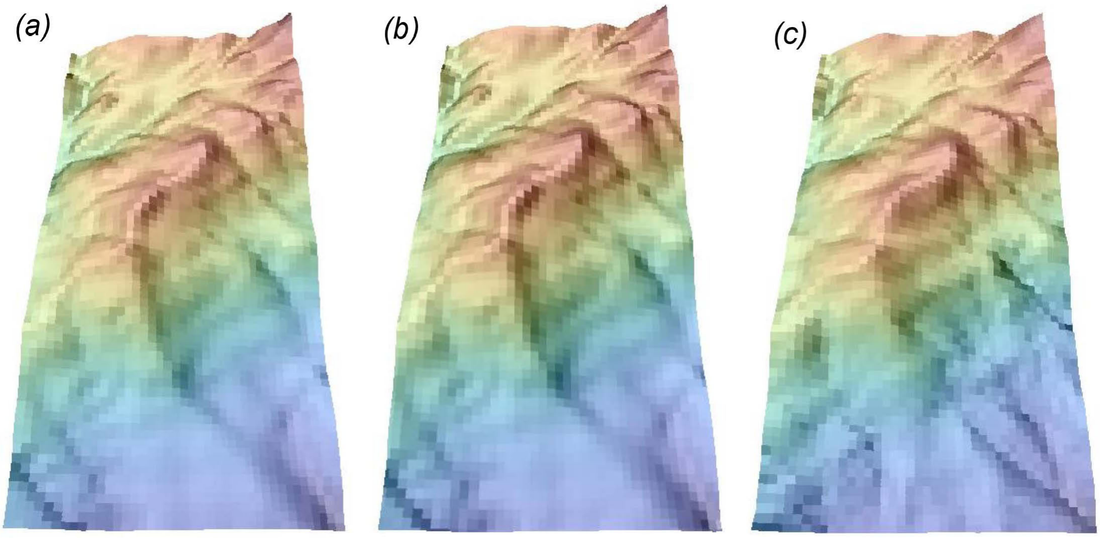

Figure 1. Comparison of DEMs derived in (a) SAGA and (b) GRASS using the 1:24k topo-map contour lines (contours.shp), as compared to the (c) DEM derived using all LiDAR points. Perspective view on the study area from the West–East direction.

The final comparison of the two DEMs shows that both software generate DEMs of approximately equal quality: the RMSE for the SAGA-derived DEM is 5.31 m, as compared to the 5.28 m for GRASS. Note also that, because the study area has a distinct topography, and because we use a smooth interpolator, both maps do not show artefacts (Fig. 1). Although the RMSE of both maps is satisfactory, it is obvious that many hydrological features in the area were missed. Neither SAGA nor GRASS are able to incorporate information on existing hydrological features (streams, and water bodies) into the generation of DEMs; compare with the ANUDEM procedure implemented in the TOPOGRID function of ArcInfo (Hutchinson, 1989).

3.2 Spatial Accuracy of Extracted Hydrological Networks

In the next exercise, we compare the drainage networks derived in SAGA and GRASS versus the stream network digitized from the topo-map. For this comparison, we use the 1 arcsec SRTM DEM dataset (DEMSRTM1.asc). In the case of SAGA, the stream network can be extracted in few steps: first we filter the spurious sinks, then extract channel network as shape file. In the case of GRASS, we first need to read the DEM into the GRASS format, and then extract the watershed using the "r.watershed" function. In the next step, we can “thin” the generated streams, so that we can also convert the stream map to vector lines.

Figure 2. Hydrological networks extracted using the 1 arcsec SRTM DEM (DEMSRTM1.asc) dataset in SAGA GIS and GRASS GIS, as compared to stream network digitized from the 1:24k topo-map (grey bold lines).

The final comparison is shown in Fig. 2. The statistical comparison of the difference between how closely the predicted streams match the streams at the topo-map shows that GRASS-derived streams are in average (median) 35.4 m from the actual stream network; for the SAGA-derived network we get 90.1 m. This difference is statistically significant (t-test statistics p-value=1.36e-06).

3.3 Processing Speed

To compare the processing speed, we tested several processing steps using the relatively large LiDAR dataset (lidar.shp). First, we use it to generate DEM using spline interpolation. This shows that there are quite some differences in the computing times: SAGA takes 279 seconds to generate a DEM (800×400 grid nodes) using Thin Plate Splines (closest 10 points) using 273,028 LiDAR points; GRASS takes about 2-3 times more. Even to derive DEMs from contour lines (2555 points) takes 81 seconds in GRASS, as compared to <1 seconds in SAGA. Second, we 480 test generation of DEM derivatives for the 800×400 grid DEM. SAGA takes 0.6 seconds to derive a slope map vs 0.4 seconds in GRASS.

There seems to be not much difference considering the image processing modules. Generation of the TWI using the multiple flow algorithm takes: 6 seconds with SAGA vs 31 seconds with GRASS. To derive the total incoming solar radiation for one year, with a hourly step of 2 hours, and a daily step of 5 days, takes 170 seconds in SAGA and 494 seconds in GRASS.

In summary, SAGA is in average about 2–3 times computationally more efficient for generation of DEMs using splines, and for hydrological and solar irradiation modeling. Functions in GRASS, on the other hand, in general provide more possibilities — they allow you to adjust the parameters and/or combine two operations within a single command line. The solar irradiation modelling in GRASS is much more sophisticated than in SAGA: it includes shadowing effects, reflected and diffuse radiation etc. GRASS also prints out the progress of processing in percentage.

3.4 Extendability

SAGA makes it easy to implement new algorithms and plug-in new libraries using Python; GRASS has an extensive and well-documented support for scripting and extension of routines. The "g.parser" module will parse specific variables in scripts (e.g. Shell, Python, Perl) and provide auto-generated graphical user interface, help page template and command line options checking, easily making simple scripts in full-featured GRASS modules. Some of the modules shipped with GRASS are in fact scripts, like "r.shaded.relief", which redirects the user options as parameters to the raster algebra module, "r.mapcalc". The GRASS-wiki AddOns lists over 100 users contributions.

In summary, GRASS supports scripting (original syntax), AddOns modules, and has a larger and more active community than SAGA. Nevertheless, modules in SAGA can also be easily extended or built from scratch but programming skills are required (C++, Python).

4. Discussion and Conclusions

The results of this set of comparisons shows that there are indeed some differences between the two software: SAGA seems to be more computationally efficient (2–3 times faster), GRASS generates more accurate streams networks, and in general offers more sophistication considering analysis of elevation data. On the other hand, much of the functionality (DEM generation, image processing, vector/raster conversion) in the two software is comparable.

The real differences exist between SAGA and GRASS in controlling the process from R and extending the functionality. SAGA seems to be slightly more user friendly considering the possibilities to manipulate maps, zoom in into the data and control the processing from external applications. GRASS, on the other hand is powerful as a tool for processing, but its interactive display characteristics are limited. SAGA’s user community is smaller, less international than in the case of GRASS. SAGA is also missing (completely!) help documents that explain different functions, how to set-up different parameters etc. In summary, there are quite big “view of the world” differences between GRASS and SAGA.

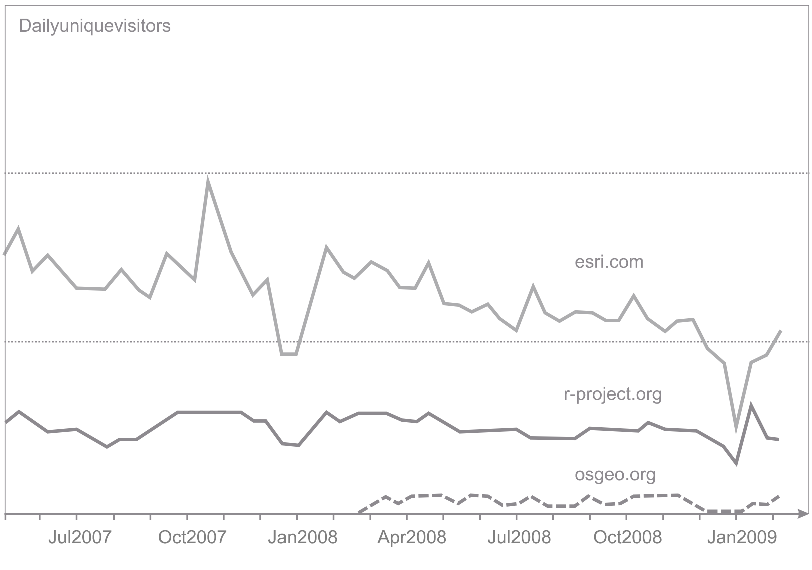

Figure 3. Trends in the web-traffic for http://esri.com, http://r-project.org and http://osgeo.org (following the http://trends.google.com statistics). Note that R users are typically more active also during the holiday periods.

Since the 1980's, the GIS research community has been primarily influenced by the (commercial) software licence practices that limited sharing of ideas and user-controlled development of new functionality (Steiniger and Bocher, 2009). With the initiation of the Open Source Geospatial Foundation (OSGeo), a new area started: the development and use of open source GIS has experienced a boost over the last few years; the enthusiasm to share code, experiences, and to collaborate on projects is growing. By comparing the web-traffic for commercial and open source GIS (Fig. 3), we can notice that there is indeed something going on — are we close to an inflection point when the open source GIS community will exceed e.g. the ESRI user's community? The open source GIS is certainly more powerful, more professional and more vital than five or six years ago. Further integration of packages such as SAGA and GRASS would increase this impression even more.

References

Bivand, R, 2005, Interfacing GRASS 6 and R. Status and development directions, *GRASS Newsletter*, 3, 11–16.

Böhner, J, McCloy, K, and Strobl, J, (eds) 2002, *SAGA — Analysis and Modelling Applications*, vol. 115 of Göttinger Geographische Abhandlungen, Verlag Erich Goltze GmbH, Göttingen.

Böhner, J, Blaschke, T, and Montanarella, L, (eds) 2008, *SAGA — Seconds Out*, vol. 19, Hamburger Beiträge zur Physischen Geographie und Landschaftsökologie, Hamburg.

Brenning, A, 2008, Statistical Geocomputing combining R and SAGA: The Example of Landslide susceptibility Analysis with generalized additive Models, In: Böhner, J, Blaschke, T, and Montanarella, L., (eds) *SAGA — Seconds Out*, vol. 19, Hamburger Beiträge zur Physischen Geographie und Landschaftsökologie, Hamburg, pp. 23–32.

Conrad, O, 2007, *SAGA — Entwurf, Funktionsumfang und Anwendung eines Systems für Automatisierte Geowissenschaftliche Analysen*. Ph.D. thesis, University of Göttingen, Göttingen.

Grohmann, C, 2004, Morphometric analysis in Geographic Information Systems: applications of free software GRASS and R, *Computers & Geosciences*, 30, 1055–1067.

Hutchinson, M, 1989, A new procedure for gridding elevation and stream line data with automatic removal of spurious pits, *Journal of Hydrology*, 106, 211–232.

Neteler, M and Mitasova, H, 2008, *Open Source GIS: A GRASS GIS Approach*, Springer, New York, 3rd edn.

Steiniger, S and Bocher, E, 2009, An Overview on Current Free and Open Source Desktop GIS Developments, *International Journal of Geographical Information Science*, in press, NA.

Wood, J, 2008, Overview of Software Packages Used in Geomorphometry, In: Hengl, T and Reuter, H, (eds), *Geomorphometry: Concepts, Software, Applications*, vol. 33 of Developments in Soil Science, Elsevier, pp. 257–267.

Proceedings of Geomorphometry 2009. Zurich, Switzerland, 31 August - 2 September, 2009

A Differential Equation for Specific Catchment Area

J. C. Gallant[1], M. F. Hutchinson[2]

[1]CSIRO Land and Water, GPO Box 1666, Canberra ACT 2601, Australia
Telephone: +61 2 62465734
Fax: +61 2 62465800
Email: John.Gallant@csiro.au

[2]Fenner School of Environment and Society, Australian National University, Canberra ACT 0200, Australia
Telephone: +61 2 61254783
Fax: +61 2 61250757
Email: Michael.Hutchinson@anu.edu.au

1. Introduction

Specific catchment area is one of the key land-surface parameters used in the fields of hydrology, geomorphology, pedology and ecology and many methods have been devised to estimate it from grid DLSMs. An accurate reference is required to test these methods, but specific catchment area has only been determined analytically for simple surfaces such as inclined planes and cones. To assess the results on the complex surfaces of natural terrain developers and users have resorted to comparisons between the results from different methods and visual inspection of the patterns of estimated specific catchment area.

This paper presents a differential equation that describes the rate of change of specific catchment area along a flow line. The equation can be solved numerically along a flow line that is derived numerically from a grid digital elevation model, allowing precise values of specific catchment area to be obtained at any location on a complex terrain surface.

The development of the concepts and exploration of the results and implications are addressed in more detail in Gallant and Hutchinson, (in preparation).

2. Stream Tubes and Specific Catchment Area

Specific catchment area, contributing area (or total catchment area, TCA) and flow width are all defined in terms of a *stream tube* (Onstad and Brakensiek, 1968) consisting of two adjacent flow lines terminating at the downstream end on the opposite ends of a contour segment (Fig. 1). Specific catchment area a is defined as

$$a = \lim_{w \to 0} \frac{A}{w} \tag{1}$$

where A is contributing area, the area of the stream tube, and w is the width of the lower end of the stream tube.

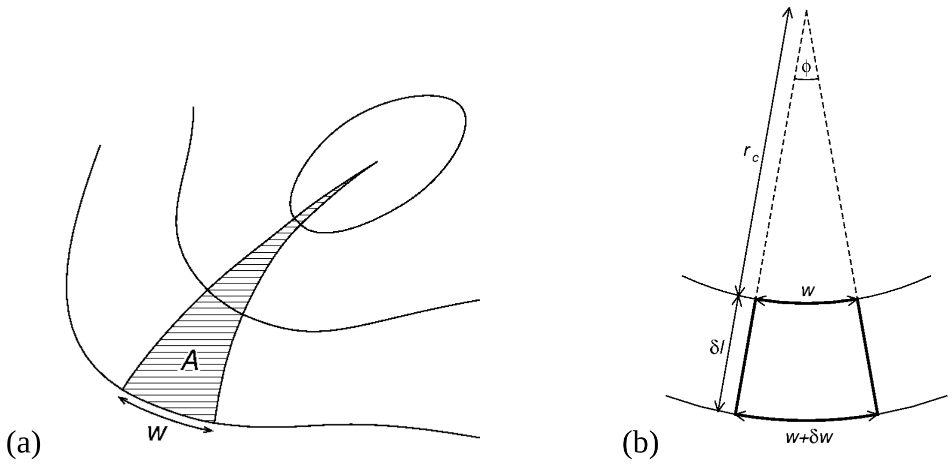

Figure 1. (a) A stream tube of area *A* defined by a contour segment of length *w*. (b) A segment of stream tube showing change in contour length determined by contour line curvature.

The area *A* at distance *l* from the hilltop is the integral of flow width *w* with respect to flow length:

$$A(l) = \int_0^l w(u)du \tag{2}$$

or equivalently

$$\frac{dA}{dl} = w \tag{3}$$

Consideration of the geometry of a short segment of stream tube where the radius of curvature of the contour lines is r_c leads to an expression for the rate of change of contour segment width *w*:

$$\frac{dw}{dl} = \frac{w}{r_c} = wK_c \tag{4}$$

where $K_c = \frac{1}{r_c}$ is the plan curvature (or contour curvature), defined here to be positive for divergent regions (as shown in Fig. 1(b)) and negative for convergent regions.

The equations for $\frac{dA}{dl}$ and $\frac{dw}{dl}$ allow a solution to the variation of specific catchment area *a* along a flow line starting from the definition of *a* at a point:

$$a = \lim_{w \to 0} \frac{A}{w} \tag{5}$$

$$\frac{da}{dl} = \frac{d}{dl} \lim_{w \to 0} \frac{A}{w} \tag{6}$$

$$= \lim_{w \to 0} \frac{w \dfrac{dA}{dl} - A \dfrac{dw}{dl}}{w^2} \tag{7}$$

$$= \lim_{w \to 0} \frac{w^2 - AwK_c}{w^2} \tag{8}$$

$$= \lim_{w \to 0} \left(1 - \frac{AK_c}{w} \right) \tag{9}$$

$$= 1 - K_c \lim_{w \to 0} \frac{A}{w} \tag{10}$$

$$\frac{da}{dl} = 1 - K_c a \tag{11}$$

Equation 11 describes the rate of change of specific catchment area a along the flow path. It is a non-linear differential equation that can be integrated numerically along a flow path constructed starting from a hilltop with $a = 0$. Under suitable conditions it can be solved analytically, although most of the analytical results can be obtained more easily by solution from first principles.

This equation has some interesting properties. The two terms on the right hand side relate to the two sources of change in specific catchment area: the constant term represents the increment due to increasing length of the flow line, while the second term captures the effects of convergence and divergence. In divergent terrain ($K_c > 0$) the two terms compete and $\frac{da}{dl}$ may increase or decrease along the flow path depending on the size of a and K_c. If $a = \frac{1}{K_c}$ the two terms balance exactly and specific catchment area remains constant along the flow path. In convergent terrain the two terms are both positive leading to an exponential increase in specific catchment area.

The use of a single flow line to determine specific catchment area becomes untenable in strongly convergent areas and in channels, where total catchment area is a more relevant quantity, but the results of Equation 11 are applicable over most of the landscape. A robust method to determine where Equation 11 ceases to be applicable; the condition $a > 5l$ is suggested in Gallant and Hutchinson (in preparation).

3. Numerical Solution

The solution of (11) on a grid DLSM requires:

- an interpolation method to create a smooth surface so that first and second derivatives can be computed at any point
- a method to construct flow lines on that surface
- a method to integrate (11) along a flow line

We use a biquadratic interpolation method (de Boor, 1978) to provide a continuous surface with continuous first derivatives. The flow lines are constructed as short straight line segments using a midpoint method with adaptive step size. At the start of each step, the local flow direction (aspect) is determined using the first derivatives of the surface, a trial half-step is taken, the direction is re-computed at the half-step point then a full step is taken in that new direction. The step size is adjusted so that the directions at the beginning and end of each step are quite close (dot product of unit vectors is greater than 0.99).

Integration of (11) is achieved by analytical solution for each segment of the flow line with appropriate assumptions on the variation of K_c along the segment. In most cases the form:

$$K_c(l) = \frac{1}{c_1 l + c_0} \tag{12}$$

is used, yielding the solution:

$$a(l) = \frac{c_0 + c_1 l}{1 + c_1} + \left(a_0 - \frac{c_0}{1 + c_1} \right) \left(\frac{c_0 + c_1 l}{c_0} \right)^{-1/c_1} \tag{13}$$

provided $c_1 \neq -1$ and $c_1 \neq 0$ and that K_c does not change sign along the line segment. If any of those conditions are not satisfied, an alternate solution with constant K_c is used:

$$a(l) = \frac{1}{K_c} - \left(\frac{1}{K_c} - a_0 \right) e^{-K_c l} \tag{14}$$

The integration commences at the top of the stream line with $a = 0$ and proceeds segment by segment to the end of the line.

The accuracy of the numerical solution will depend on the accuracy with which the flow line is constructed and the accuracy of the integration of Equation 11 along the line. The choice of the interpolation method will also have an impact on the results, although this is more a matter of choice than accuracy. In our experiments, we have used conservative parameters for the construction of the line so that many short line segments are constructed and further refinement of the line does not produce noticeable changes to either the path of the line or the integration of Equation 11. Gallant and Hutchinson (in preparation) demonstrate that the numerical results are indistinguishable from full analytical solutions on surfaces where analytical solutions are available (planes and cones).

4. Comparisons with Conventional Methods

The most valuable application of Equation 11 is as a reference against which the approximate (and much more efficient) methods of calculating specific catchment area can be compared. Figure 2 shows a flow path and stream tube calculated from a 20 m resolution DLSM in the Brindabella Ranges near Canberra in southeastern Australia (35° 21′S 148° 49′E). Figure 3 shows specific catchment area calculated along the central flow line using Equation 11 along with estimates from the most commonly used conventional methods: D8 (O'Callaghan and Mark, 1984); slope-weighted multiple flow direction here referred to as M8 (Freeman, 1991; Quinn *et al.*, 1991, 1995); DEMON (Costa-Cabral and Burges, 1994); and D∞ (Tarboton, 1997).

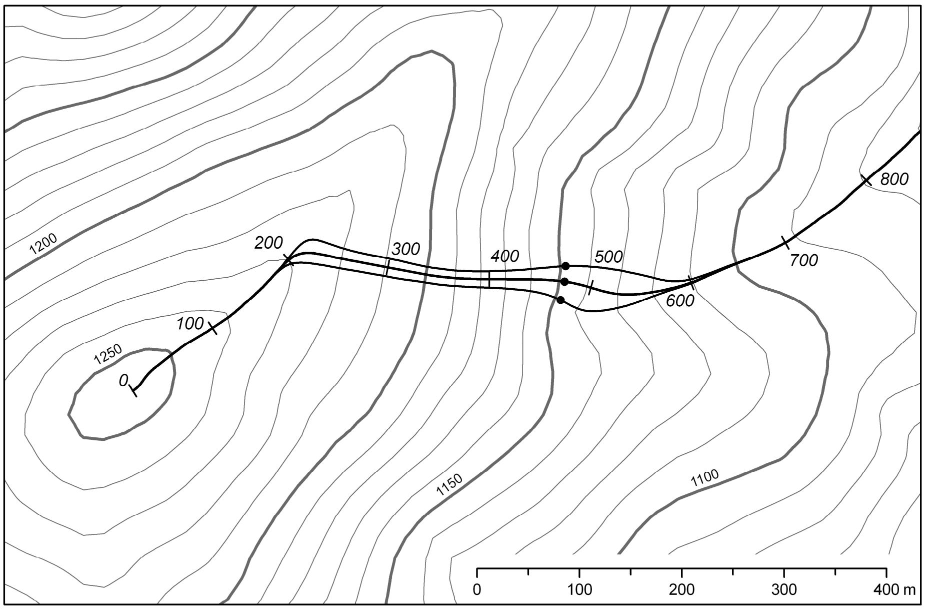

Figure 2. Flow lines derived from a 20 m resolution DLSM

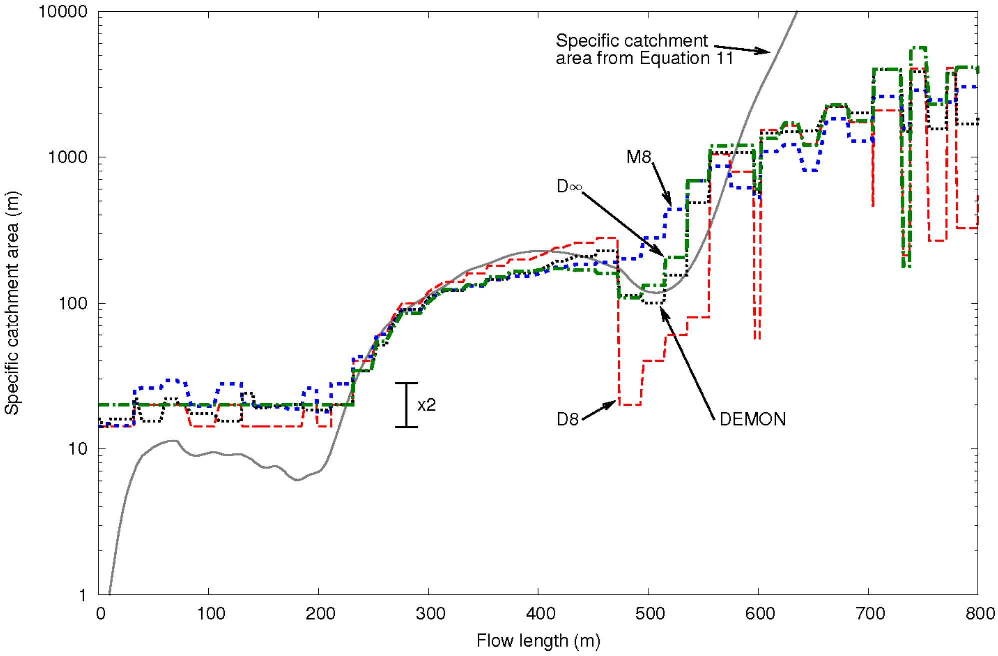

Figure 3. Specific catchment area along the flow line of Figure 2 computed using Equation 11 and four conventional methods.

Along the divergent ridgeline (flow length of 0 – 200 m) all the conventional methods over-estimate specific catchment area by about a factor of two. This is largely due to the way in which flow width is estimated in these methods; flow widths range from 1 to 1.414 times the cell size, whereas on a ridgeline flow leaves the cell over much of the perimeter of the cell.

Along the planar hillslope (200 – 400 m) all methods perform quite well with D8 giving the closest results to Equation 11. This result reflects the orientation of the flow path in a cardinal direction, where the known deficiencies of the D8 method do not occur.

Between 400 and 600 m the terrain is gently divergent then convergent. The D8 method is unable to capture this subtle variation, M8 performs better but still poorly while DEMON and D∞ behave quite well. D∞ appears to best capture the decline in specific catchment area around 450 m.

In the more convergent area beyond 600 m the result from Equation 11 increases exponentially, which is an unrealistic result that can be traced back to the assumption in Equation 1 that flow always responds to local curvature.

5. Conclusions

Equation 11 provides a method for accurately calculating specific catchment area at a specified point on a grid DEM without having to separately calculate catchment area and flow width. This method provides for the first time a means of testing approximate grid-based methods in complex terrain. A brief comparison with existing methods shows that the D∞ method best captures the variations in specific catchment area along the single flow line examined, although all methods over-estimate specific catchment area on divergent ridge lines.

References

Costa-Cabral M and Burges S, 1994, Digital Elevation Model Networks (DEMON): A model of flow over hillslopes for computation of contributing and dispersal areas. *Water Resources Research* 30(6):1681-1692.

de Boor C, 1978, A practical guide to splines. Springer-Verlag, Berlin.

Freeman T, 1991, Calculating catchment area with divergent flow based on a regular grid. *Computers and Geosciences* 17(3):413-422.

Gallant J and Hutchinson M, in preparation. Exact calculation of specific catchment area on grid DEMs, *to be submitted to Water Resources Research.*

O'Callaghan J and Mark D, 1984, The extraction of drainage networks from digital elevation data. *Computer Vision, Graphics and Image Processing* 28(3):323-344.

Onstad C and Brakensiek D, 1968, Watershed simulation by the stream path analogy. *Water Resources Research* 4(5):965-971.

Quinn P, Beven K, Chevallier P and Planchon O, 1991, The Prediction of Hillslope Flow Paths for Distributed Hydrologic Modelling using Digital Terrain Models. *Hydrological Processes* 5(1):59-79.

Quinn P, Beven K and Lamb R, 1995, The $\ln(a/\tan\beta)$ index: How to calculate it and how to use it within the TOPMODEL framework. *Hydrological Processes* 9(2):161-182.

Tarboton D, 1997. A new method for the determination of flow directions and upslope areas in grid digital elevation models. *Water Resources Research* 33(2):309-319.

A New Algorithm for Creating DEMs with Smooth Elevation Profiles

S. D. Peckham[1]

[1]University of Colorado, 1560 30th Street, Boulder, CO 80309
Telephone: (01-303-492-6752)
Fax: (01-303-735-8180)
Email: Scott.Peckham@colorado.edu

1. Introduction

Plots of longitudinal elevation profiles generated from a DEM and a corresponding D8 flow grid generally show an unrealistic step-like character, with long segments of slope zero separated by abrupt steps with steep slopes. This occurs as a result of limited vertical and horizontal accuracy in the DEM, particularly for DEMs with integer-valued elevations and a vertical resolution of one meter or one foot. The essence of the problem is that slopes on streamline elevation profiles are typically very small, on the order of 0.0001 or less. However, if the vertical resolution is Δz and the horizontal resolution is Δx, then the minimum, nonzero slope that is resolvable between two adjacent pixels is close to Δz / Δx. So, for example, if the vertical resolution is one meter and the horizontal resolution is 10 meters, slopes less than about 0.1 will be unresolvable and will usually get mapped to a value of zero. Note that even for a vertical resolution of 1 centimeter, the minimum resolvable value would be 0.001, still too large to resolve the actual along-channel slope. This issue becomes a real problem in spatially-distributed hydrologic models that use DEM-derived channel slope to compute flow velocity, v, from Manning's formula

$$v = (1/n) R_h^{2/3} S^{1/2}. \tag{1}$$

and the kinematic wave approximation. Here, n is the Manning's roughness parameter and R_h is the hydraulic radius.

When looking at a plot of a single elevation profile, it is clear that we want to apply some kind of smoothing or curve-fitting operation that replaces the elevation values on the jagged, original profile with a new, smoother set of values. Moreover, assuming that the original values are accurate to within the upper and lower bounds that are set by the vertical resolution, it seems reasonable that after rounding the new values to the same resolution we should recover the original values, if possible. What is not immediately clear is what operation we can perform on the original DEM so that all of the streamline elevation profiles will get smoothed in this way, without altering any of the original D8 flow directions.

2. A "Profile-smoothing" Algorithm

The purpose of this paper is to present one solution to this problem that is conceptually appealing and that seems to work relatively well. The idea is to first assume that Flint's Law is approximately valid over the entire DEM. Flint's Law (see all cited references) is an empirical relationship that expresses local channel slope, S, as a power-law function of basin contributing area

$$S = c A^{\theta}. \tag{2}$$

The exponent, θ, is sometimes called the concavity. Using a D8 flow grid, one then identifies the set of grid cells that lie on the streamline of the main channel in the basin of interest. Recall that the main channel is typically identified using a grid of contributing areas (computed by the D8 method) and repeatedly stepping upstream toward the D8 neighbor cell with the largest contributing area until a drainage divide is reached. Let z_0 denote the elevation of the grid cell to which the main channel's first grid cell flows. According to Flint's Law, the predicted elevation for the k^th^ grid cell on the main channel is then

$$z'_k(c,\theta) = z_0 + c\sum_{j=1}^{k} A_j^{\theta}\,\Delta L_j \qquad (3)$$

where A_j is the contributing area of the j^th^ grid cell on the main channel and ΔL_j is the horizontal distance between adjacent main-channel grid cells. A nonlinear least-squares regression procedure is then used to estimate the parameters c and θ in equation (3) that give the best fit to the main channel elevation values, z_k. If we assume that the same parameters c and θ are approximately valid for every other elevation profile in the DEM, we can then use them to compute a new grid of channel slopes from the values in the contributing area grid. This grid of channel slopes is guaranteed to decrease smoothly downstream since contributing areas computed by the D8 method always increase downstream. The final step is to modify the original elevation values so that the slope computed between every grid cell and its downstream neighbor is exactly equal to the value predicted by the new channel slope grid. We do this by using an iterative procedure, starting with the grid cells that are furthest downstream and then computing and applying the small, floating-point elevation changes that must be made to upstream neighbor cells in order to achieve the prescribed channel slope. The iteration continues upstream until every grid cell has the prescribed slope. Figure 1 shows the result of applying this procedure to the main channel of Beaver Creek, Kentucky. The smooth curve provides much better estimates of channel slope but sometimes results in fairly large differences in elevation.

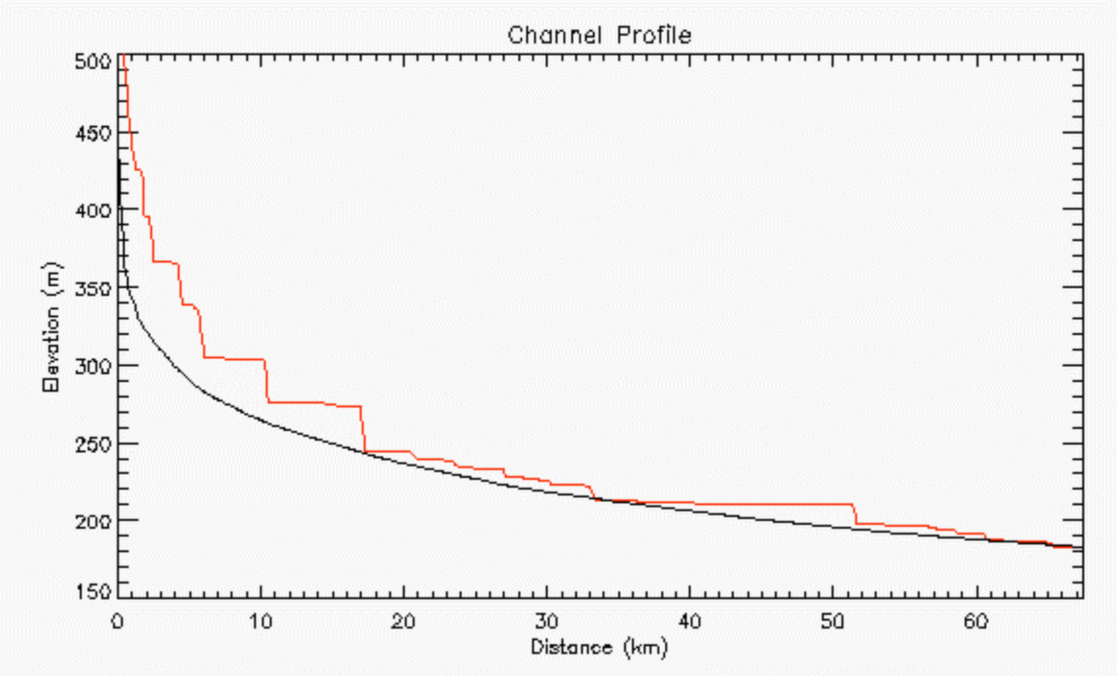

Figure 1. Comparison of main-channel elevation profiles before and after the profile-smoothing operation.

As explained previously, limited vertical and horizontal accuracy in DEMs can result in enormous errors in channel slope, S, as measured between adjacent grid cells. This is especially true for DEMs in which elevations have been rounded to the nearest foot or meter. As already illustrated, computed slopes can differ from actual slopes by a factor of 10,000 or more. However, contributing area, A, measured from a DEM depends only on the horizontal resolution and therefore the relative error in A is very small for basins that are much larger than the grid cell size. It follows that even if Flint's Law is only a crude approximation, using it to compute channel slopes from areas is likely to be more accurate than measuring slopes between grid cells in the DEM. Also, because of the inverse relationship between S and A, the relative error in A is smallest for the larger basins where the measured error in S is largest. This approach therefore allows us to trade large measurement errors in S for small measurement errors in A.

3. Conclusions

The fact that this algorithm works relatively well (at least for the fairly mature and homogeneous fluvial landscapes for which it has been tested) is somewhat surprising and points to an organizing principle in real landscapes that is not yet well-understood. Perhaps most surprising is the fact that best-fit values of c and θ obtained for the main channel produce reasonable results when applied to the landscape as a whole. In test cases the value of θ tends to be close to -0.55. This is also the average value reported by Whipple (2004). It is also about what one would expect based on combining the empirical slope-discharge equation of hydraulic geometry with an exponent close to -0.5 and a discharge-area power-law with an exponent close to 1. Note, however, that Flint's Law is not expected to apply to the concave down portion of a longitudinal profile near a drainage divide. As a result of this, the algorithm tends to produce elevations near drainage divides that are sharper than in the original DEM. However, the author has found using DEMs of different resolutions for Beaver Creek, Kentucky that the modified DEM was actually in better agreement with a higher-resolution DEM for the same area than the original DEM.

This basic "profile-smoothing" algorithm can be modified in various ways. For example, the slope value predicted from Flint's Law can be rejected if it results in an elevation change that is greater than the vertical resolution of the original DEM. One could also use all of the DEM grid cells in the nonlinear regression to estimate c and θ, instead of only those on the main channel. Work is ongoing to refine the algorithm and to make it as robust as possible.

References

Flint JJ, 1974, Stream gradient as a function of order, magnitude and discharge, *Water Resour. Res.*, 10(5): 969-973.

Schorghofer N and DH Rothman, 2002, Acausal relations between topographic slope and drainage area, Geophys. Res. Letters, 29(13): 1633.

Whipple KX, 2004, Bedrock rivers and the geomorphology of active orogens, *Annu. Rev. Earth Planet. Sci.*, 32: 151-185.

Willgoose G, Bras RL and Rodriguez-Iturbe I, 1991, A physical explanation for an observed link area-slope relationship, *Water Resour. Res.*, 30: 1697.

Wobus C, Whipple KX, Kirby E, Snyder N, Johnson J, Spyropolou K, Crosby B and Sheehan D, 2006, Tectonics from topography: Procedures, promise and pitfalls, pp. 55-74, In: *Tectonics,* *Climate and Landscape Evolution, Geol. Soc. of Am., Special Paper 398*, S.D. Willet, N. Hovius, M.T. Brandon, D.M. Fisher (eds.).

Calculation of Side-Separated Contributions to Stream Networks – A New Tool to Characterize Riparian Zones

T. Grabs[1], Jan Seibert[2], Kelsey Jencso[3], Brian McGlynn[3]

[1] Department of Physical Geography and Quaternary Geology, Stockholm University, SE-106 91 Stockholm, Sweden
Telephone: +46 (0) 768024224
Email: thomas.grabs@natgeo.su.se

[2] Department of Geography, University of Zurich, CH-8057 Zurich, Switzerland
Telephone: +41 (0) 44 6355200
Email: jan.seibert@geo.uzh.ch

[3] Watershed Hydrology Lab, Montana State University, 334 Leon Johnson Hall, Bozeman, Montana 59717
Telephone: +1 406 994 7690
Email: kelseyjencso@gmail.com, bmcglynn@montana.edu

1. Introduction

Streams play a key role in many environmental studies and research areas. From a hydrological perspective, streams and other flow pathways carry the spatio-temporally convoluted signal of all upstream, hydrologically-connected processes. Modern tools for GIS-based hydrological landscape analysis (HLA) embrace this concept for calculating values of upslope area or for aggregating upslope terrain indices. Recent studies, however, suggest that not all upslope processes contribute equally to the observed stream signal and that particularly riparian zones hold the key for a better understanding of stream responses. Riparian zones are, by nature, elongated strips of land directly adjacent to a stream network and located on both of its sides. Being the last stage before a drop of water enters a stream network, the potential imprint left by riparian zones is likely to be considerably larger than indicated by their actual extend. However, traditional HLA methods used to characterize these zones are mostly inapplicable because most methods fail to account for small extend of riparian zones and for the fact that they are located on opposite sides in a stream network.

To overcome limitations of traditional HLA methods, we developed a novel method to calculate side-separated contributions from adjacent hillslopes. Water table and elevation data from the 22 km^2 Tenderfoot Creek catchment, Montana, demonstrated clearly the importance of the new method. Separating contributions from the two sides produced significantly different results than produced by standard HLA methods. More importantly, only upslope area calculated by the new method was able to predict the hydrological connection between hillslope and riparian water tables as observed in 24 transects along the stream network.

2. Material and Methods

Our new algorithm determines the side of contributing hillslopes relative to a stream network based on geometric calculations. Since these calculations are performed separately, this method can be combined with virtually any existing flow accumulation algorithm for calculating upslope area (UA). The algorithm requires an elevation map and a stream direction map (SDM). The SDM is composed of connected stream vectors while the elevation map can be represented by various data structures such as regular grids, triangular irregular networks or contours. At this stage, we implemented the algorithm in the open-source tool SAGA GIS (Böhner et al., 2008) for use with regular grid data. Correspondingly, stream vectors in the SDM are grid cells with integer values representing different flow directions (Figure 1) and the used elevation map is a standard digital elevation model (DEM). The SDM was derived from the DEM using the "Channel Network" module in SAGA GIS (Böhner et al., 2008).

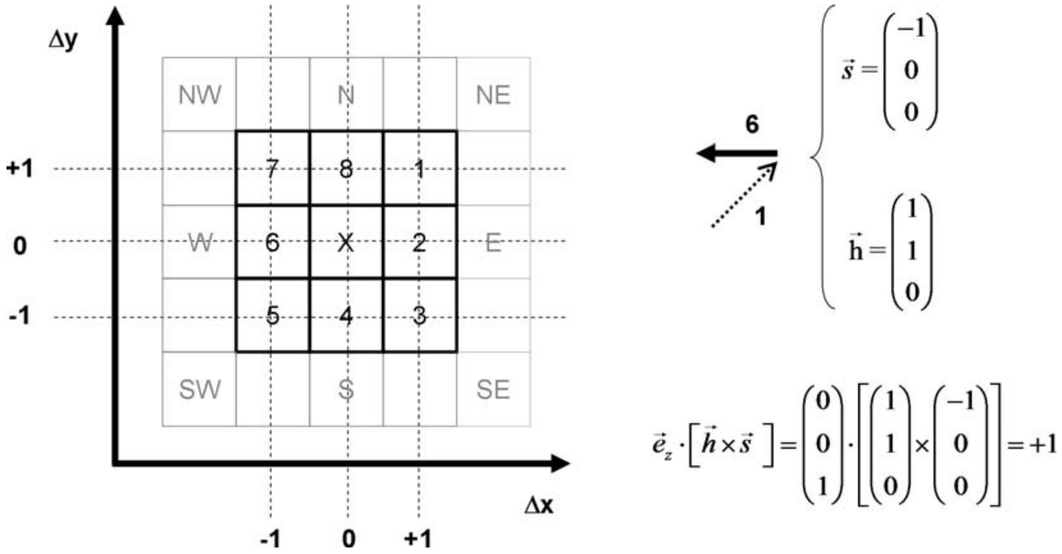

Figure 1. Directions relative to the center grid cell X are coded from 1 to 8 clockwise from northeast (NE) to north (N). The corresponding vector notation is illustrated for a hillslope vector $\vec{h}$ in direction 1 (dotted arrow) and for a stream vector $\vec{s}$ in direction 6 (plain arrow). Calculating the cross product $\vec{h} \times \vec{s}$ reveals a positive z-component and therefore the hillslope vector $\vec{h}$ is located on the left side relative to the stream vector $\vec{s}$.

The algorithm functions as follows. For every grid cell of the DEM that drains into a downslope SDM grid cell, the algorithm determines the corresponding hillslope vector $\vec{h}$ as well as the stream vector of the downslope SDM grid cell, $\vec{s}_0$, and all stream vectors $\vec{s}_{i+1}$ of upstream SDM grid cells that are directly connected to $\vec{s}_0$ (Figure 2). To find the position of the hillslope relative to the stream, the algorithm next calculates the cross products $\vec{c}_i$ of all pairs of the hillslope vector $\vec{h}$ with different stream vectors $\vec{s}_i$:

$$\vec{c}_i = \vec{h} \times \vec{s}_i , \quad i \geq 0 \tag{1}$$

Since $\vec{h}$ and $\vec{s}_i$ are horizontal vectors with z-components equal to zero, the resulting cross products, $\vec{c}_i$ are perpendicular to the map plane and only their z-components, $\vec{e}_z \cdot \vec{c}_i$, are normally different from zero. The sign of the z-components indicates the position of the hillslope relative to the considered stream vector. If left and right are defined looking in parallel direction to the stream vector $\vec{s}_0$, that is looking in downstream direction of the stream, then a negative z-component indicates that the hillslope is located on the right side relative to the stream vector. Similarly, a positive z-component indicates that the hillslope is on the left side of the stream vector. If all z-components of all cross products, $\vec{e}_z \cdot \vec{c}_i$, have the same sign the position of the hillslope can be directly inferred by from the sign of all $\vec{e}_z \cdot \vec{c}_i$. Exceptions occur when z-components have opposite signs, are equal to zero or in cases where the hillslope drains into endpoints of the stream network, which can be either sources, sinks or outlets (Figure 2). All exceptions are treated separately.

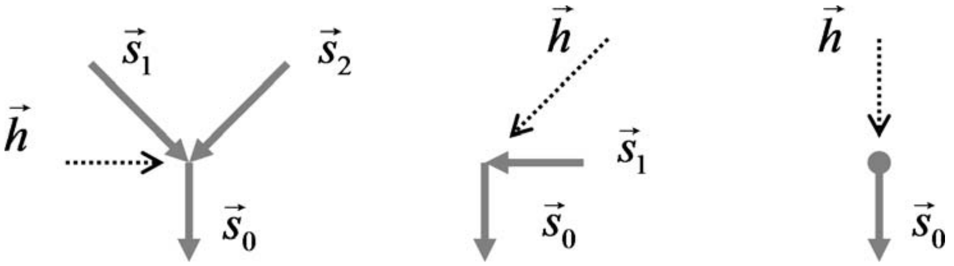

Figure 2. Different configurations of hillslope $\vec{h}$ (dotted arrows) and stream vectors $\vec{s}_i$, $i \geq 0$ (plain arrows). The left graph depicts a hillslope vector $\vec{h}$ pointing to a stream junction. In this case, the associated hillslope is attributed on the right stream side because it is on the right side relative to all stream vectors $\vec{s}_i$. A typical stream bend is shown in the middle graph. $\vec{h}$ is o the left side relative to $\vec{s}_0$ and on the right side relative to $\vec{s}_1$ and therefore on the outer side of the bend. Since the cross product $\vec{s}_1 \times \vec{s}_2$ has a negative z-component the inner bend must be located on the left stream side and hence on the right stream side. The graph on the right illustrates a hillslope upstream of a source. In this case the side of the hillslope is not definable.

3. Application and Results

We demonstrate the value of separating the stream into its left and right sides by comparing UA computed from a DEM of Tenderfoot Creek Experimental Forest (TCEF). TCEF is located in the Little Belt Mountains of the Lewis and Clark National Forest in Central Montana, USA. The research area consists of seven gauged catchments that form the headwaters of Tenderfoot Creek (22.8 km^2), which drains into Smith River, a tributary of the Missouri River. The 7 TCEF sub-catchment areas range in size from 3 to 22.8km^2. Catchment headwater zones are typified by moderately sloping (avg. slope ~ 8°) extensive (up to 1200m long) hillslopes and variable width riparian zones. Approaching the main stem of Tenderfoot Creek the streams become more incised, hillslopes become shorter (< 500m) and steeper (average slope ~20°), and riparian areas narrow compared to the catchment headwaters.

A preliminary comparison of inflows from the right side against inflows from the left side (Figure 3), all derived from a 10 m DEM of a 23km^2 catchment in (TCEF), showed no correlation between the inflows, which can be expected. This also illustrates that the total inflow is no suitable proxy for the lateral inflows from the two respective sides.

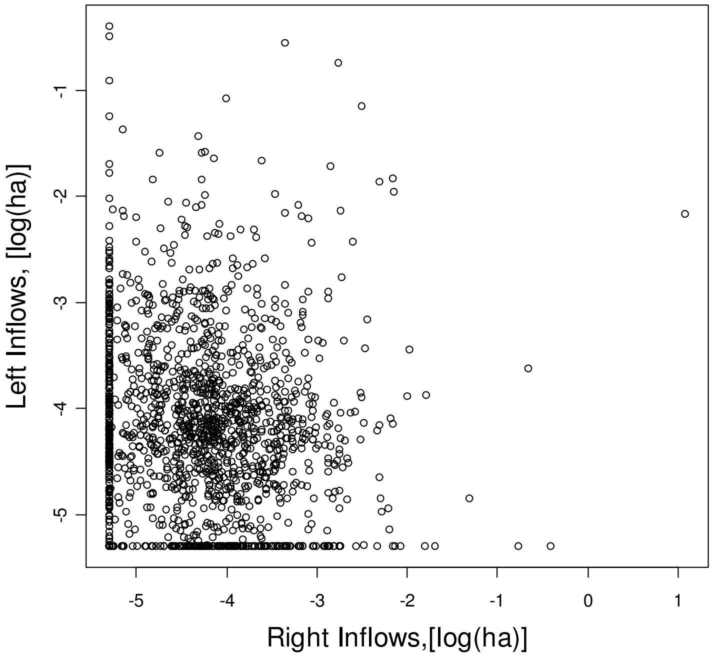

Figure 3. Scatter plot of inflows from the left versus inflows from the right side in the derived from a DEM of a 23km^2 catchment in TCEF

The distinction of opposite stream sides when calculating UA is theoretically plausible and also has practical implications. This was shown in a recent study by Jencso et al. (2009). Jencso et al. (2009) applied the suggested algorithm to same previously mentioned DEM. They compared UA to the yearly-cumulative Hillslope-Riparian-Stream (HRS) water table connectivity across twenty four transects of shallow groundwater recording wells. Hydrologic connectivity between HRS zones was inferred from the presence of saturation measured in well transects spanning the hillslope, toeslope, and riparian positions. A HRS hydrologic connection was defined as a time interval during which stream flow occurred and both the riparian and adjacent hillslope well recorded water levels above bedrock.

Meaningful relationships between UA and HRS water table connectivity were only found using side-separated UA whereas total UA seemed unrelated to HRS water table connectivity (Figure 4) which clearly demonstrates the importance of the new method.

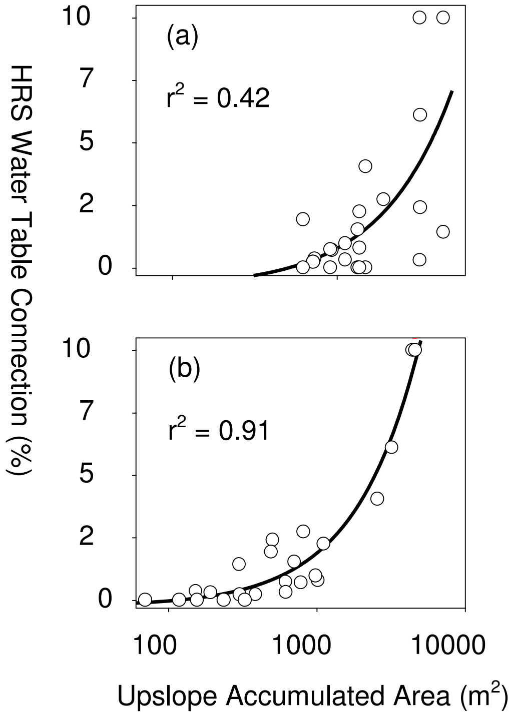

Figure 4. Hillslope UA regressed against the percentage of the water year that a hillslope-riparian-stream water table connection existed for 24 well transects. (a) Total hillslope UA from both sides of a transect cross-section. (b) Hillslope UA separated into left and right sides of the stream. A connection was recorded when there was stream flow and water levels were recorded in both the riparian and hillslope wells.

Riparian zones are also commonly referred to as buffer zones between streams and upslope areas. Any signal propagating from the upslope areas to the stream is modified, respectively buffered, by the intermediate riparian zone. To characterize the buffer capacity of riparian zones, McGlynn and Seibert (2003) introduced the ratio of riparian area to hillslope area as a new distributed terrain metric. High ratios are interpreted as high buffer capacities and vice versa. However, McGlynn and Seibert (2003) did not account for unequal lateral inflows when calculating buffer ratios. Redoing their calculations but using side-separated hillslope and riparian area ratios lead to significantly different results. For example, the catchment-wide median area-weighted buffer ratios are $1.7 \cdot 10^{-2}$ and $1.4 \cdot 10^{-2}$ for the lumped and side-separated calculations respectively, which corresponds to a relative error of about 26%. Local relative errors along the stream network even amount to 50% and more. Using the new method to compute side-separated inflows is thus an essential prerequisite for calculating realistic riparian hillslope ratios.

4. Concluding Remarks

Our findings highlight the importance and high potential benefits of using the new method to derive hydrologically meaningful characterizations of riparian zones. We are not aware of any other existing GIS-tool that allows discriminating lateral inflows.

While the need for such discrimination might depend on the type of index being calculated, it is crucial for calculating riparian-hillslope buffer ratios.

References

Böhner J, Blaschke T and Montanarella L, 2008, SAGA – Seconds Out. Hamburger Beiträge zur Physischen Geographie und Landschaftsökologie, *19, 113pp.*

McGlynn B and Seibert J, 2003, Distributed assessment of contributing area and riparian buffering along stream networks. *Water Resour. Research, 39(4): 1082, doi:10.1029/2002WR00152.*

Jencso K, McGlynn B, Gooseff M, Wondzell S, Bencala K and Marshall L, 2009, Hydrologic connectivity between landscapes and streams: Transferring reach- and plot-scale understanding to the catchment scale. *Water Resour. Research, 45: W04428, doi:10.1029/2008WR007225.*

A Viewshed Based Classification of Landscapes Using Geomorphometrics

J. Washtell, S. Carver and K. Arrell

School of Geography, University of Leeds, LS2 9JT
Tel. (+44) 0113 3433343
Fax (+44) 0113 3433308
Email s.j.carver@leeds.ac.uk

1. Introduction

Viewshed analyses are a potentially useful way of classifying landscapes for the purposes of geomorphometry as well more common applications in landscape evaluation, scenic quality assessment and associated comparative analyses (Fisher et al., 2004; Germino et al., 2001; Wilson et al., 2008;). It is theoretically possible to quantify a landscape based on openness and the cumulative visibility of a range of geomorphometric indices such as slope, aspect, curvature, roughness, ruggedness, altitudinal range, peakiness, etc (Wood, 2002, Fisher et al., 2004). This can provide the user with an indication of both how open the terrain is and what the precise characteristics of a landscape are that are visible from any point on a terrain surface. This could be implemented using standard, off-the-shelf viewshed analysis tools available in most proprietary GIS software, but the processing overheads, particularly in regard to the extremely long run times involved, where t = years rather than hours or days, make this an impractical proposition even with the most powerful processors. Of course, parallelisation of viewshed algorithms has been shown to be effective in reducing the time required for such analyses (Ware et al., 1996; Kidner et al., 1997; Ware et al., 1998) and distributed GRID computing offers still further reductions in overall run times (Rana and Sharma, 2006), but these methods do not lend themselves easily to most users of desktop GIS. Much effort has been put into developing faster and more efficient viewshed tools in GIS (Huanping et al., 2007; Izraelevitz, 2003) using a variety of algorithms such as tracking in, tracking out, approximation of line of sight, reference plane and block partitioning. This paper describes an alternative approach that utilises a novel voxel-based viewshed algorithm that can significantly reduce overall run times to acceptable levels and allow interactive, real-time evaluation of viewsheds on a standard desktop PC with large terrain models consisting of several million cells.

2. Methods

The algorithm developed uses efficient ray-casting and voxel modelling techniques popularised by realistic 3D computer games developed during the 1990s. In the voxel surface model, each of the raster cells in a digital terrain model are projected as a series of vertical columnar elements whose vertical and horizontal surfaces can be independently checked for partial visibility. At moderate cell resolutions this model produces results which are effectively indistinguishable from more sophisticated (though not inherently more accurate) interpolated surface models. Ray-casting is an efficient method of ensuring that only the parts of a terrain surface potentially visible from any viewpoint are considered in calculating the viewshed, and that calculations are not unnecessarily reproduced. The judicious combination of these techniques reduces viewshed runtimes to a fraction of those offered by algorithms available in common GIS packages such as ArcGIS and MapInfo. Individual viewsheds are accelerated to the point where observer or feature locations can be interactively auditioned in real time. This also makes "viewshed transforms" a practical possibility on a modest desk top PC, whereby the cross-visibility of every terrain cell from an observer position on every other terrain cell can be mapped. This opens up a host of sophisticated visibility-based landscape assessments that would hitherto be so time-consuming as to be impractical.

The resulting efficiencies realised means that the voxel viewshed transform is able to out-perform the equivalent calculations required by ESRI's ArcGIS software by a factor of approximately 1300. One of the immediate implications of this increase in viewshed algorithm efficiency is the ability to perform real time viewshed analyses across relatively high resolution terrain surfaces, where the total number of cells is in the region of n x 10^6. This is shown in Figure 1 and can be used to interrogate terrain data and animate viewsheds in real time. The advantages of the voxel-based model are also realised in the model's ability to incorporate calculations of both plan and profile area of features visible in the landscape, and modify these according to distance decay functions. This allows the user to load feature data representing any surface feature or index and calculate:

1. the number of distinct classes visible;
2. a discrete count (e.g. the number of individual features); and
3. a continuum (e.g. the proportion of a surface).

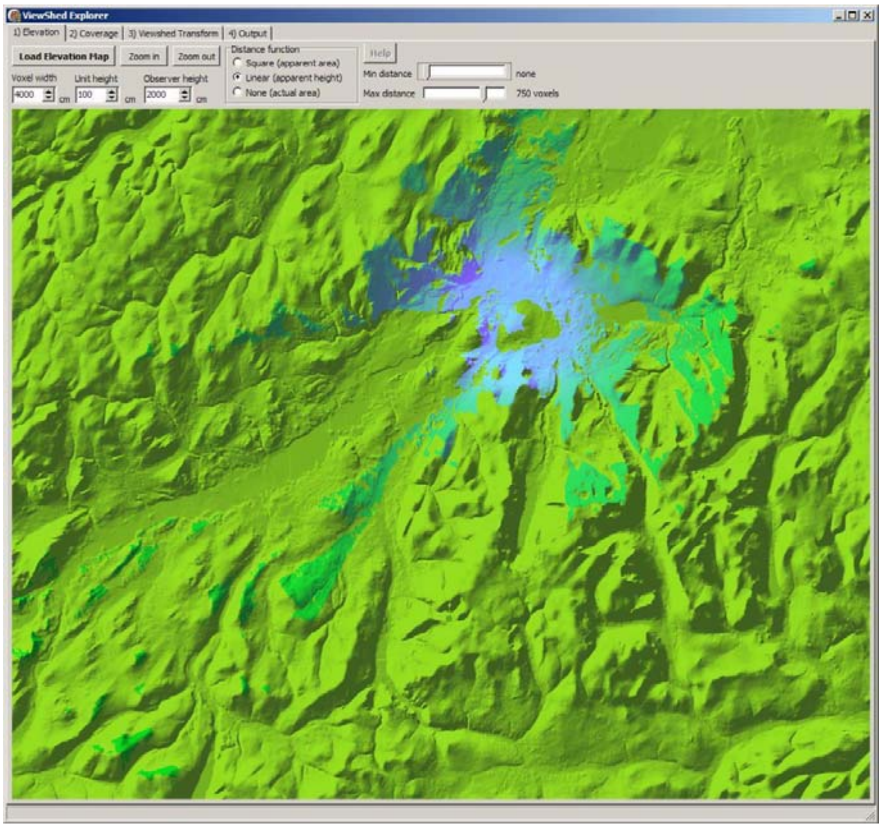

Voxel width 4000 cm

Unit height 100 cm

Observer height 2000 cm

Distance function

○ Square (apparent area)

● Linear (apparent height)

○ None (actual area)

Min distance none

Max distance 750 voxels

Figure 1. Voxel viewshed tool used to interrogate terrain data and produce real time viewsheds for a 6,000 x 10,000 cell DEM

3. Study Area

Example applications are given for the Cairngorm National Park in northeast Scotland. The Cairngorm is a high mountain plateau composed mainly of granitic rocks which is deeply incised by glacial troughs and bowls. The high plateau is the largest area of the UK above the 4000 foot contour and is nationally important for its unique arctic flora and fauna. The area is designated as a National Nature Reserve, a Site of Special Scientific Interest and was recently designated as a national park. A 5 metre resolution digital surface model and 5 metre resolution digital terrain model created from Synthetic Aperture Radar data are used to describe the land surface and surface significant features including forest and artificial structures, such as buildings and other structures, that project above the underlying terrain surface. An example is shown in Figure 2 together with a general view of the terrain. A sample dataset measuring 15 x 15 km (3,000 x 3,000 cells) is used here.

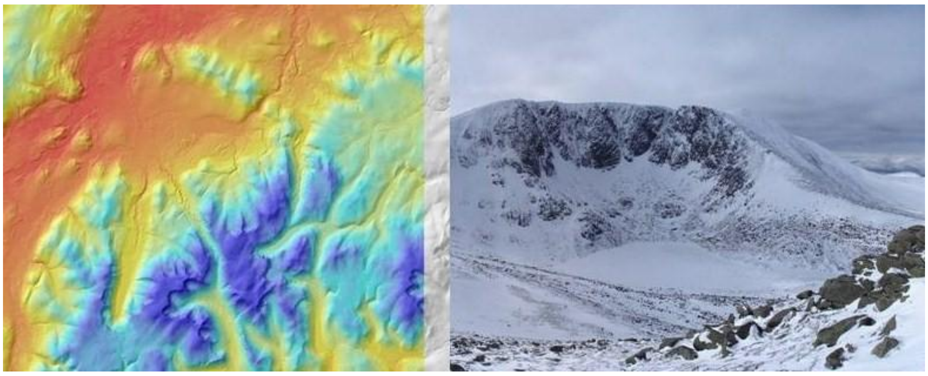

Figure 2. Cairngorm National Park and sample data

4. Results and Discussion

Results from the Cairngorm show that it is possible to classify landscapes by visible geomorphometric features. While the example runs at 5 metre resolution are possible using a ‘scavenger’ network of separate machines running in parallel on sub-samples of terrain data to speed up run times, the 1300 fold speed increase over conventional viewshed tools means that analyses can be run in a matter of days rather than years, making this level of analysis a practical proposition. The sample data for the Cairngorm National Park shown in Figure 2 are used to derive and extract a suite of terrain indices including overall openness, altitude, slope, aspect, curvature and surface significant features. Cumulative visibility totals for each of these terrain indices are shown in Figure 3 and results for surface significant features are shown in Figure 4.

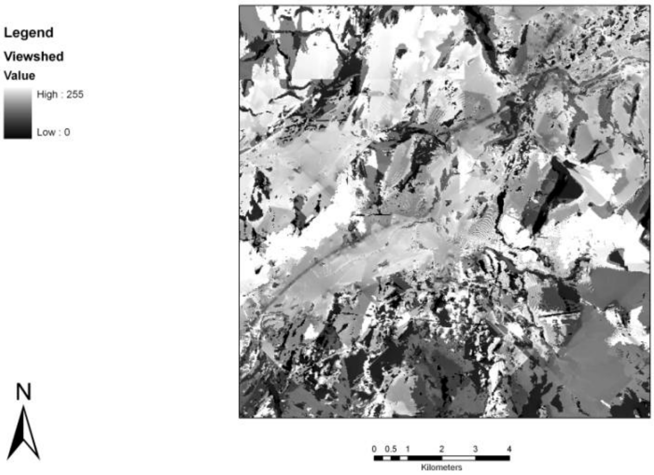

Figure 3. Openness

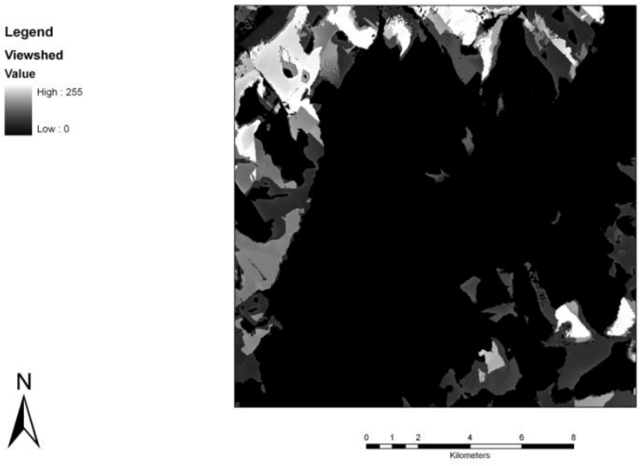

Figure 4. Surface significant features

This new algorithm can be used to generate detailed geomorphometric analyses across large, high resolution terrain models based on openness and what surface features are visible within the cumulative viewshed. This has a range of potential applications beyond geomorphometric studies including the calculation of openness for exposure modelling, radar and cellular communications, siting of viewshed critical facilities such as cell masts, observation towers and radar installations, evaluation of zones of visual influence (ZVIs) for obtrusive developments such as wind farms, landscape assessments based on a knowledge of what is visible from where, landscape planning and decision support, and comparative analysis of contrasting geomorphological regions.

References

Fisher, P., Wood, J. And Cheng, T. (2004) Where is Helvellyn? Fuzziness of multi-scale landscape morphometry. *Transactions of the Institute of British Geographers.*29: 106-127.

Germino, M.J., Reiners, W.A., Blasko, B.J., McLeod, D. and Bastian, C.T. (2001) Estimating visual properties of Rocky Mountain landscapes using GIS. *Landscape and Urban Planning*. 53(1-4): 71-83.

Huanping, W., Mao, P., Lingqing, Y. and Bing, L. (2007) A partition-based serial algorithm for generating viewshed on massive DEMs. *International Journal of Geographical Information Science*, 21(9): 955-964 .

Izraelevitz, D. 2003. A fast algorithm for approximate viewshed computation: *Photogrammetic Engineering & Remote Sensing*.69: 767-774.

Kidner, D.B., Rallings, P.J. and Ware, A. (1997) Parallel processing for terrain analysis in GIS: visibility as a case study. *GeoInformatica,* 1(2): 183-207.

Rana, S. and Sharma, J. (2006) *Frontiers of Geographic Information Technology*. Springer.

Ware, J.A., Kidner, D.B. and Rallings, P. (1996) Parallel Algorithms for Determining the Visibility Index of Digital Elevation Models. *Proc 2nd Joint European Conference and Exhibition on Geographical Information*, Barcelona, 127-136.

Ware, J.A., Kidner, D.B. and Rallings, P. (1998) Parallel distributed viewshed analysis. *Proc 6th ACM International Symposium on Advances in Geographic Information Systems*, Washington, D.C., 151-156.

Wilson, J., Lindsey, G. and Liu, G. (2008) Viewshed characteristics of urban pedestrian trails, Indianapolis, Indiana, USA. *Journal of Maps*: 108-118.

Wood J 2002b Visualizing the structure and scale dependency of landscapes. in Fisher P and Unwin D eds *Virtual reality in geography.* Taylor & Francis, London 163–74.

Correlation of Radial Profiles Extracted from Automatic Detected Circular Features, in the Search for Impact Structure Candidates

S. O. Krøgli[1], H. Dypvik[1], B. Etzelmüller[1]

[1]Department of Geosciences, University of Oslo
P. O. Box 1047, NO-0316 Oslo, Norway
Telephone: 0047 22856656
Fax: 0047 22854215
E-mail: sveinkro@geo.uio.no, henning.dypvik@geo.uio.no, bernd.etzelmuller@geo.uio.no

1. Introduction

Impact cratering is a common geological process in the Solar System and most planetary bodies display geomorphologies strongly influenced by impacts (Lowman 1997). Fresh impact craters are normally characterized by a circular morphology (Melosh 1989). This surface expression is modified on Earth by active geological processes. The variation of terrestrial impact structure expressions suggests a simple characteristic to use in automatic detection, usually the circular shape. Automatic techniques may detect candidates in regional data, but field and laboratory analysis are required to possibly confirm an impact origin by finding shock metamorphic effects or traces of meteorites (Koeberl 2004).

A first approach to detect candidates was conducted comparing typical impact crater morphologies and topography (Krøgli et al. 2007). Size-dependency scaling characteristics, e.g. relations of crater diameter, crater floor diameter and crater depth, have been established for heavily cratered areas like the Moon (Pike 1977). On Earth the catalog presently consists of 176 proven impact structures (Earth Impact Database 2009). Despite the low number, size-dependencies have also been established for terrestrial impact structures (e.g. Grieve and Pesonen 1992). To search crater-like circular depressions Krøgli et al. (2007) calculated correlations between circular templates, based on terrestrial and lunar size relations, and digital elevation models.

The geophysical properties of impacted target areas may also change during impact and can be found as anomalies in e.g. gravity and magnetic potential field data. Fracturing and brecciation of target rocks and the presence of low-density sedimentary infill cause a circular gravity low, while a central uplift of heavier rocks from deeper crustal levels may cause a circular gravity high (e.g. Grieve and Pilkington 1996). There has not been found a one to one relationship between shapes of magnetic anomalies and impact structures, but circularity may often be present (French 1998). An algorithm that detects circular orientations of slope values has been constructed to search impact structure candidates, treating regional gravity and aeromagnetic data as surface models. The algorithm, that also works on DEMs, examines only the outline of possible circular features.

Both methods (template matching and circular oriented slope values) detected features with different degrees of circularity. The number of detected features depends on the choice of threshold, but is usually large and requires further manual or automatic analysis to refine the number before field investigations. Results can be compared to maps of e.g. geology and drainage patterns and to additional methods and data (e.g. multispectral images). An approach to reduce the number of candidates is presented here as a filter technique, removing candidates from symmetry measurements.

2. Symmetry in Circular Features

The symmetry measurements are based on correlation coefficients between radial profiles in automatic detected circular features. For each circular feature the algorithm extracts eight profiles from the DEM or geophysical surface, radiating from centre to the length of the radius. These profiles are placed in a matrix consisting of a number of columns equal to the number of profiles (default eight) and a number of rows equal to the number of pixels in profiles (depending on radius). First only a part of the matrix, the first three pixels of each profile, is included in the correlation coefficient calculations. When counting pixels the first pixel of a profile is on the circular outline and the next pixel one step towards centre, and so on. A profile is marked if it does not correlate with any of the other profiles. The matrix then includes the pixels on the next step towards centre. Again a correlation coefficient calculation between profiles is performed, this time without marked profiles. This continues until all profiles are marked (no more correlation) or the end of profiles is reached (Fig. 1). Two profiles may then go the whole distance to the centre, even if situated at opposite sides. The percentage of pixels included in correlated profiles compared to total number of pixels in profiles is saved.

3. Results and Discussion

Fig. 2 displays the effect of symmetry filtering on automatic detected circular features. The reasoning behind equalizing two features having similar total profile distances is to keep features that have few but long correlation profiles, e.g. in just a corner or half of the circle. They may represent impact structures where only parts of the earlier circularity is present. Opposite, one could include a weight in order to reward if all the eight profiles are correlated a distance. The latter may exclude valleys, where two opposite ridges may have some of the characteristics of a partly circular feature. In the presented algorithm the profiles are extended from the rim an inwards, calculating correlation coefficients for each step, leaving out non-correlating profiles. This emphasizes the rim area and downgrades the middle area, which may be promising in an impact structure candidate detection. Initiating the calculations with a minor number of pixels could miss out profiles that would correlate at a later stage, if more pixels had been included. A future filter value might be calculated incorporating correlation results of profiles starting both from the outline and from the centre, or even including complete profiles. The choice of eight profiles, always with the same profile configuration, influence results. It is the profile shapes that are correlated, indicating that the profiles might be located at different elevations. Fig. 2 displays that the filter reduce the number of automatic detected impact structure candidate sites based on non-symmetrical characteristics.

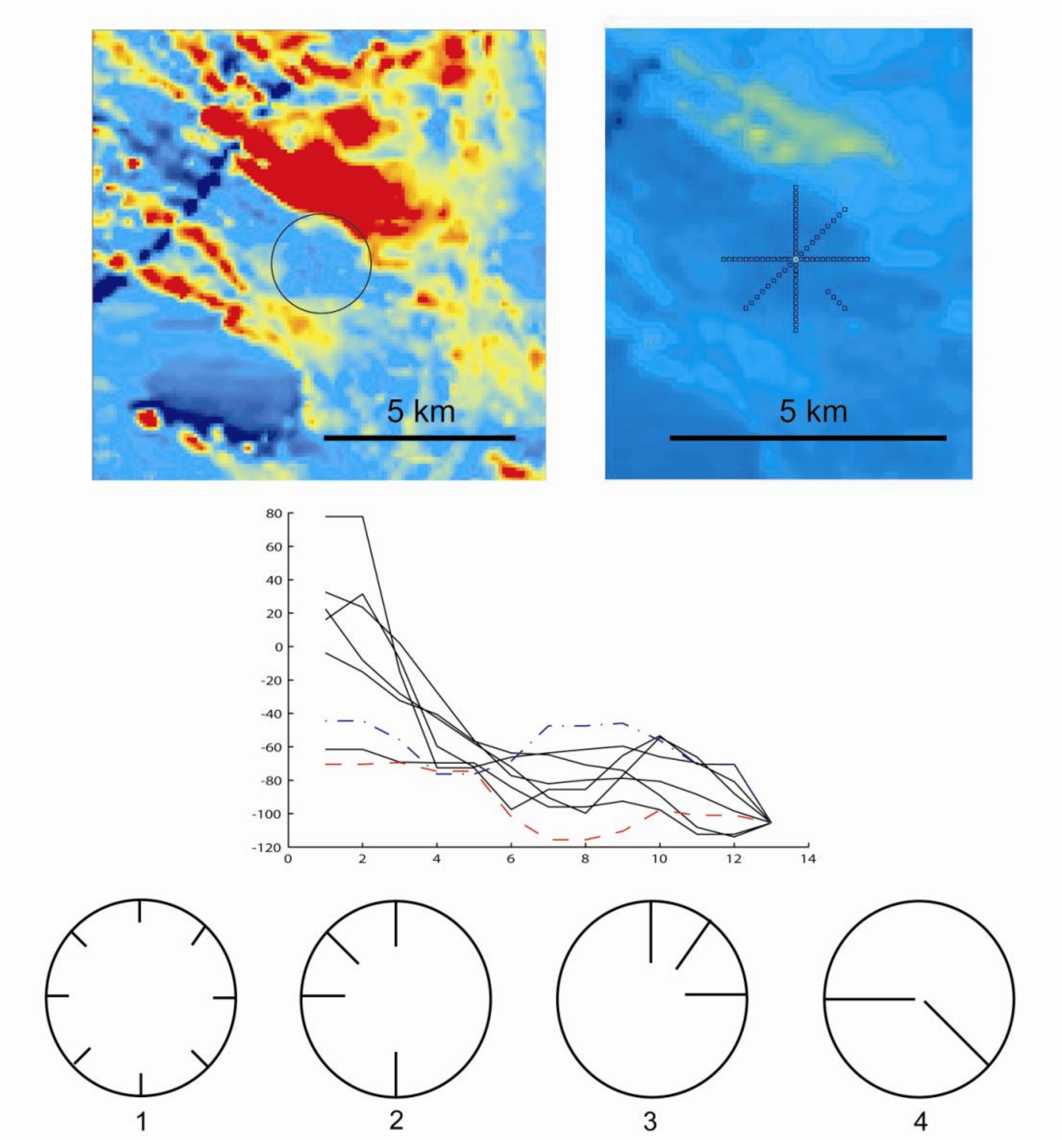

Figure 1. (Above left) Automatic detected circular feature in aeromagnetic potential field data (100 m spatial resolution, Finnmark, northern Norway). (Above right) Length of profile correlations for feature on left image. Correlation threshold 80%. Six profiles correlate the whole distance. The north-west profile does not correlate with any other. There is a gap in the circular border at that place. The south-east profile stops correlating after a while. (Middle) The eight profiles. The dashed (red) profile is the one not correlating with the others, while the dash-dotted (blue) profile stopped correlating at step 5. The y-axis is exaggerated. (Below) Four circles that display equal total profile correlation distances. If a few profiles correlate a longer distance, e.g. in a quarter of the circle (#3), it will get the same value as if all profiles correlate a smaller distance (#1). Fig. 1 is marked in Fig. 2d.

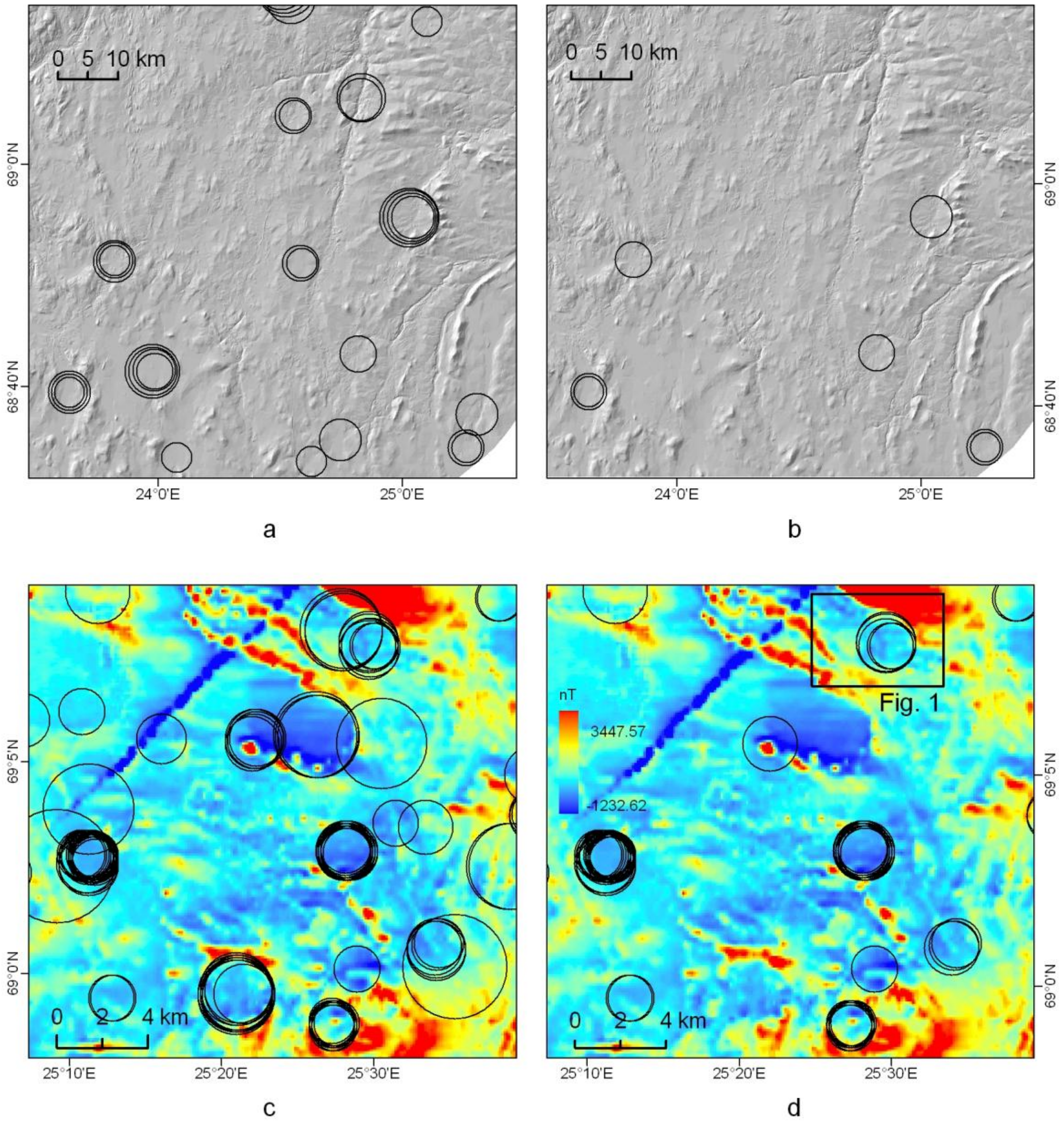

Figure 2. Figures (b) and (d) display features with a symmetry value higher than 75%, and are the filtered results of the automatic detected circular features in (a) and (c). The circular features are found by the methods of template matching on a DEM (a) and the circular outline algorithm on aeromagnetic data (c). (a) and (c) display two different areas of Finnmark, northern Norway. Both models have a spatial resolution of 100 m. The location of Fig. 1 is shown in (d).

Acknowledgements

Geophysical data were kindly provided by the Geological Survey of Norway (NGU). The project is supported by the Research Council of Norway (#170617). The comments of the Geomorphometry 2009 referees' and Programme Committee are highly appreciated.

References

Earth Impact Database. 2009: http://www.unb.ca/passc/ImpactDatabase (Accessed: 3 Mar 2009)

French BM, 1998, *Traces of Catastrophe: A Handbook of Shock-Metamorphic Effects in Terrestrial Meteorite Impact Structures*. Lunar and Planetary Institute, Houston, 120 pp.

Grieve RAF and Pesonen LJ, 1992, The terrestrial impact cratering record. *Tectonophysics* 216, 1-30.

Grieve RAF and Pilkington M, 1996, The signature of terrestrial impacts. *AGSO Journal of Australian Geology & Geophysics* 16, 399-420.

Koeberl C, 2004, Remote sensing studies of impact craters: How to be sure? *C. R. Geoscience* 336, 959-961.

Krøgli SO, Dypvik H and Etzelmüller B, 2007, Automatic detection of circular depressions in digital elevation data in the search for potential Norwegian impact structures. *Norwegian Journal of Geology* 87, 157-166.

Lowman PD, Jr., 1997, Extraterrestrial impact craters. *Oklahoma Geological Survey Circular* 100, 55-81.

Melosh HJ, 1989, *Impact Cratering: A Geologic Process*. Oxford University Press, New York, 240 pp.

Pike RJ, 1977, Size-dependence in the shape of fresh impact craters on the moon, In: Roddy DJ, Pepin RO and Merrill RB (eds.) *Impact and Explosion Cratering*, Pergamon Press, New York, pp. 489-509.

Structuring the Digital Elevation Model into Landform Elements through Watershed Segmentation of Curvature

B. Romstad[1], B. Etzelmüller[2]

[1]Department of Geosciences, University of Oslo, PO Box 1047 Blindern, 0316 OSLO, Norway
and
International Centre for Geohazards (ICG), PO Box 3930 Ullevaal Stadion, 0806 OSLO, Norway
and
CICERO Center for Climate and Environmental Research, PO Box 1129 Blindern, 0318 OSLO, Norway
Telephone: +47 2285 8530
Fax: +47 2285 8751
Email: bard.romstad@cicero.uio.no

[2] Department of Geosciences, University of Oslo, PO Box 1047 Blindern, 0316 OSLO, Norway
Telephone: +47 2285 7229
Fax: +47 2285 4215
Email: bernd.etzelmuller@geo.uio.no

1. Introduction

The spatial prediction of landforms and surface processes is an important component in the understanding and modelling of an environmental system. Therefore a fundamental research topic within geomorphometry is to extract and classify landform elements and landform types. The general topic is thoroughly introduced and reviewed in the recent chapter by MacMillan and Shary (2008) and the paper by Minár and Evans (2008), but in this paper the focus is on the matter of automatic extraction of landform elements.

Landform elements are segments characterized by simple geometry and can be viewed upon as the basic building blocks for landforms, landform types and landform systems. While many applications (implicitly or explicitly) define the grid cell itself as the basic landform element, several studies have pointed out the weaknesses of this approach (e.g. Rowbotham and Dudycha 1998, Blaschke and Strobl 2001, Romstad 2001, Dragut and Blaschke 2006). If a landform element instead can be defined by a group of connected cells, we have effectively made the transition from a field based to an object based representation of the terrain. This is a powerful approach as it allows for the calculation of contextual information such as the shape and size of regions. Important contributions on how to construct geomorphologically significant landform elements in this way include those of Friedrich (1996), MacMillan et al. (2004), Dragut and Blaschke (2006) and Strobl (2008).

The by far most common method for this type of terrain segmentation is to delineate local catchments by use of flow modelling. This type of segmentation has the favourable property that the method for delineation of regions is based on an explicitly defined physical process (hydrological flow). Thus the resulting regions represent meaningful real world objects by definition. A weakness is that this method does not ensure the geometric simplicity of the resulting elements and significant changes in slope gradient may have to be treated separately. Dragut and Blaschke (2006) delineated homogenous landform objects by applying the image segmentation algorithm described by Baatz and Schäpe (2000) to a set of topographic attributes. This algorithm convincingly created landform elements that were both geometrically simple and geomorphologically meaningful, but the algorithm is complex and relies on a number of parameters. Thus it may be difficult to predict how the algorithm will behave when applied to the same topographic attributes in different areas.

In this paper we explore whether a simple watershed segmentation of curvature maps will produce meaningful landform units. We explain how this segmentation procedure creates elements that are geometrically simple and we evaluate the method by comparing the resulting regions to a geomorphological map.

2. Method

The general concept of the method is to calculate the mean curvature from a DEM and then create a set of landform elements by applying a watershed segmentation to the curvature image. These landform elements are formed around depressions in curvature and are thus referred to as *concave elements*. A second set of landform elements is then created through a watershed segmentation of the inverse curvature image. As this will result in elements that are formed around curvature peaks we refer to them as *convex elements*. Below follows a more detailed description of each step in the method.

We used a DEM with 20m spatial resolution covering an area of 20×20 km. Before calculating the curvature the DEM was smoothed twice with a 5*5 average filter. This was done in order to reduce the effect of noise and small scale variation in the DEM. Then the *mean curvature* was then calculated for each cell with the method described by Young (Young 1978) and Evans (Evans 1979). The curvature values were expressed in units per 100m and the standard deviation of curvature values in the whole study area was about 0.11. The inverse curvature image was calculated by simply multiplying curvature with -1.

Especially in areas where the curvature is near zero there may be minor fluctuations in curvature values that represent insignificant changes of the surface geometry. This will lead to an over-segmentation of the terrain. In order to resolve this, shallow minima should be suppressed (filled) prior to segmentation. Defining what the minimum watershed depth should be will be dependent of the quality and the resolution of data and also the scale of the analysis. In our study we defined the minimum watershed depth as 10% of the standard deviation of curvature values in the dataset (a depth of about 0.01 $100m^{-1}$) and consequently curvature fluctuations below this magnitude were ignored.

Having suppressed shallow minima in both curvature images the watershed segmentation was applied. We used an algorithm that builds regions around each local minimum by simulating a gradual “flooding” of the image and watershed boundaries are formed where the “water spills over” between two neighbouring basins (Vincent and Soille 1991). The concave elements, which are the regions resulting from the curvature image, represent a cycle of curvature values with the highest values around the edge and the lowest values in its interior. As illustrated in Fig. 1 the shape of the element itself may not necessarily be concave, it could also be a planar slope or a plain that is convex near its boundary. We refer to this as a *false concavity*. Fig. 2 illustrates that the same situations occur for the regions resulting from the inverted curvature image. The convex elements may be truly convex features, or they can be *false convexities*; planar elements that are concave near their boundary.

All calculations were performed with Matlab version 7.6 using the Image Processing Toolbox.

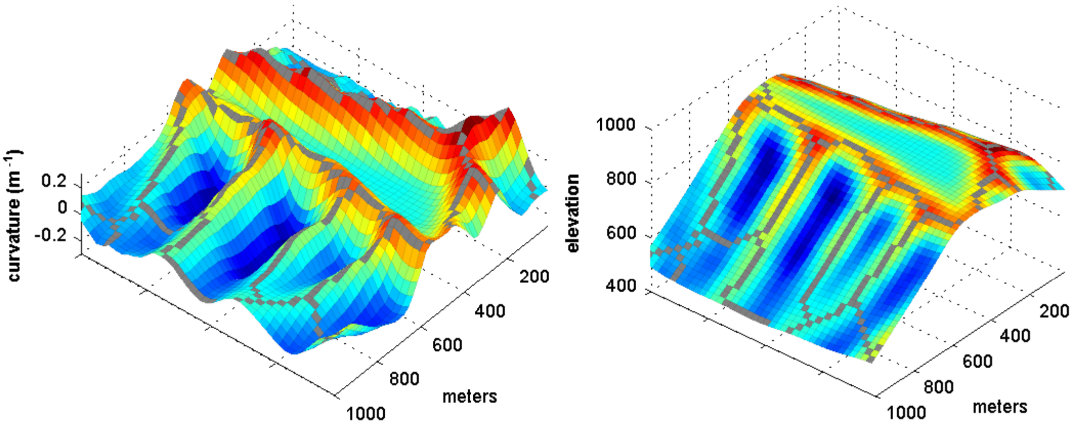

Fig. 1. Illustration of watershed segmentation of curvature (left) and the resulting concave elements draped over the original terrain surface (right).

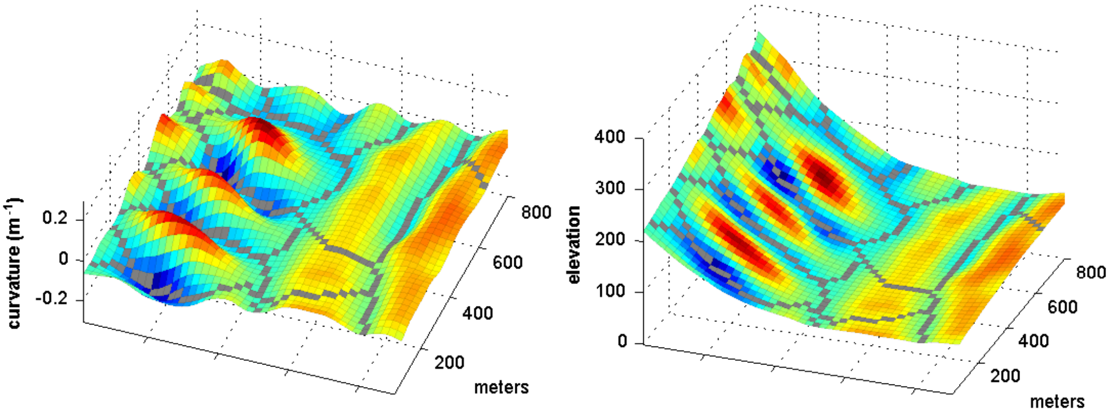

Fig. 2. Illustration of watershed segmentation of *negative* curvature (left) and the resulting convex elements draped over the original terrain surface (right).

3. Results and Discussion

The study area was located in Adventdalen, at 15.8°E and 78.2°N on Spitsbergen island in the Barents sea. This area is characterized by horizontal or slightly dipping Mesozoic sedimentary sediments, incised by both fluvial and glacial valleys with steep slopes. Permafrost is continuous and local glacierisation dominates at present. The area comprises an ensemble of glacial and periglacial landforms and sediments, dominated by gravitational processes along the slopes (talus, debris flows) and sorting processes (patterned ground) on valley bottoms and higher plateaus. To illustrate the potential of the method the regions resulting from the segmentation procedure were evaluated by qualitatively comparing their outline to different landforms and surface material types in a geomorphological map of the area published by The Norwegian Polar Institute (Tolgensbakk et al. 2000).

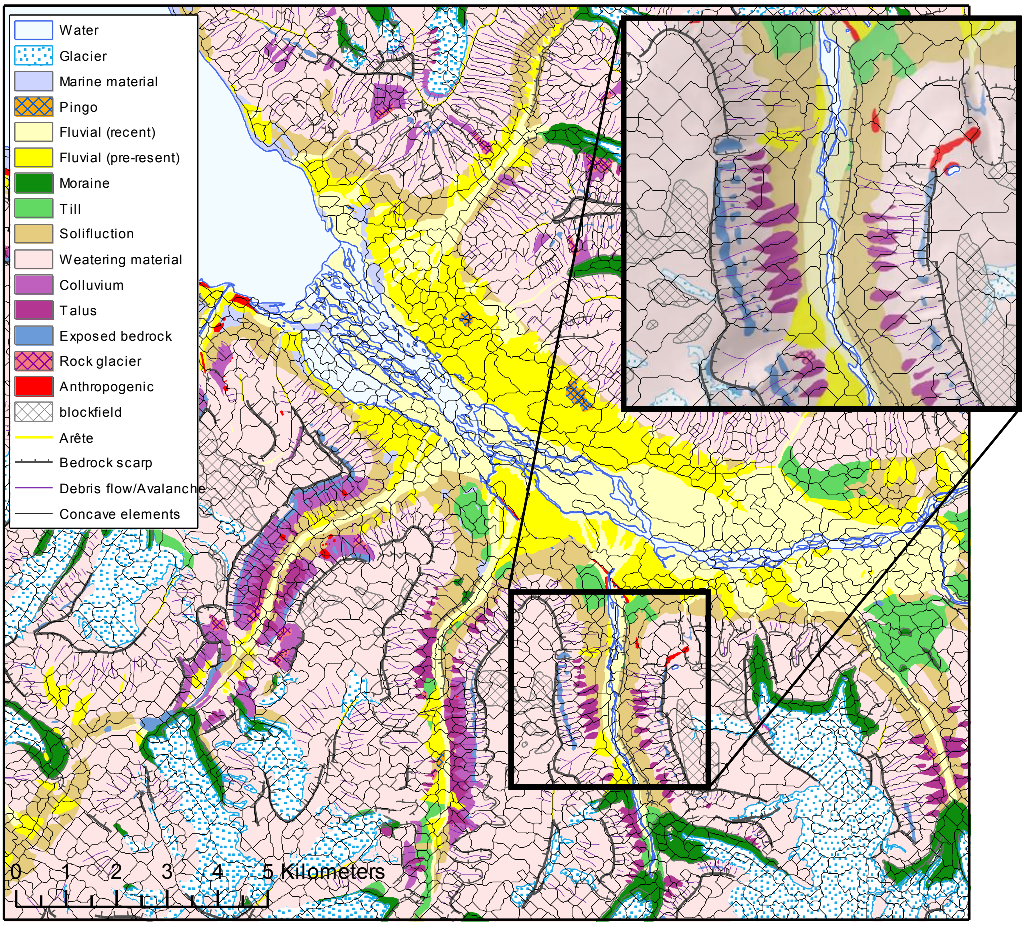

Fig. 3. Geomorphological map over the study area overlaid with concave elements. Detail from one of the valleys inset.

In Fig. 3 concave elements are shown overlaid on the geomorphological map. We observe that individual elements clearly define ravine-like features above talus and alluvial fans. Individual elements also include some larger canyons and to some extent well developed cirques are outlined by individual concave elements. All these are landforms that are typically formed by erosion and net material loss and they have a truly concave geometry. The elements can also be assumed to serve as source areas for material that is removed through mass wasting, fluvial or glacial action. The boundaries of concave elements coincide with bedrock scarps and mountain crests. For this reason isolated plateaus or mesas are well represented by concave elements. These false concavities are successfully delineated by the watershed segmentation algorithm because the convex shoulders (scarps) act as a dam around the non-curved plateau areas.

Convex elements are shown in Fig. 4. Pingos, talus, rock glaciers and some of the steeper alluvial fans are in very good agreement with individual elements. This is expected as these are landforms with a relatively simple geometry and they also have a truly convex shape. The latter is also true for mountain edges and moraines, but we observe that these landforms are split up into several elements due to undulations along the length direction. The boundary of each moraine is more or less continuously overlapped by a region boundary.

Elements in the areas described with broader surface material types (fluvial, till, solifluction, weathering material) are typically false convexities formed around planar surfaces bordered by footslopes. The footslopes define the transition from one process domain to another and thus the boundaries of the elements coincide with the boundaries in the geomorphological map.

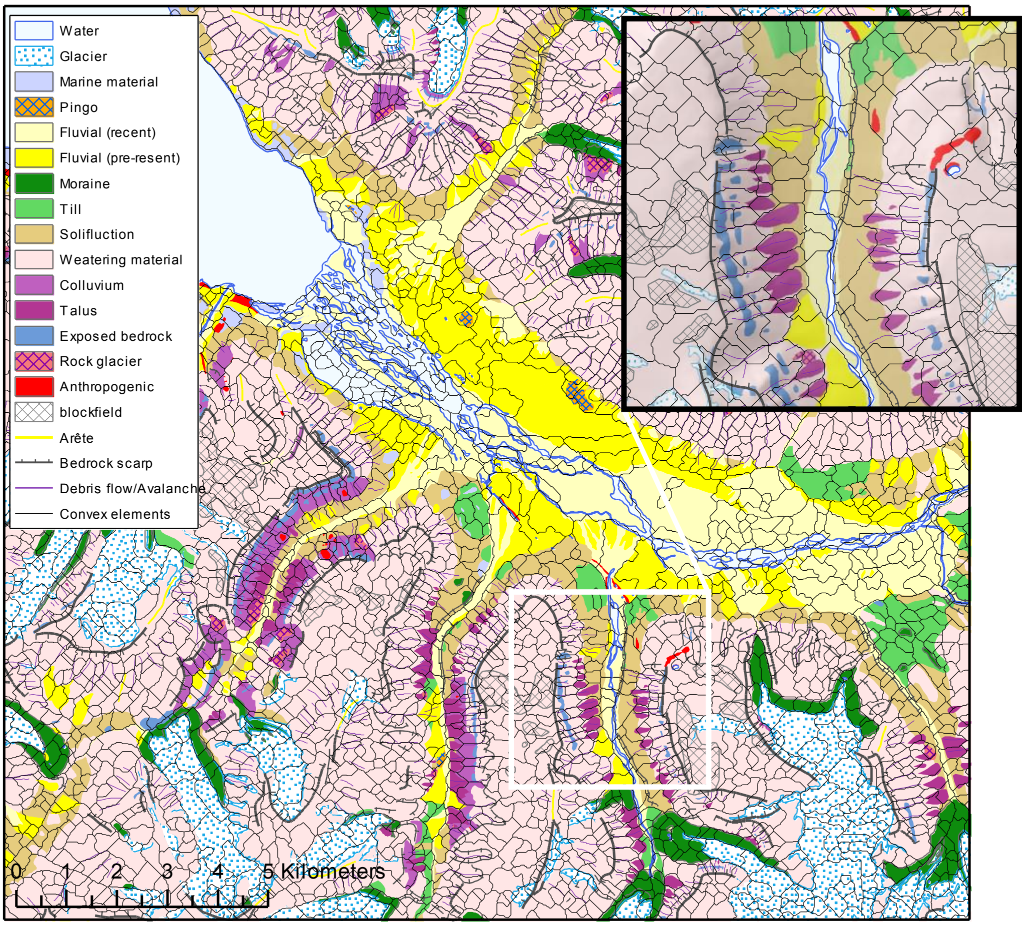

Fig. 4. Geomorphological map over the study area overlaid with convex elements. Detail from one of the valleys inset.

In general boundaries between different landforms or surface material types are respected by either the concave or the convex elements. This implies that uniform geomorphological processes can be assumed within sub elements resulting from the combination of the two sets. Each of these sub elements may be described by a combination of its own properties (geometry, shape, size...) and the properties of the concave and convex elements to which it belongs. As uniform surface processes can be assumed within each element they are suitable as spatial units in earth system modelling and analysis, e.g. in spatial modelling of slope stability, erosion processes or ground thermal regimes and freeze/thaw depth estimations.

4. Conclusions

We have presented a terrain segmentation method that is conceptually simple and makes use of computationally efficient algorithms that are implemented in most GIS. By its nature the method produces landform elements with a geometric simplicity. The elements are either characterised as curved slopes or as planar slopes or plains bordered by footslopes or shoulders. The analysis showed that the elements correspond well with the landforms and surface types represented in the geomorphological map.

Much the same way an ordinary watershed segmentation of the digital elevation model can be used to define hydrological response units a watershed segmentation of curvature may be a powerful and efficient way to define geomorphological process units. Terrain segmentation using this method is therefore expected to be meaningful for a number of applications and the method may be particularly suitable when the geomorphic objects of interest are characterized by a cyclic variation in topographical attribute.

References

Blaschke, T. and J. Strobl (2001). What's wrong with pixels? Some recent developments interfacing remote sensing and GIS. *GIS Zeitschrift für Geoinformationssysteme* 6: 12-17.

Baatz, M. and A. Schäpe (2000). Multiresolution segmentation - an optimization approach for high quality multi-scale image segmentation. In: J. Strobl, T. Blaschke and G. Griesebner, *Angewandte Geographische Informationsverarbeitung XII. Beitäge zum AGIT-symposium Salzburg 2000*, Karlsruhe, Herbert Wichmann Verlag, 12-23.

Dragut, L. and T. Blaschke (2006). Automated classification of landform elements using object-based image analysis. *Geomorphology* 81(3-4): 330-344.

Evans, I. S. (1979). An integrated system of terrain analysis and slope mapping. Final Report (Report 6) on Grant DA-ERO-591-73-G0040, 'Statistical characterization of altitude matrices by computer', Department of Geography, University of Durham, England**:** 192.

Friedrich, K. (1996). Multivariate distance methods for geomorphographic relief classification. *Proceedings EU Workshop on Land Information Systems: Developments for planning the sustainable use of land resources*, Hannover, European Soil Bureau.

MacMillan, R. A., R. K. Jones, et al. (2004). Defining a hierarchy of spatial entities for environmental analysis and modeling using digital elevation models (DEMs). *Computers, Environment and Urban Systems* 28(3): 175-200.

MacMillan, R. A. and P. A. Shary (2008). Landforms and Landform Elements in Geomorphometry. In: T. Hengl and H. I. Reuter, *Geomorphometry: Geomorphometry: Concepts, Software, Applications*, Developments in Soil Science, vol. 33, Elsevier, 227-254.

Minar, J. and I. S. Evans (2008). Elementary forms for land surface segmentation: The theoretical basis of terrain analysis and geomorphological mapping. *Geomorphology* 95(3-4): 236-259.

Romstad, B. (2001). Improving relief classification with contextual merging. *ScanGIS'2001. Proceedings of the 8th Scandinavian Research Conference on Geographical Information Science*, Ås, Norway.

Rowbotham, D. N. and D. Dudycha (1998). GIS modelling of slope stability in Phewa Tal watershed, Nepal. *Geomorphology* 26(1-3): 151-170.

Strobl, J. (2008). Segmentation-based Terrain Classification. In: Q. Zhou, B. Lees and G. A. Tang, *Advances in Digital Terrain Analysis, Series Lecture Notes in Geoinformation and Cartography*, New York, Springer, 125-139.

Tolgensbakk, J., L. Sørbel, et al. (2000). Adventdalen, Geomorphological and Quatenary Geological map, Svalbard 1:100 000, Spitsbergen Sheet C9Q, Norwegian Polar Institute.

Vincent, L. and P. Soille (1991). Watersheds in Digital Spaces - an Efficient Algorithm Based on Immersion Simulations. *IEEE Transactions on Pattern Analysis and Machine Intelligence* 13(6): 583-598.

Young, M. (1978). Terrain analysis: program documentation. Report 5 on Grant DA-ERO-591-73-G0040, 'Statistical characterization of altitude matrices by computer', Department of Geography, University of Durham, England**:** 27.

Multi-Scale and Object-Oriented Image Analysis of High-Res LiDAR Data for Geomorphological Mapping in Alpine Mountains

N. S. Anders, A. C. Seijmonsbergen, W. Bouten

Institute for Biodiversity and Ecosystem Dynamics, Computational Geo-Ecology, Universiteit van Amsterdam,
Nieuwe Achtergracht 166, 1018 WV Amsterdam, The Netherlands
Telephone: +31 (0) 20 525 7436
Fax: +31 (0) 20 525 7431
Email: n.s.anders@uva.nl

1. Introduction

Geomorphological maps are useful to a wide variety of applications, such as hazard risk analysis (Seijmonsbergen 1992), forest ecological research (Van Noord 1996) and geoconservation evaluation studies (Seijmonsbergen et al. in press). Traditional field-based geomorphological mapping strategies are often time consuming and the accuracy of these methods is questionable in steep and difficult-to-access terrain.

Topographic analysis of remotely sensed digital elevation data is a potential tool to speed up and increase accuracy of the mapping procedure. Recent studies argue that image segmentation and object-oriented classification strategies are intuitive to (semi-) automatically produce a classified hillslope or geomorphological map (Drăguţ and Blaschke 2006; Van Asselen and Seijmonsbergen 2006) based on Digital Elevation Models (DEMs) and their derivatives. However, an accurate identification and classification of individual landforms and their genesis remains a challenge, partly due to the multi-scale nature of geomorphological processes.

This research-in-progress is part of a PhD project for developing a method to classify image objects on their geomorphological nature in a multi-scale framework, based on geomorphometric parameters derived from high-resolution LiDAR (Light Detection And Ranging) data. In future research, we will integrate this detailed LiDAR-derived geomorphological information in a dynamic simulation model to facilitate landscape evolution research in complex and difficult-to-access terrain at greater detail than before.

2. Materials and Methods

Our approach is being developed and tested at several locations in the Alpine mountains of Vorarlberg (W-Austria). In this paper, we study the Gamp valley catchment (approximately 10km^2), which is characterised by a large variety of geomorphological processes and related landforms (e.g. gypsum karst, basin fill of glacially shaped valleys and steep fluvial incision of bedrock rivers). Available data of this area include a LiDAR Digital Terrain Model with 1 m spatial resolution and digital geomorphological maps in a GIS, which are digitised and hierarchically categorised from 1:10,000 field-based geomorphological maps (Seijmonsbergen 1992) and are used as ground truth reference data.

Our method is focused on extracting geomorphological information from remotely sensed LiDAR data, or more specifically, (semi-) automatically mapping geomorphological features based on their genesis. Seijmonsbergen et al. (in press) have developed a hierarchical classification scheme to apply to polygon-based geomorphological maps in a GIS. In this scheme, landforms are first distinguished on their forming process, such as fluvial or glacial processes, karst, mass movement, etc. In a second step, these classes are further separated based on erosion or accumulation processes before the final (genesis of the) landform (such as alluvial fans, karst collapse holes, fluvial incision, etc.) is determined.

In this research a comparable method will be used. Firstly, image objects are created at multiple scales, using multi-resolution image segmentation (Baatz and Schäpe 2000) of high-resolution LiDAR data, which is based on getting maximum internal homogeneity of parameter values within image objects at a user-defined scale. Secondly, image objects are classified using a rule-based hierarchical classification approach to categorise image objects on their geomorphological nature. Input arguments on which classification rules are based use DEM derivatives, such as slope gradient and curvature. In addition, topographic openness is a relatively unknown, yet promising parameter for further implementation in multi-scale image classification schemes. Openness can be defined as the degree of enclosure of a location in the landscape and is an angular measure of surface relief and horizontal distance (Yokoyama et al. 2002; Prima et al. 2006). The distance over which openness is measured is variable (Fig. 1): measurements over longer distances clearly show patterns for recognising individual landforms and processes, such as gypsum-karst collapse holes (small black spots), alluvial fan development (bright triangular shapes) and fluvial incision (dark, long and narrow shapes) at a broad scale (A), while openness measured over short distances show detailed variation at a fine scale (B and C), representing local differences of curvature (C). The multi-scale nature of topographic openness encourages a multi-scale expert rule setup for image segmentation and classification, where both broad-scale and fine-scale openness values could be incorporated. For the full theoretical and mathematical background Yokoyama et al. (2002) are referred. Fig. 2 illustrates the workflow of our approach.

2.1 Multi-Scale Image Segmentation Using Geomorphometrical Parameters

In this study, we automatically segment the image into objects of multiple scales using Definiens Developer software, based on multi-resolution segmentation using DEM-extracted slope and openness parameters. The software allows to create scale-specific image objects using a user-specified scale parameter. Broad scale image objects are derived using a set of slope, curvature and openness (measured over wide areas) parameters in combination with a large scale parameter for classifying broad-scale geomorphological features. More detail on the classification strategy is discussed in section 2.2. The broad-scale image objects will be further segmented into smaller objects using smaller scale parameters, in order to identify fine-scale geomorphological features. Such a hierarchical segmentation and classification structure facilitates the analysis of image object’s context, since small-scale objects uses classification results of broad-scale features, which in turn promotes a multi-scale analysis of image objects and geomorphological features.

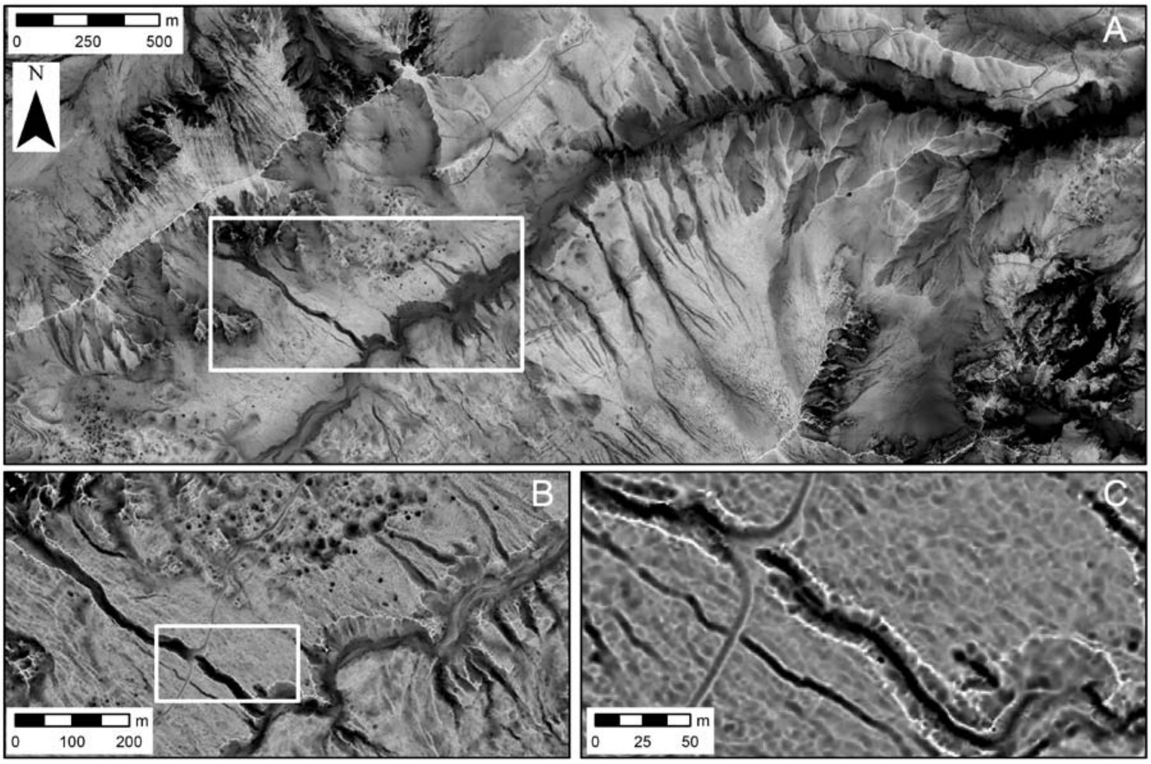

Figure 1: Topographic openness values of a subset of the Gamp valley. Bright hues represent open and wide areas, while dark hues represent enclosed, narrow areas. The values are calculated as a mean angle in eight directions, (a) measured over a diameter of 400 m; (b) measured over a diameter of 40 m; and (c) measured over a diameter of 10 m. The white boxes in (a) and (b) illustrate the locations of (b) and (c), respectively.

2.2 Rule-Based and Expert-Driven Object Classification

Each set of image objects are classified using slope, curvature and topographic openness (measured over various distances) parameters. Additional parameters are used to classify specific geomorphological features, such as flow accumulation values for identifying landforms related to fluvial processes. Internal statistics of surface parameters, relations with objects at higher scale levels and spatial properties of objects related to neighbouring objects are hierarchically used for developing a final classification of landscape features. Expert-knowledge is essential in developing the fuzzy classification rule sets.

2.3 Accuracy Assessment

The reference dataset include 1 : 10 000 symbol-based geomorphological field maps that have been translated into GIS-based polygon maps. Classification results are exported to polygon maps and are compared with the reference dataset for estimating the classification accuracy. A field campaign is set up this summer to link automatically derived objects with field geomorphology.

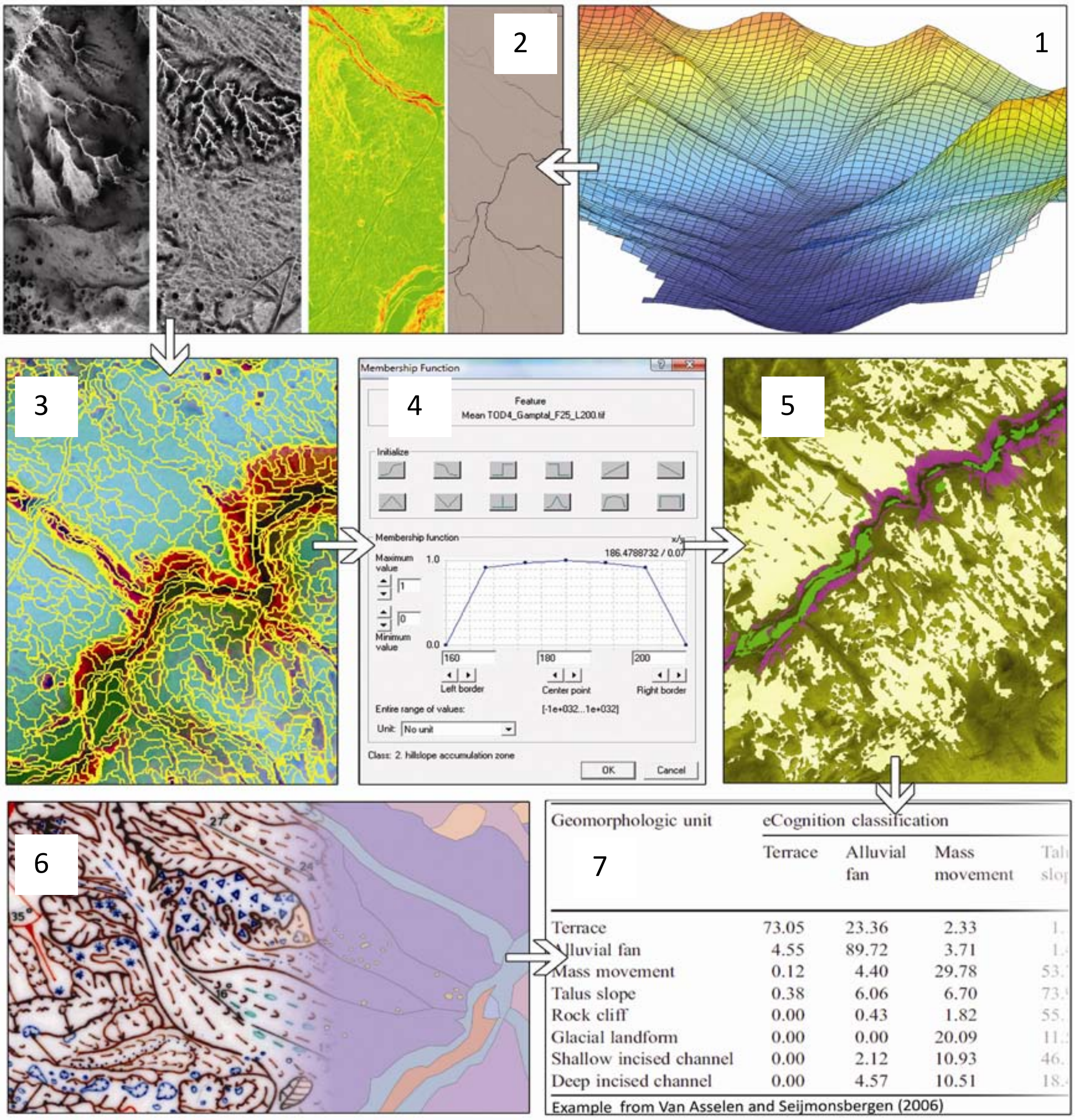

Membership Function

Feature
Mean TOD4_Gamptal_F25_L200.tif

Membership function
Maximum value 1.0
1
0
Minimum value 0.0
x/y
186.4788732 / 0.07
160
180
200
Left border
Center point
Right border
Entire range of values: [-1e+032...1e+032]
Unit: No unit
Class: 2. hillslope accumulation zone

Geomorphologic unit	eCognition classification			
	Terrace	Alluvial fan	Mass movement	Tal slo
Terrace	73.05	23.36	2.33	1.
Alluvial fan	4.55	89.72	3.71	1.
Mass movement	0.12	4.40	29.78	53.
Talus slope	0.38	6.06	6.70	73.
Rock cliff	0.00	0.43	1.82	55.
Glacial landform	0.00	0.00	20.09	11.
Shallow incised channel	0.00	2.12	10.93	46.
Deep incised channel	0.00	4.57	10.51	18.

Example from Van Asselen and Seijmonsbergen (2006)

Figure 2: Schematic overview of the methods. High-res LiDAR data (1) is used to derive various sets of geomorphometrical parameters (2) to create image objects at multiple scales (3). Internal statistics, higher level object information, spatial properties regarding neighbouring objects and expert knowledge are used create fuzzy rules (4) for mapping geomorphological features. Final classification results (5) are compared with field-based geomorphological maps (6) for estimating classification accuracy (7).

3. Results

At the time of writing this extended abstract, the research is still in progress. It is expected that a multi-scale framework of both the image segmentation and classification process will significantly increase classification results or mapping accuracy, especially if the topographic openness parameter is incorporated. First experiments of extracting gypsum karst collapse holes and fluvial landforms are promising. Image object boundaries can follow openness patterns that are measured over long distances (400 m), while internal textures of fine-scale (10 m) openness values within image objects can be incorporated—in combination with other relevant DEM-derivatives and object-oriented properties—for classifying image objects in subsequent rules following a hierarchical classification structure.

4. Future Research

Future research will integrate the automatically extracted geomorphological features with a dynamic simulation model (Anders et al. in press) to calculate alpine landscape evolution, in which channel incision is incorporated in high spatial detail. A vector-based channel incision model (CIM) calculates the longitudinal profile development of bedrock rivers at a fine spatial scale (1 m), based on a modified stream power formula, while taking into account the upstream area, channel gradient, channel disequilibrium and the geological strength against fluvial erosion. The CIM is combined with a raster-based reaction-diffusion erosion model (Minasny and McBratney, 2001) to incorporate hillslope development as a response to the fluvially incising network of river channels at a broad scale (50 m). The model is time efficient and realistically adapts to variable geological substrates, resulting in temporally and spatially variable incision values, knick-point regression and variable hillslope development. Automatically classified and detailed geomorphological information is necessary to serve as input data in the erosion model to improve results of simulated hillslope dynamics in complex terrain. Results from the landscape evolution model will be a step forward in using high-resolution data in dynamic geomorphological simulation models, to pave the way for more efficient landscape evolution research of difficult-to-access terrain and can contribute to increasing the understanding of the functioning of geo-ecological systems.

Acknowledgements

This research is supported by the Research Foundation for Alpine and Subalpine Environments (RFASE) and is carried out in the context of the Virtual Laboratory for e-Science project, which is supported by a BSIK grant from the Dutch Ministry of Education, Culture and Science (OC&W) and is part of the ICT innovation programme of the Ministry of Economic Affairs (EZ). The ‘Land Vorarlberg’ (http://www.vorarlberg.at/) has kindly allowed us to use the 1 m LiDAR DTM.

References

Anders NS, Seijmonsbergen AC and Bouten W, in press, Modelling channel incision and alpine hillslope development using laser altimetry data. *Geomorphology*.

Baatz M and Schäpe A, 2000, Multiresolution Segmentation–an optimization approach for high quality multi-scale image segmentation, In: Strobl J and Blaschke T (eds), *Angewandte Geographische Informationsverarbeitung*, Wichmann, Heidelberg.

Drăguţ L and Blaschke T, 2006, Automated classification of landform elements using object-based image analysis. *Geomorphology*, 81(3-4): 330-344.

Prima ODA, Echigo A, Yokoyama R and Yoshida T, 2006, Supervised landform classification of Northeast Honshu from DEM-derived thematic maps. *Geomorphology*, 78(3-4): 373-386.

Seijmonsbergen AC, 1992, Geomorphological evolution of an Alpine area and its application to geotechnical and natural hazard appraisal, PhD thesis, University of Amsterdam, 109 pp.

Seijmonsbergen AC, De Jong MGG and De Graaf LWS, in press, A method for the identification and assessment of significance of geomorphosites in Vorarlberg (Austria), supported by Geographical Information Systems. *Geografia Fisica e Dinamica Quaternaria*.

Van Asselen S and Seijmonsbergen AC, 2006, Expert-driven semi-automated geomorphological mapping for a mountainous area using a laser DTM. *Geomorphology*, 78(3-4): 309-320.

Van Noord H, 1996, The role of geomorphological information in ecological forest site typology in mountainous areas, a methodological study in the E-Rätikon and NW-Montafon mountains (Vorarlberg, Austria), PhD thesis, University of Amsterdam, Amsterdam: 185 pp.

Yokoyama R, Shirasawa M and Pike RJ, 2002, Visualizing topography by Openness: A new application of image processing to digital elevation models. *Photogrammetric Engineering and Remote Sensing*, 68(3): 257-265.

Use of Digital Terrain Analysis and Classification Trees for Predictive Mapping of Soil Organic Carbon in Southern Denmark

R. Bou Kheir[1], M. H. Greve[1], P. K. Bocher[1], M. B. Greve[1]

[1] Department of Agroecology and Environment, Faculty of Agricultural Sciences (DJF), Aarhus University, Blichers Allé 20,
P.O. Box 50, DK-8830 Tjele, Denmark
Email: Rania.BouKheir@agrsci.dk

1. Introduction

Soil organic carbon (SOC) is a dynamic component of the terrestrial system, with both internal changes in the vertical and horizontal directions and external changes with the atmosphere and the biosphere. Changes in SOC are attributed to both natural processes and human activities, and reflect the balance between decomposition of organic matter and input from roots and litter (Turner and Lambert 2000). In recent years, the importance of human activities has been widely recognized. Land use changes, including deforestation, biomass burning, draining of wetlands, ploughing, use of fertilisers and other agricultural practices, are regarded as the main factors causing loss of SOC and the emission of CO_2 into the atmosphere. These changes can be significant in grassland and cropland (Conant and Paustian 2002, Schuman et al. 2002) where intensive agricultural activities are carried out.

As part of international efforts to stabilize atmospheric greenhouse gas concentrations, Denmark is committed to establish inventories of the C stock in the frame of the Kyoto protocol. In this context, our study focuses on building a simple, realistic, practical and informative classification-tree model to predict the distribution of spatial patterns and changes in SOC across a study area in southern Denmark from mapped environmental variables.

2. Material and Methods

2.1 Site Description

The chosen study area, covering about 1812 km^2, is located in southern Denmark (Fig. 1). The climate is temperate with mean annual temperature ranging from 0 to 16°C, and a West-East gradient in precipitation oscillating between 900 and 600 mm/year (1961-1990). 95% of parent materials have glacial and fluvio-glacial origin. Approximately 65% of these materials were deposited during the last glacial period (between 10,000 and 100,000 years), and 20% during the previous glacial period (more than 110,000 years ago). However, the deposits from that period were all strongly redistributed by periglacial processes, and evidence of earlier soil formations is extremely rare. The area is representative of a broad region of landscapes in Denmark (i.e. weichsel moraine landscape, glacifluvial plains, saalian landscape, aeolian landscape, and post glacial marine deposits). The elevation varies from 0 m in the western part to 85 m in the eastern part. The area has been intensively cropped since the Middle Ages. Currently, 70% of the area is cultivated, 10% forested and the rest urbanized.

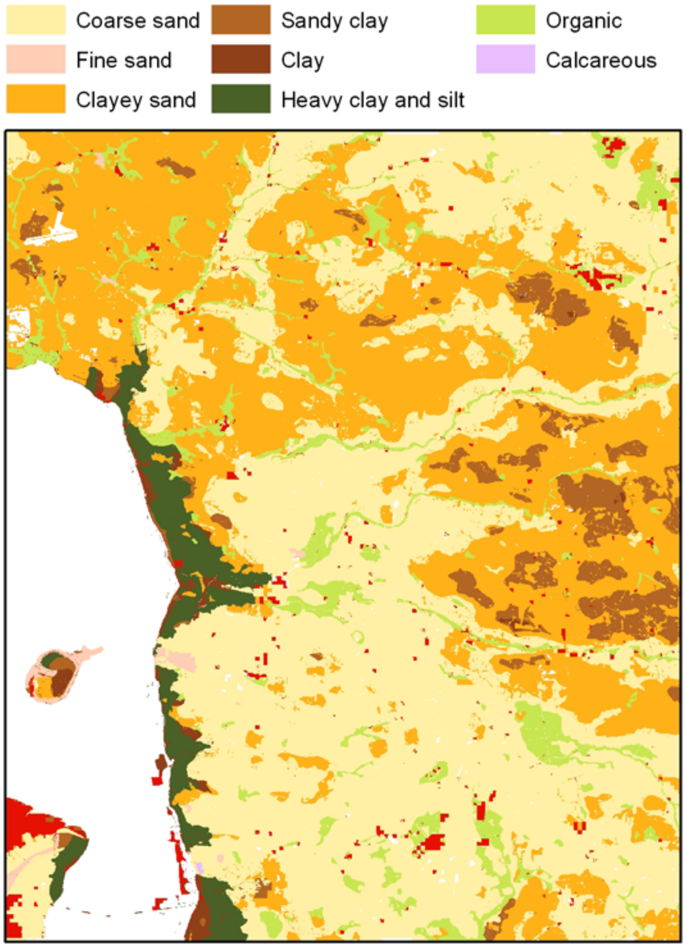

Figure 1. Soil map of the study area within Denmark (Madsen et al., 1992)

2.2 Soil Samples Collection

The soil was sampled at 1541 sites selected by four different surveys to be representative for the area. In order to avoid soil variability on a small scale, 25 bulk soil samples were taken within a radius of 50 m from a depth of 10-20 cm in the Danish Soil Classification (1975) and the Danish Profile Investigation (1990). The collected samples in these two surveys were taken to the laboratory for analysis. These samples were air-dried at room temperature and passed through a 2 mm soil sieve. Concentrations of SOC were determined by the combustion method in a LECO induction furnace, converted to % Soil Organic Matter (SOM). The other two surveys (ochre classification and well database performed in 1985) gave categorical information on parent material (e.g. peat, sand, silt and clay). This parent material information was reclassified into organic and mineral soils. In order to increase the number of samples used in the modeling process, the continuous soil organic matter (SOM) obtained in the former surveys was converted to a categorical variable using 10% SOM as a cut off value. With less than 10% SOM, soils are classified as mineral; and with more than 10% SOM, soils are considered organic.

2.3 Data Acquisition and Pre-Processing

Mapping organic soils can be achieved using decision-tree modelling through incorporating secondary spatial information into prediction (Mueller and Pierce 2003). Available digital geology (with five classes, Jakobsen and Hermansen 2007), soil (with eight classes, Madsen et al. 1992) and landscape (with five geomorphological units, Smed 1978) maps of the study area at different scales (1:20.000, 1:50.000) were converted to 30 m square grids.

A 30 m digital terrain model (DEM) was developed for the study area. The DEM resolution was chosen to match the spatial resolution of the used remote sensing data. The digital elevation data was acquired using airborn LiDaR, and a DEM of 2-meter resolution in full national scale was produced. This high resolution model was resampled to 30-meter resolution for the purpose of this study. Topographic attributes may aid spatial estimation of soil carbon, because the relief has a great influence on soil formation (McKenzie and Ryan 1999, Bou Kheir et al. 2007, 2008). They may be divided into primary and secondary attributes. Primary terrain attributes can be directly extracted from the DEM. Secondary parameters are calculated from two or more primary attributes. In this work, eight primary attributes (elevation; slope; aspect; plan, profile and tangential curvature; flow accumulation; rate of change of specific catchment area) were calculated with ArcGIS® and TerraSTREAM (Danner et al. 2007). The secondary derived attribute, quasi-dynamic topographic wetness index, was produced using the formula of Barling et al. (1994).

Besides digital elevation models, one of the most interesting sources of secondary information could be remote sensing RS, if a relationship between soil properties and spectral data could be achieved. Remotely sensed data can be useful for improving existing coarse-scale soil survey information at a regional scale (Scull et al. 2005). However, high carbon soils in Denmark can not directly be differentiated from moist soils using satellite imageries, both appearing as dark soils decreasing the spectral reflectance whenever their content increases. For that, several RS indices like the Normalized Difference Vegetation Index NDVI (based on red and NIR bands) and the Normalized Difference Wetness Index NDWI (based on near infrared and short near infrared channels) (Lillesand and Kiefer 1994) were derived from Landsat TM imageries (30 m) acquired in April 1987. NDVI was calculated to integrate vegetation status, while NDWI was extracted to compute surface moisture. The used Landsat TM imageries were chosen for many reasons: (1) being the most recent in the archive, (2) having good radiometric quality, and (3) at a minimum of plant cover shading the bare soils.

2.4 Statistical Analysis

The field survey data were split into two files, one compiling 80% of the field samples (1233 sites) used in the modelling process, and another one comprising 20% used in the validation phase (308 sites). The modelling file integrates x and y fields representing locational coordinates and the z field representing SOC. This file was converted to a square grid that matched the resolution of the constructed DEM. ArcGIS was used to assign topographic, soil, geology, landscape, NDVI and NDWI variables to each of the field survey (sampling) locations.

Spatial prediction of SOC was produced using tree-based classification models. These models are easy to interpret and discuss when a mix of continuous and categorical variables is used as predictors (Gessler 1996, McKenzie and Ryan 1999). They comprise a set of rules facilitating the classification of a categorical (classification tree) or continuous (regression tree) dependent variable based on values of the independent variables. In predictive SOC mapping, the dependent variable (SOC presence/absence) is categorical and the independent variables are both continuous (elevation; aspect; slope; plan, profile and tangential curvature; flow accumulation; rate of change of specific catchment area along the direction of flow; quasi-dynamic topographic wetness index; NDVI; NDWI) and categorical or nominal (soil type;

geological substrate; landscape type). However, the most significant advantage of tree-based models is the capacity to model non-additive and non-linear relationships in a relatively simple way (Scull et al. 2005). This is particularly useful for soil data where interactions between the response variable and environmental explanatory variables are often conditional on other explanatory variables.

Three sets of tree-models were explored based on (1) all of the variables, (2) the primary topographic variables only and (3) selected pairs of variables. Once the tree has been developed, it encodes a set of decision rules that define the range of conditions (values of environmental variables) best used to predict each SOC class.

Pruning the tree is necessary to prevent the model from being over-fit to the sample data, and to reduce tree complexity. Pruning entails combining pairs of terminal nodes into singles nodes to determine how the misclassification error rate changes as a function of tree size. We used cost-complexity pruning with an independent data set (a pruning data set) to produce a plot of training misclassification error rate versus tree size (Safavian and Norvig 1991).

2.5 Construction of SOC Map

Using the preferred classification-tree model (having the highest predictive power, and the lowest number of nodes), a predictive map of SOC was obtained under a GIS environment. This map was validated based on field surveys. An independent dataset has been chosen randomly in all landscape units, consisting of 20% (308 sites) of the total number of field sites, and the total accuracy was calculated.

3. Results and Discussion

Training misclassification error rates for the explanatory trees that were developed using all variables (Model 1) at a time or the primary topographic variables only (Model 2) varied from 23% to 26%, with quasi-identical numbers of terminal nodes (71 nodes for Model 1 and 69 nodes for Model 2). The relative importance of the predictor variables (Gini splitting method) in building those trees and splitting the corresponding nodes is shown in Table 1.

Applying cost-complexity pruning indicated that model 1 (based on all variables) would classify correctly 60% of the tested SOC selecting just seven terrain variables (with their relative importance shown in parentheses): landscape type (100%), soil type (29%), elevation (22.5%), tangent curvature (14%), NDVI (12%), aspect (11%), and slope (9%). Model 2 (based on topographic variables only) did slightly better and classified 63% of the text data accurately using five variables: (1) elevation (100%), (2) slope (36%), (3) aspect (16%), (4) tangent curvature (8%), and (5) profile curvature (5%). The number of the terminal nodes was very similar for both pruned models.

The models based on pairs of variables explained 50-68% of the variation in Soil Organic Carbon (Table 2). The model based on soil type and quasi-dynamic wetness index (TWI) (model 3) showed the highest predictive power, classifying 68% of the data correctly and pruned to fourteen terminal nodes. The TWI is a predictor of zones of soil saturation, and SOC often accumulates in lowland (concave) soils for two reasons: (1) on steep slopes, dry soil conditions prevail due to more rapid removal of water causing an important decrease in SOC, and (2) concave slopes can concentrate more water and sediments indicating the potential accumulation of a large quantity of soil organic carbon.

Predictor variables (%)	**Model 1 (explanatory tree)**	**Model 1 (pruned tree)**	**Model 2 (explanatory tree)**	**Model 2 (pruned tree)**
Elevation	70%	22.5%	100%	100%
Aspect	50%	11%	54%	16%
Slope	37%	9%	47%	36%
Profile curvature	25%	0%	23%	5%
Tangent curvature	34%	14%	12%	8%
Plan curvature	23%	0%	25%	0%
Flow accumulation	0%	0%	4%	0%
Specific catchment area	0%	0%	0%	0%
Quasi-dynamic wetness index	37%	0%	Not included in building the model	
Geological substrate	31%	0%		
Soil type	39%	29%		
Landscape type	100%	100%		
NDVI	31%	12%		
NDWI	18%	0%		
Tree size – Terminal nodes	71	9	69	10
Error rate – Training (%)	23%	33%	26%	33%
Error rate – Test (%)	-	40%	-	37%

Table 1. Relative importance of predictor variables (%) and misclassification error rates in models 1 (based on all variables) and 2 (based on primary topographic variables only).

Predictor variables	**a**	**b**	**c**	**d**	**e**	**f**	**g**	**h**	**i**	**j**	**k**	**l**	**m**	**n**
a	X	62	64	61	61	61	61	61	62	62	63	61	61	61
b		X	58	56	53	56	51	50	54	60	60	60	50	52
c			X	57	58	59	60	60	59	53	62	62	58	58
d				X	54	53	54	54	54	62	60	61	56	55
e					X	55	55	55	56	60	60	62	53	55
f						X	56	56	58	60	61	60	54	54
g							X	51	56	60	60	60	61	56
h								X	56	60	61	60	53	56
i									X	60	68	60	53	54
j										X	62	62	61	61
k											X	62	62	62
l												X	60	60
m													X	53
n														X

a = elevation, b = aspect, c = slope, d = profile curvature, e = tangent curvature, f = plan curvature, g = flow accumulation, h = specific catchment area, i = quasi-dynamic wetness index, j = geological substrate, k = soil type, l = landscape type, m = NDVI, n = NDWI

Table 2. Proportion of accuracy explained (%) for pruned tree-classification models based on pairs of variables (model 3).

Without pruning, this model gave similar results to models 1 and 2 (75% of accuracy explained), but model 3 is preferred because it is easier to understand and faster to use for making predictions. In addition, pruning the trees to their optimal size is a required task because smaller trees may provide greater predictive accuracy for unseen data than large trees. In both models 1 and 3, the predictor variable that was used statistically to generate the split from the parent node was the soil type, indicating its potential role in predicting the geographic location of SOC. The recommended model (model 3) relies on a small number of rules and just two independent predictor variables, one of which can be easily and quickly constructed whenever a DEM is available, which is the case in most countries (Fig. 2). The produced predictive map of soil organic carbon (Fig. 3) at 1:50,000 cartographic scale indicates that 7.5% of the wetlands in the study area correspond to organic soils, and 92.5% to mineral soils. The confusion matrix between the measured SOC classes and the modelled ones indicates a good overall accuracy of ca. 75%.

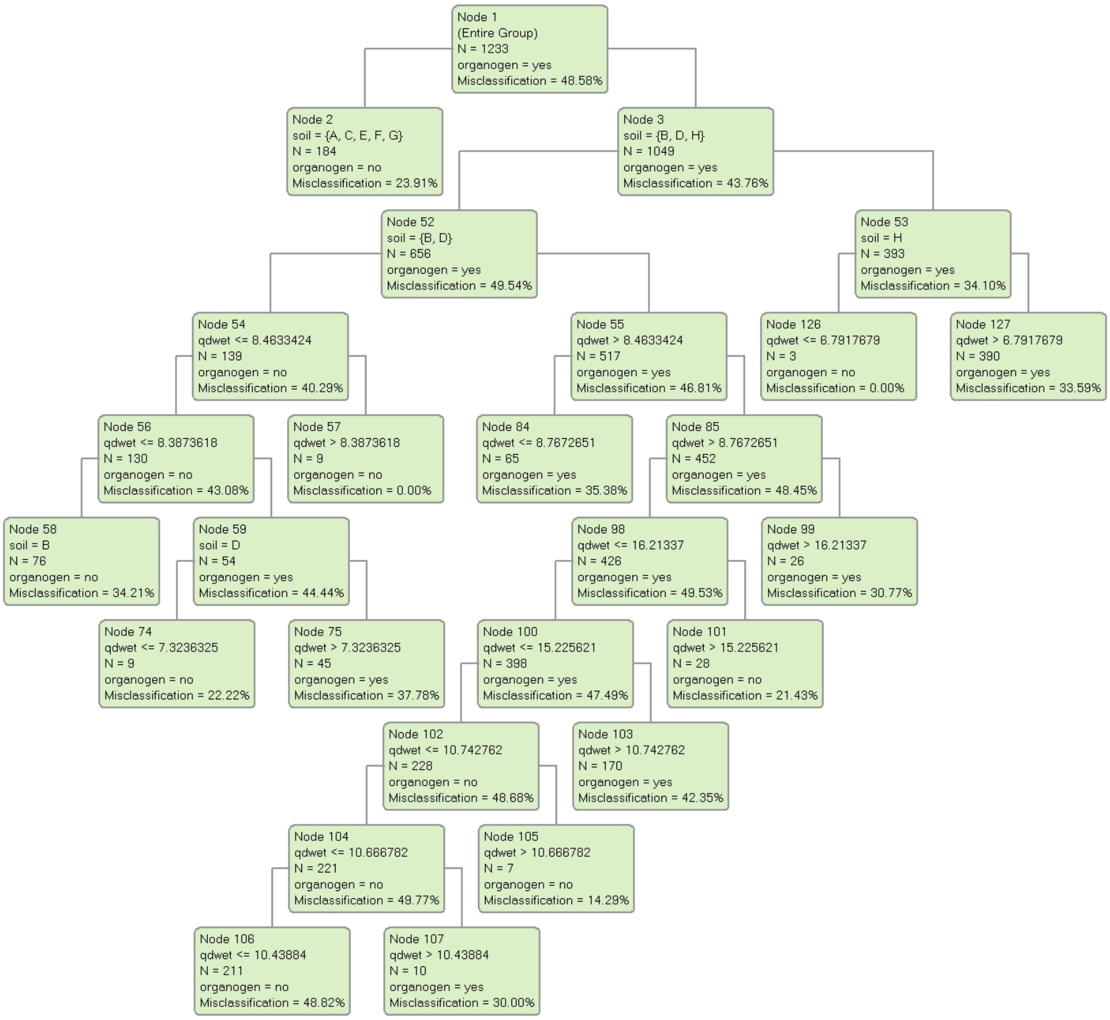

Figure 2. Classification-tree model based on the combination of soil type and quasi-dynamic wetness index for predicting the spatial distribution of SOC.

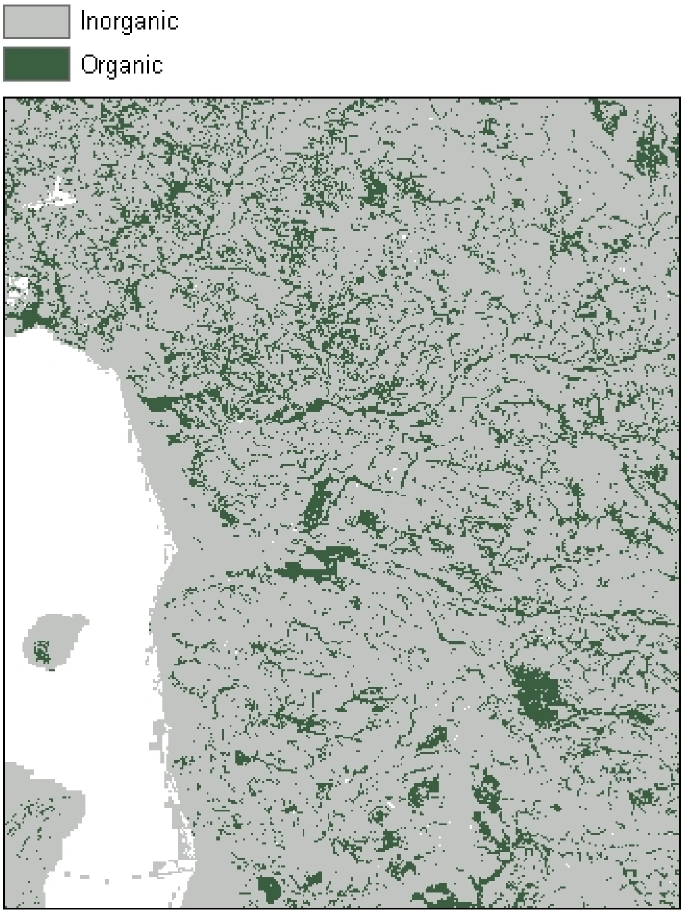

Figure 3. Soil organic carbon predicted using a classification tree model based on the combination of soil type and quasi-dynamic wetness index.

4. Conclusion

Topographic variables derived from DEMs are related to the geographic distribution of SOC. The preferred tree-based models explained 74-77% of the SOC distribution for a series of chosen field sites in southern Denmark. Two terrain variables – soil type and quasi-dynamic topographic wetness index – proved to be the most important variables, indicating that complex or secondary topographic variables show stronger relationships to SOC than primary topographic attributes. This particular pair of secondary topographic variables incorporated the effects of slope and upslope contributing area.

This modelling approach was easily implemented with available GIS (ArcGIS) and statistical (DTREG) software and is suitable for data exploration and predictive SOC mapping. It is explicit and can be critically evaluated and revised when necessary. It has the capacity to integrate easily other primary topographic attributes (e.g. slope length). The inclusion of additional variables might have explained some of the additional variation in the geographic distribution of SOC.

Future work will first compare the results from this study with those from other models (e.g. fuzzy logic, artificial neural networks, etc.), and later seek to gather additional field data so we can examine whether or not finer-scale DEMs can predict the distribution and magnitude of SOC with greater precision and reliability.

References

Barling RD, Moore ID and Grayson RB, 1994, A quasi-dynamic wetness index for characterizing the spatial distribution of zones of surface saturation and soil water content. *Water Resources Research,* 30: 1029-1044.

Bou Kheir R, Wilson J and Deng Y, 2007, Use of terrain variables for mapping gully erosion susceptibility in Lebanon. *Earth Surface Processes and Landforms,* 32: 1770-1782.

Bou Kheir R, Chorowicz J, Abdallah C and Damien D, 2008, Soil and bedrock distribution estimated from gully form and frequency: a GIS-based decision-tree model for Lebanon. *Geomorphology*, 93: 482-492.

Conant RT and Paustian K, 2002, Spatial variability of soil organic carbon in grasslands: implications for detecting changes at different scales. *Environmental Pollution*, 116: S127-S135.

Danner A, Yi K, Mølhave Th, Agarwal PK, Arge L and Mitasova H, 2007, TerraStream: From Elevation Data to Watershed Hierarchies. Proc. 15th International Symposium on Advances in Geographic Information Systems (ACM GIS), 2007.

Gessler PE, 1996, *Statistical Soil-Landscape Modeling for Environmental Management*, Ph.D. thesis, Australian National University, Canberra.

Jakobsen PR and Hermansen B, 2007, Danmarks Digitale Jordartskort. Version 3.0. Danmarks og Grønlands Geologiske Undersøgelse Rapport 2007/84, [Kun på CD-Rom].

Lillesand TM and Kiefer RW, 1994, *Remote sensing and image interpretation*. 3rd ed., John Wiley & Sons Inc., 750 p

Madsen HB, Nørr AH and Holst KA, 1992, The Danish Soil Classification. Altas of Danmark I(3). Reitzel, Copenhagen.

McKenzie NJ and Ryan PJ, 1999, Spatial prediction of soil properties using environmental correlation. *Geoderma,* 89: 67-94.

Mueller TG and Pierce FJ, 2003, Soil carbon maps – Enhancing spatial estimates with simple terrain attributes at multiple scales. *Soil Sci. Soc. Am. J.*, 67, 258-267.

Smed P, 1978, Landskabskort over Danmark. Geografforlaget, 5464 Brendrup.

Safavian SJ and Norvig P, 1991, A survey of tree classifier methodology. *IEEE transactions Syst. Man Cybern*, 21: 660-674.

Schuman GE, Janzen HH and Herrick JE, 2002, Soil carbon dynamics and potential sequestration by rangelands. *Environmental Pollution*, 116: 391-396.

Scull P, Franklin J and Chadwick OA, 2005, The application of classification tree analysis to soil type prediction in a desert landscape. *Ecological Modelling*, 181: 1-15.

Turner J and Lambert M, 2000, Change in organic carbon in forest plantation soils in eastern Australia. *Forest Ecology and Management*, 133, 231-247.

Geomorphometric Analyses of LiDAR Digital Terrain Models as Input for Digital Soil Mapping

K. Kringer[1], M. Tusch[1], C. Geitner[1,2], M. Rutzinger[3], C. Wiegand[2], G. Meißl[1]

[1]Institute of Geography, University of Innsbruck, Innrain 52, A-6020 Innsbruck
Telephone: ++43 (0)512 507 5402
Fax: ++43 (0)512 507 2895
Email: korbinian.kringer@student.uibk.ac.at, markus.tusch@uibk.ac.at, gertraud.meissl@uibk.ac.at

[2]Mountain Research: Man and Environment, Austrian Academy of Sciences, Technikerstraße 21a, A-6020 Innsbruck
Telephone: ++43 (0)512 507 4949
Fax: ++43 (0)512 507 4960
Email: clemens.geitner@oeaw.ac.at, christoph.wiegand@oeaw.ac.at

[3]International Institute for Geo-Information Science and Earth Observation (ITC), PO Box 6, NL-7500 AA Enschede
Telephone: ++43 (0)512 507 4949
Fax: ++31 (0)53 4874477
Email: rutzinger@itc.nl

1. Introduction

The delineation of supposedly homogeneous soil units for the production of high-quality soil maps usually involves intensive field work and requires comprehensive expert knowledge.

There is a need for automated, timesaving and more objective methods of digital soil mapping, which are based on available data on soil forming factors and demand only little additional field work (see McBratney et al. 2003, Lagacherie et al. 2006). This study investigates the applicability of airborne LiDAR (Light Detection and Ranging) data to delineate entities relevant for digital soil mapping using an object-based image analysis (OBIA) approach. Possible improvements of accuracy compared to the use of coarser relief data shall be exemplified.

1.1 Geomorphometrics in Digital Soil Mapping

Relief as one of the soil-forming factors identified by Jenny (1941) plays an important role in digital soil mapping. Relief data derived from digital terrain models (DTM) are used to predict soil classes and soil attributes in 80 % of the studies examined by McBratney et al. (2003). Dobos and Hengl (2008) summarise which and how surface parameters can be utilised as an input for digital soil mapping.

In mountain ranges like the Alps relief has direct (e.g., erosion and accumulation processes) and indirect impacts (e.g., distribution of unconsolidated parent material; hydrological conditions; changes of vegetation, micro-climate and land use) on soil formation, that have to be taken into account in digital soil mapping approaches (Geitner et al. 2009). Friedrich (1996) and Behrens and Scholten (2006) emphasise the importance of the relief as a major driving force in soil formation in European mid-latitude landscapes due to the topographic effects on the distribution of periglacial slope deposits.

1.2 Application of LiDAR Data

Transition zones between landform elements on a meso-scale (e.g., areas at the bottom of a slope, river terraces and embankments) tend to be blurred in conventional raster DTMs with a resolution of 10 meters and more. In the last ten years LiDAR systems and DTM filter techniques have improved so far that operational, reliable tools for the generation of DTMs with a resolution of 5 meters and less are available today. As LiDAR can penetrate the canopy of high vegetation highly accurate DTMs can be derived even for forested areas (Pfeifer and Kraus 1998). With the growing availability of high resolution DTMs from airborne LiDAR, input for medium and fine-scale applications can be improved significantly.

2. Aims and Methodology

2.1 Scope of Work

The aim of the present study is to identify landform elements which relate to specific conditions for soil formation and are referred to as soil-landform entities in this paper (MacMillan et al. 2000). As most pixel-based algorithms for the detection of landforms were developed for coarser DTMs, the applicability of these approaches on high resolution LiDAR DTMs is limited (Wood 1996). The most substantial difficulties arise from (a) the strongly varying scales of the demanded landform elements ranging from only a few metres to several kilometres, (b) random errors in the DTM (“noise”), which makes it difficult to distinguish significant changes in the relief from unwanted artefacts and (c) minor anthropogenic modifications of the relief, e.g. terraced fields or drainage channels. Instead of using a pixel-based approach, the concept of object-based image analysis (OBIA) as a new tool for morphometric analysis (e.g., Drăguț and Blaschke 2006) is applied. Derivatives of LiDAR DTMs are used as input for an OBIA-workflow that is implemented in a selected test area. Significant soil-landform entities are delineated and classified.

Classification results are compared to soil-landform entities derived from a coarser photogrammetric DTM. Benefits of airborne LiDAR DTMs for this procedure are exemplified.

2.2 Study Area and Basic Data

The study area presented in this paper is located around the city of Bruneck (Italy). It covers approximately 75 km² and has an altitudinal range from 748 to 2,276 m. The main focus is on the area below 1,000 m a.s.l. representing the basin of Bruneck. It is mainly formed by alluvial fans, flood plains and terraces of the rivers Ahrn and Rienz, and isolated outcrops of metamorphic bedrock (phyllite, schist). A LiDAR DTM (2.5 m cell size) and a photogrammetric DTM (20 m cell size) are used along with a land use map (1:10,000).

2.3 Methods

Fig. 1 shows the workflow used to develop a map of soil-landform entities from a LiDAR DTM applying an OBIA approach. The same procedure is carried out with a photogrammetric DTM to compare the results. Data on land cover is merely used to mask out rivers and areas where relief and soil formation is distorted significantly by anthropogenic influence (settlement areas, roads).

Input data for the OBIA are various terrain parameters that are derived in a first step with existing GIS-algorithms (Fig. 1, section 2). In addition to standard terrain derivatives, complex parameters are determined to detect landform elements in a heterogeneous environment. The “vertical distance to channel network” (VDCN, Bock and Koethe 2008) is adjusted and calculated separately for each watershed.

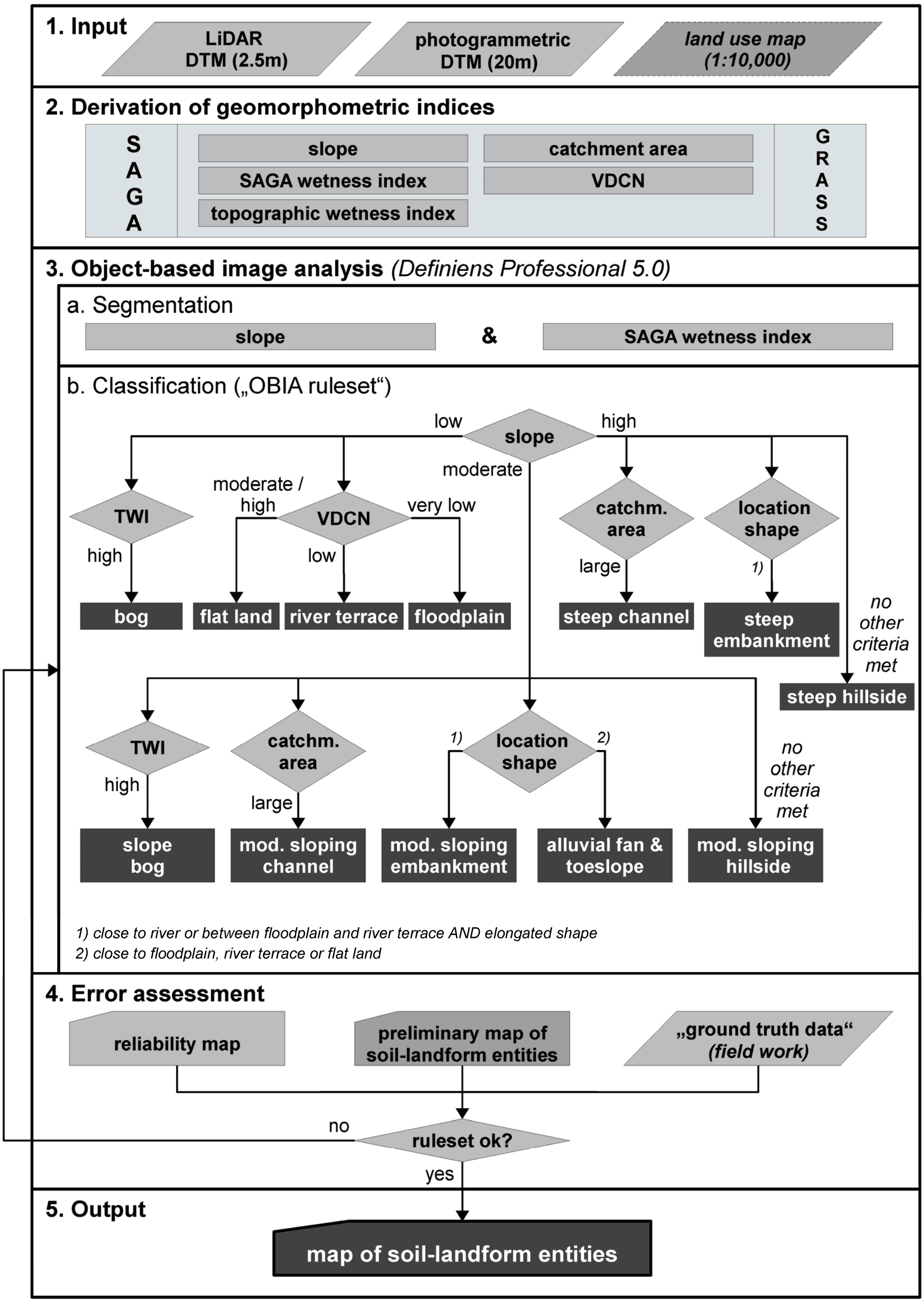

Figure 1. Workflow of the OBIA for Bruneck.

In a next step, OBIA is carried out applying an expert-driven semi-automated approach for the segmentation and classification process (van Asselen and Seijmonsbergen 2006, Schneevoigt et al. 2008). Multi-resolution segmentations based on the equally weighted parameters slope and SAGA wetness index (Boehner et al. 2002) are used to create a hierarchical segmentation with an increasing level of detail by decreasing the scale parameter (Baatz and Schäpe 2000). The compound terrain parameter SAGA wetness index proved to return better results than the basic terrain parameter catchment area, due to its capability of smoothing out small variations in flat areas (Böhner et al. 2002). The scale parameters used for the LiDAR DTM (10 on the highest level of detail) and the photogrammetric DTM (2) have to be chosen independently to guarantee segments of comparable size. Measures of curvature were integrated in the segmentation process first, but did not improve results due to a high sensitivity to the problems mentioned above (chapter 2.1) and are not used in this approach.

For the classification, a set of rules based on expert knowledge is developed to describe the relevant soil-landform entities (Fig. 1, section 3b). Instead of strict threshold values fuzzy classifiers are used to capture characteristics of the relief as a gradually alternating object. In a first classification step areas with similar slope processes are detected using the fuzzy membership function shown in Fig. 2. This first allocation reflects the distinctive gravitational influence of the relief on soil formation in a mountainous environment. Our choice of fuzzy membership functions is based on Schneevoigt et al. (2008) and observations from field work prior to the elaboration of the rule set.

In a second classification step river terraces and floodplains are separated from other objects with shallow slopes by their vertical proximity to a major river. Embankments are defined as objects of elongated shape, steep slope and adjacency to a river terrace or a floodplain. Hillside objects are distinguished from alluvial fans and areas at the bottom of slopes (toeslope) by analysing whether an adjoining object is classified as flat land, floodplain or river terrace. Other landform elements are identified according to the parameters shown in Fig. 1.

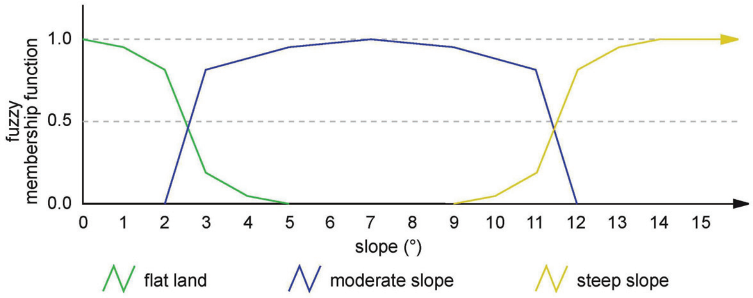

Figure 2. Fuzzy membership function of "slope" for the first classification step.

3. Results

The final outcome is a map of landscape elements including both geomorphic and hydromorphic features (Fig. 3a and b). It is intended to assist the field work for fine-scale soil mapping and to provide an input for subsequent digital soil mapping algorithms. Rather than geomorphologic units the map shows a classification of terrain in view of different conditions for soil formation (soil-landform entities).

Tab. 1 (split in two parts for lack of space) summarizes a first quality assessment of the OBIA classification. The columns show which percentage of the area assigned to each class derived from the LiDAR DTM is covered by each class derived from the photogrammetric DTM. Entities that cover large areas, such as steep hillside slopes and alluvial fans & toeslopes are congruent to a high degree. Entities of limited extent in at least one direction (e.g., embankments) are identified poorly. Small soil-landform entities based on hydrologic features (bogs) are excluded from this comparison since no meaningful representation is possible from the photogrammetric DTM.

		Classification of LiDAR DTM (2.5m)								
	class	flood plain	river terrace	flat land (unspecified)	alluvial fan & toeslope	steep hillside	mod. slop. hillside	moderate embankm.	steep embankm.	unclassif.
Classification of photogrammetric DTM (20m)	flood plain	**58,81**	11,78	1,13	1,16	0,06	0,02	17,64	7,03	0,00
	river terrace	3,06	**55,60**	10,18	2,36	0,02	0,00	7,72	1,60	0,00
	flat land (unspecified)	0,00	0,11	**37,12**	2,85	0,07	0,17	0,02	0,21	0,00
	alluvial fan & toeslope	26,47	23,19	42,80	**75,57**	2,67	2,85	49,37	32,24	40,89
	steep hillside	1,08	0,57	1,83	11,85	**91,95**	47,80	6,96	35,22	49,77
	mod. sloping hillside	0,43	2,28	2,60	4,50	5,17	**48,61**	1,50	2,74	9,34
	moderate embankment	4,12	4,01	0,12	1,03	0,04	0,03	**13,39**	15,93	0,00
	steep embankment	0,13	0,20	0,00	0,06	0,01	0,00	1,42	**3,48**	0,00
	unclassified	5,90	2,26	4,24	0,62	0,02	0,53	1,99	1,55	**0,00**

Table 1. Comparison of landform classification of LiDAR DTM and photogrammetric DTM (%).

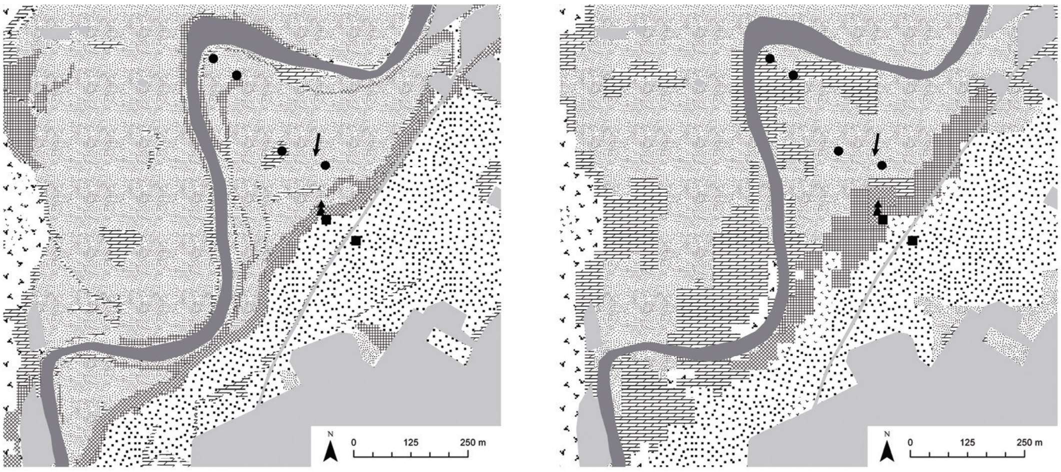

(a) Landform classification of LiDAR DTM

(b) Landform classification of photogrammetric DTM

(c) Orthophoto

(d) Photo from field work

Figure 3. Comparison of landform classification of (a) LiDAR DTM and (b) photogrammetric DTM with orthophoto (c) and field photo of flood plain and embankment (d).

Further error assessment is made by comparing field data to the results of both classifications. More than 260 soil profiles were sampled with a Pürckhauer auger and the associated landform was recorded. Fig. 3a and b show the results of both classifications for a small section of the river Ahr and adjacent flood plains, river terraces and embankments as well as the location of seven soil profiles. The comparison to the same section in the orthophoto (Fig. 3c) shows that a correct classification under forest canopy is only possible by using the LiDAR DTM as an input. The poor classification of embankments using the photogrammetric DTM can also be observed by comparing Fig. 3a and 3b to the field work data (location of soil profiles and Fig. 3d).

4. Conclusions and Future Work

The presented study shows the potential of LiDAR data for geomorphometric analysis as input for soil mapping. A method to detect homogeneous areas, in terms of unique conditions for soil formation, from secondary data sources shall reduce time consuming field work to a minimum. However, for highly populated, mountainous regions, it is obvious that an automatically derived map from terrain parameters and land use data cannot fully replace but at least assist conventional soil mapping (Friedrich 1996). Verification of soil-landform delineations in the field will always be necessary.

More sophisticated ground truth data using differential GPS will be collected. Specific landform entities and topographic profiles will be surveyed to determine the spatial accuracy of the results derived from the LiDAR DTM. An error assessment will be made by comparing mapped landform entities to classification results as shown in Table 1. Finally the transferability of the approach will be tested by comparing the results obtained in this study to the results from a second test area in the Inn Valley (Kramsach, Austria) with different topographic conditions.

Results will also be integrated in a digital soil mapping approach using classification and regression trees to derive comprehensive conceptual soil maps for the investigation areas. Soil classes and specific soil properties will be assessed and are used for an evaluation of natural soil functions as additional input for spatial planning procedures.

Other fields of application include the research on soil formation processes in Alpine areas. A special focus is set on the influence of relief on various scales and the investigation of hydraulic properties of soils to determine the relevance of soil for the development of storm water runoff in Alpine catchments.

Acknowledgements

We thankfully acknowledge funding from the Translational Research Programme of the Austrian Science Fund (FWF) for project L352 “Ökologische Bodenbewertung im mittleren Maßstab” and from the Autonomous Province of Bozen/Bolzano - South Tyrol for project “LASBO - Einsatz von Laserscanning zur Unterstützung der Bodenkartierung in Gebirgsräumen”.

References

Baatz M and Schäpe A, 2000, Multiresolution segmentation – an optimization approach for high quality multi-scale image segmentation. In: *Angewandte Geographische Informationsverarbeitung XII. Beiträge zum AGIT-Symposium Salzburg 2000*. Herbert Wichmann Verlag, Karlsruhe, 12-23.

Behrens T and Scholten T, 2006, Digital soil mapping in Germany – a review. *Journal of Plant Nutrition and Soil Science*, 169:434-443.

Benz C, Hofmann P, Willhauck G, Ligenfelder I and Heynen M, 2004, Multi-resolution, object-oriented fuzzy analysis of remote sensing data for GIS-ready information. *ISPRS Journal of Photogrammetry & Remote Sensing,* 58:239-258.

Bock M and Koethe R, 2008, Predicting the depth of hydromorphic soil characteristics influenced by ground water. *Hamburger Beiträge zur Physischen Geographie und Landschaftsökologie,* 19:13-22.

Böhner J, Köthe R, Conrad O, Gross J, Ringeler A and Selige T, 2002, Soil regionalisation by means of terrain analysis and process parameterisation, *European Soil Bureau – Research Report,* 7:213-222.

Dobos E and Hengl T, 2008, Soil Mapping Applications. In: Hengl T and Reuter H (eds), *Geomorphometry: Concepts, Software, Applications.* Developments in Soil Science, 33, Elsevier, Amsterdam, 461-480.

Drăguţ L and Blaschke T, 2006, Automated classification of landform elements using object-based image analysis. *Geomorphology,* 81:330–344.

Friedrich K, 1996, *Digitale Reliefgliederungsverfahren zur Ableitung bodenkundlich relevanter Flächeneinheiten*. PhD thesis, Frankfurter Geowissenschaftliche Arbeiten, 21, Frankfurt.

Geitner C, Tusch M, Meißl G, Kringer K and Wiegand C, 2009 (submitted), Der Einfluss des Reliefs auf die räumliche Verteilung der Böden: Grundsätzliche Überlegungen anhand von Beispielen aus den Ostalpen (Tirol und Südtirol). *Zeitschrift für Geomorphologie*.

Jenny H, 1941, *Factors of soil formation. A system of quantitative pedology.* Dover Publications, New York.

Lagacherie P, McBratney AB and Voltz M (eds), 2006, *Digital Soil Mapping: An Introductory Perspective*. Developments in Soil Science, 31, Elsevier, Amsterdam.

MacMillan RA, Pettapiece WW, Nolan SC and Goddard TW, 2000, A generic procedure for automatically segmenting landforms into landform elements using DEMs, heuristic rules and fuzzy logic. *Fuzzy Sets and Systems*, 113:81-109.

McBratney AB, Mendonça Santos ML and Minasny B, 2003, On Digital Soil Mapping. *Geoderma*, 117:3-52.

Pfeifer N and Kraus K, 1998, Determination of terrain models in wooded areas with airborne laser scanner data. *ISPRS Journal of Photogrammetry & Remote Sensing*, 53:193-203.

Schneevoigt NJ, van der Linden S, Thamm HP and Schrott L, 2008, Detecting Alpine landforms from remotely sensed imagery. A pilot study in the Bavarian Alps. *Geomorphology*, 93:104-119.

van Asselen S and Seijmonsbergen AC, 2006, Expert-driven semi-automated geomorphological mapping for a mountainous area using a laser DTM. *Geomorphology*, 78:309-320.

Wood J, 1996, *The Geomorphological Characterisation of Digital Elevation Models*. PhD thesis, University of Leicester, UK.

Terrain-related Revision of Existing Soil Maps

M. Möller[1], T. Koschitzki[1], K.-J. Hartmann[2]

[1]Geoflux GbR, Lessingstraße 37, D-06114 Halle (Saale)
Telephone: 00493451352244
Fax: 00493452394019
Email: moeller@geoflux.de

[2]State Institute for Geology and Natural Resources Saxony-Anhalt, Köthener Straße 34, 06118 Halle (Saale)
Telephone: 04493455212117
Email: hartmann@lagb.mw.sachsen-anhalt.de

1. Introduction

In Germany, federal geological surveys are responsible for mesoscale soil mapping.In the federal state Saxony-Anhalt, the soil map 1:50,000 results from an integration process of already existing soil maps (Hartmann 2006). These maps were mainly surveyed in the former East Germany where another classification system was valid. The data integration process was subjectively realized by soil surveyors and aimed primarily at the semantic transformation to the current valid classification system of the German Handbook of Soil Mapping (Ad-hoc-AG Boden 2005). While the former soil unit boundaries were generally taken over, the soil attributes were semantically aggregated. That means that the soil units, which originally represented genetically linked soils, were now described by only the dominant soil.

The resulting soil map does not contain any quality information and is therefore labeled as "preliminary" (*in German*: Vorläufige Bodenkarte 1:50,000 or VBK 50). Thus, a simple quality assessment of VBK 50 should be applied in a reproducible manner by the following general conditions:

- Implementation of expert knowledge should be ensured.
- No training or validation information was available for automatic classification approaches.

In this paper, on the example of VBK 50 we present a cost- and time-effective terrain-related revision of mesoscale soil maps. The revision bases on a state-wide available Digital Elevation Model with a resolution of 20 x 20 m (DEM 20) and focuses on the terrain-related soil properties *floodplain membership*, *colluvium membership* and *humus layer thickness*.

2. Methods

The procedure can be distinguished in five steps: First, soil-related terrain attributes were derived which had been proved to be suitable for the classification of the above mentioned target soil properties (section 2.1). Second, terrain attributes were segmented into landform elements and then geometrically overlaid with aggregated VBK 50 units (section 2.2). Third, the resulting landform soil elements (LSE) were statistically analyzed and classified by fuzzy membership functions (section 2.3). Finally, the classified LSE were semantically and geometrically aggregated (section 2.4) as well as assessed regarding their terrain-related plausibility by means of a quality measure (section 2.5).

2.1 Terrain Analysis

The target soil properties *colluvium membership* and *humus layer thickness* are related to the terrain attribute *mass balance index MBI*. The index is calculated by the combination of the terrain attributes *slope*, *vertical distance to channel network* and *profile curvature* (Fig. 1 e). Negative *MBI* values represent areas of net deposition such as depressions, positive *MBI* values represent areas of net erosion such as hill slopes, *MBI* values close to 0 indicate areas with a balance between erosion and deposition such as plain areas (Fig. 1 a, c; Möller et al. 2008).

The floodplainindex *FPI* enables the detection of floodplains (Fig. 1 b, d). They can be characterized by a maximal value of *topographic wetness index TWI*, low slope values and minimal values of *vertical distance to channel network* (Fig. 1 f).

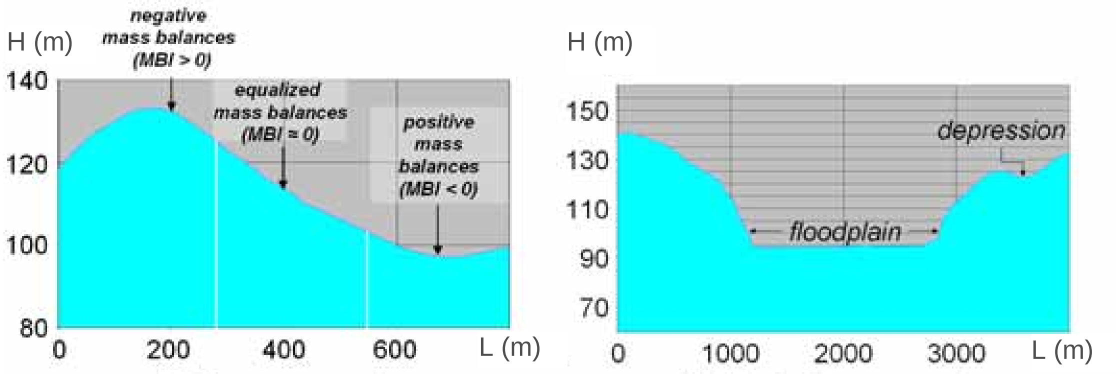

(a) Slope cross section (b) Floodplain cross section

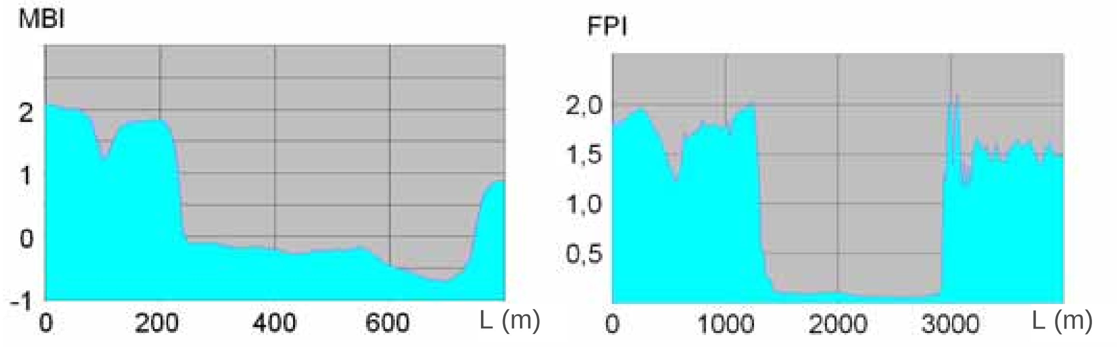

(c) *MBI* cross section (d) *FPI* cross section

$$MBI = \begin{cases} f(vk) \times (1 - f(n)) \times (1 - f(ht)) \text{ for } f(vk) < 0 \\ f(vk) \times (1 + f(n)) \times (1 + f(ht)) \text{ for } f(vk) > 0 \end{cases} \quad FPI = (1 - f(TWI)) \times (1 + f(n)) \times (1 + f(ht))$$

with $MBI \in [-1,3]$ with $FPI \in [0,2]$

(e) *MBI* calculation (f) *FPI* calculation

Figure 1. Relations between DEM cross sections (a, b) and value ranges of *MBI* (c) and *FPI* (d) | H, height (m) | L, length of cross section (m) | *vk*, profile curvature | *n*, slope | *ht*, vertical distance to channel network | *TWI*, topographic wetness index

2.2 Segmentation

Segmentation algorithms applied on terrain attributes have been established as an approach for the reproducible delimitation of soil-related landform elements (Möller et al. 2008, Minár and Evans 2008, MacMillan and Shary 2009). In this study, the fractal net evolution algorithm (FNEA) was used which is described in detail by Benz et al. (2004). The FNEA belongs to hierarchical region-growing algorithms starting with raster cell groups (seeds) representing local minima within raster grid and cluster of smallest Euclidean distance within the associated n-dimensional feature space. Those seeds are growing as far as a halting criterion is reached. Halting criteria are defined by the average heterogeneity of resulting segments or landform elements. The segmentation process generates different aggregation levels of discrete landform elements. Each level represents a specific target scale consisting of segments with a comparable heterogeneity. The segmentation results can be influenced by parameters which allow the adaptation of the target segment's heterogeneity and shape.

The overlay of landform elements and aggregated VBK 50 soil units led to landform soil units (LSE). The VBK 50 aggregation was performed semantically (not geometrically). Soil types, representing a horizon-related classification according to soil forming processes, were summarized to soil classes considering similar terrain-related soil forming conditions (Ad-hoc-AG Boden 2005).

2.3 Classification

The classification process corresponds to a data base query applied on LSE mean *MBI* and *FPI* values using fuzzy set theory (Zadeh 1965). The crucial point while defining fuzzy membership functions is the identification of appropriate fuzzy sets. Following Kuo et al. (2009), memberships were derived from *k means* clustering of LSE mean values of each soil class within the R statistics environment (cf. Reimann et al. 2008).

2.4 Assignment und Aggregation

The classification can be considered as a test if LSE terrain properties and the associated soil classes fit together. If so, the original soil unit attributes can be confirmed and taken over. If not, new suitable soil information has to be assigned. Therefore, we created a lookup table containing soil information of all possible spatial neighbors. Applying a Boolean value, all combinations were expert-based judged regarding their plausibility. The actual GIS-based aggregation routine searches in an iterative manner for the best contextual fitting neighbor delivering its soil information whereas every iteration step produces new neighborhood relations. Finally, all classified and assigned LSE are aggregated: On condition that all original VBK 50 boundaries are retained unchanged, all neighbors are merged geometrically and semantically if they have an area smaller than 2.5 ha and belong to the same soil class. This operation should ensure that only scale relevant geometric boundary modifications are taken into account which affect the cartographic presentability for the target scale of 1:50,000.

2.5 Assessment

Fuzzy classification results can be assessed by the best class membership $Z1$ and classification stability $Zrel$. While $Z1$ indicates simply the height of the best class membership (0 = low; 1 = high), $Zrel$ results from the combination of the first and second best class memberships $Z1$ and $Z2$ according to Equation 2.

$$Zrel = \frac{Z1 - Z2}{Z1} \qquad (2)$$

High $Zrel$ values indicate that the first class membership is considerably higher that the second one. The classifications can be considered as *stable*. Low $Zrel$ values stand for *instable* classifications because $Z1$ and $Z2$ values are similar. Finally, a classification can be highly esteemed if $Zrel$ and $Z1$ values are high.

The integral consideration of $Z1$ and $Zrel$ gives a so called plausibility measure PM which is applied separately on confirmed, new classified and not classified LSE.

PM is calculated from the *k means* cluster analysis of $Z1$ and $Zrel$ values, their following cluster related summation $(Z1, mean + Zrel, mean)$ and ranging according to equation (4).

$$PM = \frac{(Z1, mean + Zrel, mean) - (Z1, mean + Zrel, mean)_{\min}}{(Z1, mean + Zrel, mean)_{\max} - (Z1, mean + Zrel, mean)_{\min}} \tag{4}$$

3. Study Area

The approach was applied for the total area of Saxony-Anhalt (20,443 km^2) but we have visualized some results on the example of a study area with heterogeneous soil and relief conditions (Fig. 2). This area corresponds to the official German topographic map 4336 at a scale of 1:25,000 with a size of about 100 km^2 (cf. Möller et al. 2008).

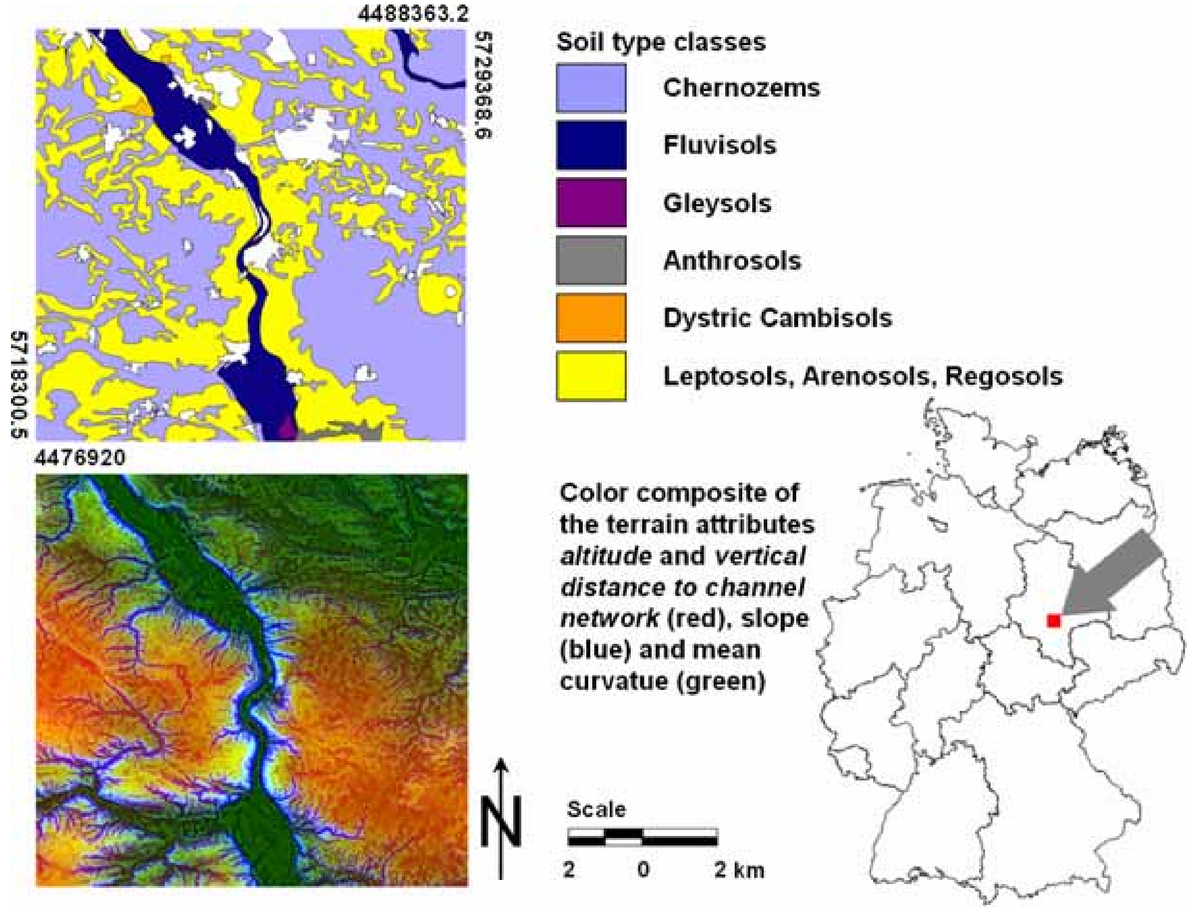

Figure 2. Study area: Soil type classes and color composite of selected terrain attributes.

4. Results

The upper image in Fig. 3 shows the segmentation and classification results on the example of the study area. Related to Saxony-Anhalt, the overlay of segmentation result and VBK 50 led to 469,430 LSE. The original number of soil units was 36,636.

Fig. 4 shows on the example of the soil class *Chernozem* class specific membership functions which result form *k means* cluster analysis. The cluster number was chosen subjectively (here: 10 cluster). The frequency charts of each cluster give a clue of the cluster relevance. The lower and upper cluster quartiles as well as cluster means revealed fuzzy sets for the used membership function types (mft) smaller than and about range (cf. Definiens 2008).

The lower image of Fig. 3 clarifies the effects of the applied aggregation operation: Only scale relevant modifications were made. In Saxony-Anhalt, the aggregation led to a decrease in LSE number from 469,430 to 87,012.

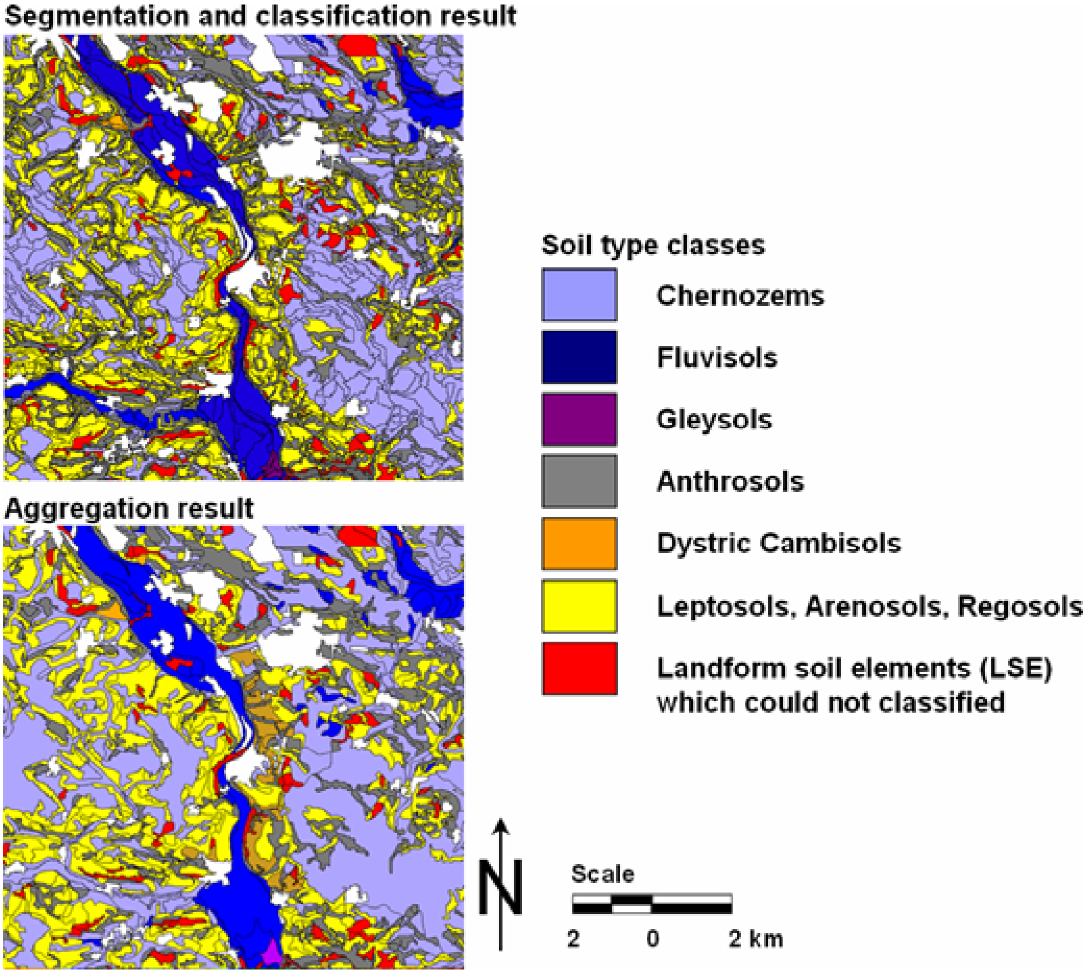

Figure 3. Visualization of segmentation, classification and aggregation results on the example of the study area Könnern.

Fig. 5 uncovers that the proportion of the soil type class *Anthrosol* (Y1) had been increased considerably to the disadvantage of other soil type classes. The information about colluvium's occurrence was hidden in the semantic attributes of the original soil maps which got lost during the semantic transformation process (section 1). Thus, the classification result represents a geometric disaggregation revealing original semantic terrain-related information.

57 % of all LSE could be confirmed or assigned with new soil information (classes A, B-L, D, G, R, S-P, T, Y), 36 % could be classified but not assigned (classes A1, A2, O1, R1, Y1) and 7 % could be neither classified nor assigned (class REST). Finally, Table 1 contains the plausibility measure *PM* for each confirmed or new classified LSE derived from clustered and summarized $Z1$ and $Zrel$ values.

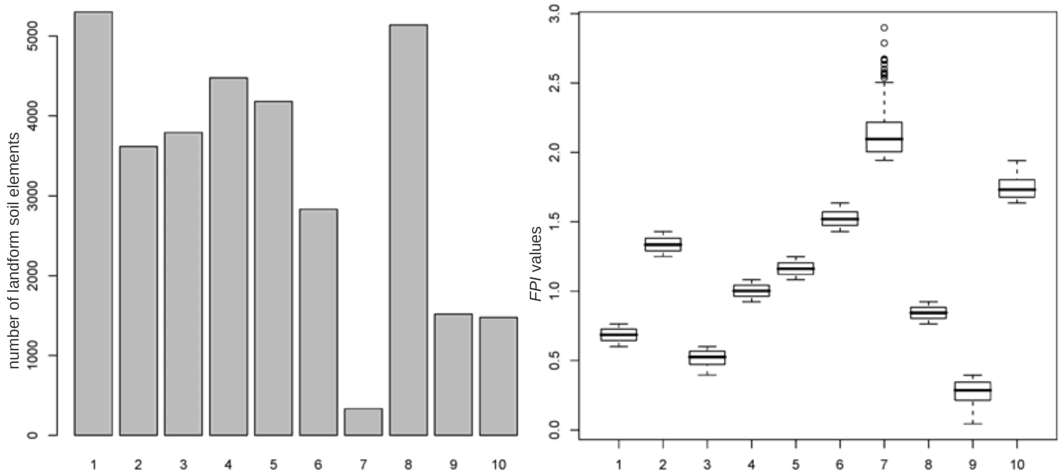

(a) *FPI* cluster barplots (b) *FPI* cluster boxplots

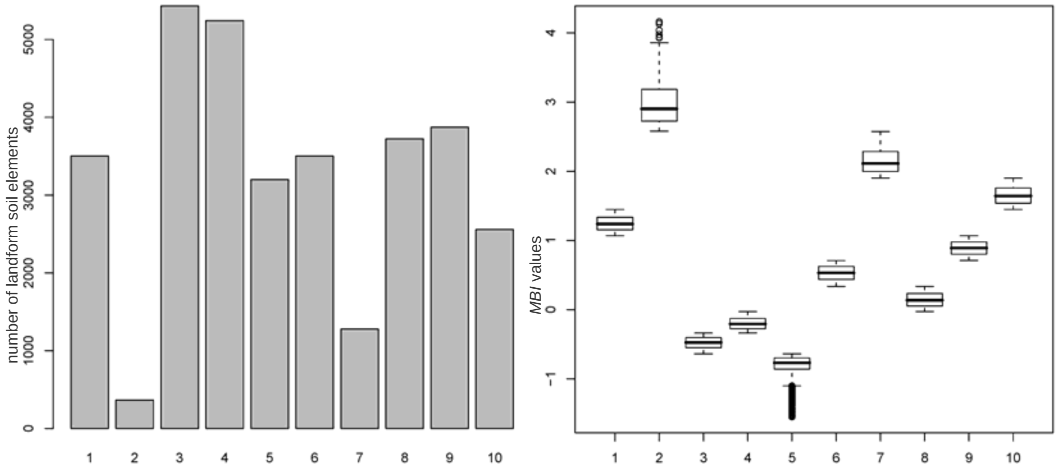

(c) *MBI* cluster barplots (d) *MBI* cluster boxplots

- Class *Chernozem*
    - *feature MBI*: *mft* about range *border* 0.1 … 1.3 (used cluster. 4: 1, 6, 8, 9)
- Class *Chernozem to Floodplain*
    - *feature FPI*: *mft* smaller than *border* 0.3 … 0.7 (used cluster: 1, 3, 9)
- Class *Chernozem to Anthrosol*
    - *feature MBI*: *mft* smaller than *border* -0.8 … 0 (used cluster: 3, 4, 5)
- Class *Chernozem to Leptosol, Arenosol or Regosol*
    - *feature MBI*: *mft* smaller than *border* 1.6 … 2.9 (used cluster: 2, 7, 10)

(e) Class definitions

Figure 4. Frequency charts (a, c), Box Whisker plots (b, d) of *FPI* and *MBI* cluster as well as membership functions (e) for the soil class *Chernozem* related to the total area of Saxony-Anhalt.

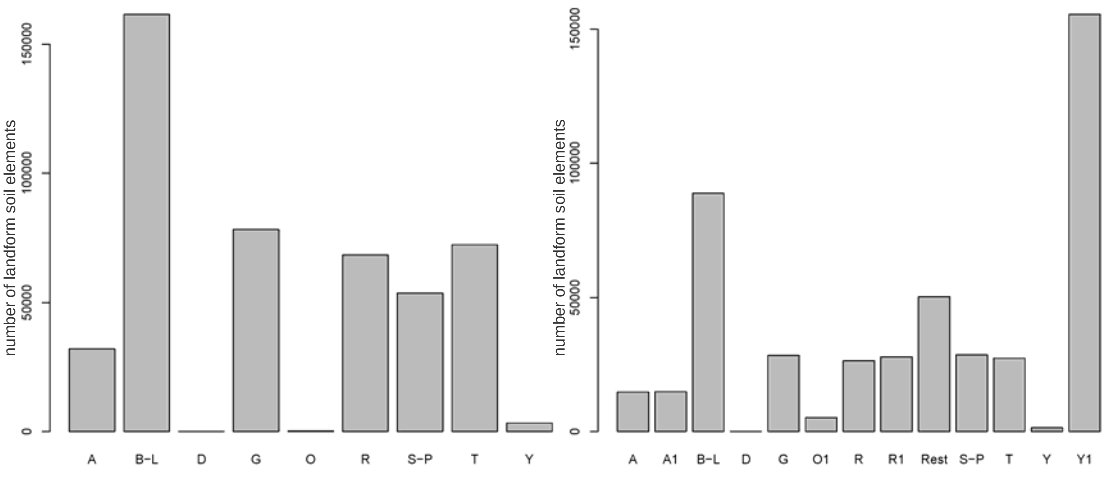

(a) (b)

Figure 5. Frequency charts of the original VBK 50 (a) and the modified LSE number (b) (A1, O1, R1 and Y1 = new classified soil classes. REST = LSE could neither classified nor assigned).

$Z1, mean$	$Zrel, mean$	PM
0.01	0.01	0.00
0.88	0.09	0.48
0.34	0.24	0.28
0.86	0.45	0.65
0.47	0.62	0.54
0.90	0.75	0.83
0.62	0.92	0.77
0.29	0.94	0.61
0.85	0.97	0.91
0.99	1.00	1.00

Table 1. Clustered $Z1$ and $Zrel$ mean values and related PM values.

5. Conclusions

We presented an effective algorithm to integrate terrain information into existing mesoscale soil maps. The applied approach bases on the segmentation of terrain attributes into landform elements. On the resulting object data sets a fuzzy classification based on two-dimensional membership functions was carried out. The membership function borders were defined by a preceding *k means* cluster analysis. The classification result was aggregated considering scale and neighborhood relations as well as cartographic readability. All algorithm steps were affected by expert knowledge.

The modified soil units contain additional information to their terrain related plausibility. We are aware that the derived quality measures cannot replace a semantic and geometric validation (cf. MacMillan 2008). However, this approach can help to get an idea about the terrain related accuracy of existing older soil maps which often contain no quality information. Finally, the classification and assessment results can be used for the definition of training areas for automatic classification approaches (cf. Scull et al. 2003, MacMillan 2008) which be subject of further work.

References

Ad-hoc-AG Boden. 2005. *Bodenkundliche Kartieranleitung*. E. Schweizerbart'sche Verlagsbuchhandlung. 5th edition. Hanover. Germany.

Benz U C. Hofmann P. Willhauck G. Lingenfelder I and Heynen M. 2004. Multi-resolution. object-oriented fuzzy analysis of remote sensing data for GIS-ready information. *Journal of Photogrammetry & Remote Sensing*. 58: 239–258.

Definiens. 2008. *Definiens User Guide*. Document Version 7.0.5.968. Definiens AG. München. Germany.

Hartmann K-J. 2006 . Bodeninformationen. In: Feldhaus D and Hartmann K-J (eds). *Bodenbericht Sachsen-Anhalt 2006: Böden und Bodeninformationen in Sachsen-Anhalt*. Landesamt für Geologie und Rohstoffe Sachsen-Anhalt. Halle (Saale). 71–87.

Kuo R J. Chao C M and Liu C Y. 2009. Integration of *k means* algorithm and AprioriSome algorithm for fuzzy sequential pattern mining. *Applied Soft Computing.* 9: 85–92.

Minár J and Evans I S. 2008. Elementary forms for land surface segmentation: The theoretical basis of terrain analysis and geomorphological mapping. *Geomorphology.* 95: 236–259.

Möller M. Volk M. Friedrich K and Lymburner L. 2008. Placing soil genesis and transport processes into a landscape context: A multiscale terrain analysis approach. *Journal of Plant Nutrition and Soil Science.* 171: 419–430.

MacMillan R A. 2008. Experiences with applied DSM: Protocol. availability. quality and capacity building. In: Hartemink A E. McBratney A and Mendonca-Santos M L (eds). *Digital soil mapping with limited data.* pp. 113–136. Springer. Heidelberg. New York

MacMillan R A and Shary P A. 2009. Landforms and landform elements in geomorphometry. In: Hengl T and Reuter H I (eds). *Geomorphometry: concepts. software. application.* Developments in soil science. volume 33: 227–254. Elsevier: Amsterdam.

Reimann C. Filzmoser P. Garrett R and Dutter R. 2008. *Statistical Data Analysis Explained: Applied Environmental Statistics with R*. Wiley & Sons. Chichester. West Sussex. UK.

Scull P. Franklin J. Chadwick O and McArthur D. 2003. Predictive soil mapping: a review. *Progress in Physical Geography*. 27: 171–197.

Zadeh L. 1965. Fuzzy sets. *Information and Control*. 8: 338–353.

Mapping Continuous Soil Depth Functions in the Edgeroi District, NSW, Australia, Using Terrain Attributes and Other Environmental Factors

B. P. Malone, B. Minasny, A. B. McBratney

Faculty of Agriculture, Food & Natural Resources
The University of Sydney
Telephone: 0011 +61 9568 4113
Email: b.malone@usyd.edu.au

1. Introduction

To benefit from the ecological and economical functions of soil, land holders, corporate stakeholders and, governmental departments need access to quantitative soil information. Such information confers weight to decisions regarding the management of the land and soil resources. To facilitate this need, we must first comprehend the functions and pertinent factors contributing to not only soil variability across a landscape but also soil variability with depth down a profile.

The variation of soil properties down a profile is usually continuous (Ponce-Hernandez et al. 1986). Soil depth functions are often created to represent the depth-wise variation of soil properties. However, with traditional sampling of soil profile horizons, it is often assumed that the horizon value of a particular attribute represents the average value for that attribute for the depth interval of that horizon. With this paradigm, in effect what should be a continuous function, the data often appears discontinuous or stepped.

A flexible and accurate method for fitting continuous functions of soil data is the use of smoothing splines (Erh 1972) and equal-area spline functions as proposed by Ponce-Hernandez et al. (1986). Essentially, a spline function is a set of local quadratic functions tied together with ‘knots’ that describe a smooth curve through a set of points. Bishop et al. (1999) demonstrated their superiority over other continuous soil depth functions when they predicted various types of soil properties.

However, in a spatial context, a collection of spline functions for individual site observations will ultimately lead only to point observation data sets. To the parties concerned, such data will be of little use for mapping soil variability. The response to this demand has been answered partly in the way of digital soil mapping, where soil properties are mapped based on their relationship with environmental variables (Minasny et al. 2008). The *scorpan* factors as proposed by McBratney et al. (2003) provide a valuable predictive framework for determining soil variability in areas with limited soil data.

Given the predictive capabilities of soil depth functions and an explosion in the capabilities of digital soil mapping in areas with limited data (Lagacherie 2008), it seems only logical for there to be an amalgam of both methods to quantitatively predict the vertical and lateral variation of soil properties across a defined area. In this paper we propose a novel method for predicting the vertical and lateral variation of soil properties in areas where limited soil data exists. Using soil carbon as our exemplar soil property we want to firstly determine whether terrain attributes alone are feasible for predicting its lateral and vertical variation or whether it is better described with the inclusion of other environmental factors relating to parent materials and landuse into the predictive models. With the most parsimonious model we want to map carbon storage to a depth of 1m in our defined study area and then demonstrate the functionality of the underlying soil geo-database for data enquiry by mapping the depth at which soil carbon falls below 1%.

2. Methods

2.1 Study Area and Soil Data

The study site (1500km^2) is situated near Narrabri (30.32S 149.78E), 500km NNW of Sydney, NSW, Australia. Agricultural enterprises such as cropping and pastoral farming are predominant in the area. There are also some significant tracts of land covered with remnant vegetation (Fig. 1).

The soil dataset consists of 341 soil profiles (Fig. 1). The dataset describes and quantifies various soil morphological, physical and chemical attributes at depth intervals of 0–0.1, 0.1–0.2, 0.3–0.4, 0.7–0.8, 1.2–1.3 and 2.5–2.6m (McGarry et al. 1989). Soil carbon storage is of greatest interest in this study. For our subsequent analyses, carbon was assessed on a volume basis (kg m^{-3}) of which was derived from the measured organic carbon percentages using pedo-transfer functions.

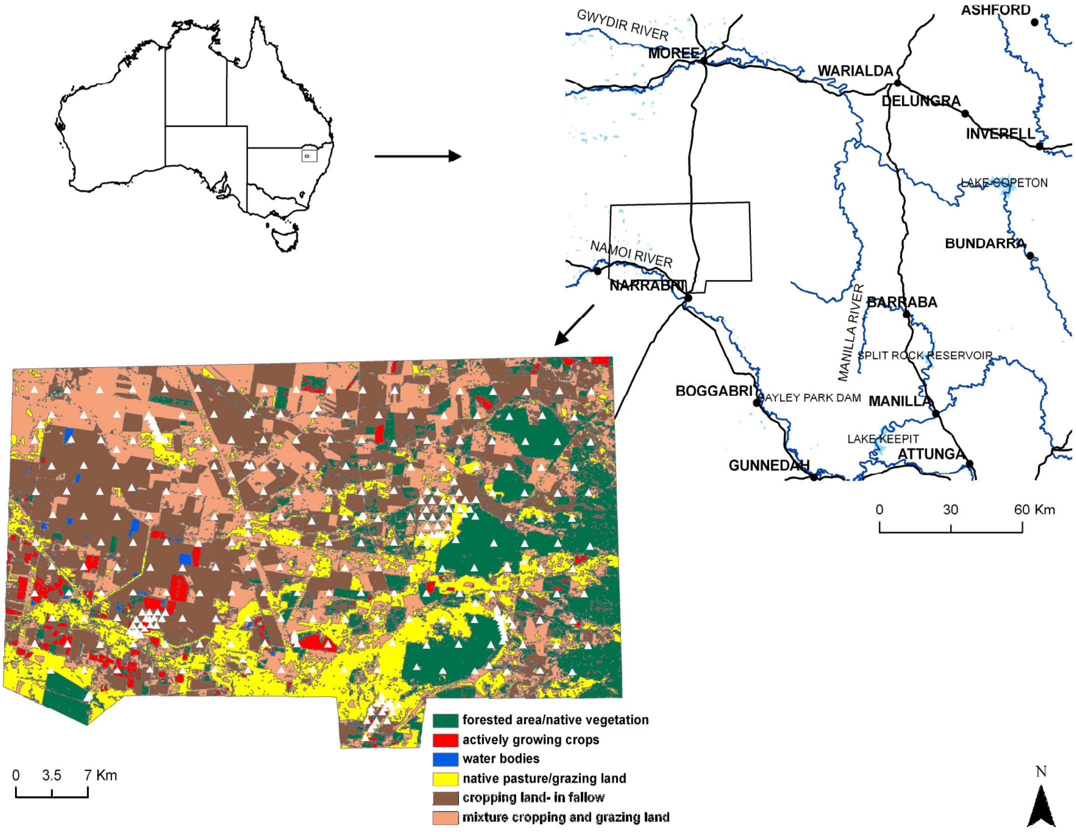

Figure 1. The Edgeroi study area

2.2 Environmental Data

A number of environmental covariates were sourced and interpolated onto a common grid of 90m resolution. These included:

- 3 arc-second (90m) digital elevation model (DEM). First and second derivatives, namely: slope, aspect, terrain wetness index (TWI), flow length, slope length factor (LS-factor), area above channel network (AOCN) and stream power index (SPI) were determined.

- Landsat 7 ETM+ images from 2003. The Landsat bands were used for the estimation of land cover and land use. Vegetation cover and type was estimated using the Normalised Difference Vegetation Index (NDVI). Furthermore, the band ratios or more commonly, soil enhancement ratios of b3/b2, b3/b7 and b5/b7 were also derived.
- Gamma-radiometric survey data (Geosciences Australia 2008), which provides a measure of the spatial distribution of three radioactive elements (potassium-K, thorium-Th and uranium-U) in the top 30-45 cm of the earth's crust. This data was used to determine the distribution of various parent materials over the landscape.

2.3 The Equal-Area Smoothing Spline

The spline model we used is a generalisation of the quadratic spline model of Bishop et al. (1999). The model by Bishop et al. (1999) is when data are averages over adjacent horizons or layers in a soil profile. The model used in this paper is more general where the data are again averages of soil layers, but the supports of the data are not adjacent.

Splines were fitted to each of the 341 point using code written in Matlab (Mathworks 2005). For modelling purposes, the mean values at depth intervals; 0–10, 10–20, 20–30, 30–40, 40–50, 50–70, 70–80 and 80–100cm were derived from the splines.

2.4 Data Analysis and Modelling

JMP software (SAS) was used to construct neural networks for the depth-wise modelling of carbon storage. Prior to this, 50 data points were randomly selected and omitted from the dataset for the purpose of model validation.

Firstly, a neural network was constructed using only the DEM data and derived terrain attributes as predictor variables. Secondly, using the best combination of environmental factors as determined from stepwise regression another neural network was constructed. Profile formulae for each depth interval were saved for later use to predict in areas where data observations were not available. Residuals were calculated and then kriged (local) onto the common 90m grid.

For model validation, the profile formulae were applied to the 50 withheld data points. Residuals, calculated by inverse kriging from the 90m grid of residuals were added to the estimated depth values to give an amended prediction. Splines were then reconstructed and then compared to the raw data values as derived from the inputs provided by McGarry et al. (1989).

Using the best neural network, the profile formulae were applied to the common 90m grid geo-database in order to map total carbon storage for the study area. The kriged residuals were added to the predictions. For demonstration of functionality, the resulting geo-database of soil information generated in this study was queried to determine the depth at which carbon storage decreases to below 1% using computer programming code written in Matlab (Mathworks 2005).

3. Results

Table 1 shows the best combination of terrain attributes used for each layer. In the top depth interval (0–10cm) all terrain attributes except flow length were pertinent where

35% of variation could be explained. Elevation is critical at all depth intervals except at 80–100cm. Other important factors include altitude above channel network, stream power index and terrain wetness index.

Depth Interval (cm)	Terrain Attributes	R^2
0–10	Elevation, aspect, slope, terrain wetness index (TWI), altitude above channel network (AOCN), LS-factor, stream power index (SPI)	35%
10–20	Elevation, AOCN, LS-factor, SPI	22%
20–30	Elevation, AOCN, SPI	12%
30–40	Elevation, AOCN, SPI	11%
40–50	Elevation, AOCN, TWI, SPI	12%
50–70	Elevation, AOCN, TWI, flow length, SPI	15%
70–80	Elevation, AOCN, TWI, flow length, SPI	16%
80–100	TWI, AOCN, flow length, SPI	12%

Table 1. Depth wise variation in terrain attributes to predict soil carbon storage

With the inclusion of other environmental factors, the most parsimonious combination was found to comprise of elevation, slope, and altitude above channel network, stream power index, potassium (from radiometric survey), and Landsat bands #3, #4 and #5 and the band ratios 3/7and 5/7. On average 35% of the variation could be explained with these factors.

Using all the available terrain attributes as factors, the neural network for carbon prediction was found to explain 57% of the variation. Upon the automated cross-validation procedure, 0% of dataset could be accurately modelled. Conversely, using the most parsimonious set of environmental factors, the neural network model explained 60% of the variation. 4% of the variation was explained when the model was cross-validated.

Five data points were selected at random from the 50 validation points to graphically represent model predictions with the raw values derived from McGarry et al. (1989) (Fig. 2) As expected, the fitted splines, fit closely to the raw data. When using the terrain attributes only or the best combination of factors, the predictions display a fair agreement with the raw data values. The fits from both neural networks at *ed002*, *ed147* and *ed218* (Figures 2a, c, d) are reasonably similar. However, at *ed044* and *ed340* it appears that using the most parsimonious set of factors generates more accurate results (Figures 2b, e).

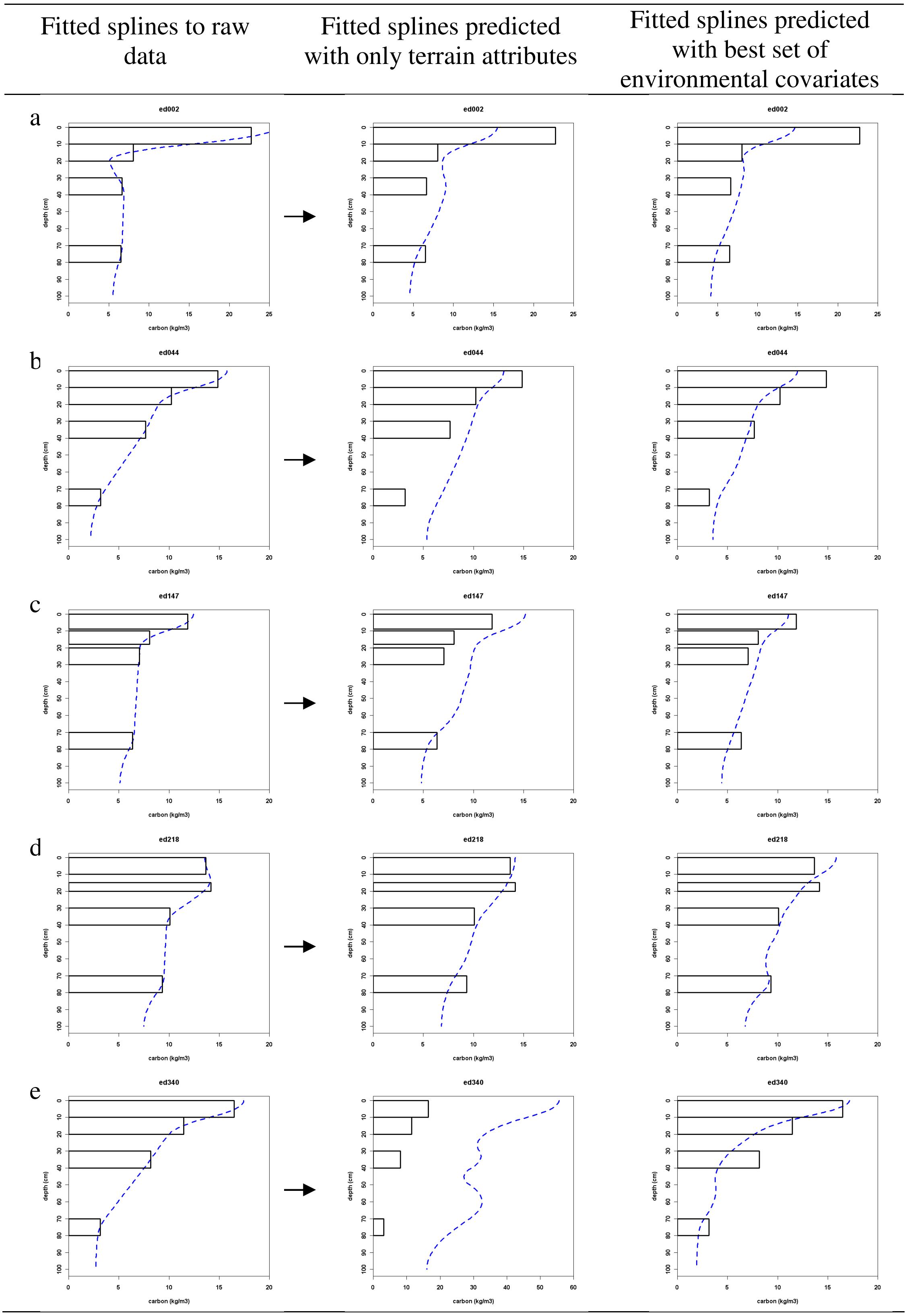

Figure 2. Fitted splines (dashed lines) of raw data and carbon predictions using either terrain attributes only or the most parsimonious set of environmental factors. (Polygons are the raw data values from McGarry et al. 1989).

The model with the best combination of environmental factors was used to map total carbon storage in the soil across the study area. Soil carbon ranged between 1–80kg m^{-2} to a depth of 1m (Figure 3). The total average carbon storage was 9.5kg m^{-2}, with the highest levels found to the eastern and southern sections of the area (8–80kg m^{-2}). These areas coincide with landuse not dedicated to cropping for example in forested areas, along watercourses and grazing areas. The cropping areas, situated in the northern and western sections of the area have the lowest carbon storage (1–7kg m^{-2}).

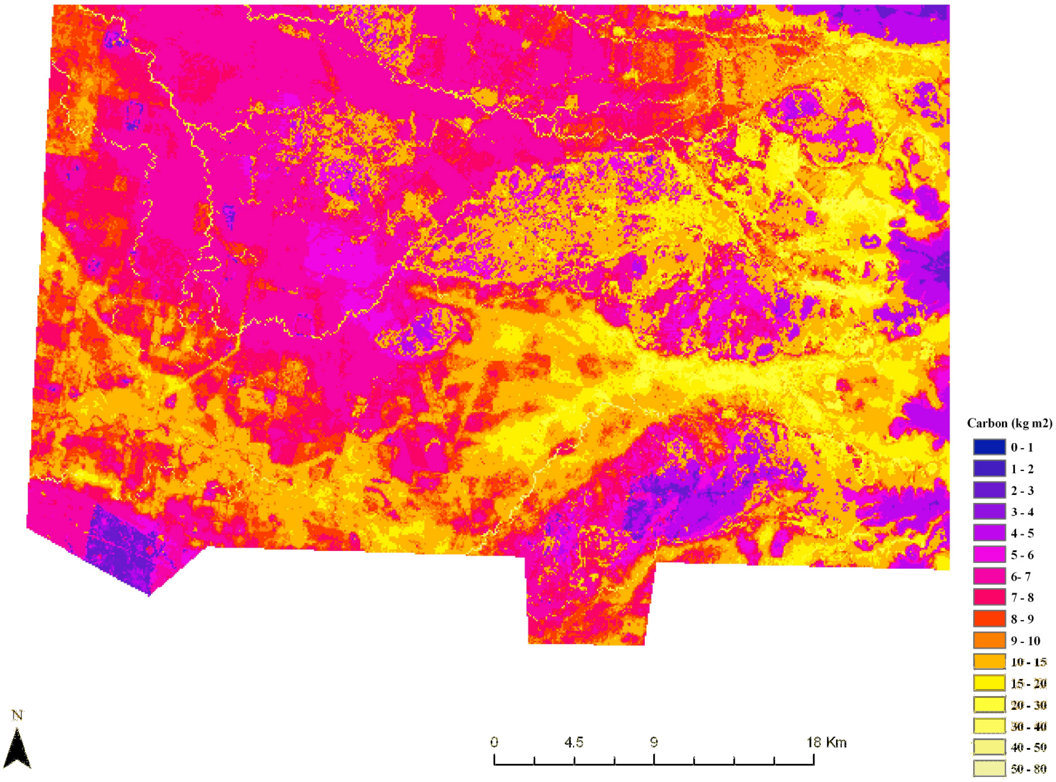

Figure 3. Total carbon storage across the Edgeroi study area.

As can be observed in Figure 4 the depth at which soil carbon drops below 1% is quite variable across the study area where it ranges from 1cm to over 1m, with the average depth at 21cm. The cropping areas situated mostly to the western areas of the study area have the highest concentration of soils where in the top 5cm, soil carbon falls below 1%. Conversely, the areas that do not appear to be cropped maintain soil carbon levels above 1% to greater depths. The range of depths at which soil carbon decreases to below 1% is much larger than that observed in the areas where cropping is practiced and would be predominantly due to land use (grazing as apposed to dense vegetation etc) and other factors such as parent materials and proximity to waterways.

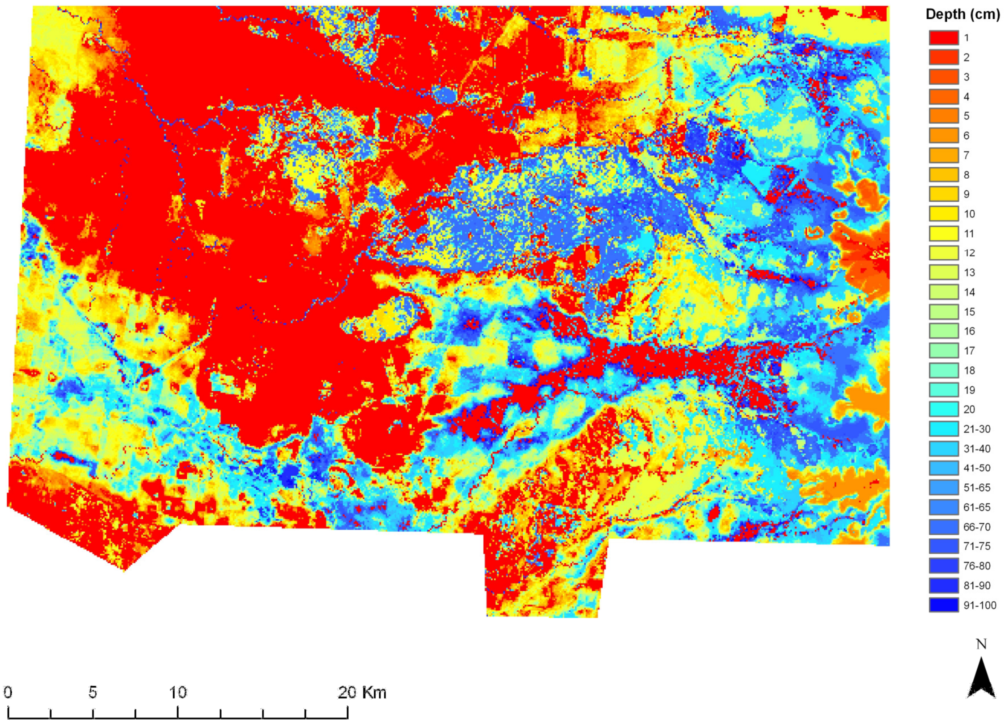

Figure 4. Depth at which soil carbon decreases to below 1% across the Edgeroi study area.

4. Discussion and Conclusions

Previous studies have identified the impact that land use has on soil carbon storage where areas under remnant vegetation have considerably more soil carbon than areas that have been cleared and used for agricultural pursuits (Knowles and Singh 2003). A similar trend was observed for this particular project. Additionally, the generated results of total carbon storage in the Edgeroi area are reflective of those of Minasny et al. (2006) who used an exponential decay to model soil carbon storage.

Alone, the terrain attributes provide a valid framework in which soil carbon can be mapped both vertically and laterally as observed by the re-constructed splines at certain points. This would indicate that the geomorphology of the study area is partly deterministic of the variation of soil carbon where elevation, slope, altitude above channel network and stream power index are important attributes. However, without the inclusion of other environmental factors the predictive accuracy of the model framework is reduced by comparison.

Nevertheless, this study provides an example where a rich soil attribute geo-database can be generated from a limited soil dataset. The functionality of this database for enquiry will suit the purposes of people concerned with the management of land. However, future work will attempt to address some of the structural and metrical uncertainty identified in this study.

References

Bishop TFA, McBratney AB, Laslett GM, 1999, Modelling soil attribute depth functions with equal-area quadratic smoothing splines. *Geoderma*, 91(1-2): 27-45.

Erh KT, 1972, Application of spline functions to soil science. *Soil Science*, 114(5): 333–338.

Knowles TA, Singh B, 2003, Carbon storage in cotton soils of northern New South Wales. *Australian Journal of Soil Research*, 41(5): 889-903.

Lagacherie P, 2008, Digital soil mapping: a state of the art. In: AE Hartemink, AB McBratney, ML Mendonca-Santos (Editors), *Digital Soil Mapping with Limited Data*. Springer Science, Australia, pp. 3–14.

McBratney AB, Mendonca-Santos ML, Minasny B, 2003, On digital soil mapping. *Geoderma*, 117(1-2): 3-52.

McGarry D, Ward WT, McBratney AB, 1986, Soil studies in the Lower Namoi Valley: methods and data. The Edgeroi Dataset. CSIRO Division of Soils, Adelaide.

Minasny B, McBratney AB, Mendonca-Santos ML, Odeh IOA, Guyon B, 2006, Prediction and digital mapping of soil carbon storage in the Lower Namoi Valley. *Australian Journal of Soil Research*, 44(3): 233-244.

Minasny B, McBratney AB, Lark MR, 2008, Digital soil mapping technologies for countries with sparse data infrastructures. In: AE Hartemink, AB McBratney, ML Mendonca-Santos (Editors), *Digital Soil Mapping with Limited Data*. Springer Science, Australia, pp. 15–30.

Ponce-Hernandez R, Marriott FHC, Beckett PHT, 1986, An improved method for reconstructing a soil-profile from analysis of a small number of samples. *Journal of Soil Science*, 37(3): 455-467.

Physiographic Classification of the Ocean Floor: A Multi-Scale Geomorphometric Approach

M. A. V. Gorini

Departamento de Geologia - LAGEMAR /UFF
Av. General Milton Tavares de Souza, 4º andar, Niterói - RJ
CEP24210-346 - Brasil
Telephone: 55 (21) 2629-5930
Fax: 55 (21) 2629-5931
Email: gorini@gmail.com

1. Introduction

Physiography, in this paper, is the study and classification of the surface features of Earth. In the oceanic domain, the Physiographic Diagram of the North Atlantic by Heezen *et al.* (1959) forged our knowledge of the actual form of the ocean basins. Since then, much has been published about the morphology of continental margins, the geology of oceanic trenches and the continuity of the mid-oceanic ridge. In most of these studies, however, the pioneer work of Bruce Heezen and his colleagues proved to be precise, despite being grounded upon sparsely collected data and a lot of "scientific imagination".

Presently, the increasing availability of high-resolution and/or globally distributed Digital Elevation Models (DEMs), together with innumerous improvements in geomorphometry – the quantitative analysis of topography – stimulates objective classifications of the physiography of landscapes. In particular, the Smith and Sandwell (1997) global digital bathymetric database represents an invaluable contribution to ocean floor mapping. However, while classifications of topography of continental landscapes (Dikau *et al.* 1991, Brabyn 1997, Iwahashi and Pike 2007), or even of planetary landscapes (Miliaresis and Kokkas 2003, Stepinski and Bagaria 2009) are becoming common subjects of geomorphometry, submarine environments are rarely investigated through quantitative geomorphological techniques (Micallef *et al.* 2007), especially at physiographic scales. Also, the basic problem in geomorphometry – the fact that all measures vary with the scale of analysis (Evans 1972) - is seldom considered in submarine mapping efforts.

Therefore, the intention of this paper is to develop and test a geomorphometric classification procedure to be applied to the global Smith and Sandwell (1997) database. The geometric signature concept - "*a set of measures that describes the topographic form well enough to distinguish among topographically disparate landscapes*" (Pike 1988) - will be used to describe the ocean floor in a multi-scale approach and to classify topography in distinct physiographic domains. The main idea is to evaluate if there can be a "recipe" for the automated identification of physiographic provinces and how such classification correlates with the established knowledge.

2. Methodology

2.1 Study Areas

A test-DEM (Fig.1A) corresponding to a broad portion of the Northwest Atlantic Ocean (centred at 35°28'35.6"N and 122°3'9.2"E) was extracted from the Smith and

Sandwell (1997) database (2 arc minutes spatial resolution) and re-interpolated to a grid spacing of 3,700 meters in Mercator projection. This area was chosen for its wide range of physiographic features in diverse geological settings, representing an appropriate sample of the world's ocean floor. In a second phase, the methodology was applied to a much more extensive DEM, encompassing the entire ocean floor between the parallels 50° S and 50° N (Fig.1B).

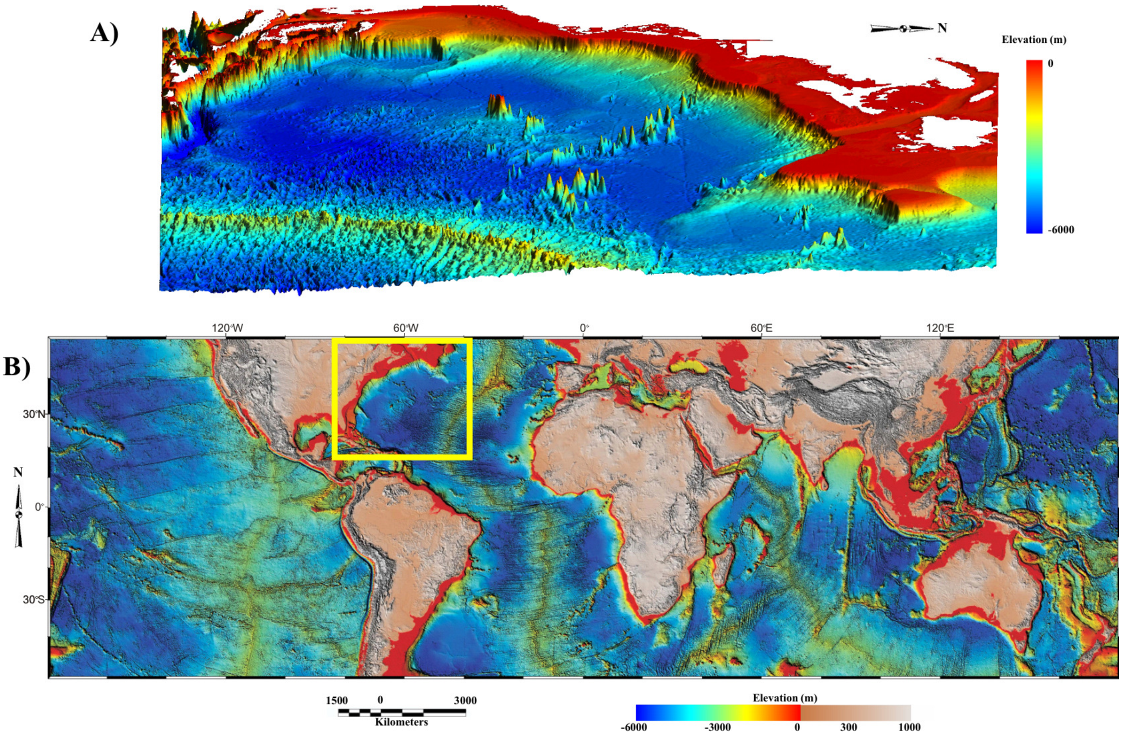

Figure 1. Oblique view of the test-DEM (A) and map of global DEM used in the application of the methodology (B - yellow box locates the test-DEM).

2.2 The Geometric Signature

In order to define appropriate variables, the *Landserf* software (©Wood, 1996–2008, http://www.soi.city.ac.uk/~jwo/landserf/landserf230/) was used for multi-scale surface parameterisation and feature extraction of the test-DEM. *Landserf* uses least squares regression to fit a quadratic surface through any arbitrary set of points, allowing surface measures to be taken for the same location over a range of spatial extents (Wood 1996).

In this way, the scale dependency of five terrain parameters (elevation, gradient, aspect, profile and plan curvature), as well as six surface features (pits, peaks, channels, ridges, passes and planes) were analysed by interactive probing through *Landserf*. A maximum spatial extent of analysis of 33x33 grid cells was considered to incorporate the majority of scale variations and, thus, used for the calculation of multi-scale variables.

These new variables summarized the behaviour of scale for each point on the surface by either (i) the mean of the surface characteristic over multiple scales to represent its central tendency or (ii) the standard deviation to represent its dispersion (Wood 1996).

This multi-scale approach yielded a three-part geometric signature (Fig.2A) – *multi-scale gradient* (mean of gradient), *roughness* (standard deviation of feature classification, *i.e.*, the scaled *entropy*) and *organization* (standard deviation of aspect) - as well as two auxiliary variables (Fig.2B) – *elevation* (scale independent) and *multi-scale profile curvature* (mean of profile curvature).

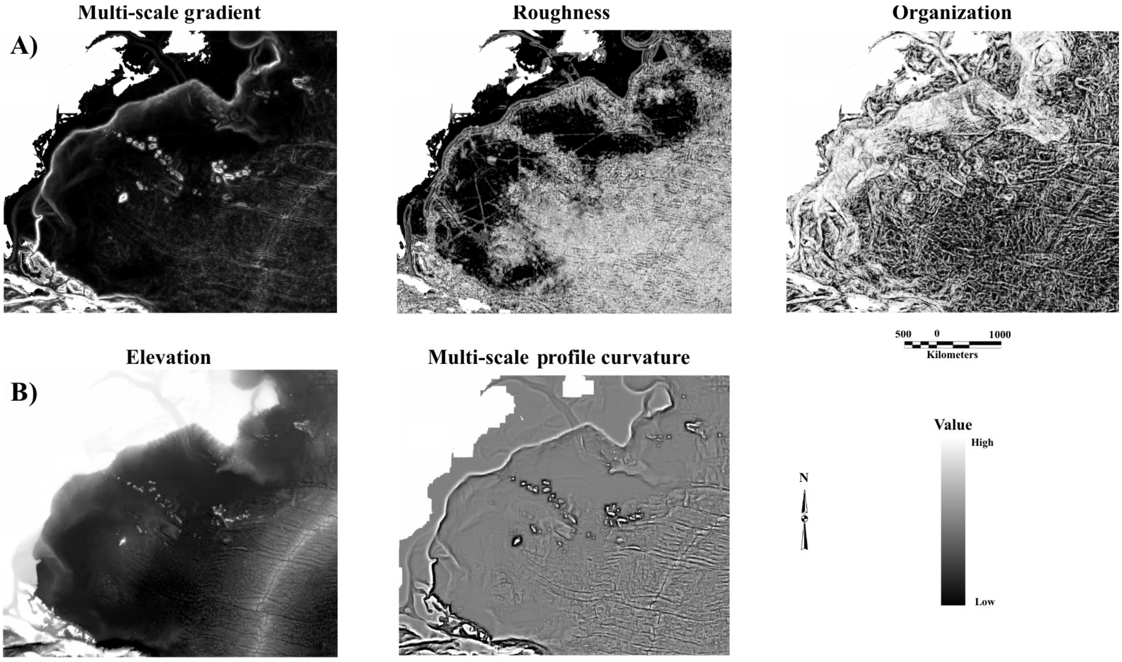

Figure 2. Greyscale images of the geometric signature (A) and auxiliary variables (B). Note the clear spatial independence of the three variables in (A).

2.3 The Classification Procedure

A classification procedure (Fig.3) was devised to combine the geometric signature with the auxiliary variables in four sequential stages. The two first stages were based on unsupervised techniques and the last two were supervised by the author's experience.

1) Initially, each attribute map was submitted to a statistical unsupervised classification algorithm (ISOCLASS) yielding morphometric classes defined by the inherent frequency distributions of each variable (Table 1). Visual and histogram analyses of the original maps indicated the optimal number of classes to be pre-set in the algorithm;

Geometric signature			Auxiliary variables	
Gradient (tg α)	Roughness (0-1)	Organization (0-1)	Bathymetry (-m)	P. Curvature (+-)
flat (< 1:82)	smooth (< 0.210)	disorganized (0.55 – 0.77)	shallow (<1,588)	concave (-)
sloping (1:82 – 1:32)	rough (0.21 - 0.50)	organized (> 0.77)	intermediate (1,588 - 3,444)	convex (+)
steep (1:32 – 1:16)	very rough (> 0.50)		deep (3,444 - 4,602)	
scarped (> 1:16)			abyssal (> 4,602)	

Table 1. Morphometric classes of the selected variables.

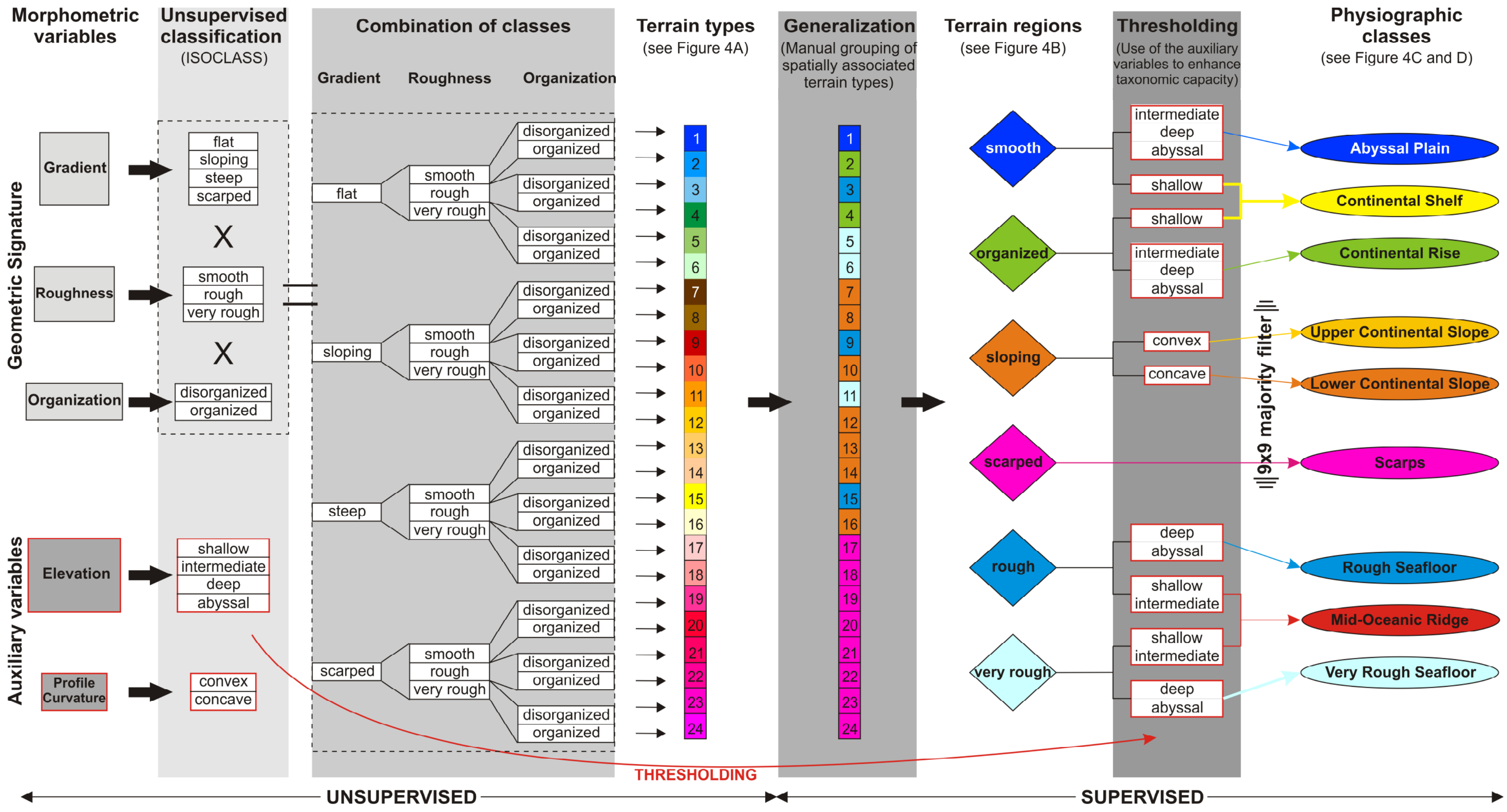

Figure 3. Flow chart of the classification procedure.

2) The resultant classes were then combined (4x3x2) to form 24 distinct terrain types (Figs.3 and 4A);

3) After that, manual grouping of spatially associated terrain types was used to generalize the classification into 6 terrain regions (Figs.3 and 4B);

4) Finally, the auxiliary variables were used as thresholds to enhance taxonomic capacity resulting in 9 physiographic classes (Figs.3, 4C and D). A 9x9 post-classification majority filter was used to consolidate scattered occurrences of classes.

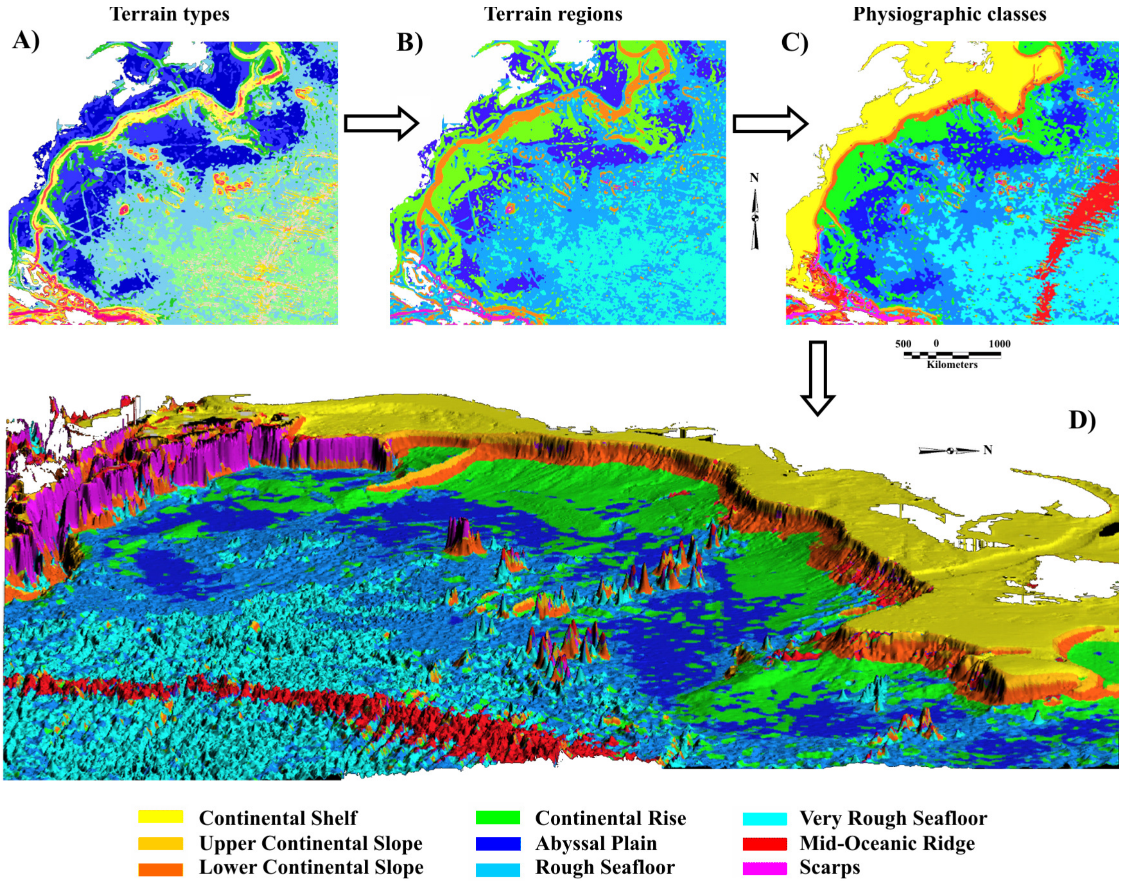

Figure 4. Classified maps of the test-DEM showing 24 terrain types (A), 6 terrain regions (B) and 9 physiographic classes (C). Oblique view of the classification draped over the test-DEM (D). See Fig.3 for colour-code of (A) and (B).

3. Results and Discussion

In order to assess the effectiveness of the classification achieved, the Physiographic Diagram of the North Atlantic (Heezen *et al*. 1959) was directly overlaid to the classified map (Fig.5). Clear similarities can be seen with respect to the spatial distribution of the continental slope, continental rise and abyssal plains, although no traditionally accepted thresholds (*e.g.* gradient of 1:40 for continental slopes and 1:1000 for abyssal plains) were used in their classification. The concentration of scarps in the southwest portion of the map indicated the association of this class with the landward slopes of trenches. Some individual seamounts were also classified as scarps.

The physiographic classes *rough seafloor* and *very rough seafloor* were defined mainly by the use of entropy as a roughness parameter but were not directly equivalent to known physiographic provinces. They are more related to distinct textures of the ocean floor where abyssal hills, the mid-oceanic ridge and its fracture zones are included. A depth threshold was necessary to individualize the mid-oceanic ridge as well as to distinguish the continental shelf among smooth and organized terrain.

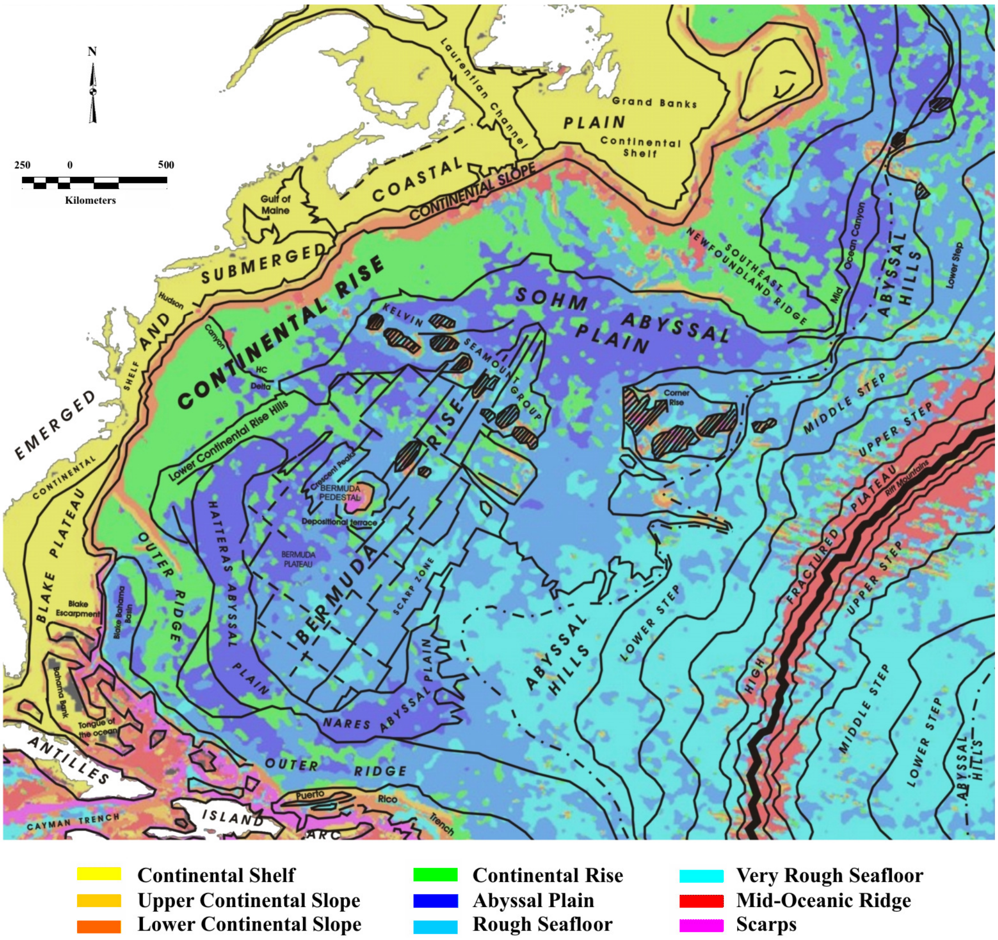

Figure 5. Visual comparison between the Physiographic Diagram of the North Atlantic (Heezen *et al*. 1959) and the present study.

The application of the classification scheme to the global DEM (Fig.6) allowed further evaluation of the methodology Continental rises and scarps concentrated, respectively, in the Atlantic and Pacific oceans differentiating passive from active margins (Fig.6C). The central portion of the mid-oceanic ridge was identified in every ocean giving a desirable structure for the classification. Different textures of the deep ocean were identified both regionally (Fig.6A and D) and locally (Fig.6B).

The selective use of auxiliary variables avoided over-segmentation of the surfaces in meaningless classes while still enhancing taxonomic capacity. The elevation parameter was not included in the geometric signature due to the directional trend of the ocean basins (down from the shoreline to the deep ocean and back up to the mid-oceanic ridge crest), which tend to create “natural” broad regions with high pattern coherence but low geomorphological content. Profile curvature was also excluded from the geometric signature for its statistical correlation with gradient and for producing local convex and concave features with limited significance for a physiographic assessment.

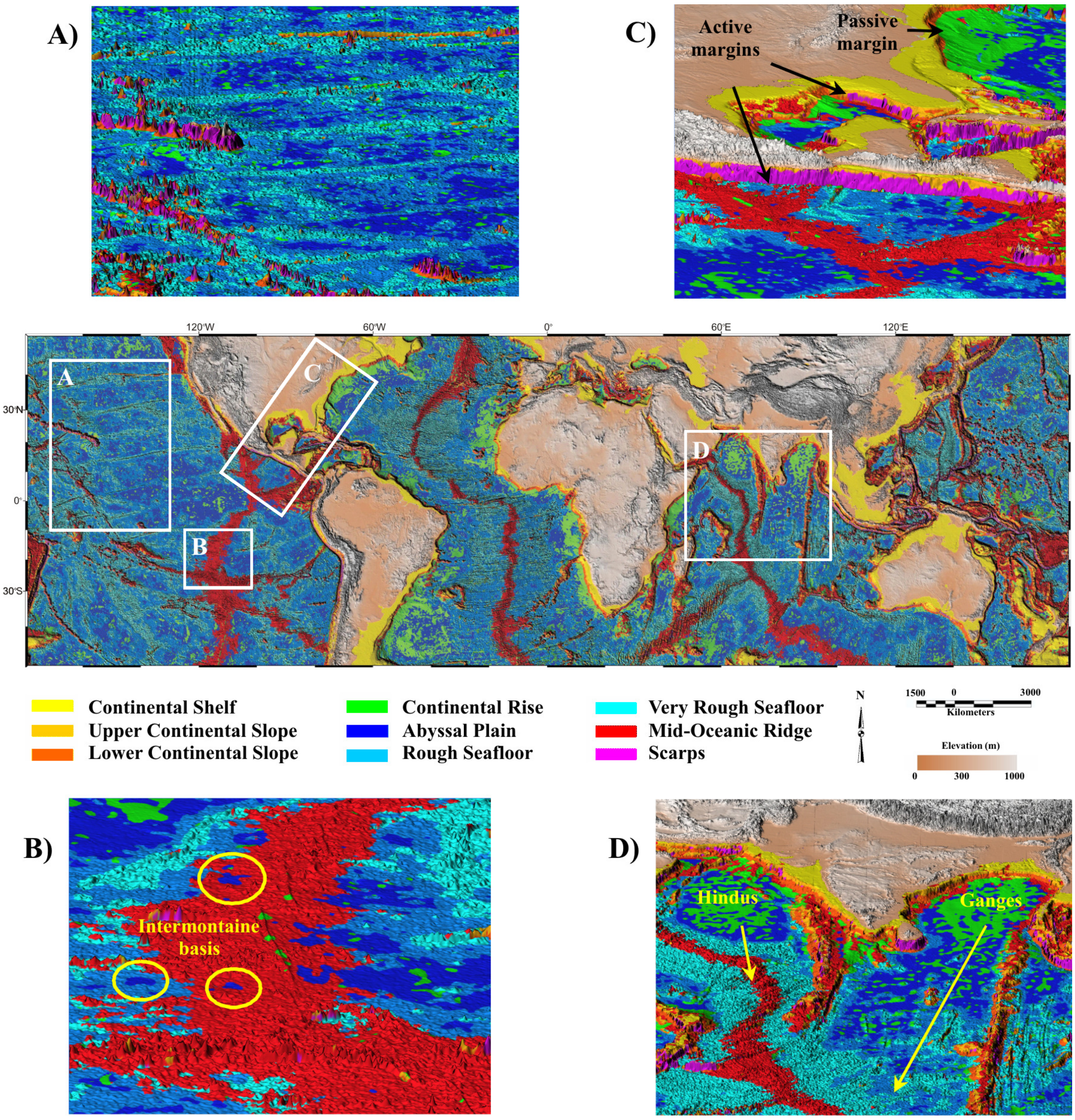

Figure 6. Global physiographic map. A) Regional pattern of rough and very rough seafloor intertwined with abyssal plains in the Pacific Ocean; B) Local intermontaine basins identified among the flanks of the mid-oceanic ridge; C) Clear differentiation between passive and active margins; D) Characterization of abrupt (Hindus Fan) and gradational (Ganges Fan) regional changes in relief.

4. Conclusions

Important geometric properties of physiographic provinces were captured by the morphometric variables used, thus allowing the consistent identification of physiographic classes through a semi-automated classification procedure. The global physiographic map showed that classes usually formed large spatial assemblages coherent with certain physiographic provinces. However, some isolated occurrences of classes were not related to a physiographic province *per se*, but to local geomorphological characteristics.

The multi-scale description attempted to cope with the influence of scale in geomorphometry but was oversimplified by a fixed limit size of analysis and by collapsing the scale variation dimension in one simple measure. More sophisticated approaches like Schmidt and Andrew (2005) that identifies dominant scales may be a good alternative for the method to better reflect the inherent *scale tendency* of the data.

While different geometric signatures should be tested to enhance taxonomic capacity, it is hard to believe that the spatial arrangement of the classes alone will define all the physiographic provinces. Not only the use of auxiliary variables proved to be essential, but it also indicated that each physiographic province may have its own unique set of descriptors, which should be investigated in further development of the method. This objective reassessment of the physiography of the ocean floor, far from contradicting the established knowledge, may represent a path for new discoveries and, without doubt, many new questions.

Acknowledgements

I thank Marcus Gorini, Ph.D. for his unconditional support and inspiration. I also thank the entire MAG staff for all the scientific conversations and pleasant work environment.

References

Brabyn LK, 1997, Classification of macro landforms using GIS. International Institute for Geo-information Science and Earth Observation Journal 1: 26–40.

Dikau R, Brabb EE and Mark RK, 1991, Landform Classification of New Mexico by Computer. Open-File Rep. (U. S. Geol. Surv.) 91–634 15 pp.

Evans IS, 1972, General geomorphometry, derivatives of altitude and descriptive statistics. In: Chorley, RJ (Ed.), Spatial Analysis in Geomorphology. Harper & Row, London, pp. 17–90.

Heezen BC, Tharp M and Ewing M, 1959, The floors of the oceans, 1: The North Atlantic. The Geological Society of America Special Paper, 65, 122p.

Iwahashi J and Pike RJ, 2007, Automated classifications of topography from DEMs by an unsupervised nested means algorithm and a three-part geometric signature: *Geomorphology*, doi:10.1016/j.geomorph.2006.09.012, in press.

Micallef A, Berndt C, Masson DG and Stow DAV, 2007, A technique for the morphological characterization of submarine landscapes as exemplified by debris flows of the Storegga Slide: *Journal of Geophysical Research*, vol.112, F02001, doi: 10.1029/2006JF000505.

Miliaresis G and Kokkas N, 2003, The geomorphometric signature of Valles Marineris from M.O.L.A DEM. American Society for Photogrammetry & Remote Sensing, Anchorage, Alaska, 5-9, 9 p.

Pike RJ, 1988, The geometric signature: quantifying landslide-terrain types from digital elevation models. Math. Geol. 20: 491–511.

Schmidt J and Andrew R, 2005, Multi-scale landform characterization. Royal Geographical Society (with The Institute of British geographers), 37(3): 341-350.

Smith WHF and Sandwell DT, 1997, Global seafloor topography from satellite altimetry and ship depth soundings, Science, v. 277, p. 1956-1961.

Stepinski TF and Bagaria C, 2009, Automatic mapping of martian physiography: application to Tharsis region. 40th Lunar and Planetary Science Conference, Houston, USA.

Wood J, 1996. The geomorphological characterisation of digital elevation models. PhD Thesis, University of Leicester, UK. Web publication available at this URL address http://www.soi.city.ac.uk/~jwo/phd/.

Proceedings of Geomorphometry 2009. Zurich, Switzerland, 31 August - 2 September, 2009

Global Survey of Organized Landforms: Recognizing Linear Sand Dunes

P. L. Guth[1]

[1] Department of Oceanography, US Naval Academy
572C Holloway Rd, Annapolis MD 21402 USA
Telephone: 00-1-410-293-6560
Fax: 00-1-410-293-2137
Email: pguth@usna.edu

1. Introduction

The Shuttle Radar Topography Mission (SRTM) provided an unrivalled view of Earth's topography and a rich data set for geomorphometry (Farr et al. 2007). The 30" overview data set shows regional trends and can fit on a single CD-ROM, and the 3" local data set shows an incredible amount of detail with required storage of about 35 GB. The increasing availability of 1 meter Lidar topography highlights the possibility of looking at landscapes at a wide range of scales; SRTM provides the big and medium pictures for looking at the entire world or individual continents.

Guth (2007) described the creation of a geomorphometric atlas from the 3" data. This paper will use that atlas to look at terrain organization, focusing on the identification of linear dune fields (Lancaster 1995).

2. Geomorphometric Atlas

The earth’s land surface between 60°N and 56°S contains about 7.4 million blocks 2.5’ (arc minutes) on a side. The blocks range in size from 4.6 x 4.6 km at the equator, to 4.0 x 4.6 km at 30° latitude, and 3.0 x 4.6 km at 60° latitude. The atlas contains grids for 37 parameters (Evans 1998; Pike 2001), computed from 2601 points in each block, sufficient for robust statistics describing terrain. Each data grid contains 8640x2784 values, about 70% of which are voids covering the oceans. The atlas allows color coding each parameter on a map, as well as the creation of filters based on selected values for any parameter, and rapidly combining filter results.

Terrain organization (Guth 2003) provides a key characteristic to identify several categories of terrain, including drumlin fields, folded mountains, fault block mountains, and linear dune fields (Guth 2007). Organization measures the tendency for ridges and valleys to share the same spatial orientation. Drumlin fields may not have a large enough spatial scale for identification in the geomorphometric atlas, but this study will use to the atlas to locate and identify large linear dune fields.

3. Linear Dunes

Lancaster (1995) described three categories of linear dunes (Table 1). Despite some overlap in size measures, the three types generally reflect an increase in all three size measures. Figure 1 shows an SRTM shaded relief map and a topographic profile across complex dunes in Saudi Arabia. While simple dunes clearly show up in the SRTM 3 second data , they may be difficult to discriminate because the smaller wavelengths include only a few 90 m grid postings, and the dune height approaches the inherent radar speckle in flat regions. This work therefore seeks to investigate the geomorphometry of compound and complex linear dunes.

Linear Dune Type	Spacing (m)	Width (m)	Height (m)
Simple	430-2346	220-290	4-21
Compound	990-2080	650-940	24-48
Complex	1500-3300	900-1500	40-200

Table 1. Linear dune statistics (after Lancaster 1995).

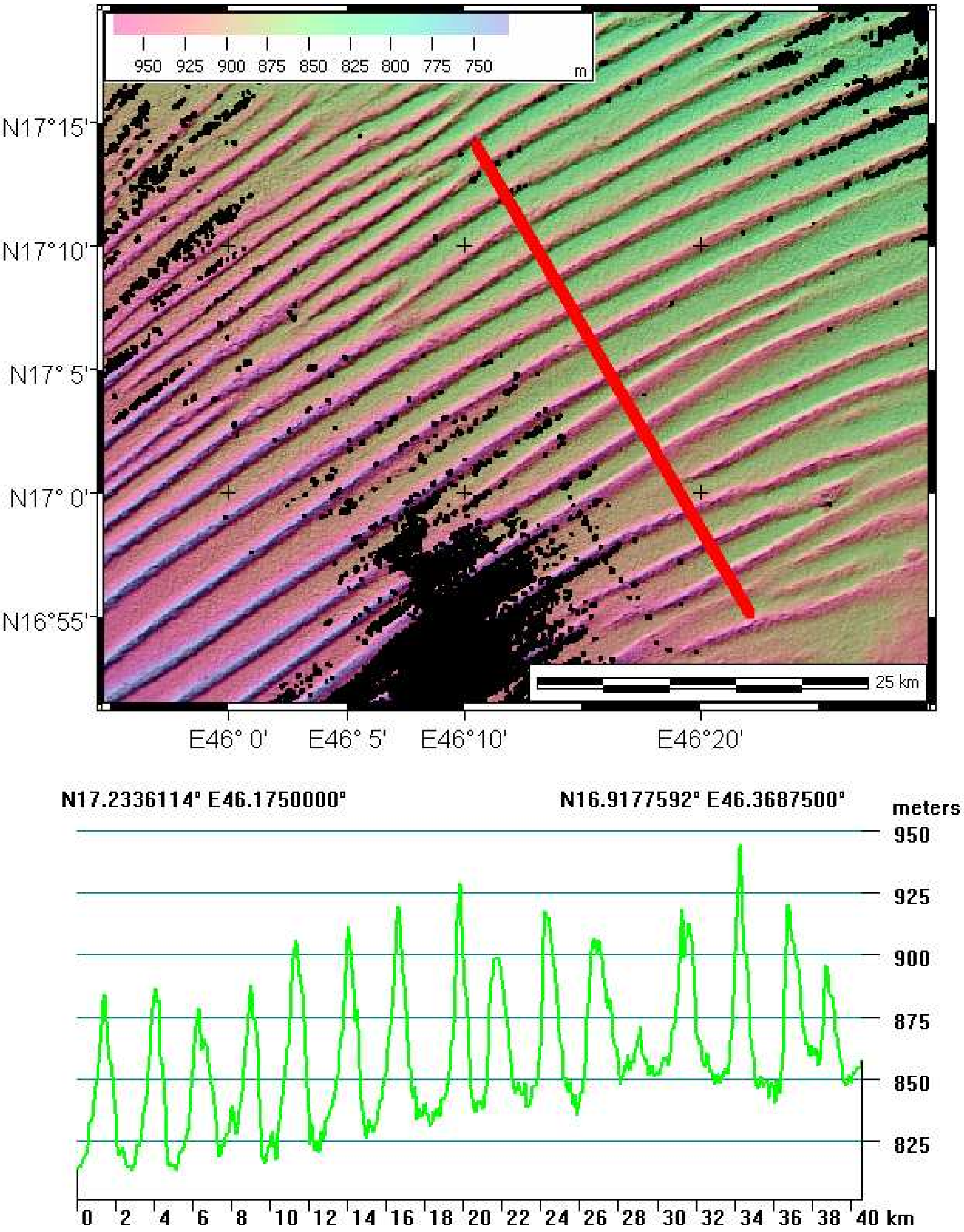

Figure 1. Complex dunes in southwestern Saudi Arabia in map view and profile. The tallest dunes are about 100 m high.

4. Methods

Geomorphometric parameter maps can be viewed in conjunction with maps derived form SRTM-30 and SRTM-3, with colored symbols from the atlas overlaid on grayscale shaded relief to provide context, or on satellite imagery. Where necessary, Google Earth provides rapid access to high quality imagery to verify interpretations. Initial examination of the global terrain organization map, focusing on the high values, shows that large linear dune fields are among the features that stand out.

An initial classification identified dune regions, and Figure 2 shows bivariate scatter plots for 25 geomorphometric parameters from the atlas. Each parameter appears in a column and a row, with the principal diagonal showing the parameter plotted against itself. The gray color indicates the entire data set, and the red the linear dune fields. Parameters that do a good job discriminating linear dunes should show a tight distribution of the red points. Similar graphs with univariate histograms show how the linear dunes compare with other landforms for values of a single parameter.

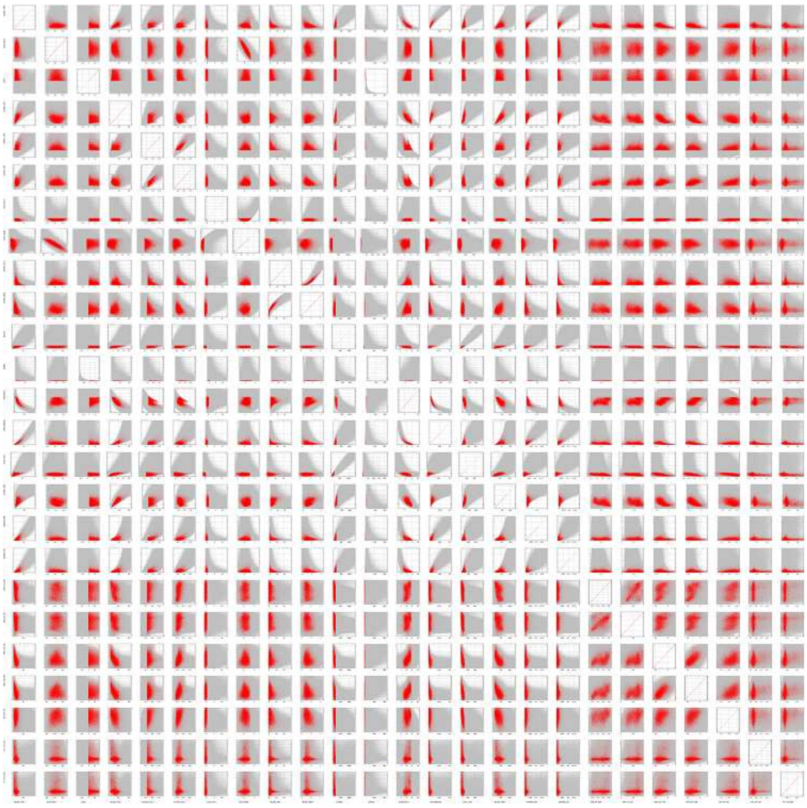

Figure 2. Bivariate scatter plots for 25 parameters, with linear dunes in red and all SRTM data in gray.

Selection of parameter values can use either the absolute value, or the percentile range which avoids problems with some extreme values in the data set related to SRTM holes and other statistical anomalies. Figure 3 shows the approximately highest 10% of cells in terms of terrain organization, and three other parameters selected because they appear to discriminate dunes from other features. Homogeneity, the kurtosis of the elevation distribution, easily differentiates linear dunes from star or isolated dunes. Curvature in profile, the standard deviation of the profile curvature distribution, and relief, further appear to differentiate linear dunes. Table 2 shows the parameters selected for dune discrimination.

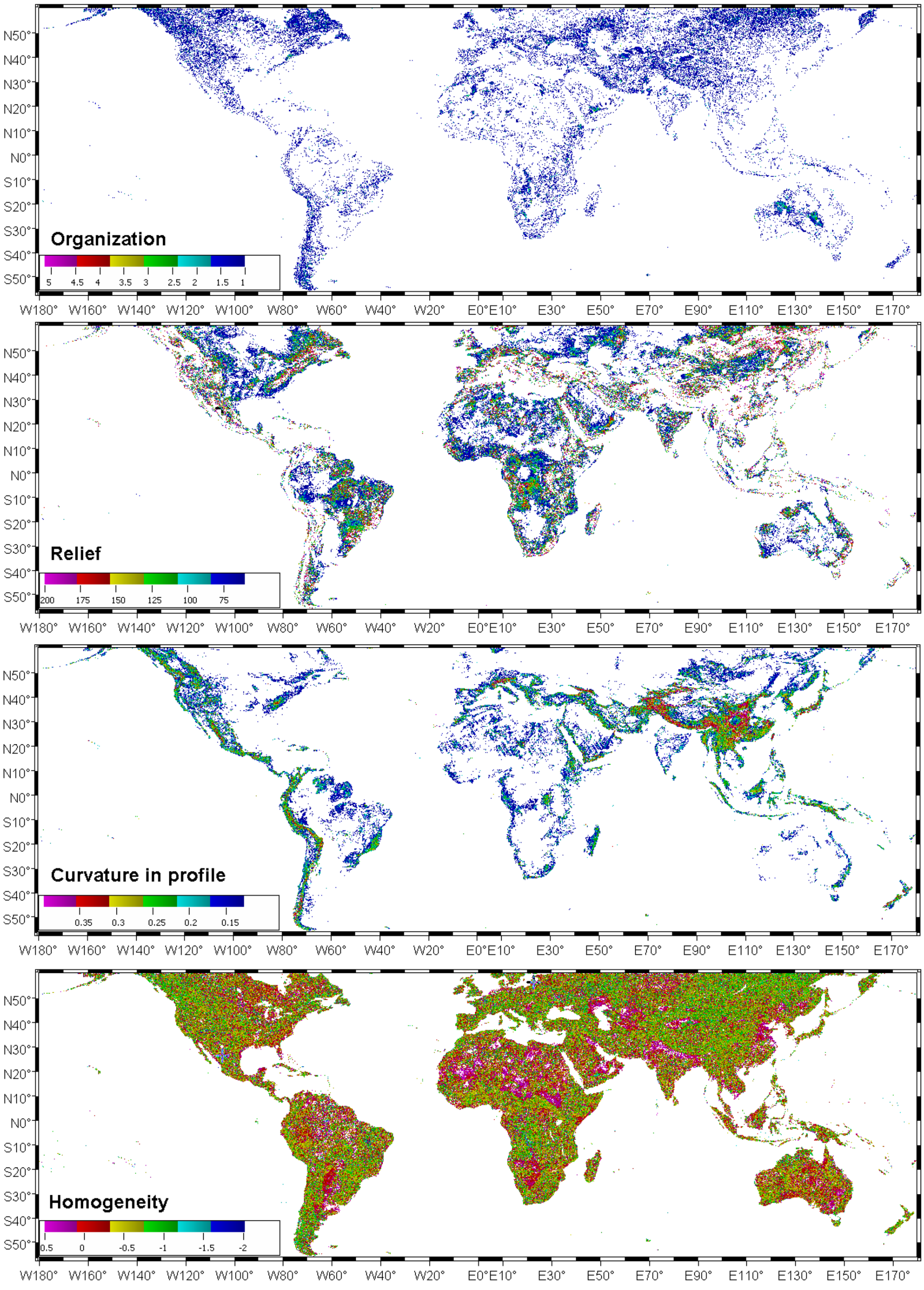

Figure 3. Four of the parameters used to identify linear dune fields. Colored points show locations that match the individual criteria; the map display exaggerates the proportion of the earth's surface actually matching each criterion.

We created masks for each parameter for the cells that matched the criteria, and then combined masks to find candidate regions. Because of the noise in the resulting maps, we filtered the data to find all cells that had at least 65 neighbours within an 11x11 neighbourhood (54% of the region) that met the criteria. This meant that we were looking for dune fields covering 50 x 50 km at the equator, 44 x 50 km at 30° latitude, and 33 x 50 km at 60° latitude

Parameter	Range	Percentile Range
Organization	1 to 5.15	88.8 to 99.9
Relief	60 to 200	41.4 to 71.8
Steepness (Average slope)	3 to 25	45.2 to 89.8
Homogeneity (elevation kurtosis)	-2.02 to 0.5	0.1 to 75.1
Massiveness (elevation skewness)	0.1 to 50.94	41.9 to 99.9%
Curvature in profile (standard deviation)	0.12 to 0.4	73.1 to 99.6

Table 2. Parameters used to classify dunes.

5. Results

Table 3 shows the results of using 4 combination of parameters. All cases use organization, average slope, and relief. The raw matches show the number of cells meeting the criteria out of the 4.7 million in the world covered by the SRTM, and the region matches show the number that belong to a region, typically about 10% of the raw matches. Figure 5 shows the results for the three parameter solution, and regional matches clearly remove a great deal of noise with isolated cells (so that they appear on the map, the size of the matches are exaggerated for display). While the three parameter model located a number of dune fields in the northern hemisphere desert belt, it also identified a large region east of Hudson Bay (Figure 6) and a number of regions along the coasts of the Black Sea, Caspian Sea, and similar latitudes farther east in central Asis. Table 3 and Figure 6 show that adding the standard deviation of profile curvature does the best job of removing these non-dune regions.

Figure 6 shows the dune fields identified with this algorithm. Google Earth imagery confirms that all regions shown in green represent large linear dune fields.

Parameters	Raw Matches	Region Matches
Organization, average slope, and relief	223,566	21,323
Organization, average slope, relief, and **elevation kurtosis**	171,357	13,650
Organization, average slope, relief, and **elevation skewness**	133,211	9103
Organization, average slope, relief, and **standard deviation of profile curvature**	32,379	4464

Table 3. Classification results with 4 combinations of parameters.

Although not obvious at the scale of Figure 3, the curvature map shows anomalies in the SRTM processing that follow the shuttle orbital pattern (Guth 2006). Figure 8 shows 3 arc second SRTM elevation data, overlaid with regional atlas data for organization and profile curvature. Large square symbols meet the criteria for linear dunes, and small triangles do not; the colors show the value of the parameter. The diagonal patterns of SRTM holes repeat at about 60 km spacing, which match the width of the four portions of the 225 km SRTM swath width. Particularly for the curvature in profile parameter, alternating bands have low values (which do not meet the dune field criteria) and higher values (which do meet the criteria).

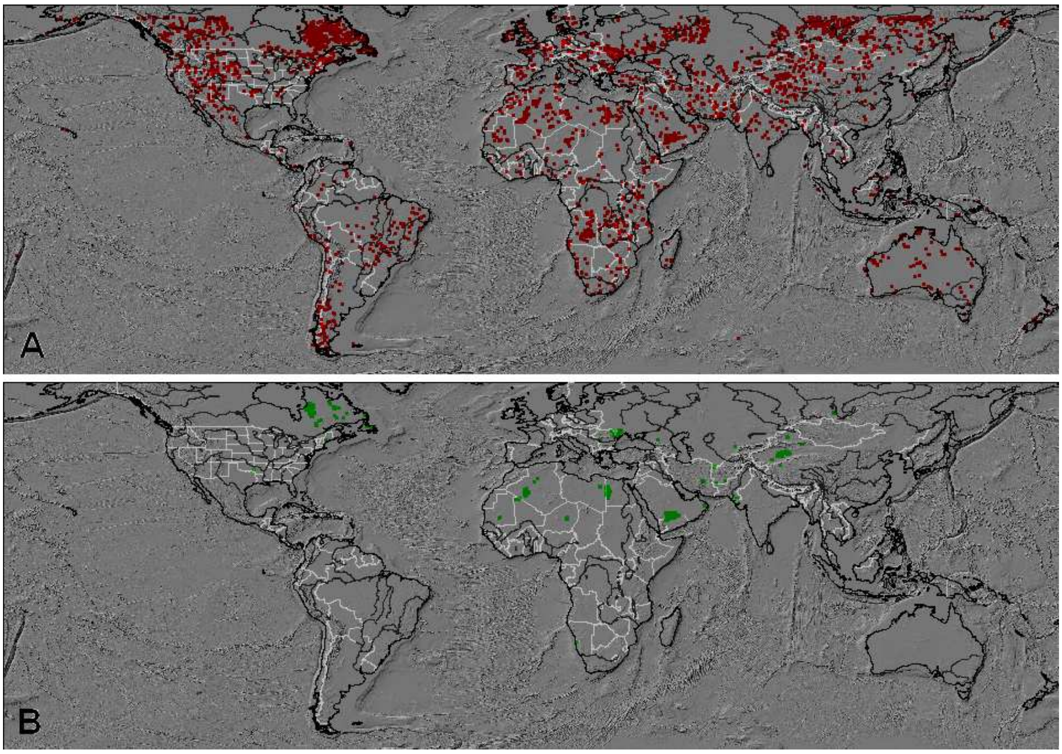

Figure 4. Classification using organization, average slope, and relief. Figure 4A shows the raw matches, and Figure 4B the filtered regional matches.

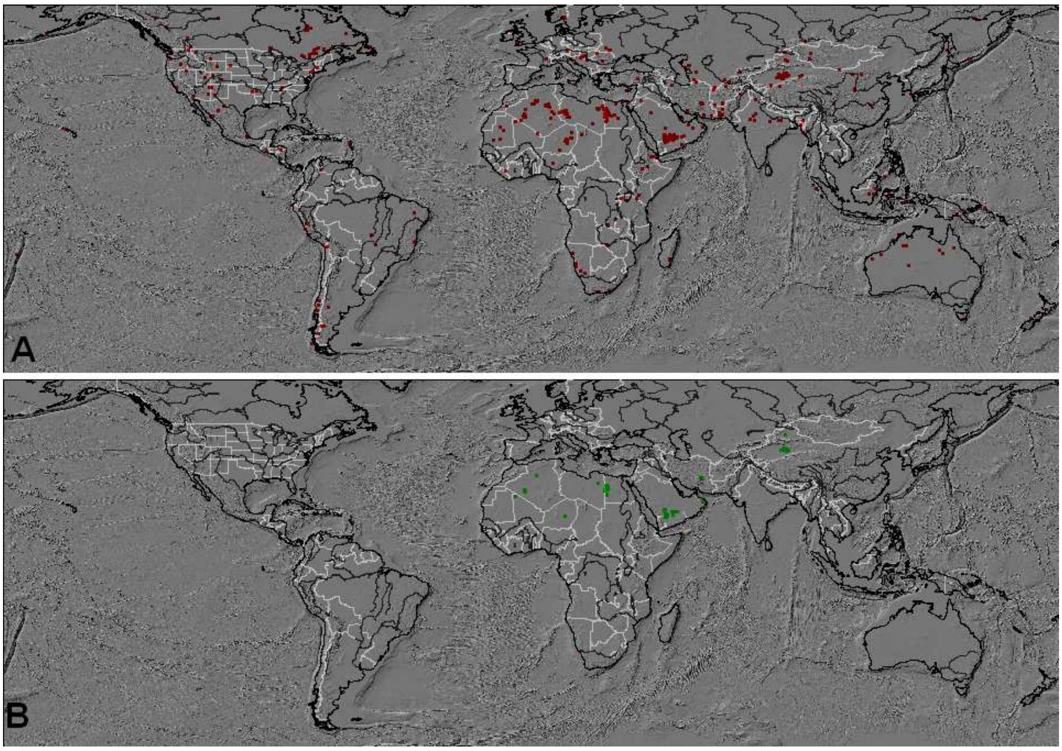

Figure 5. Classification using organization, average slope, relief, and standard deviation of profile curvature. Figure 5A shows the raw matches, and Figure 5B the filtered regional matches.

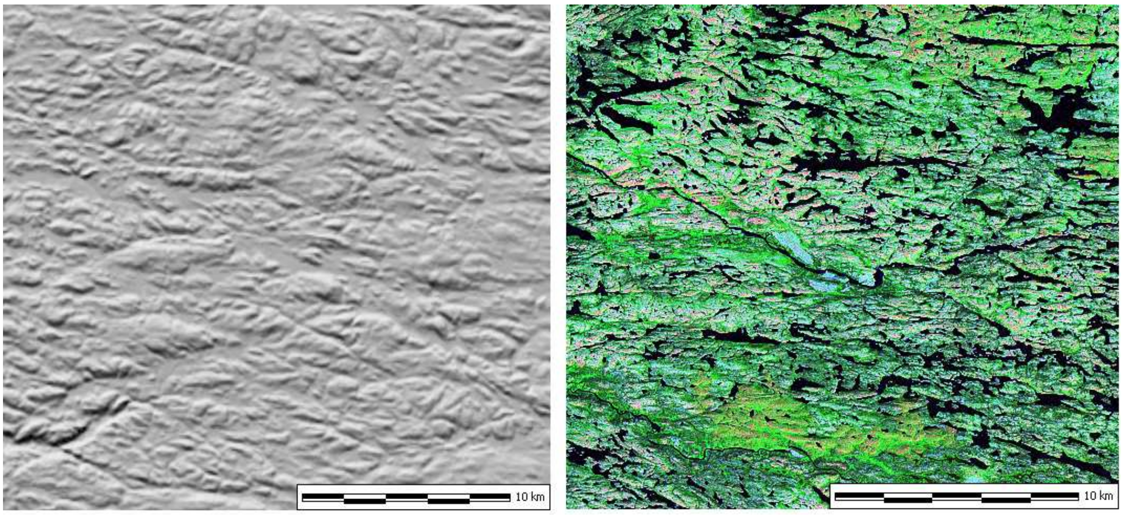

Figure 6. Glacial topography east of Hudson Bay, in shaded relief from the SRTM 3" dataset on the left and the Geocover 2000 Landsat imagery on the right.

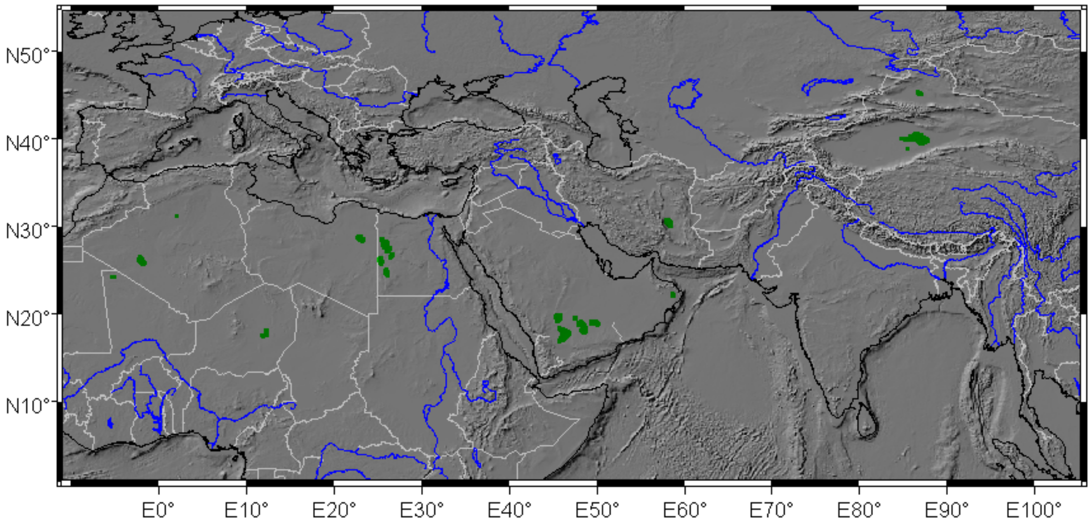

Figure 7. Blowup of Figure 5B, showing the large linear dune fields identified using geomorphometric criteria.

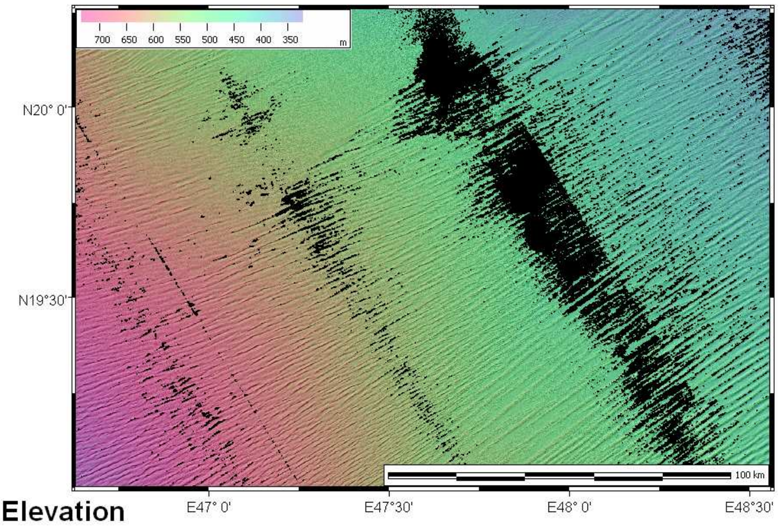

Elevation

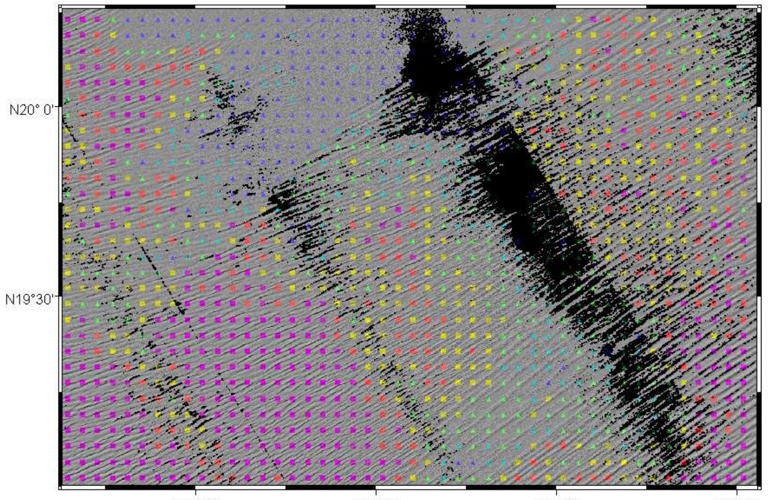

Organization

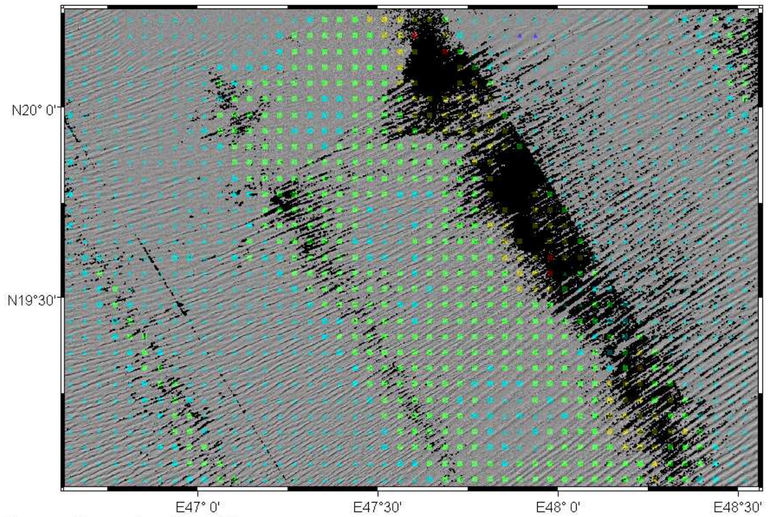

Curvature in Profile

Figure 8. Map of a region in southwestern Saudi Arabia that includes Figure 1. The elevation map shows SRTM-3" data, and the bottom two maps overlay organization and curvature in profile.

6. Future Work

Figure 9 shows complex dunes in the Rub' al Khali region in southeastern Saudi Arabia. These are taller, and less linear than those shown in Figures 1 and 8, and in fact the algorithm does not identify much of this area as being composed of linear dunes. Additional work will focus on (1) better identifying large complex dunes and small simple dunes; (2) adjusting the criteria ranges, or adding additional criteria to reliably identify smaller regions of linear sand dunes; and (3) extending the work to additional categories of landforms, such as drumlins and folded mountains. Finally, we would like to quantify the results, which will require an independent digital data set with the locations of specific landforms.

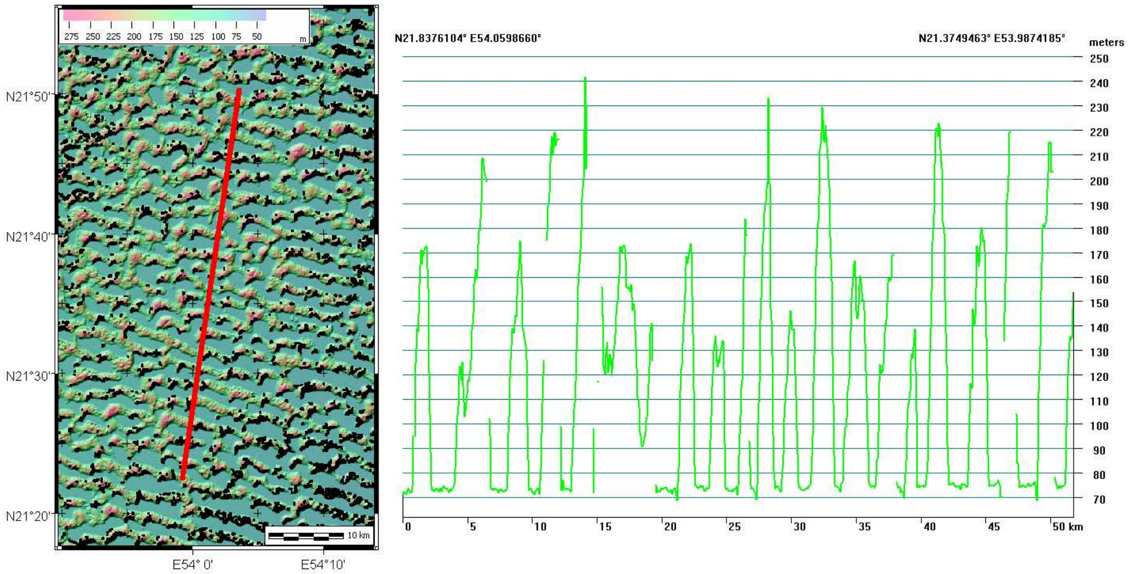

Figure 9. Complex dunes in the Rub' al Khali region in southeastern Saudi Arabia. These dunes are much taller and less linear than those successfully identified by the current algorithm.

Acknowledgements

This work used the freeware MICRODEM program (Guth 2008). It would not have been possible without the partnership between NASA and NGA (then NIMA) to create the SRTM dataset. I thank the three reviewers for helpful comments on the manuscript.

References

Evans, IS, 1998, What do terrain statistics really mean?, In Lane, S.N., Richards, K.S., and Chandler, J.H., (Eds.) *Landform monitoring, modelling and analysis*, J.Wiley, Chichester, 119-138.

Farr, TG, Rosen, PA, Caro, E, and 15 others, 2007, The shuttle radar topography mission: *Reviews of Geophysics*: 45(2): RG2004, doi:10.1029/2005RG000183.

Guth, PL, 2003, Eigenvector analysis of digital elevation models in a GIS: Geomorphometry and quality control: in Evans, I.S., Dikau, R., Tokunaga, E., Ohmori, H., and Hirano, M., eds., *Concepts and Modelling in Geomorphology: International Perspectives*: Terrapub Publishers, Tokyo, 199-220.

Guth, PL, 2006, Geomorphometry from SRTM: Comparison to NED**:** *Photogrammetric Engineering & Remote Sensing*, 72(3): 269-277.

Guth, PL, 2007, Global SRTM geomorphometric atlas: Geocomputation 2007, NUI Maynooth, Ireland, 3-5 September 2007, 6 page paper #P07 on Conference proceedings on flash drive.

Guth, PL, 2008, Geomorphometry in MICRODEM, In Hengl, T., Reuter, H.I. (eds), *Geomorphometry: concepts, software, applications:* Developments in Soil Science Series, Elsevier, 351-366.

Lancaster, N, 1995, *Geomorphology of desert dunes*: London, Routledge, 290 p.

Pike, RJ, 2001, Geometric signatures—Experimental design, first results, In Ohmori, H., ed., DEMs and Geomorphometry, *Special Publications of the Geographic Information Systems Association, Proceedings of the symposia on New Concepts and Modeling in Geomorphology and Geomorphometry*, *DEMs and GIS*, held 24-26 August, 2001, Tokyo, Fifth International Conference on Geomorphology, ISSN 1346-7417, Vol.1, 50-51.

Worldterrain – A Contribution to the Global Geomorphometric Atlas

H. I. Reuter[1], A. D. Nelson[2]

[1]Independent spatial consultant
Fax: (+49-3212-8912839)
Email: gisxperts@web.de

[2] Independent spatial consultant
Email: dr.andy.nelson@gmail.com

1. Introduction

A Digital Elevation Model (DEM) is one of the most useful sources of information for spatial modeling and monitoring, with applications as diverse as: Environment and Earth Science, e.g. catchment dynamics and the prediction of soil properties; Engineering, e.g. highway construction and wind turbine location optimisation; Military, e.g. land surface visualisation, and; Entertainment, e.g. landscape simulation in computer games (Hengl and Evans 2007). The extraction of land surface parameters – whether they are based on 'bare earth' models such as DEMs derived from contour lines and spot heights, or 'surface cover' models derived from remote sensing sources that include tree top canopies and buildings for example – is becoming more common and more attractive due to the increasing availability of high quality and high resolution DEM data (Gamache 2004).

Global DEM datasets are available in a different variety of resolutions. At 1km resolution the GTOPO30, GLOBE, SRTM30 and ACE2 datasets are available. However certain processes and function can only be detected at much finer scales. One of the most widely used DEM data sources is the elevation information provided by the 90m resolution Shuttle Radar Topography Mission (SRTM) (Coltelli et al. 1996, Farr and Kobrick 2000, Gamache 2004). A new 30m DEM of the world is expected to be released in June 2009 based on 1.5 Million single ASTER DEM scenes covering the whole world.

This detailed elevation data can be used to generate a geomorphometric atlas, which is particularly useful as a resource of surface measures and objects in support of decision-making and projects over a broad spectrum of applications (Gessler et al, 2007). Several attempts have been made - for example the USGS global 1 km HYDRO1k Elevation Derivative Database or the River and Catchment Database at 250 m for Europe (Vogt et al., 2003). Guth (2009) already showed some results for a SRTM based high-resolution continental geomorphometric atlas. The work performed did not contain some of the number of criteria that these dataset should inherit (Gessler et al. (2007): 1) precision, 2) multi scale, 3) open structure, 4) web access and 5) quality. However with the current datasets usually these parameters are not satisfied. Additional important points are the reuse of the generated parameters and the description in terms of metadata. This is of outmost importance as different software packages - even different versions of the same software - produce different results.

This paper describes a procedure to generate a geomorphometric atlas, which as a start will fulfill several of these criteria. The atlas is extendable to include additional parameters, whereupon suitable algorithms could be chosen to map them. The objective is to provide a standardized workflow and format, which can accommodate the expected growth in Geomorphometry applications in the future.

2. Method

The method projects a given input DEM (SRTM) to a UTM projection using a cubic convolution algorithm. Secondly, it checks for a spikes and sinks above/below 100 compared to its surrounding and filters them out if possible. Third, it calculates terrain parameters (TP) and aggregates them to specified commonly used resolutions (i.e. matching the resolutions of existing environmental datasets: 250m, 500m, 1km and 10km). There is no single source for a global high resolution DEM, but the SRTM data comes close. SRTM has an approximate resolution of 90 m and covers all land masses between 60N and 60S. If a more detailed global datasets appears (e.g. ASTER GDEM), then the smallest reported resolution could be as small as 100m. For local conditions (e.g. LiDAR data of 1 m resolution) the reporting resolution could be even more detailed: 5, 10 and 50 meters for example.

In the current version the calculated parameters include elevation, aspect, slope, profile curvature, plan form curvature, flow direction, flow accumulation, ridges, and a number of elevation residuals at different window sizes reflecting various landscape scales . Additionally, since the parameters are computed at fine scale and then aggregated, we report for each given output cell the following statistical parameters: Minimum, Maximum, Mean, Median, Standard Deviation, Range, Sum and for integer TP also the Majority and Minority Values. An example for a derived TP in its original resolution is given in Figure 1.

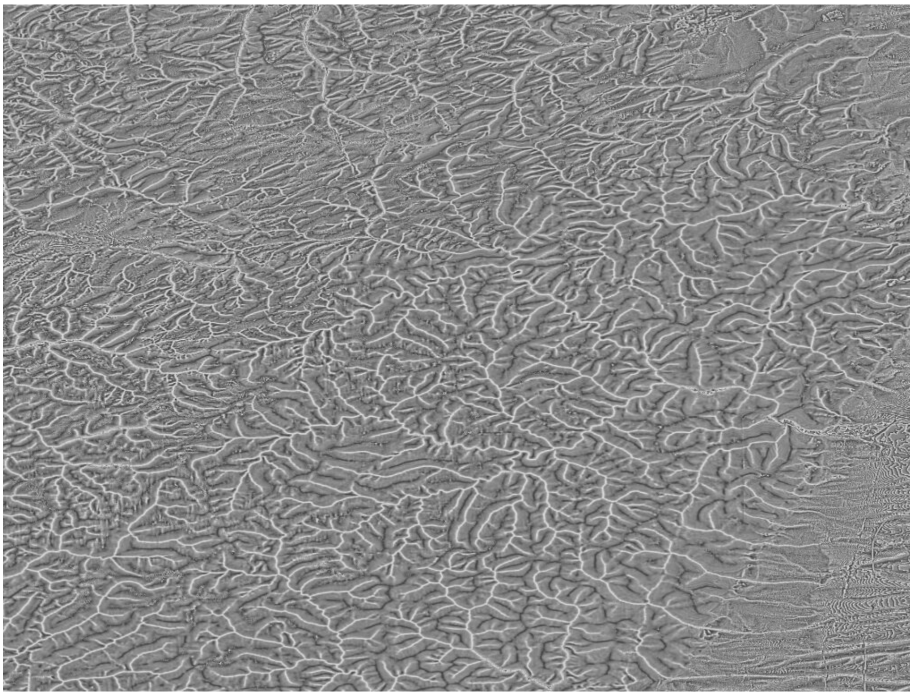

Figure 1 Deviation for a 5 x 5 window for a DEM

A aggregated version of the elevation values calculated from SRTM for some parts of the tropics in danger for deforestation is shown in Figure 2.

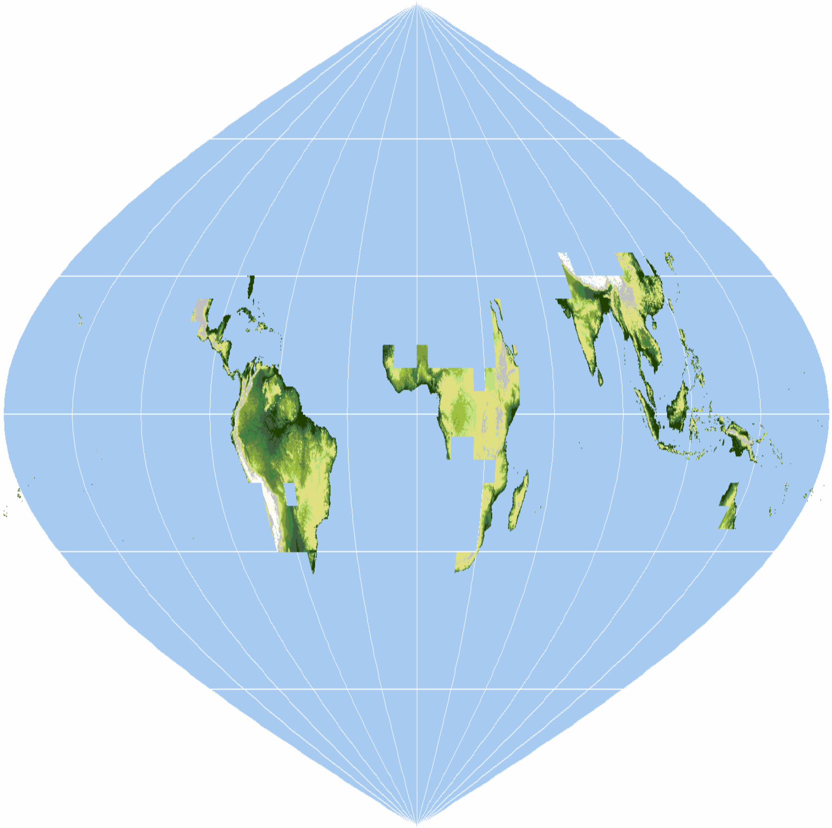

Figure 2 Mean Elevation at 1km resolution generated from SRTM for the tropics.

3. Conclusion

The Geomorphometric Atlas will deliver essential parameters for understanding global, regional and local problems and solutions for example for the global soil map project (www.globalsoilmap.net) for fighting poverty in Africa, for understanding deforestation in the tropics or for calculations of travel times to major cities (Nelson, 2008). We expect that with the increase in computer power the calculations will evolve and new algorithms/sensors will allow for decision making in different spatial-temporal scales. The atlas will fill an important gap and aims to become a key dataset for environmental and socioeconomic applications.

References

Coltelli, M., Fornaro, G., Franceschetti, G., Lanari, R., Migliaccio, M., Moreira, J. R., Papathanassiou, K. P., Puglisi, G., Riccio, D. and Schwabisch, M., 1996, SIR-C/X-SAR multifrequency multipass interferometry: A new tool for geological interpretation, *Journal of Geophysical Research*, 101, 23127-48.

Farr, T. G. and Kobrick, M., 2000, Shuttle Radar Topography Mission produces a wealth of data, *American Geophysical Union*, 81, 583-85.

Gamache, M., 2004, Free and Low Cost Datasets for International Mountain Cartography, Available online at: http://www.icc.es/workshop/abstracts/ica_paper_web3.pdf (accessed 01/08/2006).

Gessler, P., Pike, R.J., MacMillan,R.A., Hengl, T.,Reuter,H.I., 2008, The Future of Geomorphometry. In: Hengl, T. and Reuter, H.I. (Eds), Geomorphometry: Geomorphometry: Concepts, Software, Applications. *Developments in Soil Science*, vol. 33, Elsevier, 637-652.

Guth, P., 2008. Geomorphometry in MicroDEM. In: Hengl, T. and Reuter, H.I. (Eds), Geomorphometry: Geomorphometry: Concepts, Software, Applications. Developments in Soil Science, vol. 33, Elsevier, 351-366.

Hengl, T. and Evans, I. S., 2008, Geomorphometry: A brief guide. In: Hengl, T. and Reuter, H.I. (Eds), Geomorphometry: *Geomorphometry: Concepts, Software, Applications*. Developments in Soil Science, vol. 33, Elsevier, 3-30.

Nelson, A., 2008, Travel time to major cities: A global map of Accessibility. Global Environment Monitoring Unit - Joint Research Centre of the European Commission, Ispra Italy. Available at http://gem.jrc.ec.europa.eu/

Vogt, J.V., Colombo, R., Paracchini, M.L., de Jager, A., Soille, P., 2003, CCM River and Catchment Database for Europe, Version 1.0, EUR 20756 EN. EC-JRC, Ispra, Italy.

Surface Roughness Scaling Trends

K. Arrell, S. Carver

School of Geography, University of Leeds, LS2 9JT
Tel. (+44) 0113 3433343 Fax (+44) 0113 3433308
Email k.arrell@leeds.ac.uk

1. Introduction

Greater accuracy and higher resolution terrain data from direct measurements (for example SAR/LiDAR/TLS) have created a wide range of opportunities for detailed landscape analyses previously hampered by a lack of suitable data. Further, the increasing size and volume of these datasets necessitate quantitative data generalisations and metadata that can inform process studies, for example drainage density and relative relief. A number of studies have attempted to extract geomorphically significant measures from digital elevation data (Pellegrini, 1995; Wood, 1996; Burrough, et al., 2000; Arrell et al., 2007), these have largely attempted to characterise landscape elements and thus infer geomorphic process. Attempts to characterise or classify landscapes holistically still remain under developed and would provide useful metrics for digital elevation data analysis and geomorphological applications for example landscape evolution modelling. This paper looks at the development of measures of surface roughness as a multi-scale index for characterising landscape types.

We propose that the methods outlined here can provide landscape characterisations that reflect surface geomorphology, differentiating between surface types e.g. fluvial vs. glacial, erosional vs. depositional, soft vs. hard geology, when these landscape types exhibit different surface roughness scaling trends. We propose that scaling roughness trends will provide meaningful measures where local variability in surface properties governs the convergence and divergence of mass and energy which form critical controls on surface processes.

2. Study Area

2 m LiDAR data for the upper Wharfe Yorkshire, the Aire valley, and Cley-next-to-the-Sea and 5 m NEXTMap data for parts of the Cairngorms were used as test datasets. These varied landscapes were selected to assess the robustness of the outlined technique to differentiate between landscapes of differing characteristics and roughness. Further multi-resolution analyses were performed for the Wharfe using 2, 10, 50 and 75 m data. These data are all from proprietary sources, including both direct measurement and interpolated DEMs. There are summarised in Table 1.

Resolution	Type	Source
2 m	Direct measurement	EA LiDAR
10 m	Interpolation from1:10k map data	Ordnance Survey Landform Profile™
50 m	Interpolation from 1:50k map data	Ordnance Survey Landform Panorama™
75 m	Direct measurement	NASA SRTM

Table 1. DEM data sources.

3. Methods

A number of different measures of surface roughness were used to assess their ability to differentiate between landscape types. Roughness was measured as the standard deviation of each elevation, slope, the sine of aspect and finally curvature, comprising four different measures. These roughness indices are characterising the topography in different ways and consequently are therefore quantifying different surface features and trends. Here roughness is used as tool for differentiating between landscape types; the roughness data themselves do not form the primary focus of the study. Indeed any geomorphometric measure could be used, and the suitability of different measures will be the focus of future studies.

Surface roughness was measured within increasing kernel windows from 3x3 cells upward and stored per pixel for each different kernel size. The average roughness within the raster for each kernel resolution was calculated and plotted against kernel window size to look at local, focal and global trends in surface roughness. The confidence with which the average roughness value can account for the variability within the data will be explored in future work. This process was repeated with each of the four quantifications of surface roughness.

Data for each study area were plotted and used to characterise trends for landscape types. A theoretical representation is shown in Figure 1, where landscape types can be defined by their scaling trends. These may reflect key landforms or constituent landscape elements present at specific scales. Optimal landscape differentiation and hence classification will occur where surface roughness is different for different landscape types at the same kernel size and where surface roughness changes for the same landscape type at different kernel sizes.

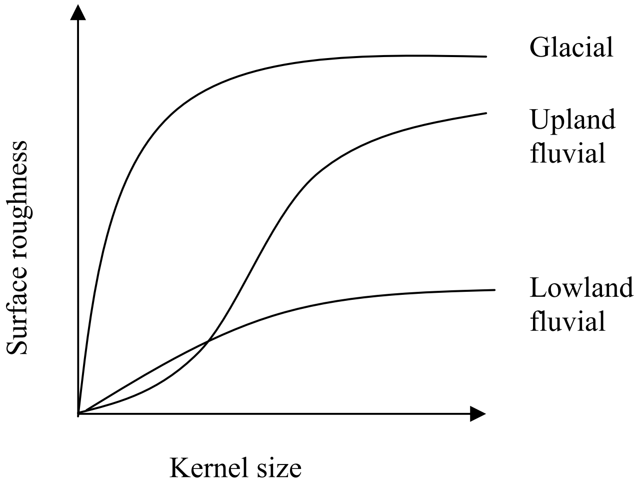

Figure 1. Schematic of plotted landscape types.

4. Results and Discussion

Initial results show that different landscapes exhibit different roughness scaling trends (Figure 2). The results show that indicative roughness trends for different landscapes exist through analysis of absolute magnitudes of, and scaling trends in, surface roughness.

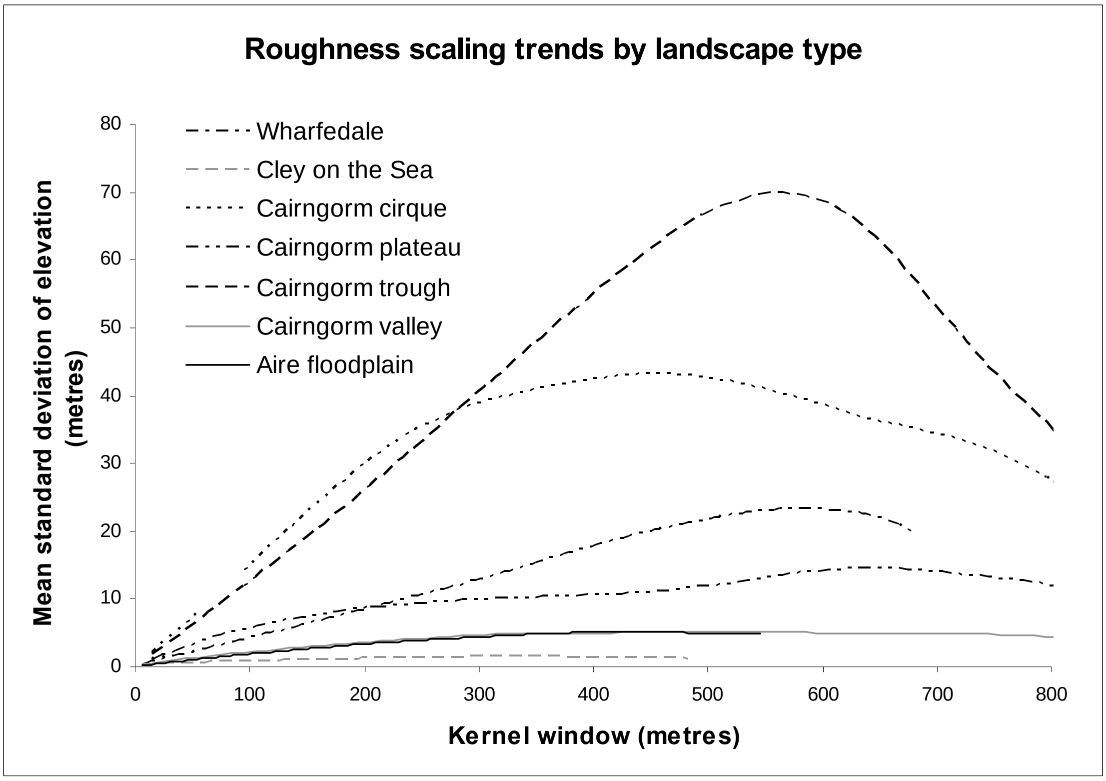

Figure 2. Measured roughness scaling trends.

Coastal and glacial valley floor landscapes exhibit a nominal scaling trend where surface roughness remains largely constant with kernel window size. Glacial landscapes, namely cirques and troughs exhibit a very different pattern, where surface roughness increases rapidly initially as cirque and valley walls are encountered. Both landscapes exhibit a marked inflection point in surface roughness after which elevations become increasingly less rough (more similar). These inflection points are felt to reflect landform spacing and frequency. This is supported by an average valley floor width of ~ 600 metres within the Cairngorm trough dataset. The Cairngorm plateau results suggest the possibility of two distinctive components which may represent palaeosurfaces.

Experiments were repeated with three other surface roughness measures which show similar trends but indicate different sensitivities to surface roughness scaling (Figure 3). Although these in part reflect differing units the gradient of the inflection point and the scaling relationships vary, these results are currently being investigated further.

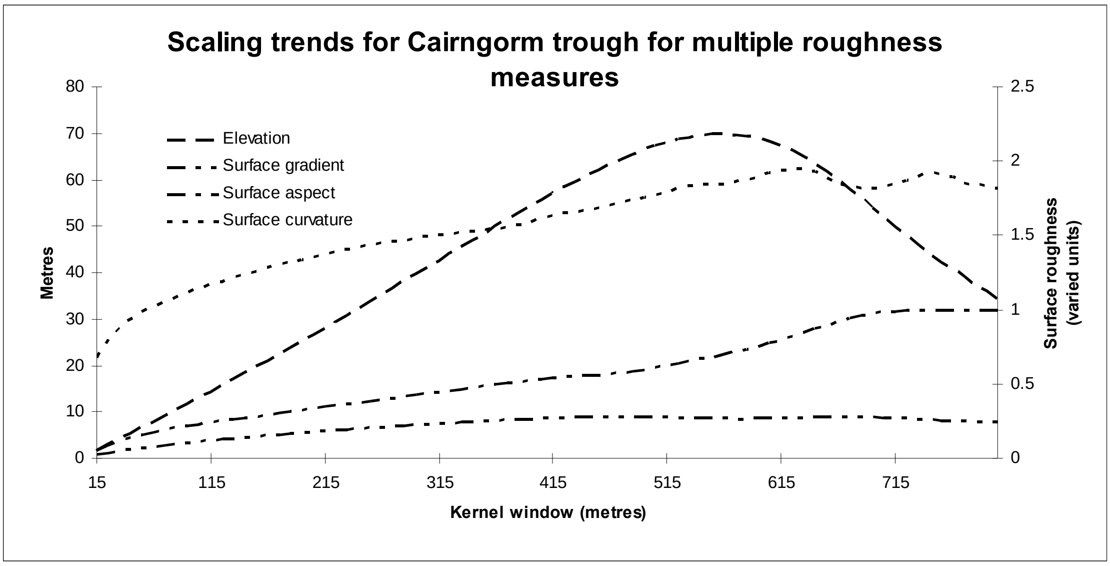

Figure 3. Multiple roughness measures.

Experiments were also undertaken with differing resolution data for the Wharfedale study area, these showed that trends were stable at multiple resolutions, where the point of inflection and scaling trends held for a landscape type using different resolution data.

The method proposes the identification of key or indicative kernel sizes for different landscape types defined by the scale of key landforms (for example valleys, slopes, cliffs). Initial results indicate that this methodology can also identify and extract geomorphologically meaningful data, for example cirque and valley spacing. A measure of the robustness of this technique to classify landscape types and the ability of different roughness measures to differentiate between different landscape types will be assessed by testing the resulting classifications on a range of “unseen” terrain models.

References

Arrell KE, Fisher, P, Tate N, Bastin L (2007) A fuzzy c-means classification of elevation derivatives to extract the morphometric classification of landforms in Snowdonia, Wales, *Computers & Geosciences* 33 pp. 1366–1381.

Burrough PA, van Gaans P, MacMillan R, (2000) High resolution landform classification using fuzzy k-means. *Fuzzy Sets and Systems* 113 pp. 37–52.

Pellegrini G (1995) *Terrain shape classification of digital elevation models using eigenvectors and Fourier transforms* Ph.D. Dissertation, State University of New York College of Environmental Science and Forestry, Syracuse, NY.

Wood J (1996) *The geomorphological characterisation of digital elevation models*. PhD Dissertation, University of Leicester, http://www.soi.city.ac.uk/_jwo/phd/S (accessed 13 April 2007).

Laplace-Gradient Wavelet Pyramid and Multiscale Tensor Structures Applied on High-Resolution DEMs

M. Kalbermatten[1], D. Van De Ville[2], S. Joost[1], M. Unser[2] , F. Golay[1]

[1] Ecole Polytechnique Fédérale de Lausanne (EPFL), GIS laboratory, Station 18, 1015 Lausanne, Switzerland
Telephone (+41) 21 693 57 83
Fax: (+41) 21 693 57 90
Email: {michael.kalbermatten, stephane.joost, francois.golay}@epfl.ch

[2] Ecole Polytechnique Fédérale de Lausanne (EPFL), Biomedical Imaging Group, Station 17, 1015 Lausanne, Switzerland
Telephone: (+41) 21 693 51 42
Fax: (+41) 21 693 37 01
Email: {dimitri.vandeville, michael.unser}@epfl.ch

1. Introduction

Wavelet decompositions are a powerful tool for multiscale image analysis. Their use in DEMs (Digital Elevation Models) analysis is still limited. Nevertheless, some researchers (De Boer 1992, Wilson & Gallant 2000) demonstrated that scale and structure play an important role to determine the elementary shape of landscape features. Wavelets are ideally localized functions fulfilling that condition (Mahler 2001, Gallant & Hutchinson 1996).

Wavelet analysis of high-resolution (1-meter) DEMs is highly complementary to morphometric indicators (Wood 1996); e.g., applications include multiscale filtering and enhancement. Here, we introduce various methods using wavelets and structure tensors in order to show the multiscale nesting of landscape features. The method was applied on a DEM including a well-known landslide, and the results were compared to an ordinary geomorphological analysis. The aim is to show the potential of this method and to give hints for further development of such tools in terrain analysis systems.

2. Methodology

2.1 Laplace-Gradient Wavelet Pyramid

Classical wavelet transforms (Mallat 1996, Mallat 2000) act like a smoothed multiscale derivative operator when applied to the data. Usually, multidimensional data is processed in a separable way, i.e. dimension-by-dimension, which leads to multiple wavelets at each scale making the interpretation difficult. The recently introduced “Marr wavelet pyramid” (Van De Ville et al. 2008b) is an intrinsic 2-D wavelet design inspired on David Marr’s theory of primate’s vision (Marr 1982) that circumvents these limitations. Each scale is characterized by a single wavelet that acts like a Laplace-complex gradient operator. Consequently, the wavelet coefficients are complex-valued and their phase provides directional information.

Marr’s theory proposes that vision (or human visual capabilities) is linked to information cells tuned into different spatial frequencies, thus making it possible to do multiscale analysis. For this purpose, wavelets are a useful tool for DEM analysis.

The starting point of the wavelet pyramid is the identification of the Laplace-complex gradient, which characterizes the complete family of shift-invariant, scale-invariant, and rotation-covariant convolution operators (Equation 1, Van De Ville & Unser 2008b).

$$L_{\gamma,N} = (-\Delta)^{\frac{\gamma-N}{2}} \left(-j\frac{\partial}{\partial x} - \frac{\partial}{\partial y} \right)^{N} \tag{1}$$

Next, the associated wavelet function is a multiscale version of this operator; i.e., the wavelet is defined as $\psi = L_{\gamma,N}(\phi)$, where ϕ is an appropriate smoothing kernel.

The scaling function associated with the wavelet pyramid is the so-called complex polyharmonic B-spline $\beta_{\gamma,N}$ in 2-D (Van De Ville et al. 2008b, Van De Ville et al. 2005); its scaling relation for dyadic subsampling (factor of 2 in each dimension) can be expressed conveniently in the Fourier domain by the low-pass filter *H* (Equation 2).

$$\hat{\beta}_{\gamma,N}(2\boldsymbol{\omega}) = \frac{1}{4} H(e^{j\boldsymbol{\omega}})\hat{\beta}_{\gamma,N}(\boldsymbol{\omega}) \tag{2}$$

The wavelet function is embedded in the finer approximation scale; i.e., the high-pass filter *W* expresses the relationship in Equation 3.

$$\hat{\psi}_{\gamma,N}(2\boldsymbol{\omega}) = \frac{1}{4} W(e^{j\boldsymbol{\omega}})\hat{\beta}_{\gamma,N}(\boldsymbol{\omega}) \tag{3}$$

Here, we use $\gamma = 3$ (number of vanishing moments) and $N = 1$ (order of the complex gradient). Consequently, the wavelet transform corresponds to a multiscale version of the operator $L_{3,1}$ (Equation 1).

To obtain the pyramid decomposition of the signal of interest, we apply the efficient filterbank algorithm depicted in Fig. 1. The decomposition is applied iteratively to the low-pass coefficients $c_{i-1}[\mathbf{k}]$. The wavelet coefficients are not subsampled, which leads to a pyramid structure with mild redundancy. In this paper, we chose up to eight decomposition levels.

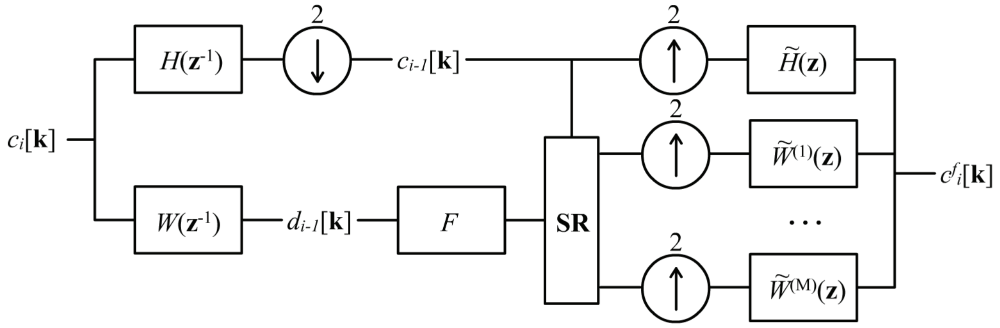

Figure 1. Laplace-gradient wavelet pyramid filterbank
(adapted from Van De Ville et al. 2008b).

Before applying the synthesis procedure, we can process the wavelet coefficients ($d_{i-1}[\mathbf{k}]$), as embodied in the box *F* of Fig. 1. The synthesis procedure uses a so-called subband regression method to obtain the most consistent reconstruction with respect to the (redundant) decomposition (box **SR** in Fig. 1, see Unser & Van De Ville 2008 for more details).

2.2 Structure Tensors

Structures tensors are a representation of pixel value changes in a local neighbourhood. The complex-valued wavelet coefficients can be interpreted directly as the gradient of a Laplace-filtered and multiscale smoothed version of the data; i.e., we have $\nabla g_i[\mathbf{k}] = [\mathrm{Im}\{d_i[\mathbf{k}]\}, \mathrm{Re}\{d_i[\mathbf{k}]\}]$. Therefore, the wavelet coefficients can be used to compute a multiscale structure tensor (Van De Ville et al. 2008a):

$$\mathbf{J}_i(\mathbf{k}) = \sum_{\mathbf{n}\in\Omega} w[\mathbf{n}](\nabla g_i(\mathbf{k}+\mathbf{n})\nabla g_i(\mathbf{k}+\mathbf{n})^T) \tag{4}$$

where w is a fixed-size smoothing window with positive weights.

The eigenvectors and eigenvalues of the structure tensor provide robust and essential information about the signal variation at a given scale. Specifically, we did use the following three measures, obtained from the tensor (Van De Ville et al. 2008a):

- *Orientation*: orientation shows the dominant direction of the local structure. It is less prone to noise than the coefficient-wise orientation. Since the tensor is a second-order descriptor, there is no difference between a "positive" and a "negative" edge; i.e., gradients pointing in opposite directions are considered equally ($orientation \in [-\pi/2, \pi/2]$).
- *Energy*: energy of the the local gradient.
- *Coherency*: the ratio between the mean square magnitude of the gradient and the magnitude of the orientation vector gives an indicator called the coherency ($coherency \in [0,1]$). Large coherency shows that there is a dominant orientation in the local neighbourhood (depending on the Gaussian window's size) and small coherency indicates isotropy (Van De Ville et al. 2008a, Jähne 2005).

In order to have a comprehensive visualization of these measures, the 3 components are combined in a composite HSB (hue-saturation-brightness) image. The orientation was coded in the hue level (colour tint), the coherence in the saturation level and the energy in the brightness level. We applied histogram equalization to the energy component, since some initial adjacent pixels (elevations) have markedly different values. These ones induce much higher energy values than most of the other pixels. A root function (3rd or 4th order, depending on the decomposition level) was used to soften this effect.

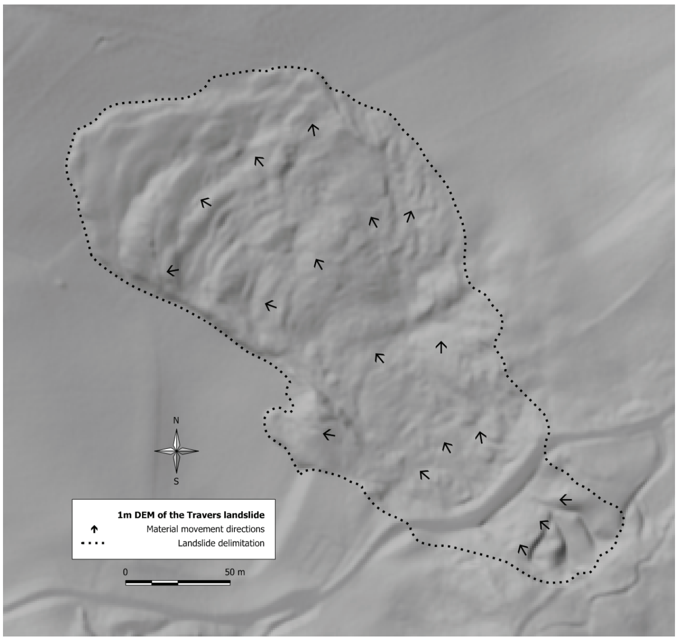

Figure 2. Landslide context in Travers, Switzerland, DEM©SITN.

3. Application on High-Resolution DEMs

The proposed methodology was applied on a high resolution DEM (base resolution 1m) covering a recent landslide (2007) in Travers – Canton de Neuchâtel, Switzerland. The DEM was generated using TIN (Triangular Irregular Network) interpolation on raw scan2map[1] airborne LiDAR (Light Detection And Ranging) points. The resulting shaded DEM and the delimitation of the contained landslide are shown in Fig. 2.

3.1 Phase and Magnitude of the Complex Wavelet Subbands

The wavelet coefficients are complex-valued: phase (inverse tangent of the real and the imaginary parts) indicates the orientation and magnitude (squared root of the squared real and the squared imaginary parts) represents the strength. An example is shown in Fig. 3.

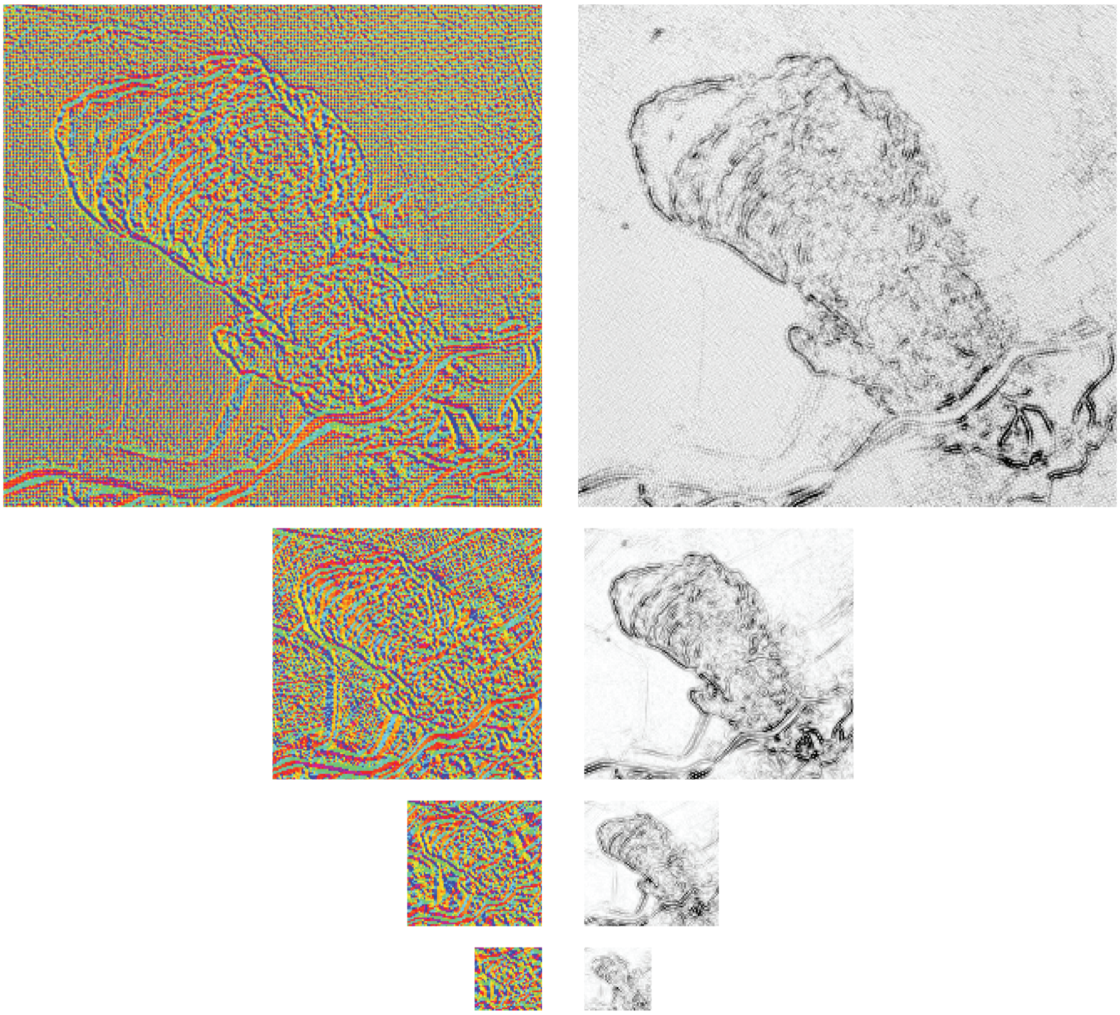

(a) (b)

Figure 3. Phase (a) and magnitude (b) results on the landslide region for the first four decomposition levels (i.e. resolutions of 1, 2, 4 and 8 meters).

---

[1] scan2map is a research project of the Geodetic Engineering Laboratory at the Ecole Polytechnique Fédérale de Lausanne (TOPO-EPFL, see http://topo.epfl.ch/laserscanning/)

Phase and magnitude can also be combined to create a multiscale vector field. Each decomposition level shows the behaviour of its associated resolution. In Fig. 4, we show gradient vector fields using different decomposition levels.

We observe that the magnitude reveals interesting structural features depending on the decomposition level (thus the equivalent resolution of the feature shape) and phase the azimuth of the feature. Both of these indicators may be used for multiscale Canny edge detection, but this was not undertaken in this paper.

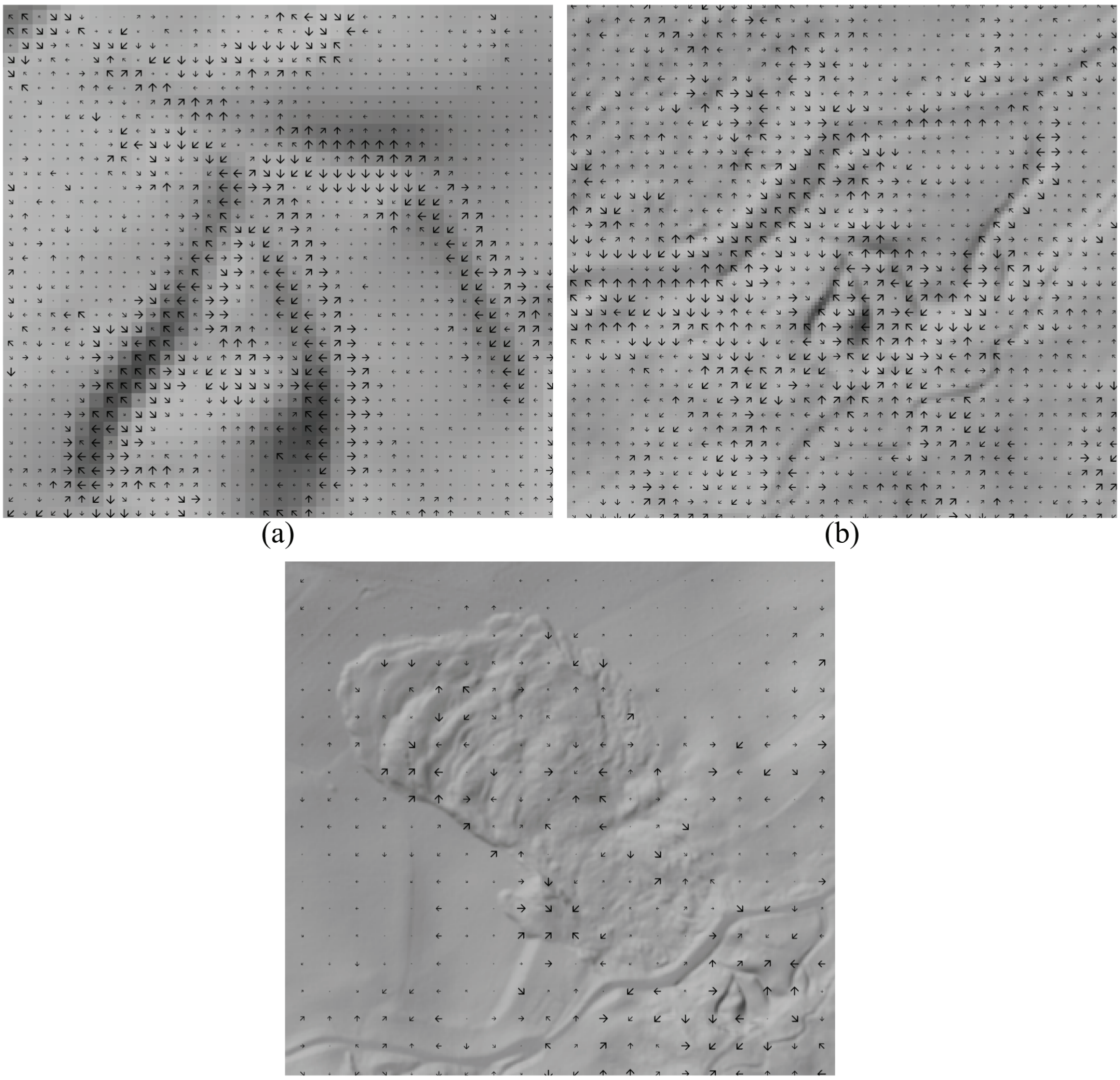
(a) (b)

(c)

Figure 4. Phase-magnitude vector field for the first decomposition level (1m resolution) (a), for the third decomposition level (4m resolution) (b) and for the fifth decomposition level (16m resolution) (c).

3.2 Subband-selective Reconstruction

Reconstruction from specific subbands allows to choose which elements, based on their resolution (i.e. decomposition level), should be reconstructed to the finest scale (1 meter resolution). Fig. 5 shows the combination results of the different decomposition levels. The following procedure was used to create these images:

- The high resolution DEM was analysed until the nth level.
- The resulting low pass grid was suppressed.
- The Marr pyramid was reconstructed using the subband regression.

The images in Fig. 5 are normalised ([-100,100]) coefficients with a colour saturation level at [-20,20]. Negative values are given in blue and positive values in red. The coefficients of the different levels were not enhanced (frequency boosting), but this could be done easily, depending on the interest of the geomorphologist.

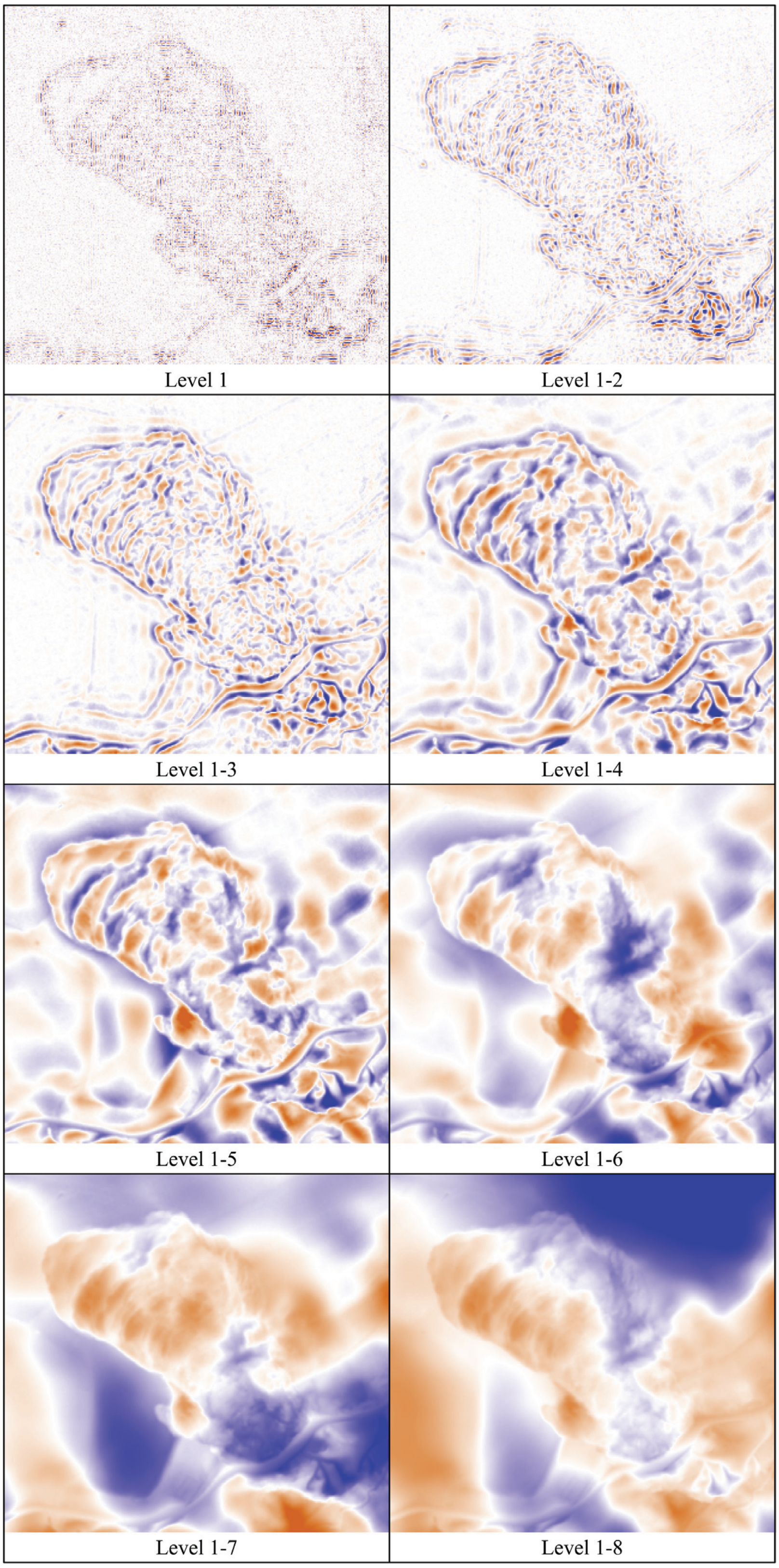

Figure 5. Subband reconstruction for cumulative high pass coefficients, from level 1 to cumulative level 1-8.

Fig. 5 illustrates the nesting of landscape structures and helps for the identification of pertinent morphological elements of the landslide. Any levels (filtered version or not) could be combined, to help multiscale feature recognition.

3.3 Structure Tensor of the Different Decomposition Levels

The different measures obtained from the multiscale structure tensor (coherency, energy and orientation) also provide excellent characterization of landscape elements. In Fig. 6, we show the results for the first decomposition level. As expected, coherency shows the isotropic behaviour of this level structures (whitest pixels) and energy (3rd root) the local energy of the coefficients. Fig. 6 was created using a 3x3 moving-average window.

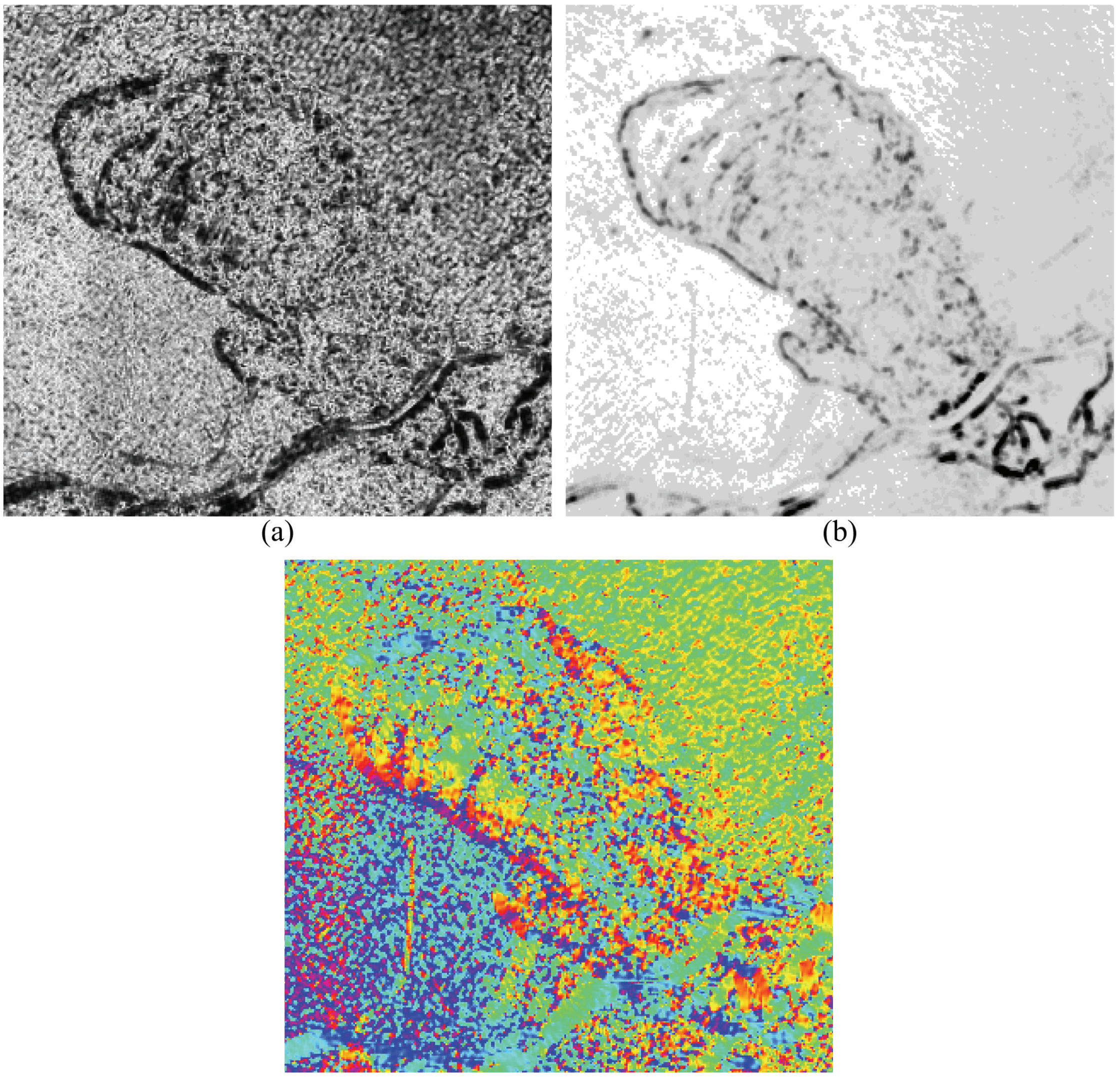
(a) (b)

(c)

Figure 6. Structure tensor results for the first decomposition level, (a) coherency, (b) energy and (c) orientation.

Another representation of these results is given in Fig. 7 where the three new layers are coded in HSB image (H = orientation, S = coherency, B = energy). Going through the decomposition level, the images show more and more generalized structures.

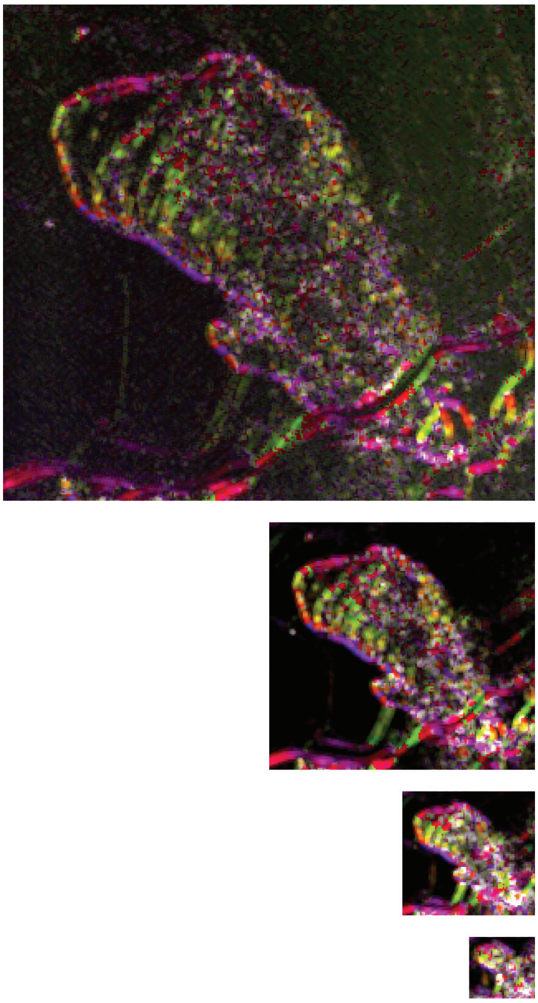

Figure 7. HSB images of structure tensor results for the first four decomposition levels.

4. Conclusion

We propose a novel DEM multiscale analysis approach. It is built upon recent advances in multidimensional wavelet design, in particular the Laplace-gradient wavelet pyramid. The phase and magnitude of the complex wavelet coefficients provide a unique representation of multiscale nested features. The combination of coefficients from distinct decomposition levels permits to obtain scale dependent structures corresponding to the needs of geomorphologists.

Localized and oriented multistructural information, as well as structure tensors, provide additional analytical elements. Combined to usual morphometry (Wood 1996), the proposed way of incorporating scale and structure may be useful to further elaborate landscape geomorphological processes.

References

De Boer D H, 1992, Hierarchies and spatial scale in process geomorphology: a review, *Geomorphology*, 4:303-318.

Gallant J C and Hutchinson M F, 1996, Towards an understanding of Landscape Scale and Structure, *Third International Conference/Workshop on Integrating GIS and Environmental Modeling*, Santa Fe, USA.

Jähne B, 2005, *Digital Image Processing, 6th revised and extended edition*, Springer, Berlin, Germany.

Mahler E, 2001, *Scale-Dependent Filtering of High Resolution Digital Terrain Models in the Wavelet Domain*, MSc Thesis, Department of Geography, University of Zurich, Switzerland

Mallat S, 1996, Wavelets for a vision, *Proceedings of the IEEE*, 84(4):604-614.

Mallat S, 2000, *Une exploration des signaux en ondelettes*, Les éditions de l'école polytechnique, France.

Marr D, 1982, *Vision: a computational investigation into the human representation and processing of visual information*, W. H. Freeman and Company, San Francisco, USA.

Unser M and Van De Ville D, 2008, The pairing of a wavelet basis with a mildly redundant analysis via subband regression, *IEEE Transactions on Image Processing*, 17(11):2040-2052.

Van De Ville D, Blu T and Unser M, 2005, Isotropic Polyharmonic B-splines: Scaling Functions and Wavelets, *IEEE Transactions on Image Processing*, 14(11):1798-1813.

Van De Ville D, Sage D, Balac D and Unser M, 2008a, The Marr wavelet pyramid and multiscale directional image analysis, *EUSIPCO08*, Lausanne, Switzerland.

Van De Ville D, and Unser M, 2008b, Complex wavelet bases, steerability, and the Marr-like pyramid, *IEEE Transactions on Image Processing*, 17(11):2063-2080.

Wilson J P and Gallant J C , 2000, *Terrain Analysis, Principles and Applications*, John Wiley & Sons, New-York, USA.

Wood J, 1996, *The Geomorphological Characterisation of Digital Elevation*, PhD Thesis, City university, London, UK.

A Comparison of Methods to Incorporate Scale in Geomorphometry

Lucian Drăguț [1,2], Clemens Eisank[1], Thomas Strasser[1], Thomas Blaschke[1]

[1]Department of Geography and Geology, University of Salzburg, Hellbrunnerstraße 34, Salzburg 5020, Austria

[2]Department of Geography, West University of Timişoara, V. Pârvan Blv. 4, Timişoara 300223, Romania
Telephone: (+43) 662 8044 5293
Fax: (+43) 662 8044 5260
Email: lucian.dragut@sbg.ac.at

1. Introduction

Although debated, it seems to be unsettled if scales in digital representations of the land surface are explicitly detectable, or if scale is a ‘window of perception’ (Marceau 1999).

In geomorphometry, scale is predominantly considered as a function of DEM resolution (Hengl and Evans 2009; MacMillan and Shary 2009). Increasing availability of high resolution DEMs is leading to a shift of paradigm regarding scale issues in geomorphometry. While in the past researchers were looking for finer resolution DEMs as a premise for improving analysis, now when they are available there is growing evidence that higher levels of detail represent just noise for some applications. This raises interest for considering scale issues in geomorphometry.

The scale dependency of land-surface parameters and objects derived from DEMs has been demonstrated in a number of studies (Wood 1996, 2009; Florinsky and Kuryakova 2000; Evans 2003; Fisher et al. 2004; Schmidt and Andrew 2005; Hengl 2006; Arrell et al. 2007; Drăguț et al. 2009) and methods to account for scale through DEM generalization have been proposed. However, a comprehensive assessment of scaling methods- particularly from the perspective of their suitability of enabling scale detection- is still missing. This motivates our work.

Several methods to generate scale levels were selected to comparatively evaluate their performances under controlled conditions.

2. Modelling and Data

Scale levels at constant increments were produced for slope gradient with the following methods:

a. Resampling. The input DEMs were resampled using bilinear interpolation;
b. Smoothing the DEM with focal mean statistics. The input DEM was filtered using focal mean statistics within constantly increased windows, then slope was calculated for each derived dataset;
c. Smoothing slopes with focal mean statistics. Slopes were calculated in a 3X3 window, then filtered using the previous method;
d. Multiscale surface characterization (Wood 1996). Slopes were calculated globally within increasing neighbourhood using LandSerf (Wood 1996);
e. Object-based image analysis (OBIA). Multiple scale levels were produced by increasing the scale parameter within a multi-resolution segmentation process using Definiens Developer® (see Drăguț and Blaschke 2006 for details on segmentation method).

Scale sensitivity of up-scaling methods was evaluated both against field measurements and using the method of local variance (Woodcock and Strahler 1987). In the former case, relationships between measured and calculated values of slope gradient were assessed through Spearman’s rank of correlation coefficient and Root Mean Squared Error (RMSE). Both estimator values were plotted against scale levels. The latter evaluation method is based on local variance (LV), defined as the average of standard deviation (SD) within a small neighbourhood (3X3 rowing window passing over the entire area). For details on the reason behind this method see Woodcock and Strahler (1987). To assess the LV dynamics from a scale level to another, we used a measure called rate of change (ROC) of LV (Drăguț et al. in review). Values of LV and its ROC were plotted against scale levels as well.

The research is carried out in two test areas, each of them of 3X3 km in size, located in the Federal State of Salzburg, Austria (Fig. 1). Test areas cover two types of land surface in terms of roughness: relatively flat (Eugendorf) and mountain (Schlossalm) (Fig. 1). For each test area, LiDAR DEMs at 1 m spatial resolution are available. 50 points per test area were randomly generated (Fig. 1), then slope values were measured at each point, with a digital inclinometer (HEDÜ, display accuracy: 0,1°).

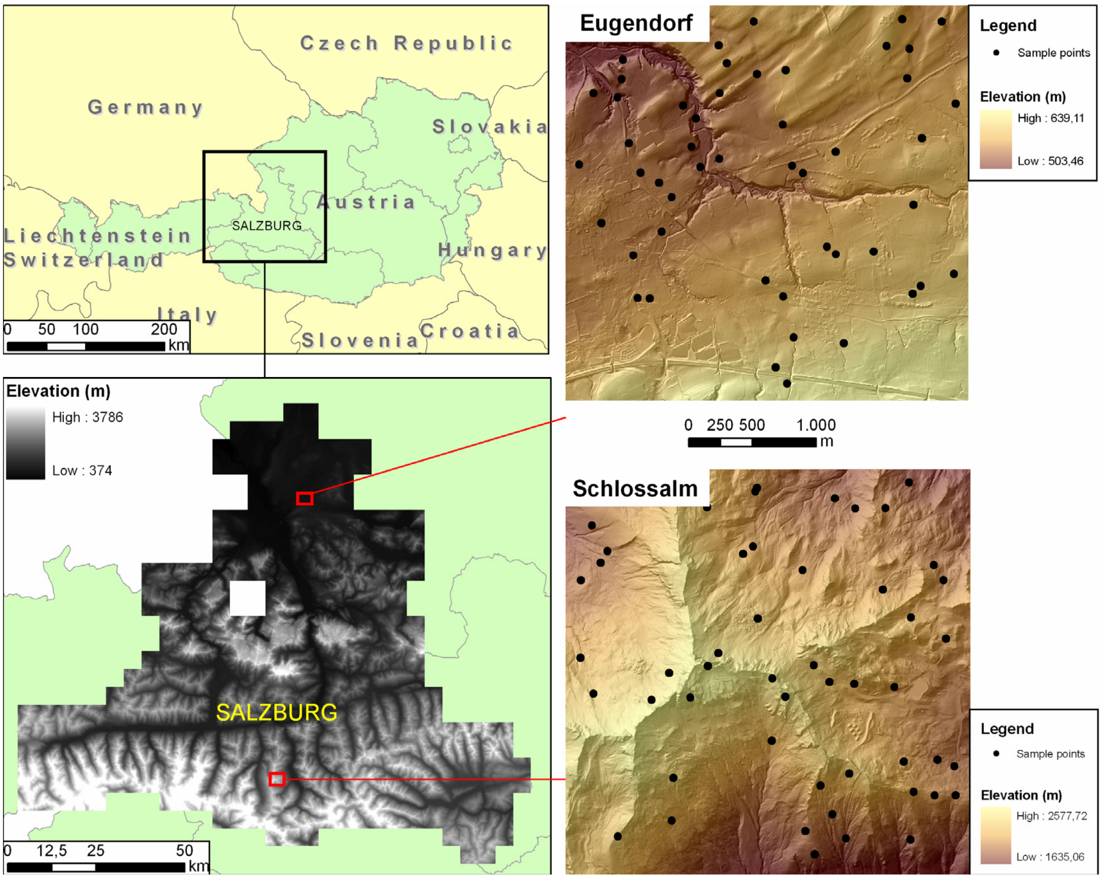

Figure 1. Locations of test areas. Black dots represent locations of field measurements.

3. Results and Discussion

In this experimental research we aim to test whether the graphs obtained as described above could help in detecting characteristic scales in geomorphometric analysis.

Similar to concepts in landscape ecology and remote sensing, breaks in constant evolutions of land-surface parameters across scales might reveal levels of organization in the structure of data as a consequence of the occurrence of similar sized spatial objects. Here 'objects' are not defined as classical geomorphologic objects (e.g. landforms), but rather as 'morphometric primitives' (Gessler et al. 2009) or pattern elements, carriers of information on slope gradient. This term is seen as bridge between 'real' objects and their representation. Morphometric primitives can be further classified in landform elements and integrated in nested hierarchies (Minar and Evans 2008; Evans et al. 2009), but this falls beyond the scope of this paper.

For each scaling method, specific scale signatures (sense Wood 2009, but applied globally) have been obtained (Fig. 2) in scale ranges up to 21 for cell-based methods, and up to 100 for OBIA respectively. Thresholds in trends of curves have been comparatively analysed.

In contrast to OBIA and resampling, all other methods produce decreasing curves of LV (Fig. 2). This is because these methods do not emulate real world 'objects', as resampling does (e.g. through different cell sizes, which may or may not approximate characteristic dimensions of homogeneous slopes at given scale). Therefore, LV does not increase as a consequence of contrasting neighbour cells, but reduces with raising spatial autocorrelation. Further, thresholds in R and RMSE curves only occasionally indicate similar scale levels.

For resampling and OBIA, LV graphs are provided in two versions to reveal thresholds at higher scale (otherwise obscured due to huge values of ROC at lowest levels).

For OBIA, four thresholds in LV and ROC curves (corresponding to scale parameters of 10, 25, 40 and 85) have been identified for Eugendorf, and three (20, 50 and 90) for Schlossalm. Thresholds at these values or close to them are visible in R and RMSE curves as well. For Schlossalm, thresholds in curves of R, RMSE, and LV show a notable fit, despite aforementioned indicators were calculated on different basis.

For resampling methods, two thresholds have been identified for each of the two test areas, at the same scales: 5 and 19. Except for the threshold at 5 in Schlossalm, all others appear on R and RMSE curves, too. For Eugendorf, a misfit between R and RMSE curves duplicate the threshold at 19, suggesting an interval from 15 to 19 rather than a single value.

Results were visually evaluated for OBIA, and through profiles for resampling. Figure 3 displays slope profiles at scales as in Figure 2 (resampling). Variations in profiles correspond to levels of generalization of land-surface. While profiles at scales 5 and 19 show distinct representations of slopes (which suggests good performance of LV method in detecting meaningful scale levels), scale levels are the same for both study areas, regardless of differences in topography.

In Figure 4, areas of similar homogeneity are delineated with OBIA for Schlossalm, with the scale parameters presented above. Good agreements between slope values and their aggregation in objects at these scale levels are depicted. In OBIA, anisotropy is readily incorporated in analysis, contrary to cell-based methods (see Schmidt and Andrew 2005, pp. 347, for details). Thus, various features in terms of size and shape (from extremely elongated to circular) occur in the same scale level, according to land-surface patterns (Fig. 4). Well individualized features may persist across scales without changing shape (e.g. elongated features inside the polygon at scale 90 persist at finer scales).

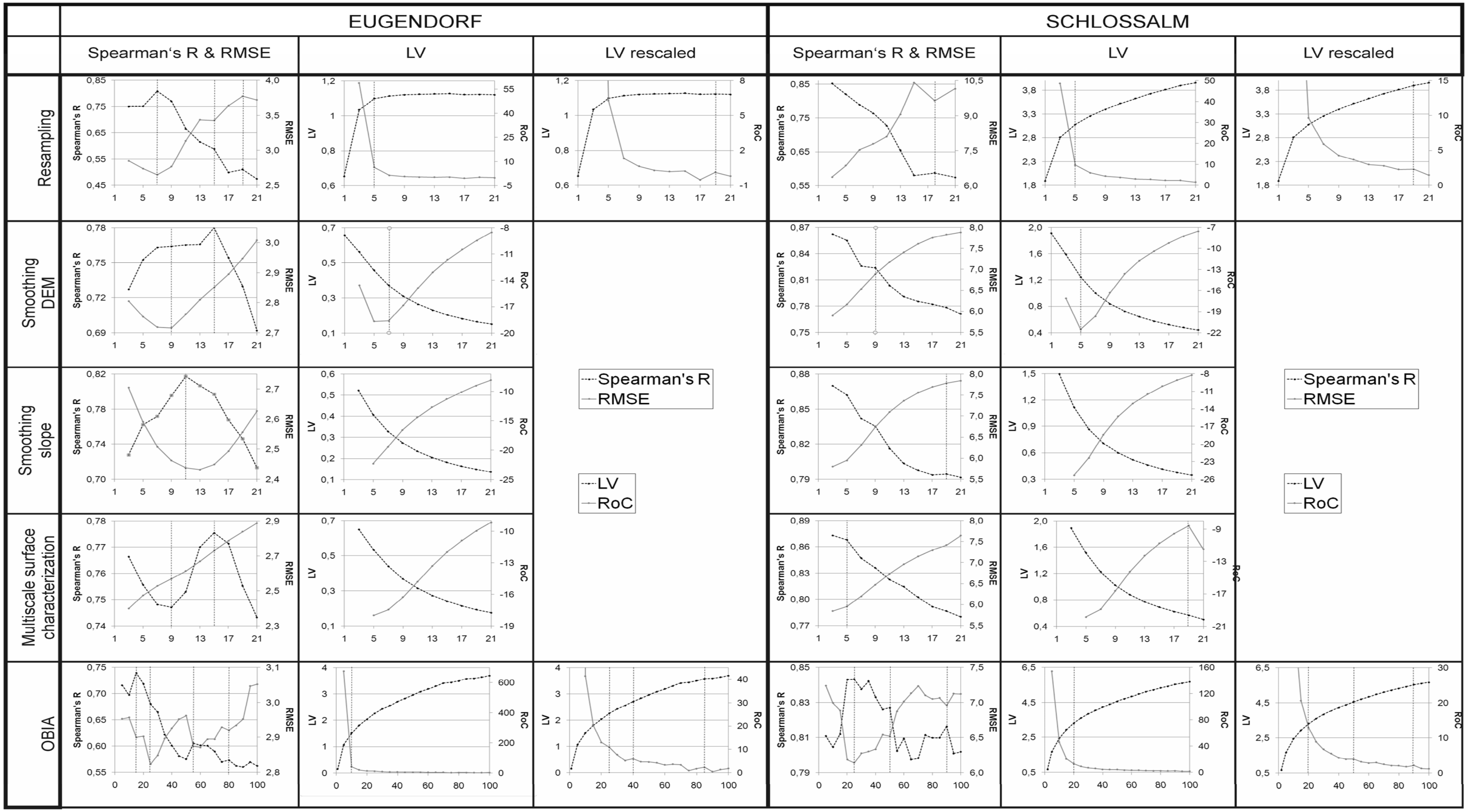

Figure 2. Comparative view of scale signatures. Where applicable, vertical lines in graphs represent scale thresholds.

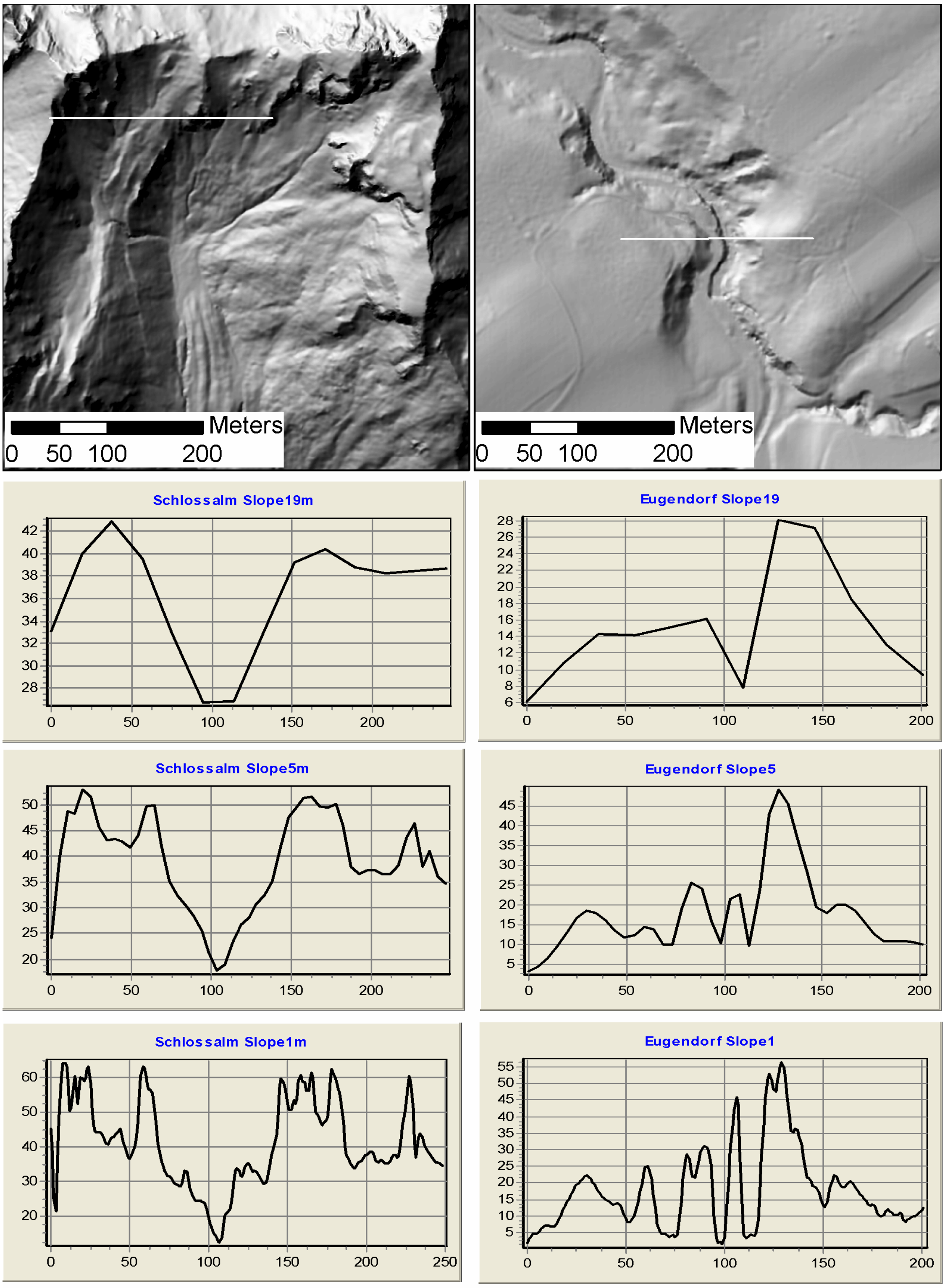

Figure 3. Slope profiles at original and detected scales for Schlossalm (left) and Eugendorf (right). White lines on shaded maps show profile locations.

Li (2008) suggested the LV method should be applicable to DEM data (pp. 79). In this study, we compared scale sensitivity of five up-scaling methods using both LV and field-based methods. We found that filtering and multi-scale surface characterization do not enable scale detection in slope maps with the methods presented here. More research is needed (particularly on other parameters and larger scale ranges) to evaluate the suitability of resampling for scale detection. OBIA produced visually appealing representations of homogeneous slopes at scales detected by all methods. Although land-surface ‘objects’ are characterized by smoother transitions in comparison with land cover objects, the application of LV method on segments looks promising for multi-scale analysis in geomorphometry too.

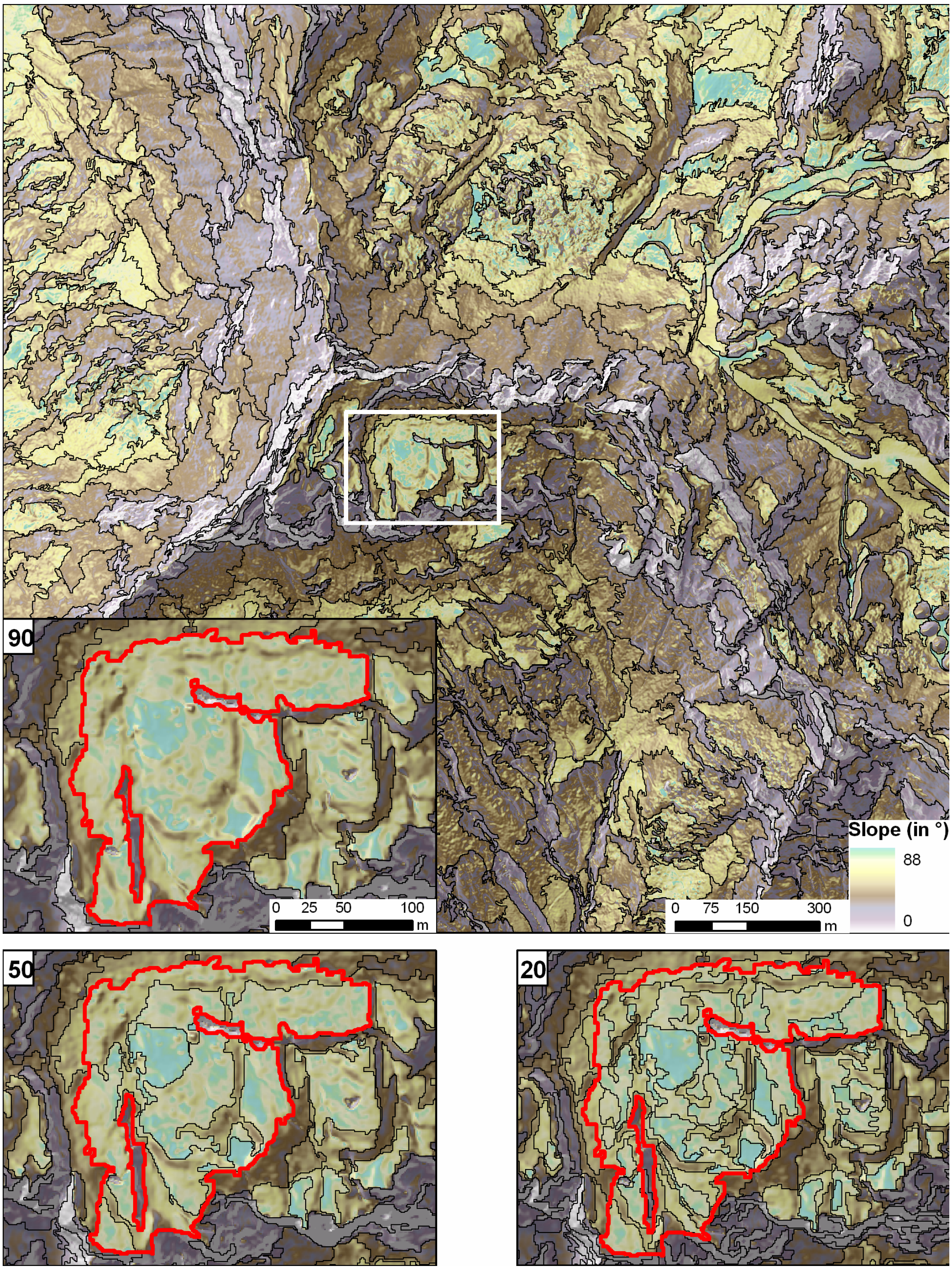

Figure 4. Multi-scale object representation in OBIA environment. Results of segmentations with detected scale parameters (SP) are visible. The whole Schlossalm test area (top) with slope segments delineated at a SP of 90. For the object marked in white rectangle, detailed views are provided at SPs of 90, 50 and 20.

Acknowledgements

This research was supported by the Austrian Science Fund (FWF) through a Stand-alone project, and by a Marie Curie European Reintegration Grant within the 7th EC Framework Programme. DEM data was provided by the regional government of Salzburg (SAGIS, Land Salzburg). Correction files for accuracy improvement of GPS field measurements were provided by the Austrian Railway System (ÖBB). Gerald Griesebner helped in GPS corrections.

References

Arrell KE, Fisher PF, Tate NJ and Bastin L, 2007, A fuzzy c-means classification of elevation derivatives to extract the morphometric classification of landforms in Snowdonia, Wales. *Computers & Geosciences,* 33:1366-1381.

Drăguţ L and Blaschke T, 2006, Automated classification of landform elements using object-based image analysis. *Geomorphology,* 81:330-344.

Drăguţ L, Schauppenlehner T, Muhar A, Strobl J and Blaschke T, 2009, Optimization of scale and parametrization for terrain segmentation: an application to soil-landscape modeling. *Computers & Geosciences*, doi:10.1016/j.cageo.2008.10.008.

Drăguţ L, Tiede D and Levick S, in review. ESP: a tool for estimating the scale parameter in multiresolution image segmentation of remotely sensed data. *International Journal of Geographical Information Science*.

Evans IS, 2003, Scale-Specific Landforms and Aspects of the Land Surface. In: Evans IS, Dikau R, Tokunaga E, Ohmori H and Hirano M (eds), *Concepts and Modelling in Geomorphology: International Perspectives.* Terrapub, Tokyo, 61-84.

Evans IS, Hengl T and Gorsevski P, 2009, Chapter 22 Applications in Geomorphology. In: Hengl T and Reuter HI (eds), *Geomorphometry-Concepts, Software, Applications. Developments in Soil Science, vol. 33*, Elsevier, Amsterdam, 497-525.

Fisher P, Wood J and Cheng T, 2004, Where is Helvellyn? Fuzziness of multi-scale landscape morphometry. *Transactions - Institute of British Geographers,* 29:106-128.

Florinsky IV and Kuryakova GA, 2000, Determination of grid size for digital terrain modelling in landscape investigations - exemplified by soil moisture distribution scale. *International Journal of Geographical Information Science,* 14:815-832.

Gessler P, Pike R, MacMillan RA, Hengl T and Reuter HI, 2009, Chapter 28 The Future of Geomorphometry. In: Hengl T and Reuter HI (eds), *Geomorphometry-Concepts, Software, Applications. Developments in Soil Science, vol. 33*, Elsevier, Amsterdam, 637-652.

Hengl T, 2006, Finding the right pixel size. *Computers & Geosciences,* 32:1283–1298.

Hengl T and Evans IS, 2009, Chapter 2 Mathematical and digital models of the land surface. In: Hengl T and Reuter HI (eds), *Geomorphometry-Concepts, Software, Applications. Developments in Soil Science, vol. 33*, Elsevier, Amsterdam, 31-63.

Li Z, 2008, Multi-scale terrain modelling and analysis. In Zhou Q, Lees B and Tang GA. (eds.), *Advances in Digital Terrain Analysis*. Springer, Berlin, Heidelberg, 59-83.

MacMillan RA and Shary PA, 2009, Chapter 9 Landforms and landform elements in geomorphometry. In: Hengl T and Reuter HI (eds), *Geomorphometry-Concepts, Software, Applications. Developments in Soil Science, vol. 33*, Elsevier, Amsterdam, 227-254.

Marceau DJ, 1999, The scale issue in social and natural sciences. *Canadian Journal of Remote Sensing,* 25:347-356.

Minar J and Evans IS, 2008, Elementary forms for land surface segmentation: The theoretical basis of terrain analysis and geomorphological mapping. *Geomorphology,* 95:236-259.

Schmidt J and Andrew R, 2005, Multi - scale landform characterization. *Area,* 37:341–350.

Wood J, 1996, The Geomorphological Characterisation of Digital Elevation Models, Ph.D. Dissertation, University of Leicester, England, http://www.soi.city.ac.uk/~jwo/phd/.

Wood J, 2009, Chapter 14 Geomorphometry in LandSerf. In: Hengl T and Reuter HI (eds), *Geomorphometry-Concepts, Software, Applications. Developments in Soil Science, vol. 33*, Elsevier, Amsterdam, 333-349.

Woodcock CE and Strahler AH, 1987, The Factor of Scale in Remote-Sensing. *Remote Sensing of Environment,* 21:311-332.

Surface Roughness of Topography: A Multi-Scale Analysis of Landform Elements in Midland Valley, Scotland

C. H. Grohmann[1], M. J. Smith[2], C. Riccomini[3]

[1] Institute of Geosciences – University of São Paulo – Rua do Lago, 562, São Paulo, SP, Brazil, 05508-080
Telephone: +55 11 3091- 4216
Fax: +55 11 3091-4258
Email: guano@usp.br, carlos.grohmann@gmail.com

[2] School of Geography, Geology and the Environment, Kingston University, Kingston-upon-Thames, Surrey, KT1 2EE, UK
Telephone: +44 (0) 207 099 2817
Fax: +44 (0) 870 063 3061
Email:michael.smith@kingston.ac.uk

[3] Institute of Geosciences – University of São Paulo – Rua do Lago, 562, São Paulo, SP, Brazil, 05508-080
Telephone: +55 11 3091- 4126
Fax: +55 11 3091-4207
Email: riccomin@usp.br

1. Introduction

Surface roughness is a key variable used across the earth and planetary sciences (Hobson 1972) to both identify individual landforms and determine the processes acting upon them. In geomorphometry, roughness is described using surface elevation values and can be used to characterise landforms over a variety of different scales.

Throughout this article, we use the term *surface roughness* as an expression of the variability of elevation of a topographic surface *at a given scale*, where the scale of analysis is determined by the size of the landforms or geomorphic features of interest, either local or regional.

In this paper we briefly review a selection of measures of surface roughness, with specific application to grid based digital elevation models (DEMs). A selection were assessed for the behaviour of roughness at different spatial scales and dataset resolutions using moving-window and raster algebra steps to a test area in the Midland Valley, Scotland.

1.1 Measures of Surface Roughness

The *area ratio* evaluates the similarities between the surface (real) area and flat (plan) area of square cells or triangles defined by input points, by calculating the ratio of these values. According to Hobson (1972) flat surfaces would present values close to one, whilst with irregular surfaces the ratio shows a curvilinear relationship which asymptotically approaches infinity as the real area increases.

Different measurements of *vector dispersion* (or orientation) were used as a proxy for surface roughness (e.g., Hobson 1972; Day 1979; Guth 2003; McKean and Roering 2004). An array of regularly spaced elevation values can be divided into planar triangular surfaces and normals to these planes represented by unit vectors. Values of vector mean, strength (R) and dispersion (k) can be calculated for each square cell. In smooth areas, with similar elevations, vector strength is expected to be high and vector dispersion to be low, since the vectors will become parallel, as R approaches N. In rough areas, the non-systematic variation in elevation readings will result in low vector strength and high vector dispersion.

Several authors define surface roughness in terms of the *variability of elevation* values, generally expressed as the absolute standard deviation of all values within a window, or as the deviation from a best-fit plane (e.g, Haneberg et al., 2005, Frankel and Dolan 2007, Evans 1984). As the *slope* denotes the rate of change of elevation, *profile curvature (profc)* measures the rate of change of slope. Area ratio, vector dispersion, SD_{elev}, SD_{slope} and SD_{profc} were selected for further study.

The selected methods are suited to array-based calculations using DEMs as primary input data and were implemented as shell scripts in GRASS-GIS (Neteler and Mitasova 2007, GRASS Development Team 2008) as sequences of neighbourhood (i.e. moving-window) and raster map algebra analysis steps.

Moving-window operators were adopted because the morphometric parameter is calculated for all input cells, so there is no risk of ”missing" any terrain feature (Grohmann and Riccomini 2009). The flexibility of array-based calculations also means that a multi-scale study can be performed simply by changing the neighbourhood size.

2. Methodology and Study Area

A study area located in the Midland Valley, Scotland (Fig. 1), was selected. The NEXTMap Britain (Smith et al., 2006) DEM was considered suitable as the input dataset. This product was acquired and produced by Intermap Technologies using airborne InSAR at a spatial resolution of 5 m.

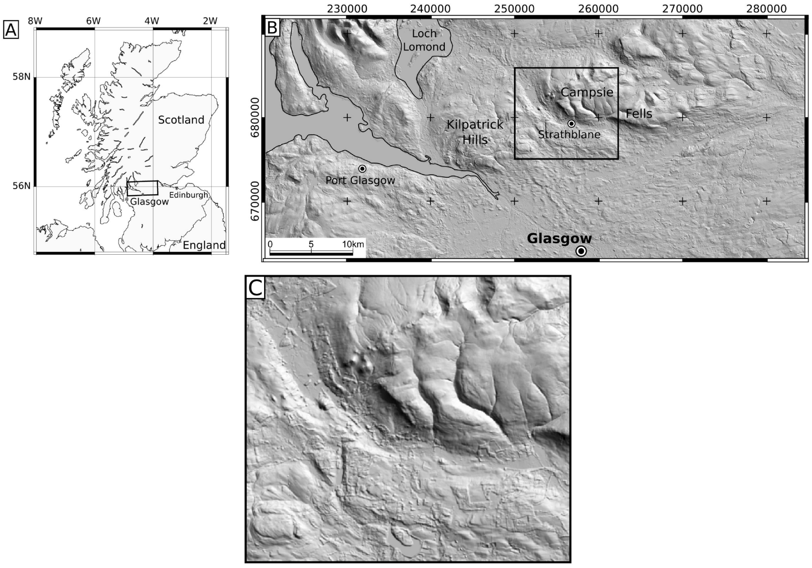

Figure 1. Shaded relief image depicting the location of the study area (illumination 045º, elevation 30º, no vertical exaggeration).

To evaluate the effects of spatial resolution, the original DEM was resampled by calculating the mean elevation value at resolutions of 10, 25, 50 and 100 m. To evaluate scale effects of roughness, the selected methods were applied to all DEMs using moving-windows of 3x3, 5x5, 7x7, 9x9, 11x11, 13x13, 15x15, 17x17, 19x19, 21x21, 31x31 and 51x51 cells. Roughness was calculated for the 5 resolutions and 12 window sizes, giving a total of 300 individual model runs.

To calculate area ratio, the surface area of individual cells was calculated from the trigonometric relationships between the square (horizontal) pixel and its inclined projection, given by slope (Grohmann 2004).

To calculate vector strength (*R*) and dispersion (*1/k*), compass-oriented aspect, colatitude (90^o-*slope*), direction cosines (Equation 1) and sum of direction cosines in a neighbourhood (Equation 2) were calculated. Vector strength was derived according to equation 3 and vector dispersion as the inverse of equation 4.

$$x_i = \sin \theta_i \cos \varphi_i \qquad y_i = \sin \theta_i \sin \varphi_i \qquad z_i = \cos \theta_i \tag{1}$$

$$\bar{x} = \sum_{i=1}^{N} x_i \qquad \bar{y} = \sum_{i=1}^{N} y_i \qquad \bar{z} = \sum_{i=1}^{N} z_i \tag{2}$$

$$R = \sqrt{\bar{x}^2 + \bar{y}^2 + \bar{z}^2} \tag{3}$$

$$k = (N - 1)/(N - R) \tag{4}$$

Standard deviation outputs were calculated using common moving-window tools.

3. Results and Discussion

Initial results are depicted in Fig. 2 A-D, where surface roughness, calculated using a 11x11 moving-window over the DEM with 10 m spatial resolution, are presented for the selected methods (area ratio, vector dispersion, SD_{elev}, SD_{slope} and SD_{profc}). Shades of yellow correspond to smoother areas, green-blue tones to intermediate values and purple-red to rough areas. It should be noted that the original roughness values were normalized, in order to provide a direct comparison of the maps.

For the area ratio output (Fig. 2A), the predominance of cyan-blue tones indicates that this method fails to distinguish features with similar elevation. The scarps of Campsie Fells are marked with high roughness values, since they have steep slope angles, even though they may be considered as smooth [inclined] surfaces.

For the vector dispersion output (Fig. 2B), the predominance of blue-purple tones indicates the sensitivity of this method to short-scale (i.e. local) variations in elevation, which are common in InSAR datasets over vegetated and urban areas. In this image the scarps of the Campsie Fells are depicted as smooth areas, with low vector dispersion.

The output for SD_{elev} (Fig. 2C) shows a predominance of low values (yellow-green tones), with the scarps of the Campsie Fells marked with high values due to the steep slopes. This method is also sensitive to local strong variations in elevation, which can be caused by spurious data.

SD_{slope} (Fig. 2D) is sensitive to sudden changes in the original slope values, and highlights the boundaries of urban and forest areas. The scarps of the Campsie Fells are correctly identified as smooth areas, with high values located over the slope break, indicating that this method is suitable for terrain analysis.

SD_{profc} (FigFig. 2E) does not identify the slope break of the Campsie Fells scarps. The higher values are found in urban and vegetated areas, indicating a sensitivity to strong variations in slope, as seen in urban features.

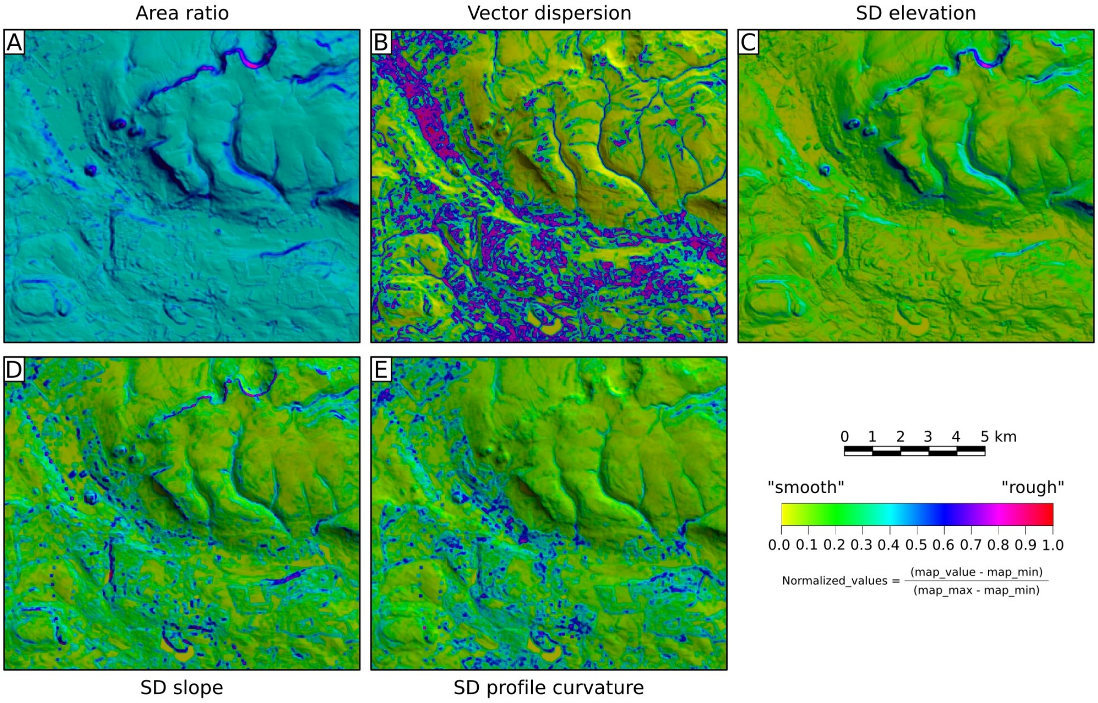

Figure 2. Sample output for surface roughness calculations. A) area ratio; B) vector dispersion (*1/k*); C) standard deviation of elevation ; D) standard deviation of slope; E) standard deviation of profile curvature. All outputs were calculated using a 11x11 neighbourhood for the 10 m DEM.

Fig. 3 shows the effect of changing the spatial resolution of the DEM for vector dispersion and SD_{slope}. Fig. 4 shows the effect of changing the moving-window size for vector dispersion and SD_{slope}. Fig. 5 depicts density plots of window size at four DEM resolutions (10, 25, 50 and 100 m) for all selected methods.

Our tests demonstrate that for area ratio the broad pattern of roughness does not change across scales or window sizes. Whilst smoothing does occur at coarser resolutions and larger window sizes, area ratio is generally scale independent.

The results for vector dispersion show a more complex relationship with resolution and window size. As resolution decreases and window size increases, roughness increases. Whilst vector dispersion is less sensitive to outliers, it only depicts roughness at certain scales and doesn't identify regional roughness features (i.e. mountain blocks). Unlike area ratio, it does (correctly) depict uniform slopes as smooth.

SD_{elev} shows an increase in roughness as resolution and window size increases, with the effect greater at coarser resolutions. In particular, breaks-of-slope are identified so that at coarser resolutions and larger window sizes, regional relief is identified.

SD_{slope} shows an increase in roughness as resolution and window size increases. Density plots exhibit a transition from unimodal distributions to bimodal or multimodal distributions with increasing window size, a behaviour enhanced at low spatial resolutions.

SD_{profc} shows a fast increase in roughness as window size increases even with moderately high resolution (20 m), Interestingly, with 50 m spatial resolution, density curves for windows from 11x11 to 21x21 pixels present a peak at about the same value.

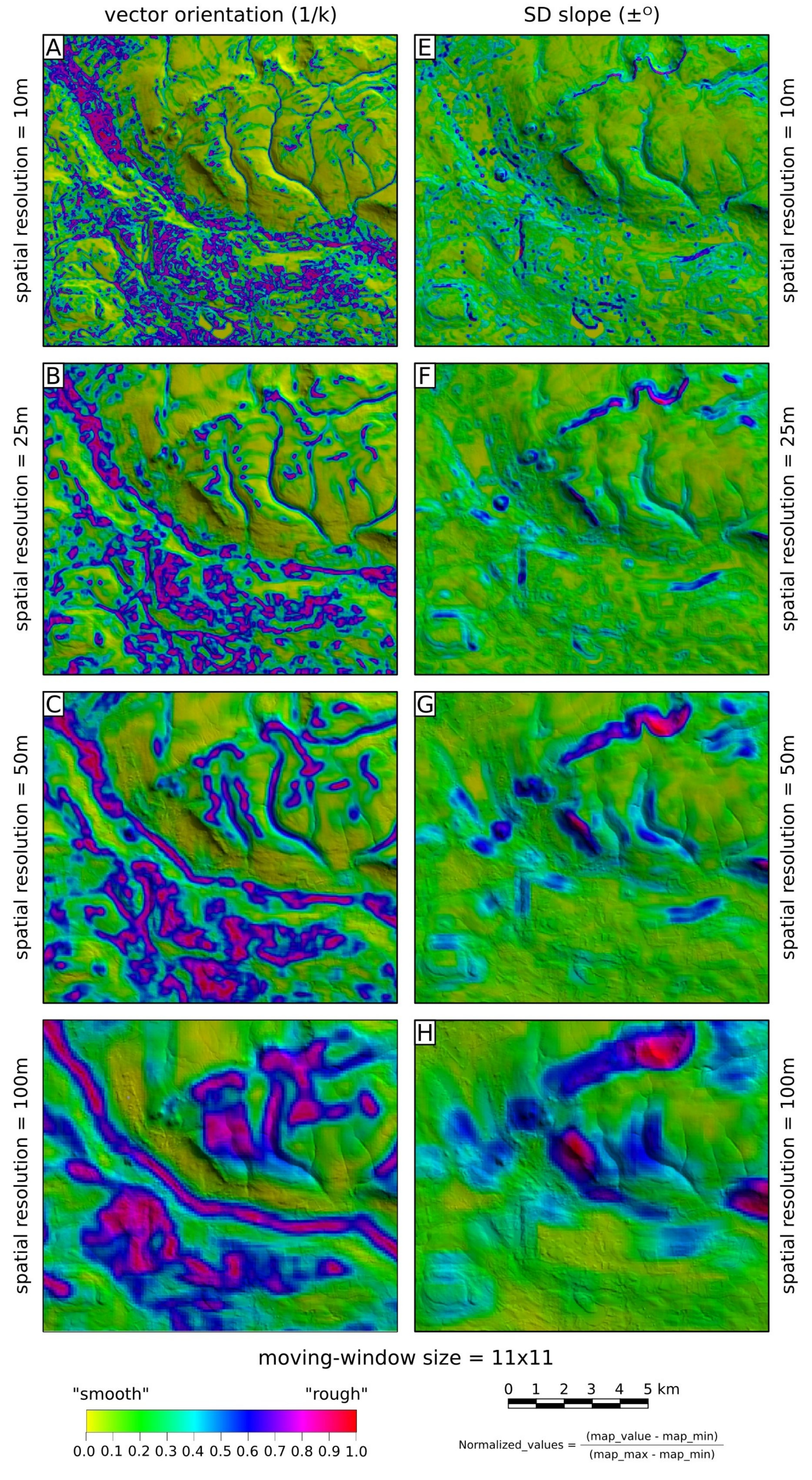

Figure 3. Effect of changing spatial resolution of the input DEM. Vector dispersion and SD_{slope} calculated using a 11x11 moving window.

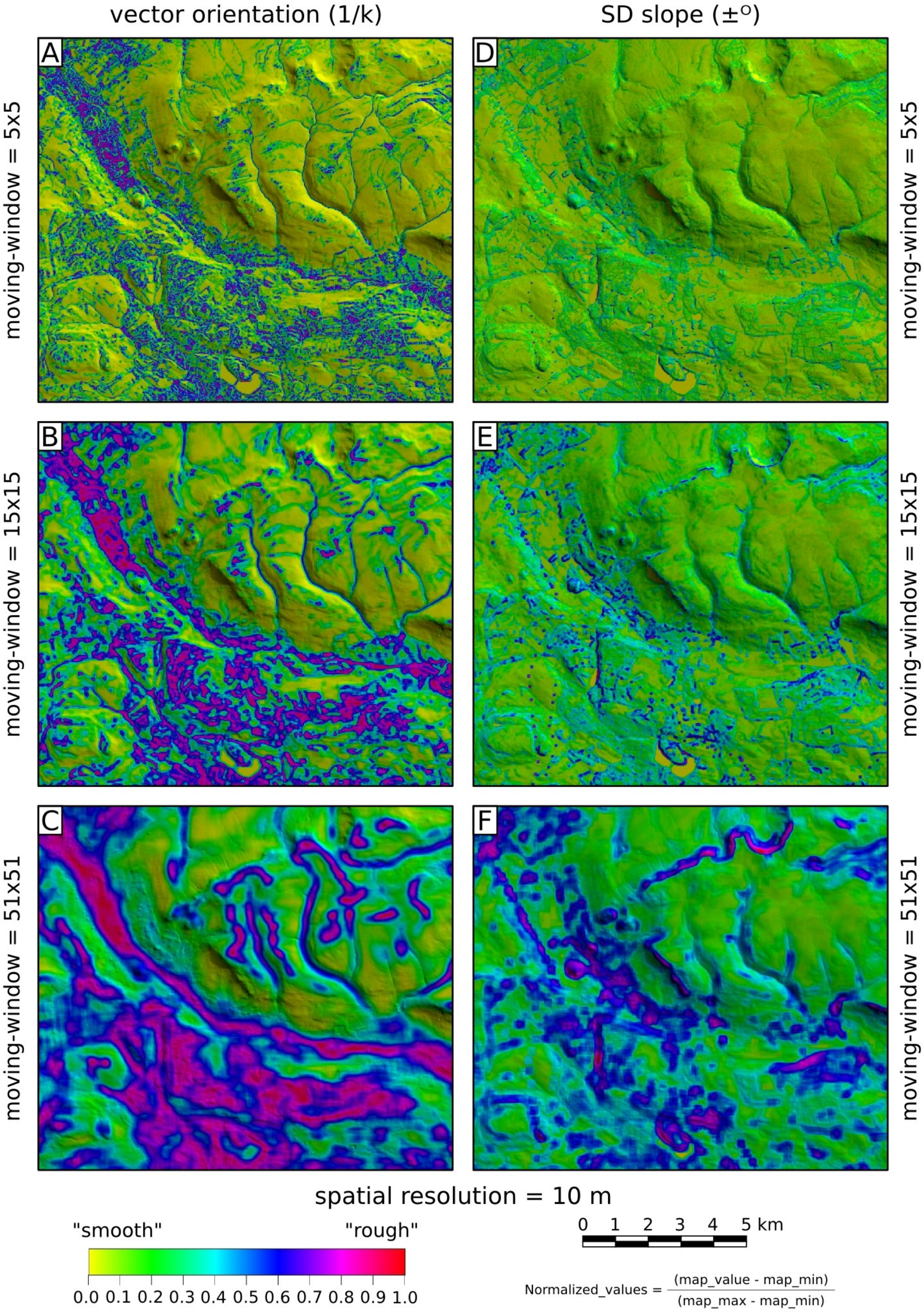

Figure 4. Effect of changing moving-window size for vector dispersion (A-C) and SD_{slope} (D-F). Output is calculated over the DEM with 10 m spatial resolution.

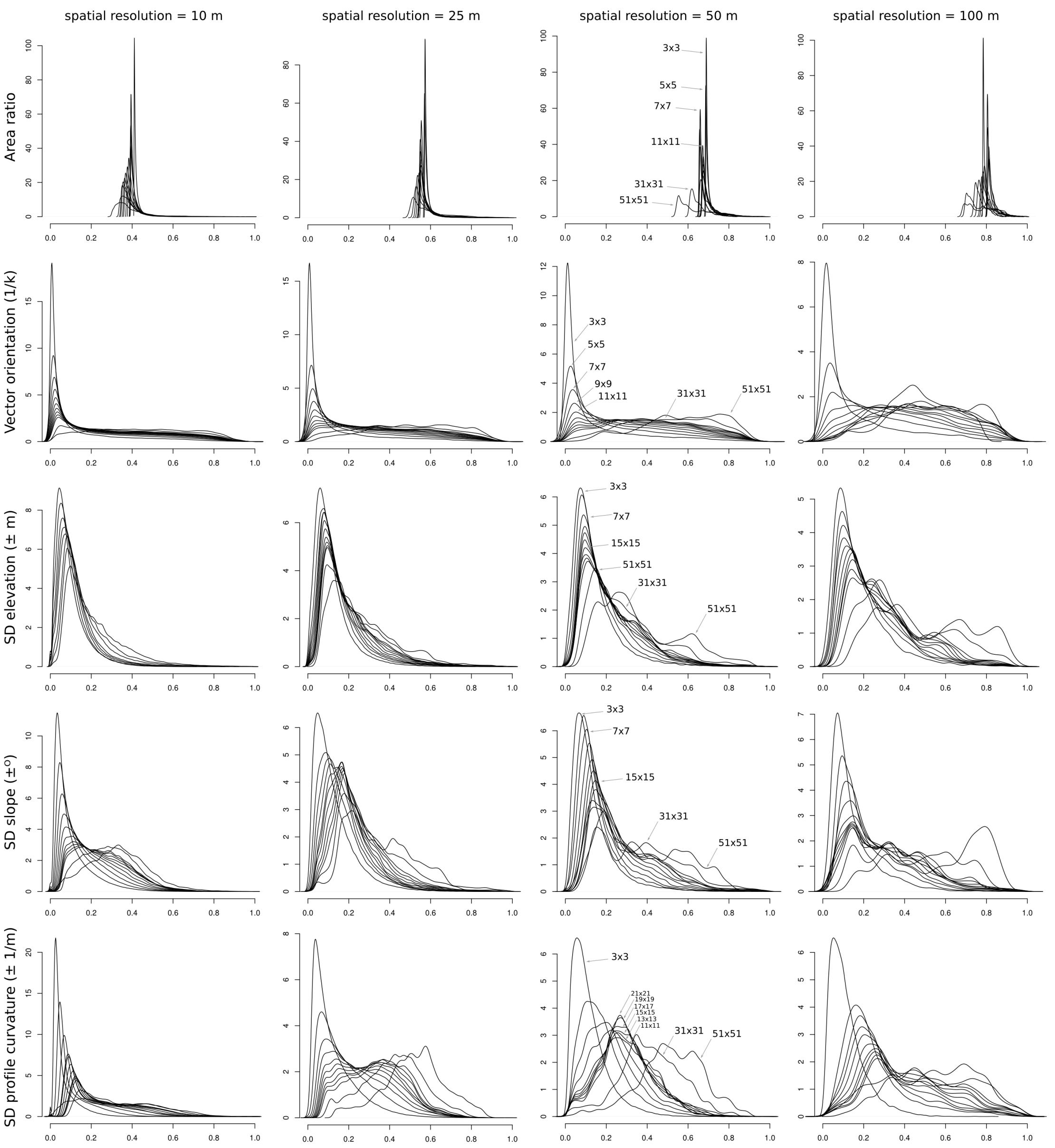

Figure 5. Density curves for the selected roughness methods plotted at four spatial resolutions (10, 25, 50 and 100 m) for 12 moving window sizes.

4. Conclusions

There is a general trend of inclusion (or exclusion) of features into homogenous neighbourhoods at coarser resolutions and larger window sizes. Large landscape elements are not depicted by small neighbourhoods while local, “fine scale”, features are obliterated over wide areas. Spatial resolution is important here when, for example, studying landforms hundreds of metres wide. In this instance there is little advantage in using a detailed, fine-resolution DEM, as a large neighbourhood will be required and the number of cells within the window grows exponentially. This dramatically increases the computational time involved in roughness calculations.

In summary, area ratio operates independently of scale, providing a consistent result which means that coarser resolution DEMs should produce similar results to detailed DEMs. This is a significant advantage, although it should be noted that steep, smooth, slopes will appear as rough terrain and that this method fails in distinguishing features with similar elevations.

Vector dispersion produces a much wider range of results with increasing roughness (and homogenization of terrain) at coarser resolutions and larger window sizes. Whilst steep, smooth, slopes will have low roughness values, breaks-of-slope are not readily delimited and regional relief is more difficult to identify. However vector dispersion is good at identifying fine-scale roughness features and there is the potential for its use in automating the removal of "surface clutter" from DEMs.

SD_{elev} identifies breaks-of-slope and is therefore good at detecting regional relief. Even at fine resolutions and small window sizes it remains good at identifying small features, although standard image processing techniques (such as contrast stretches) may be required to emphasise them.

Finally, SD_{slope} correctly identifies steep smooth slopes and areas of "surface clutter" (e.g. forest stands) whilst also identifying breaks-of-slope across scales.

SD_{profc} does not identify breaks-of-slope, and is very sensitive to sudden changes in slope, as seen in urban features.

In addition to good performance at a variety of scales, both SD_{elev} and SD_{slope} benefit from the simplicity of the calculation which is perhaps their single greatest benefit. A final word of caution should be exercised with the use of output from SD_{slope} as any noise or error in the original elevation data may be enhanced.

Acknowledgements

This study was supported by CAPES/PDEE-BEX Grant 5176/06-9 and FAPESP Grant 04/06260-5 to Grohmann. Riccomini is a Research Fellow of CNPq, Grant 304649/2005-8. We gratefully acknowledge Intermap Technologies for the supply of NextMap Britain data.

References

Day MJ, 1979, Surface roughness as a discriminator of tropical karst styles. *Zeitschrift fur Geomorphologie*, Suppl.-Bd. 32:1–8.

Evans IS, 1984, Correlation structures and factor analysis in the investigation of data dimensionality: statistical properties of the Wessex land surface, England. *International Symposium on Spatial Data Handling*, Zurich, 1:98–116.

Frankel KL and Dolan JF, 2007, Characterizing arid region alluvial fan surface roughness with airborne laser swath mapping digital topographic data. *Journal of Geophysical Research (Earth Surface)*, 112:F02025.

GRASS Development Team 2008, *Geographic Resources Analysis Support System (GRASS GIS)* Software, version 6.3.0. http://www.grass.osgeo.org

Grohmann CH, 2004, Morphometric analysis in Geographic Information Systems: applications of free software GRASS and R., *Computers & Geosciences*, 30:1055–1067.

Grohmann CH and Riccomini C, 2009, Comparison of roving-window and search-window techniques for characterising landscape morphometry. *Computers & Geosciences, in press*. DOI: 10.1016/j.cageo.2008.12.014

Guth PL, 2003, Concepts and Modelling in Geomorphology: International Perspectives, chapter *Eigenvector Analysis of Digital Elevation Models in a GIS: Geomorphometry and Quality Control,* page 199-220. TERRAPUB, Tokyo.

Haneberg WC, Creighton AL, Medley EW and Jonas DA, 2005, Use of LiDAR to assess slope hazards at the Lihir gold mine, Papua New Guinea. In: Hungr O, Fell R, Couture R, and Eberhardt E, (eds), *Proceedings of International Conference on Landslide Risk Management,* Vancouver, Canada, Supplementary CD.

Hobson RD, 1972, Surface roughness in topography: quantitative approach. In Chorley, R. J., editor, *Spatial analysis in geomorphology*, pages 225–245. Methuer, London.

McKean J and Roering J, 2004, Objective landslide detection and surface morphology mapping using high-resolution airborne laser altimetry. *Geomorphology*, 57:331 351.

Neteler M and Mitasova H, 2007, *Open Source GIS : A GRASS GIS Approach*, Third Edition (The Kluwer International Series in Engineering and Computer Science), volume 773. Springer.

Smith MJ, Rose J, and Booth S, 2006, Geomorphological mapping of glacial landforms from remotely sensed data: An evaluation of the principal data sources and an assessment of their quality. *Geomorphology*, 76:148–165.

Enhancing the SRTM Data for Australia

J. C. Gallant[1], A. Read[2]

[1]CSIRO Land and Water, GPO Box 1666, Canberra ACT 2601, Australia
Telephone: +61 2 62465734
Fax: +61 2 62465800
Email: John.Gallant@csiro.au

[2]CSIRO Land and Water, GPO Box 1666, Canberra ACT 2601, Australia
Telephone: +61 2 62465782
Fax: +61 2 62465800
Email: Arthur.Read@csiro.au

1. Introduction

The SRTM dataset is a near-global DEM derived from interferometric radar data collected by NASA's Space Shuttle in February 2000. It is unique in providing reasonably good quality topographic data over most land masses but suffers from a number of artefacts including: voids in high relief areas and some other locations; striping artefacts; and offsets due to woody vegetation. It was produced at 1 second (about 30 m resolution) but degraded to 3 second resolution for public release except for the USA.

In Australia, the SRTM data provides better quality topographic information than other available sources over much of the continent. Its utility is hampered by the artefacts, particularly the offsets induced by vegetation. Many rivers in inland Australia are surrounded by remnant native vegetation while the surrounding land is cleared for agriculture; the rivers thus appear as raised features in the SRTM data preventing any useful hydrological analysis.

This paper describes methods developed to treat the artefacts in the SRTM data to produce a usable DLSM. Negotiations with Australia's Defence Imagery and Geospatial Organisation (DIGO) have resulted in access to the 1 second version of the SRTM data and permission to release processed versions of that data at 1 second resolution to government agencies within Australia. Reduced resolution 3 second versions will be publicly available.

The methods described could be applied to SRTM data in other areas that lack better quality DEM data, such as Africa, so long as vegetation mapping is also available to support the removal of vegetation offsets. The methods could also be adapted to treat similar offsets in other radar or photogrammetric products that do not directly map land surface heights in vegetated areas.

2. Removal of Striping Artefacts

The first step was to remove striping artefacts, which are clearly visible in some areas of low relief Australia. The stripes have a typical wavelength of about 800 m with an amplitude of about 0.2 – 4 m and are aligned diagonally in a pattern that suggests a close relationship to the orbital paths. A software tool was developed to display tiles of the raw SRTM data (¼ × ¼ degree) and a 2-D Fourier transform of the data and support identification and removal of frequency components corresponding to the stripes (Figure 1). The tool was used by a team of analysts to remove striping wherever stripes could be discerned across the continent.

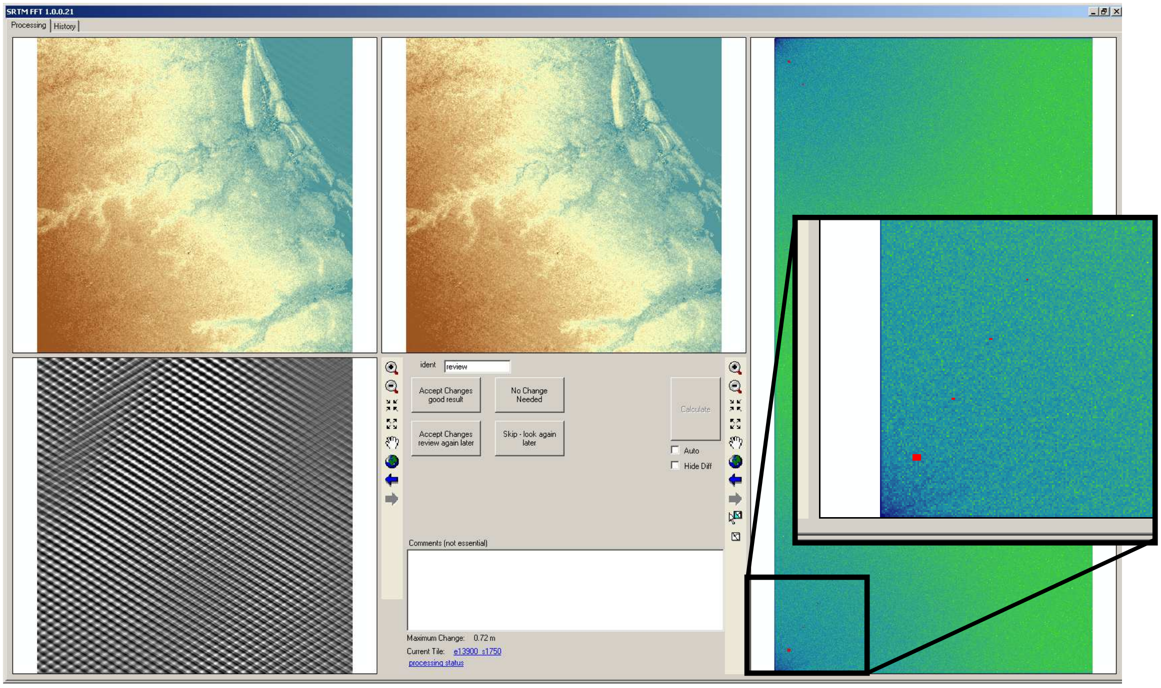

ident: review

Maximum Change: 0.72 m

Current Tile: e13900_s1750

Figure 1. The SRTM striping removal tool. The DEM in top centre shows the stripes, the treated DEM is at top left. The removed stripes are at lower left and the right hand pane shows the magnitude of the Fourier transform with red boxes around frequency components to be removed (expanded in inset).

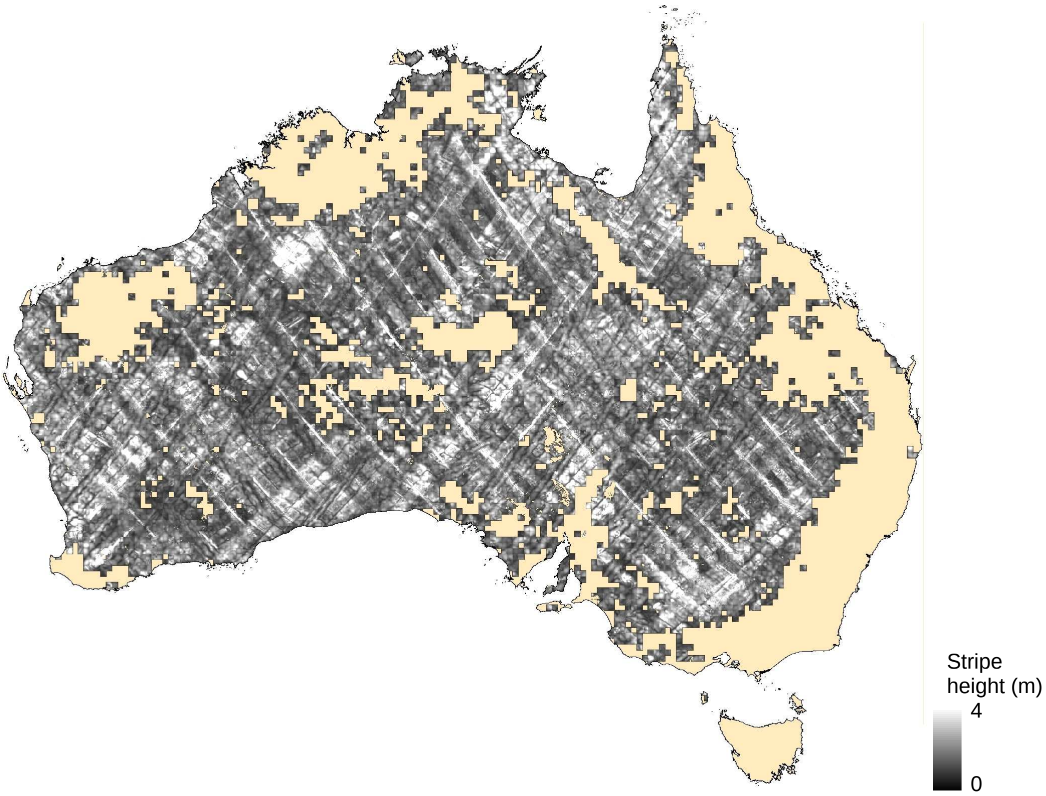

Figure 2. The magnitude of stripes removed across Australia. The tan areas were not treated because the striping was not visible in the higher relief terrain.

This processing took about 8 weeks for four analysts, and revealed that striping at varying levels occurred everywhere except where it was obscured by high topographic relief. Figure 2 shows the pattern and level of striping that was removed.

3. Filling Voids

Voids were filled using a modification of the delta surface fill method (Grohman *et al*., 2006). The Geodata 9 second DEM (Geoscience Australia, 2008) was used as the infill data. The delta surface fill method was modified to use natural neighbour interpolation (Sibson, 1981; implemented in ArcGIS 9.3) to create the delta surface, and the mean plane inside the larger voids was not used. The delta surface fill method was chosen because it offered better prospects of filling extensive voids in rugged terrain (such as those shown in Figure 3) than an interpolation-based algorithm.

The void filling process provides an effective fill in both flat and high relief terrain, although many voids in low relief terrain are surrounded by erratic heights that propagate into the void. Figure 3 shows an example of void filling.

The product of the destriping and void filling is a cleaned digital surface model (DSM) that still includes offsets due to vegetation and constructed features but is a valuable product for some applications such as calculating line of sight and illumination angles for correcting remotely sensed imagery.

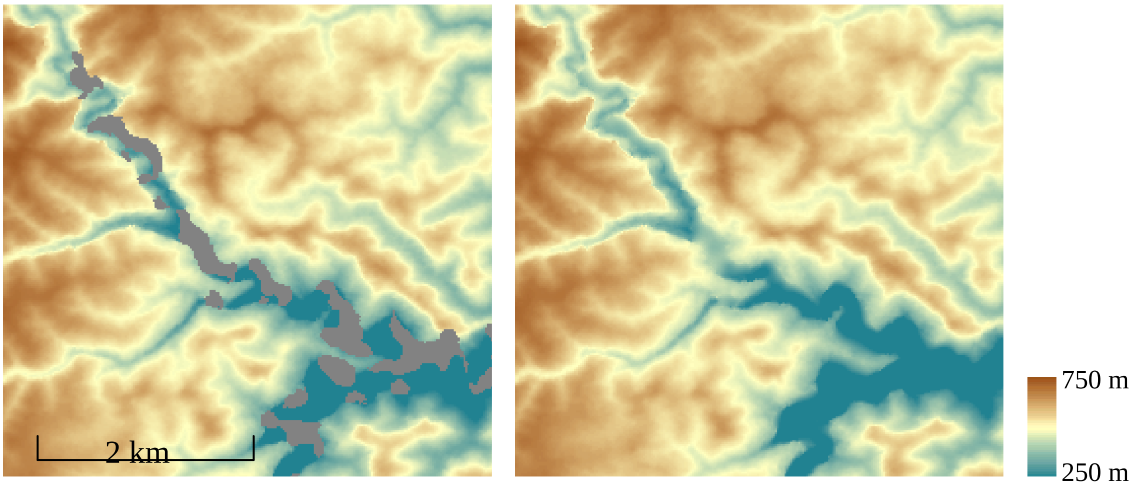

Figure 3. An example of void filling. The voids due to terrain shadowing are replaced with adjusted lower resolution data. Some areas at the base of the deep valleys are not accurately represented but the results are much better than would be achieved using interpolation across the voids.

4. Removing Vegetation Offsets

The removal of vegetation offsets is the most complex part of the cleaning process. The strategy taken here is to identify areas that are affected by vegetation offsets, estimate the height offsets around the edge of each patch and derive a vegetation offset surface that is then subtracted from the destriped SRTM data to produce a bare-earth elevation model.

Vegetation patches are identified using woody vegetation mapping based on satellite remote sensing, supplemented by detection of narrow linear features directly from the SRTM data. The edges of the patches are adjusted to match changes in height in the DEM. The vegetation height is estimated by fitting a surface to elevations in a circle of 5 cell radius; the surface is represented as:

$$z(x,y) = a_0 + a_1x + a_2y + a_3xy + a_4m \qquad (1)$$

where $a_0 \ldots a_3$ are parameters of the land surface, a_4 is the vegetation height and m is the vegetation mask smoothed by a Gaussian filter to match the response of the SRTM data to sharp edges. The estimates of vegetation height are accepted where the fit of

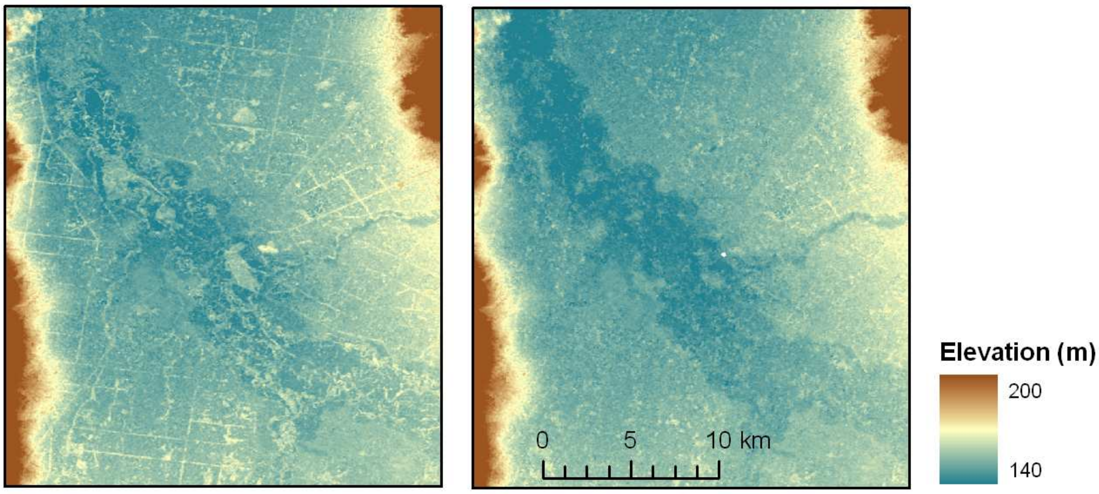

Figure 4. An example of vegetation removal. The elevated linear features are due to trees along roads, while the larger elevated features are patches of forest among cleared land. Most of the offsets are completely removed, revealing the inset floodplain of the river flowing through the centre of the image.

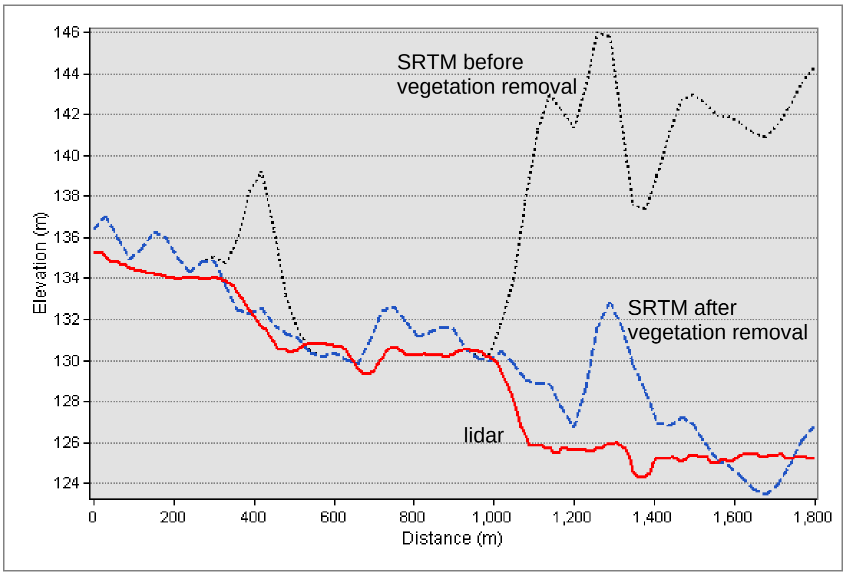

Figure 5. Profiles through SRTM data before and after vegetation removal, compared with lidar data. The profiles are on a transect from cleared farming land (left) through a narrow tree line (~400 m) into forested floodplain (right).

Equation 1 produces sufficiently low fitting error and they satisfy some sanity checking and the acceptable estimates are then interpolated to form a continuous vegetation height surface. The vegetation height surface multiplied by the smoothed vegetation mask m is subtracted from the destriped SRTM data.

The vegetation-removed product is a digital land surface model (DLSM) that is a good source for many geomorphic and ecological applications but lacks drainage connectivity in low relief areas. A comprehensive manual quality assurance process was used to assess the quality of vegetation removal and identify any issues with the product.

Figure 4 shows an example of the removal of vegetation offsets. Figure 5 compares the SRTM data before and after vegetation removal with elevations from a lidar DEM; most (but not all) of the vegetation offsets have been removed and the resulting DLSM is a reasonably good match to the lidar data considering the inherent uncertainty in the SRTM data.

5. Drainage Enforcement and Smoothing

The vegetation-removed bare-earth DLSM lacks drainage connectivity in lower relief areas, due to both the noise in the SRTM data and to the effects of vegetation along drainage lines. In much of inland rural Australia the land is cleared for agriculture except for riparian woodlands and forests along waterways that obscure the channel itself. Mapped streamlines derived from aerial or satellite imagery are required to support enforcement of drainage lines in the terrain surface. This has been achieved using ANUDEM (Hutchinson 1989, 2000, 2006), modified to improve its performance with dense noisy data such as SRTM (Hutchinson *et al*, 2009). The ANUDEM processing also produces a modest degree of smoothing that reduces the noise in the surface.

The finest scale of mapped drainage lines covering all of Australia is 1:250,000, which is a much coarser scale than the SRTM data which has an effective scale of approximately 1:50,000. Finer scale drainage line data is expected to be acquired for much of Australia over the next few years and will be incorporated into the SRTM products (and subsequent better quality terrain data) as they become available.

6. Discussion

The cleaning of the digital surface model has not resolved all issues with that data. Broad-scale striping with a wavelength of about 30 km (compared to about 800 m for the fine striping removed) has been detected in one area of southern New South Wales. There are abrupt changes in height of up to 5 m in some areas, random height variations due to noise are as large as ± 10 m in some areas, and one area of grossly incorrect height has been detected in a canyon west of Sydney. With some effort, and with supporting data, the areas of incorrect height can be detected and corrected, and noise can be reduced by adaptive smoothing.

The method to remove vegetation offsets performs well where the vegetation patches are well mapped and where the distance between estimated heights is not too large. Within larger vegetation patches the estimates of vegetation height are dependent on interpolation from distant edges and become less reliable. Some additional information on vegetation height would help to constrain the heights in these areas.

As of May 2009, the destriping and void filling is complete, vegetation removal is complete and drainage enforcement for the Murray-Darling basin is expected to be complete by June 2009.

The production of a continental DLSM at 1 second resolution from SRTM data represents a major advance in digital terrain data from Australia. The current best continental coverage is at 9 second resolution interpolated from 1:250,000 and 1:100,000 topographic data. The 1 second data is expected to support many new applications including study of landforms in the arid and low relief areas of Australia.

The methods developed for this project are applicable to other parts of the world that lack high resolution digital terrain data, provided the supporting data – mapping of woody vegetation in particular – are available. Use of the methods to remove vegetation offsets in other digital surface models, such as those derived from ASTER data, is also under investigation.

Acknowledgements

This work was funded by CSIRO’s Water for a Healthy Country research flagship and by the Bureau of Meteorology.

The 1 second resolution SRTM data for Australia was provided by Australia’s Defence Imagery and Geospatial Organisation (DIGO). The products of this work can be obtained from Geoscience Australia at 1 second resolution for Australian Government users and at 3 second resolution for other users.

References

Geoscience Australia, 2008, GEODATA 9 Second DEM and D8:Version 3 and Flow Direction Grid 2008, http://www.ga.gov.au/nmd/products/digidat/dem_9s.jsp.

Grohman G, Kroenung G and Strebeck J, 2006, Filling SRTM voids: The delta surface fill method. *Photogrammetric Engineering and Remote Sensing* **72** (3):213-216.

Hutchinson MF, 1989, A new method for gridding elevation and streamline data with automatic removal of pits. *Journal of Hydrology* 106:211-232.

Hutchinson MF, 2000, Optimising the degree of data smoothing for locally adaptive finite element bivariate smoothing splines. *Australian & New Zealand Industrial and Applied Mathematics Journal* 42(E):C774-C796.

Hutchinson MF, 2006, ANUDEM Version 5.2. Fenner School of Environment and Society, Australian National University. Available online at: http://fennerschool.anu.edu.au/publications/software/anudem.php (accessed Feb 2009).

Hutchinson MF, Stein JA and Zhu T, 2009, Locally adaptive gridding of noisy high resolution topographic data. In R Anderssen, R Braddock and LTH Newham, MODSIM09 International Congress on Modelling and Simulation, Cairns, 13-17 July 2009. Modelling and Simulation Society of Australia and New Zealand.

Sibson R, 1981, A brief description of natural neighbour interpolation. In V. Barnet, editor, *Interpreting Multivariate Data*, pages 21-36. John Wiley & Sons, Chichester.

Preprocessing of Digital Elevation Models – derived from Laser Scanning and Radar Interferometry – for Terrain Analysis in Geosciences

R. Köthe[1], M. Bock[1,2]

[1]scilands GmbH, Goetheallee 11, D-37073 Göttingen, Germany
Telephone: +49 551 5315870
Fax: +49 551 5315873
Email: koethe@scilands.de

[2]University of Hamburg, Bundestraße 55, 20146 Hamburg, Germany
Telephone: +49 040 42838-7418
Email: mbock@scilands.de

1. Introduction

The application and availability of digital elevation models (DEM) and digital terrain models (DTM) is increasing since many years. Whereas in former years DTM were often derived from contour lines of topographic maps and stereoscopic measurements form aerial images nowadays small scale DEM are often derived form radar interferometry such as the well known DEM from the Shuttle Radar Topography Mission (SRTM) (http://www.jpl.nasa.gov/srtm/) which covers 80% of the earth's landmass (Guth 2006). Large scale DTM are based increasingly on laser scanning which allows the interpolation of high resolution DTM with cell sizes < 1m.

However you can observe that the terms DEM and DTM are often used inaccurately. Another aspect is that for terrain analysis in geosciences often the DEM of other surfaces than the terrain (earth's surface) is used. For example: using SRTM DEM in flat regions for calculating drainage basins will produce watersheds on forest canopies because SRTM DEM is (approximately) a DEM of the vegetation surface.

This article aims – beside clarifying terms as DEM and DTM - on presenting approaches of preprocessing DEM/DTM to enable advanced terrain analysis in geoscience. The emphasis is on reducing elevation of forest canopies in radar based DEM (SRTM) and identifying and eliminating man-made terrain features in laser based DTM.

2. Definition of DEM, DTM and Earth's Surface

Going back to the suggestions of Hofmann (1986) and corresponding to the compendium Maune (2007) gave in his “DEM Manual” the following definitions may help to clarify the terms DEM/DTM:

Definition of digital elevation model (DEM): Digitally stored xyz triples of a surface. It is necessary to always mention *which surface* is represented by the DEM (for example DEM of the vegetation surface, DEM of the ground water surface).

Definition of digital terrain model (DTM): Digitally stored xyz triples of the *earth's surface.* Thus a DTM is simply one special case of the common term DEM: a DTM is a DEM of the earth's surface.

Therefore it is obvious that terrain analysis which calculates geomophometry or classifies terrain features should use a *DTM* as data base.

Nowadays most of the DEM/DTM are provided as raster (square grid) data. As the original measurements (xyz triples) in most cases are irregularly spaced, various interpolation techniques (which impact the quality) are used to create the grid data.

Definition of earth's surface: The earth's surface is commonly defined as the boundary layer between the solid crust and the atmosphere or water bodies.

You have to distinguish between different types of the earth's surface: *natural surface and man-made surface*. (A third type the *quasi natural surface,* relief formed by natural processes caused by human activity such as soil erosion, is not considered in this paper.)

3. Consequences of the Definitions for Terrain Analysis

From the above definitions a number of problems arise for terrain analysis:

a) It is not suitable to use DEM which represent the vegetation surface when morphometric parameters of the earth's surface should be calculated. In chapter 6 is presented an approach to convert SRTM DEM into a DTM.

b) Depending on the objective of the terrain analysis you have furthermore to distinguish between the natural surface and the man-made surface. Whereas contour lines in topographic maps show the natural surface (man-made terrain forms are omitted) especially laser based DTM always represent the man-made surface in all details. For modelling the surface runoff (e.g. for soil erosion or phosphate washout) the man-made terrain features are very important. For supporting digital soil mapping however man-made features cause problems. An example: the crossing of river flood plains by embankment dams has consequences for calculating soil relevant complex terrain parameters based on overland flow and stream lines, such as wetness indexes, relative elevation above stream lines or erosion/accumulation indexes.

c) Another problem is the identification and the handling of water bodies in DTM. Whereas SRTM provides water bodies as very useful information, DTM from laser scanning normally do not have this information. Without this information modelling hydrological parameters, such as flow accumulation or stream lines, is problematic. Solutions for these problems are still under development and therefore not presented in this paper.

4. Noise Reduction

A first step of preprocessing DEM/DTM is noise reduction. Both, laser and radar based DEM/DTM imply a certain noise. This noise (variation of elevation in local neighbourhood) does not contain any information for terrain analysis. In the case of radar based DEM the noise is immanent and termed 'thermal noise'. The noise of DTM derived from laser scanning depends on the roughness of the different measured surfaces (forest floors, fields, meadows, etc.).

To reduce or eliminate the noise advanced filter techniques are required which identify and eliminate the noise while saving the terrain information hidden under the noise. We used a modified and extended version of a multi directional noise filter (Lee 1980) to achieve this objective. In a first step the implemented filter creates bands of cells in all directions (e.g. with a length of 9 and a width of 3 cells) around every grid cell. Then the standard deviation (of elevation) is calculated for every band (direction). The new value (elevation without noise) for the grid cell is calculated from the mean elevation of the band with the lowest standard deviation and the original elevation of the cell. The weighting between mean and original value is controlled by the noise level and a user given noise reduction parameter (the more noise the more the weighting tends to the mean - and vise versa). To avoid bulges on slopes (parallel to contour lines) optionally the above calculations can be executed on slope gradient instead of elevation.

The results of the noise reduction are presented in fig. 1B, 2b and 3b.

5. Identifying and Eliminating Man-made Terrain Features in DTM Derived from Laser Scanning

DTM based on laser scanning (Liu 2008) are highly accurate models of the earth's surface. Buildings as well as trees are normally already filtered and provided as additional DEM of buildings and vegetation surface. However laser based DTM also show all man-made modifications of the earth's surface. As already mentioned (3.) for modelling relief controlled processes under natural conditions, it is necessary to identify the man-made terrain features and to "reconstruct" the natural surface. (Surely this attempt will find its limits within urban areas.)

As no high resolution spatial information about these terrain features is available, the developed filter to identify man-made features works without any additional data (e.g. about traffic buildings). Certainly manual control and correction of the result is definitely necessary. The functionality of the filter shall be briefly explained on the example of embankment - the most wide-spread man-made terrain feature outside of settlements:

The filter is based on a resampling module to generalise grid data. The developed algorithm calculates the values for the generalised grid cells under consideration of local maxima and minima within a given radius. For the maxima and minima the "trend" is calculated:. e.g. if the surface is flat within the radius but a pit exists there is a high trend for a local minimum. If pits and bumps are canceling each other the trend tends to "0". Thus the resampling module is able to conserve maxima and minima - or used in an inverse function to eliminate both which creates a very smooth surface.

The embankments normally show a much sharper shape than natural terrain features. Furthermore the dam crests mark local maxima of the elevation. These facts are utilised by the filter using the resampling approach described above. The difference of the original DTM and the version where maxima and minima are eliminated, contains nearly all man-made features (fig. 2a,c). Additional algorithms such as skeletonising crest lines and modified relief intensity are used to enhance the result. After manual controling the identified terrain features are eliminated and interpolated (fig. 2b) using standard gap filling module of free GIS SAGA (http://www.saga-gis.org/).

6. Estimating Elevation of Forest Canopies in DEM Derived from Radar Interferometry

The research leading to these results has received funding from the European Community's Seventh Framework Programme (FP7/2007-2013) under grant agreement number 211578. The processed data for EU countries will be distributed on a ftp server of the European Commission's Joint Research Centre. The mentioned grant agreement number stands for the e-SOTER project, the regional pilot platform as EU contribution to a Global Soil Observing System.

The spatial resolution of elevation measurements by radar signals and optical remote sensors is normally much lesser than that recorded by laser scanners. DEM derived from radar interferometry (e.g. SRTM) as well as from satellite images (e.g. ASTER) represent the earth's surface only in areas with low or sparse vegetation and low building densities. Particularly forest canopies cause problems for terrain analysis.

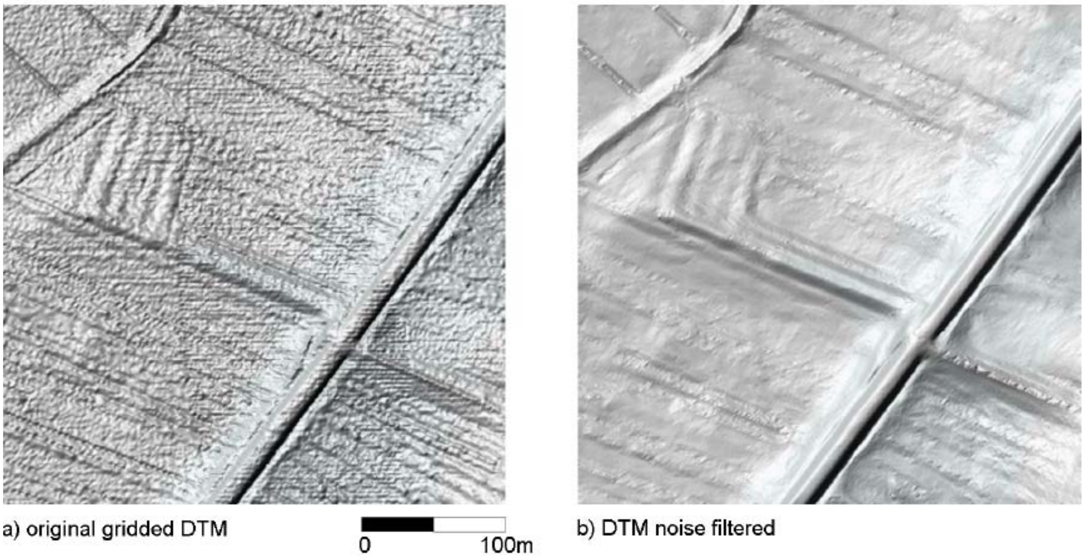

a) original gridded DTM

b) DTM noise filtered

Figure 1. Noise Filtering for a DTM from Laser Scanning (1m grid cell size)

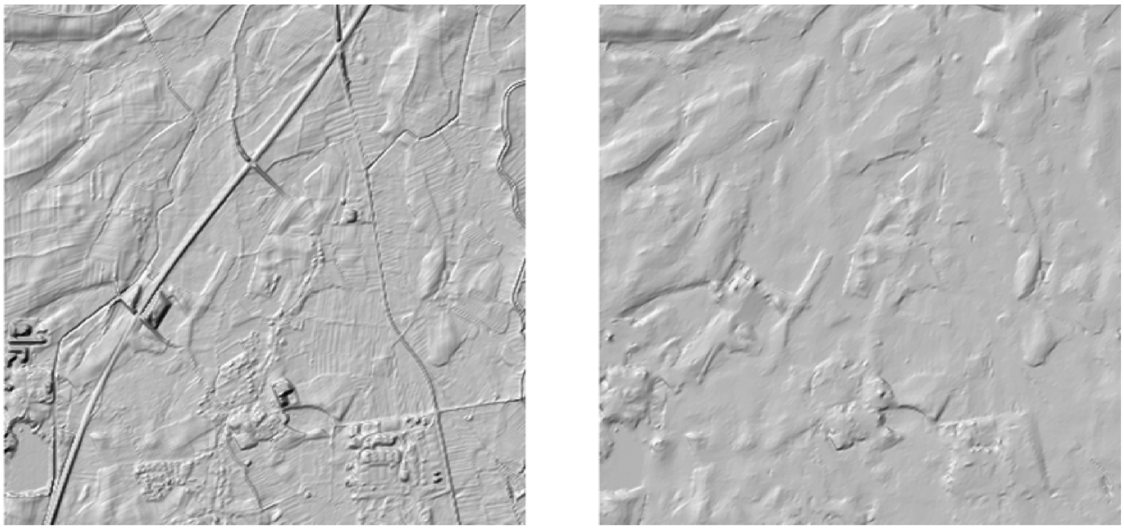

a) DTM including man-made Terrain Features

b) DTM man-made Terrain Features filtered

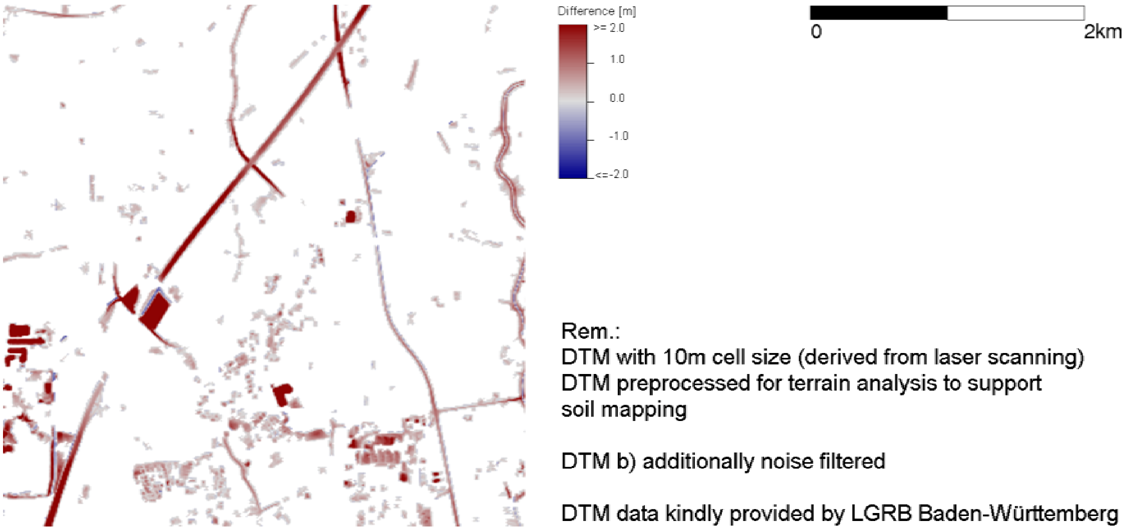

Rem.:
DTM with 10m cell size (derived from laser scanning)
DTM preprocessed for terrain analysis to support
soil mapping

DTM b) additionally noise filtered

DTM data kindly provided by LGRB Baden-Württemberg

c) man-made Terrain Features (Difference a - b)

Figure 2. Identifying and Eliminating man-made Terrain Features

The objective of the presented approach is the conversion of a DEM of the vegetation surface into a DTM. Calculating the elevation of forest canopies from a DEM representing the vegetation surface without having any information about tree/forest heights certainly is a "mission impossible". But the estimation of forest elevation - to a certain degree - is possible.

In contrast to the identification of man-made terrain features (see 5.) the estimation of forest elevation needs information about the *location* (not height) of forests. In Europe this information is available for large areas. For the processing of SRTM DEM we used the Pan-European Forest/Non-Forest Map (FMAP) 2000 version 1.4 (Pekkarinen 2009) for forest locations (Rem.: CORINE landcover data turned out as too coarse for SRTM DEM with a cell size of 3 arc sec. (approx. 75 to 90m).

The estimation of forest elevation is only possible at the forest borders. The flatter the terrain the better is the estimation. At first the forest borders - including a fringe of 3 grid cells inside and outside the forests - are located. The fringe is necessary because the 90m cell size of the DEM imply generalisation of the forest borders. For the cells of the "inside forest fringe" the positive relief intensity (a) is calculated. The "positive relief intensity" is defined as the altitude of a given cell minus the lowest of the lower neighbour cells within a given radius (here: 3 cells). In our case only cells of the "outside fringe" are considered as lower neighbour cells. Next the "negative relief intensity" (similar to "positive" but only higher cells are considered) is calculated for cells located only in the inside fringe. This second value (b) is subtracted from the positive relief intensity (a). The result is the estimated forest elevation. The subtraction a - b may result in "0" which means that the relief intensity inside the forest fringe is greater than the potential forest height. In this case it is impossible to estimate forest elevation.

The next step is to interpolate the forest elevation from the forest borders into the woods. This is achieved by an approach which creates fringes of 1 cell width from the borders into the centers of the forest bodies. With the increasing fringe number the radius for calculating mean values (of forest elevation) also increases (including a inverse distance weighting).

The last step is to subtract the estimated forest elevation from the DEM to get the DTM.

This is only a brief description of the approach which implies some more details than described. Moreover there are still some problems to solve (e.g. with small clearings and big forest bodies).

Figure 3 presents the result of the attempt to convert SRTM DEM into a DTM. The improvement of the data is also demonstrated by the change of the summary statistics of the deviation of a reference DTM from the two SRTM versions: Subtracting the reference DTM from the SRTM DEM (fig 3d) only for forest cells indicated by FMAP2000 results in an artithmetic mean of 7.98 meters with a standard deviation of 6.54 meters. After the procedure to create a DTM (fig 3e) the subtractions arithmetic mean is reduced to 1.91 meters with a remaining standard deviation of 4.44 meters.

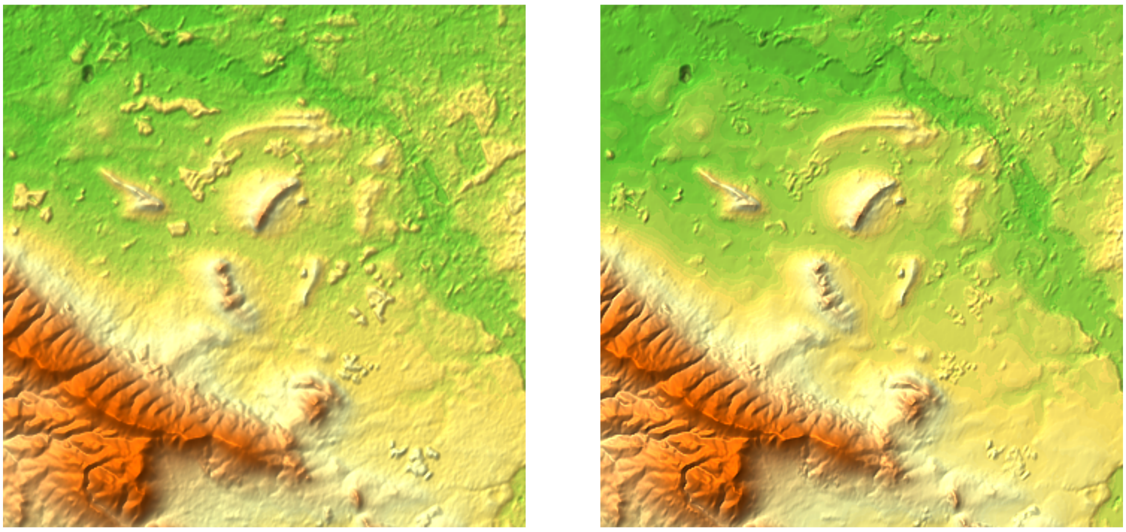

a) SRTM DEM with Forest Canopies

b) preprossed DTM without Forest Canopies, noise filtered

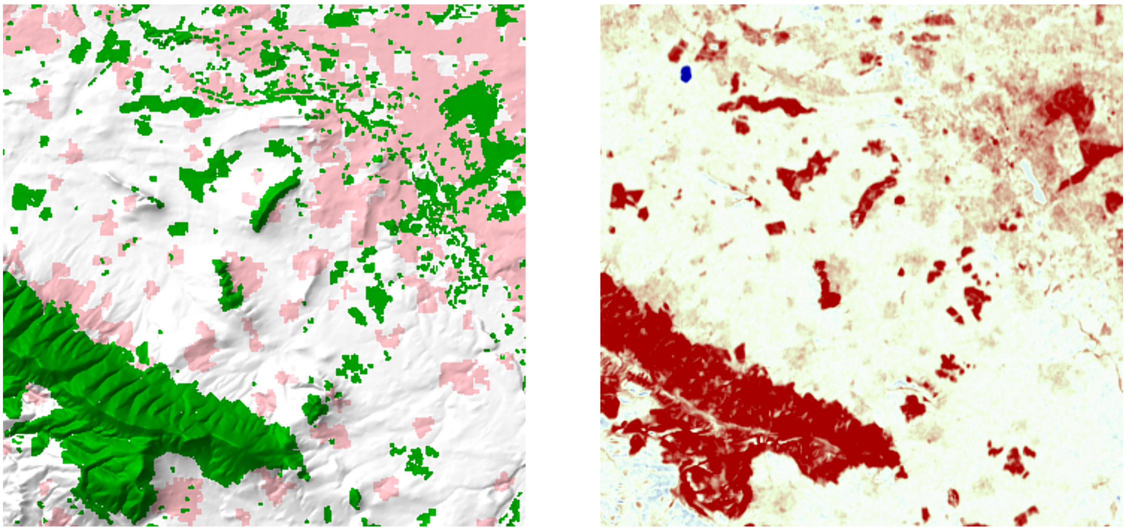

c) green: JRC Forest map, pink: settlements (CORINE)

d) Elevation Difference:
reference DTM - original DTM (fig. 3a)

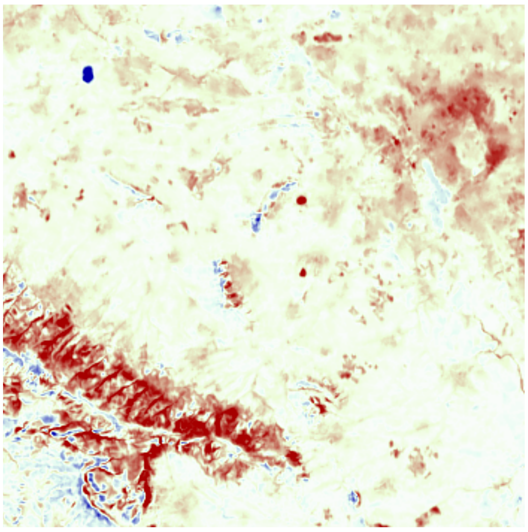

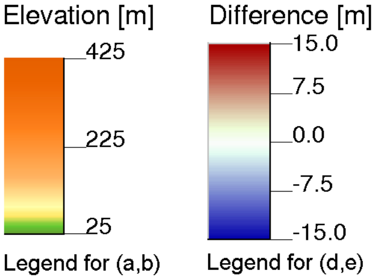

Rem.:
please notice also the impact of settlements (see c,d) on SRTM elevation

Reference DTM kindly provided by
LBEG Niedersachsen

e) Elevation Difference:
reference DTM - preprocessed DTM (fig. 3b)

Figure 3. Converting SRTM DEM into a DTM

References

Guth, P (2006): Geomorphometry from SRTM: Comparison to NED. - Photogrammetric Engineering & Remote Sensing, 72 (3): 269–277.

Hofmann, W. (1986): Wieder einmal: Das Digitale Gelände-/Höhenmodell. - Bildmessung u. Luftbildwesen, 54 (1): 31-31; Karlsruhe.

Lee, J.-S. (1980): Digital Image Enhancement and Noise Filtering by Use of Local Statistics. - IEEE Transactions on Pattern Analysis and Machine Intelligence, PAMI-2 (2): 65-168.

Liu, X. (2008): Airborne LiDAR for DEM generation: some critical issues. Progress in Physical Geography 32 (1): 31-49.

Maune, D. F. (ed.) (2007): Digital elevation model technologies and applications. The DEM users manual, 2nd edition. Maryland.

Pekkarinen, A., Reithmaier, L. & Strobl, P. (2009): Pan-European forest/non-forest mapping with Landsat ETM+ and CORINE Land Cover 2000 data. - ISPRS Journal of Photogrammetry and Remote Sensing, 64: 171-183.

Investigations on the Relation of Geomorphological Parameters to DEM Accuracy

H. Papasaika, E. Baltsavias

Institute of Geodesy and Photogrammetry
ETH Zurich
Wolfgang-Pauli-Str. 15, CH-8093, Zurich, Switzerland
Telephone: +41 44 6336808
Email:(haris, manos)@geod.baug.ethz.ch

1. Introduction

In recent years, collection and processing techniques for Digital Elevation Models (DEMs) generation have improved rapidly, providing DEMs with higher resolution and accuracy. Each DEM contains errors due to the primary data acquisition technology and subsequent processing software, the surface relief and landcover (Li 1992). Parameters such as elevation, aspect, slope, vertical curvature and tangential curvature are useful to identify and describe geomorphological characteristics. Preliminary research studies have partially addressed the correlation between DEM accuracy and terrain relief (Toutin 2002, Crosetto and Crippa 2000). The morphology of the terrain and the sampling density used can have a significant influence on the accuracy of the DEM (Li 1992, Gao 1995, Gao 1997, Weng 2002). Some geomorphological parameters, such as average terrain slope, seem to be positively correlated with the decrease in accuracy of the DEM (Felicísimo 1992).

Our work is embedded within the EU FP6 project Pegase (Pegase, 2009), which aims at the development of an autonomous landing and take-off system for aircrafts. This system should use geodata on-board of each aircraft and DEMs are a crucial part of this geodata. To generate higher quality products covering all airports worldwide, DEM fusion is needed. DEM (and generally data) fusion needs first a quality characterisation of each input. Unfortunately, almost all available DEMs come with one global accuracy measure, which does not represent correctly the local accuracy variations. Thus, we try to exploit various parameters that influence the DEM accuracy, in order to assign to the DEM locally (ideally for each DEM point) a quality factor. The parameters that influence DEM accuracy are many, including geomorphology, landcover, DEM generation technology etc. with interrelations among them. In this paper, we report on investigations regarding the relation of some geomorphological parameters to the accuracy of DEMs. As DEMs, we mean both Digital Terrain Models (DTMs) and Digital Surface Models (DSMs). Till now, we have worked mostly on DSM fusion. Although Pegase relates to airports, the DEM fusion process should be applicable to any dataset.

After developing the basic methodology, a test, using various DEMs at a site with varying terrain relief and landcover, was conducted and discussed here.

2. Methodology

We compare five DEMs in the region of Thun, Switzerland produced with different technologies. The only available a priori information on the DEMs is their generation technology (e.g. airborne laser scanning, image matching, SAR interferometry, map contour digitisation), a global DEM accuracy measure and the raw data acquisition date. To perform the comparison of multiple DEMs, the procedure described below is proposed.

First, the DEMs are converted to a common coordinate reference system (CH1903). Then, the DEMs are co-registered to remove remaining global systematic errors, and the 3D differences between the DEMs are computed. After the DEM co-registration, we calculate geomorphological parameters (slope, roughness and aspect), using the DEM with the highest resolution and accuracy. Finally, we analyse the relation between the DEM differences after co-registration and these geomorphological parameters.

2.1 Co-registration

The input DEMs must be co-registered in order to compensate major systematic discrepancies between them. The DEMs are co-registered using the ETHZ software LS3D (Gruen and Akca 2005). The method performs 3D least squares matching. After the co-registration, the Euclidean distances (E) between the two DEMs are computed point-wise, together with their X, Y, Z components. The distances are computed as slave minus master DEM, where slave is the nominally less accurate DEM. The Euclidean distances and their X, Y, and Z components provide the so-called “residual maps”. LS3D generally uses a 7-parameter similarity transformation but in most cases three translations suffice.

2.2 Geomorphological Characteristics

Geomorphological parameters (slope, aspect, roughness, curvature, etc.) can be derived from a DEM using local operations. Three geomorphological parameters (slope, aspect and roughness) were calculated and their relation to co-registration residuals was analyzed. Slope and roughness relate to DEM quality for many DEM generation technologies, with DEM quality deteriorating with increasing slope and roughness. Aspect, in relation with significant slopes, relates mainly to shadows that cause DEM errors, when the DEM is generated by image matching. It also relates to DEM errors produced by SAR interferometry and airborne laser scanning, but to estimate these relations one needs more detailed knowledge of the data acquisition parameters (e.g. flight path, viewing angle), which we assume that are unknown.

Slope gives the deviation from the horizontal. Slope is the first derivative of a surface.

Aspect indicates the direction that slopes are facing. Aspect is defined as the direction of the biggest slope vector on the tangent plane projected on the horizontal plane, and here it is measured clockwise from 0 (North) to 360 degrees.

Roughness is a particular useful diagnostic tool because of its sensitivity to local elevation changes in the DEM. There are many ways to calculate the DEM roughness (e.g. standard deviation, variance, fractal dimension, entropy). We experimented with all these methods and found out that the entropy method performs best for our purposes. Entropy is a statistical measure of randomness (Haralick et al. 1973) that can be used to characterize the local variation of the input DEM. This measure is low when the heights within a local window have similar values and high when they vary significantly. Each output grid cell contains the entropy value within a n-by-n neighbourhood around an input DEM grid cell. In our case, we use a neighbourhood 9-by-9. For grid cells at the borders, symmetric padding is used.

3. Test Area and Data Description

The study site is an area around the town of Thun, Switzerland, characterized by steep mountains, smooth hilly regions and flat areas, both rural and urban. The elevation range is more than 1600m, varying from 530m to 2190m. The landcover is extremely variable with both dense and isolated buildings, open areas, forests, rivers and a lake. The available DEM data are:

- **SRTM C-band**, with 90 m grid spacing and estimated accuracy ± 5-15 m. The acquisition year is 2000.
- **DHM25** (Swisstopo), with 25 m grid spacing and estimated accuracy for the Thun tile ± 2.5 m. The digital height model DHM25 was essentially derived from the height information of the Swiss National Map 1:25,000 (NM25). It is a DTM. The raw data acquisition date is the year 1981.
- **Lidar DSM** (Swisstopo), with 2 m grid spacing and estimated accuracy (1 sigma) of 0.5m and 1.5m for vegetation and buildings. The acquisition date is spring 2000. The initial raw point density is about 1 point per 2 m^2.
- **A photogrammetric DSM**, with 4 m grid spacing. Over this test area, two IKONOS image triplets were acquired in December 2003 and a DSM was produced using image matching techniques with the ETHZ software Sat-PP. The estimated accuracy (RMS) is 1−2m in open areas, about 3m on the average in the whole area, excluding vegetation and 8m in vegetated areas (Baltsavias et al. 2006).
- **Reference 3D DEM**, obtained through automatic image matching of SPOT-5 HRS stereopairs. The grid spacing is 1 arcsecond (~ 30 m at the equator, varying according to latitude), the absolute elevation accuracy is 10 m for slopes < 20° and the absolute planimetric accuracy is 15 m. The acquisition date is November 2006.

Fig. 1 shows the shaded Lidar DSM.

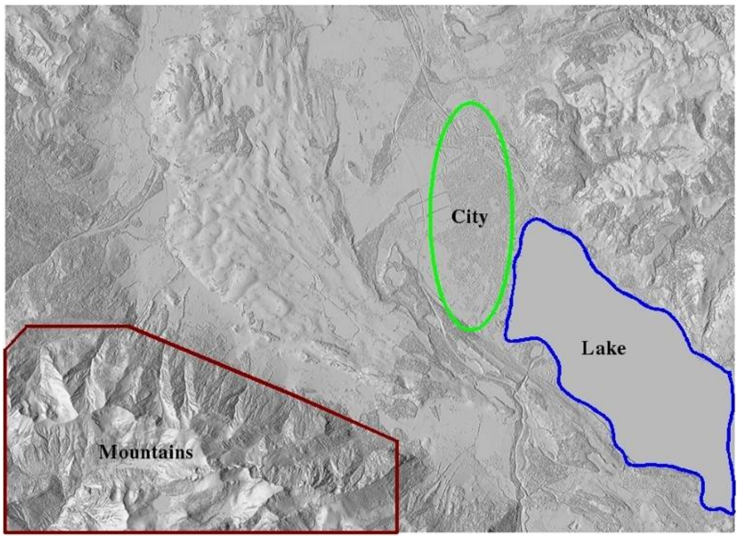

Figure 1. The Lidar DSM visualized in shaded mode.

4. Results and Discussion

At the co-registration step, we set as master DEM the lidar DEM. Among the 7 parameters, only the three X, Y, Z shifts were significant. The results of the co-registration step are summarized in Table 2. After co-registering the DEMs, the Euclidean distances between the two datasets are computed, as well as the X, Y, Z components, and their statistics. The residual distribution (see Figs. 2 and 3) shows that the larger ones are mainly located on the southern part, especially in the shadowed northern steep mountain region.

Template DEM	Slave DEM	Sigma a Priori (m)	Sigma a Posteriori (m)	Iterations	Tx (m)	Ty (m)	Tz (m)
Lidar	**Ikonos**	1.00	5.49	17	1.77	-3.97	0.45
Lidar	**DHM25**	1.00	9.07	6	3.73	8.60	4.50
Lidar	**SRTM**	5.00	9.11	5	42.69	83.42	1.35
Lidar	**Ref3D**	5.00	10.64	8	-24.17	-17.61	2.57

Table 1. Results of the co-registration of the available DEMs for the test area of Thun, Switzerland. T shows the translations.

	Lidar- SRTM					Lidar-Ikonos				
Residuals	**Minimum (m)**	**Maximum (m)**	**Mean (m)**	**St. Dev. (m)**	**RMSE (m)**	**Minimum (m)**	**Maximum (m)**	**Mean (m)**	**St. Dev. (m)**	**RMSE (m)**
E	-721.27	88.45	-0.61	15.68	15.69	-85.69	88.41	0.04	5.96	5.97
X	-333.79	235.47	-0.06	5.23	5.23	-51.78	57.47	0.01	2.62	2.62
Y	-325.59	305.66	-0.11	9.39	9.39	-79.91	78.78	0.04	3.08	3.08
Z	-632.70	69.96	-0.23	11.44	11.44	-50.87	54.41	-0.01	4.38	4.38
	Lidar-DHM25					**Lidar-Ref3D**				
Residuals	**Minimum (m)**	**Maximum (m)**	**Mean (m)**	**St. Dev. (m)**	**RMSE (m)**	**Minimum (m)**	**Maximum (m)**	**Mean (m)**	**St. Dev. (m)**	**RMSE (m)**
E	-64.37	63.48	-0.13	9.07	9.07	-147.09	170.50	0.34	11.84	11.84
X	-29.79	54.11	0.00	2.31	2.31	-70.28	131.58	0.03	3.65	3.65
Y	-36.36	36.70	-0.00	2.81	2.81	-112.69	130.90	0.10	5.88	5.88
Z	-64.00	36.87	0.00	8.31	8.31	-128.67	130.22	0.10	9.60	9.60

Table 2. Statistics of the residual maps (E = Euclidean distances, and their X, Y, Z components) after co-registration of the available DEMs for the test area of Thun, Switzerland.

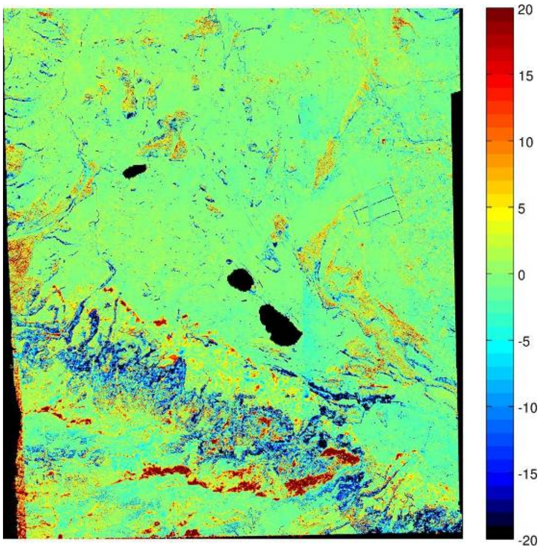

Figure 2: Color-coded Euclidean distance residuals (in m) between the Ikonos and the Lidar DSMs after co-registration.

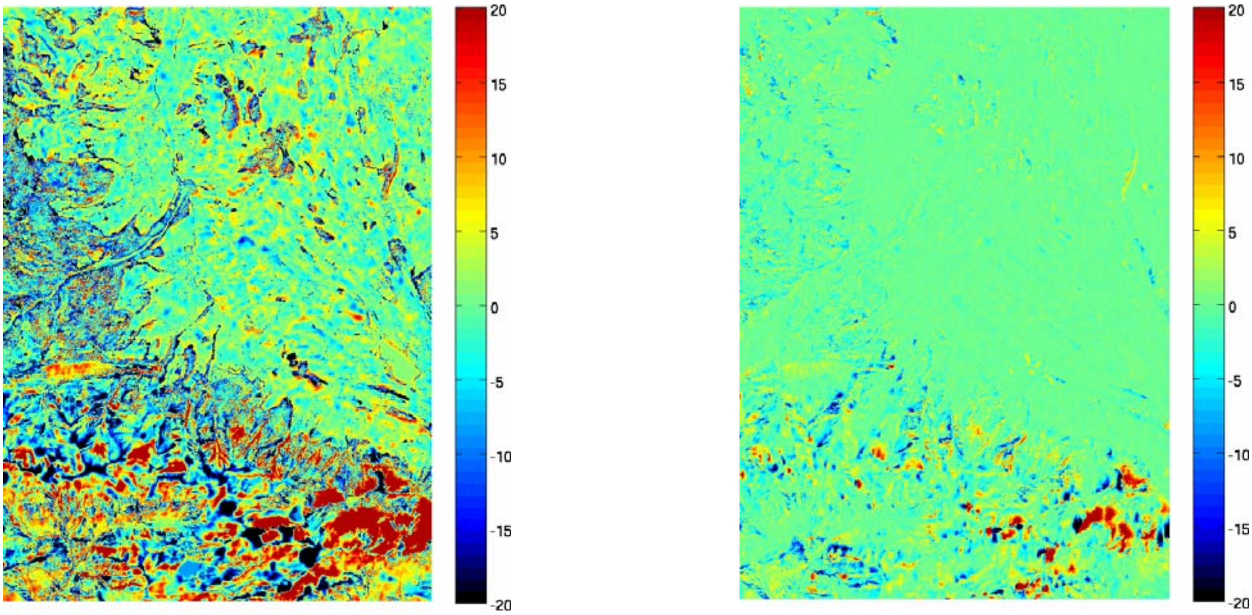

(a) Euclidean residuals (b) X residuals

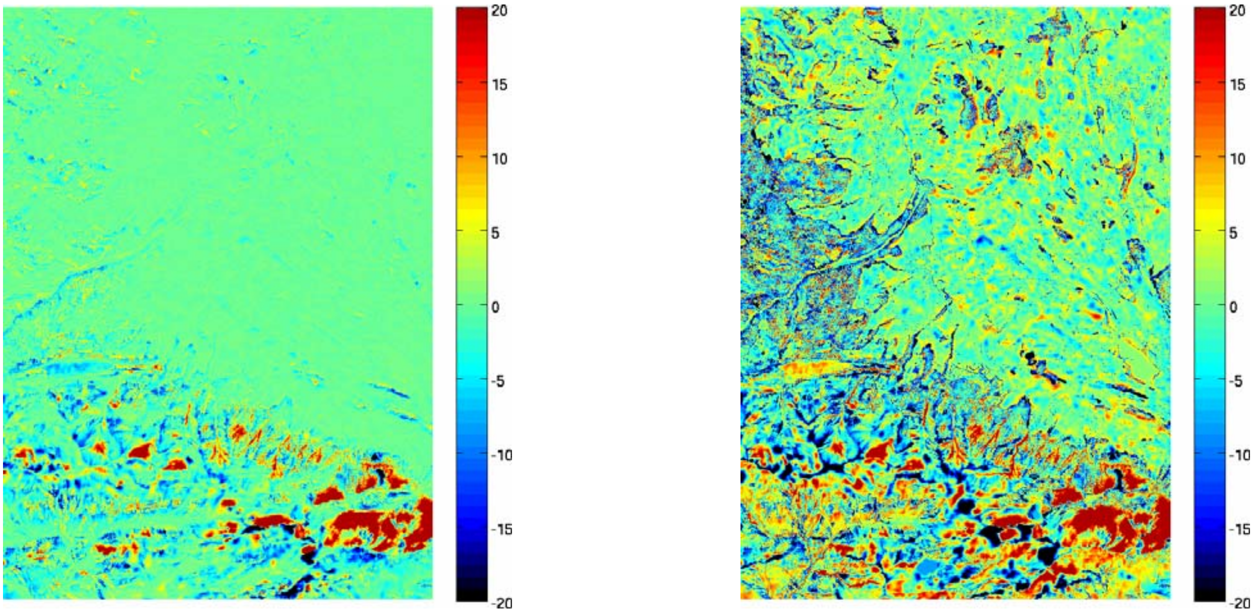

(c) Y residuals (d) Z residuals

Figure 3: Color-coded residuals (in m) between the Reference3D and Lidar DSMs after co-registration.

The residuals between the DSMs were studied in relation to the geomorphologic characteristics, which were previously computed. By plotting the residuals with respect to slope, aspect and roughness (see Fig. 4), it can be noted that:

- Slope is one of the principal parameters that relates to the differences between the DSMs. The steeper the slope is, the larger the differences between the DSMs, whatever the aspect (Fig.4a).
- Northern aspect correlates with the highest residuals. It corresponds to shadows, especially at mountain slopes, in the Ikonos images where the matching DSM has large errors because of the low image texture but also high slope and roughness (Fig 4b).
- Differences increase consistently as roughness increases. In general, above a certain roughness, elevation accuracy and roughness are almost linearly correlated (Fig 4c).

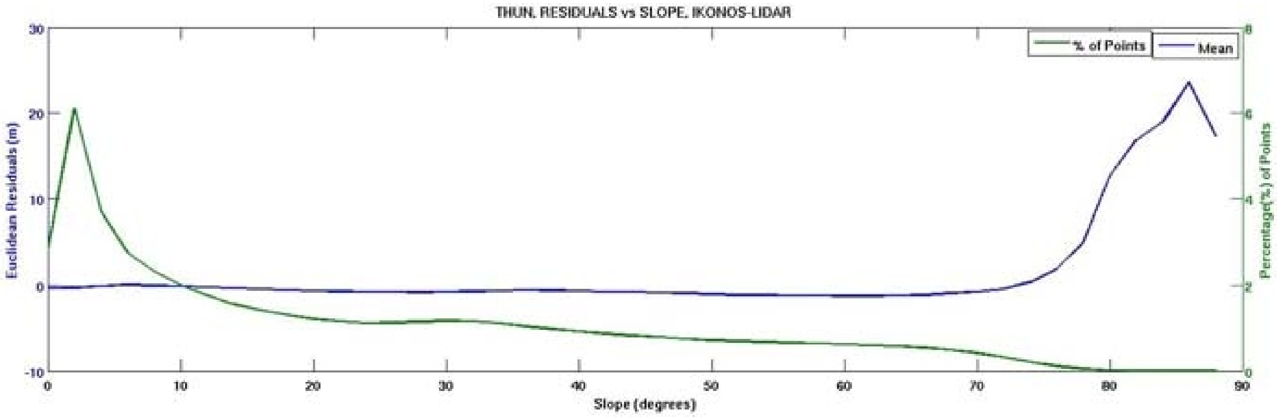

(a) Euclidean distances (mean every degree) versus slope. The green line shows the percentage of points.

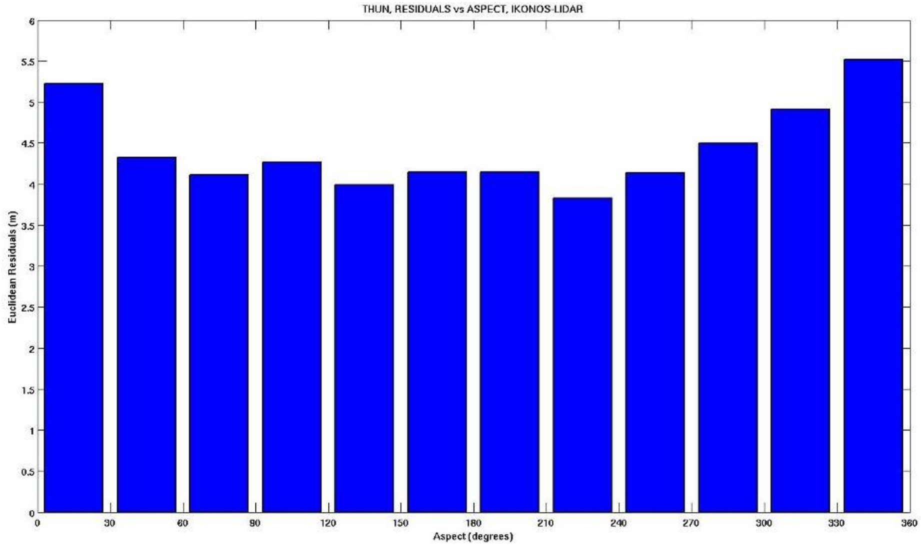

(b) Euclidean distances (mean every 10 degrees) versus aspect. Grid cells with slope <10◦ are not used; 0◦ : North, 90◦ : East, 180◦ : South, 270◦ : West.

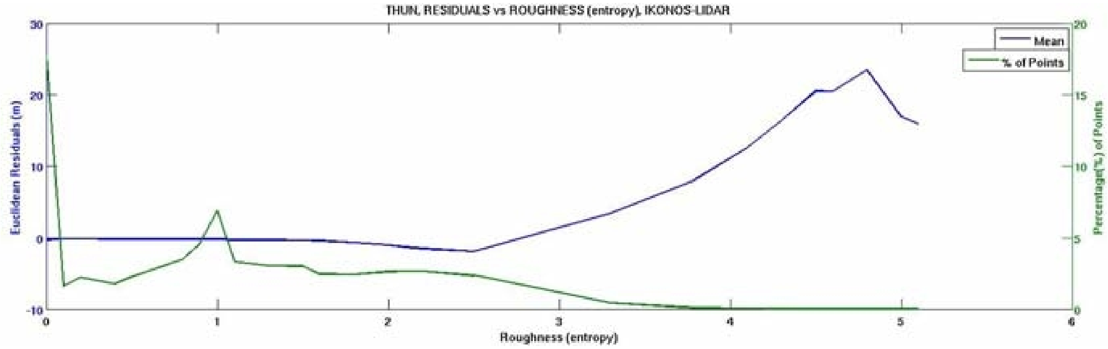

(c) Euclidean distances (mean values every 0.2 units of entropy) versus roughness. The green line shows the percentage of points.

Figure 4: Plots of the 3D residuals (mean values) as a function of the (a) slope, (b) aspect, and (c) roughness of the Lidar DSM.

The above mentioned results demonstrate a combined correlation between DEM accuracy and DEM slope, aspect and roughness.

Further work is needed regarding usage of other geomorphological parameters (like DEM surface discontinuities), the quantification of the influence of each geomorphological parameter on DEM accuracy and the combination of these influences (as well as others relating to landcover and DEM generation technology) in order to derive local DEM accuracy measures, ideally for each DEM point.

Acknowledgements

This work is part of the EU FP6 PEGASE project (Pegase, 2009). We also acknowledge Swisstopo for providing ETHZ with the Lidar DSM.

References

Aguilar F.J., Agüera F., Aguilar M.A., Carvajal F., 2005, Effects of Terrain Morphology, Sampling Density, and Interpolation Methods on Grid DEM Accuracy. *ISPRS Journal of Photogrammetry and Remote Sensing*, 71(7): 805-816.

Baltsavias E., Zhang L., Eisenbeiss H., 2006, DSM Generation and Interior Orientation Determination of IKONOS Images Using a Testfield in Switzerland. *Photogrammetrie, Fernerkundung, Geoinformation*, (1): 4154.

Crosetto M., Crippa B., 2000, Quality assessment of interferometric DEM. *International Archives of Photogrammetry and Remote Sensing*, 33(B1):146-153.

Felicísimo A.M., 1992, Digital Terrain Models and their Application to Environmental Sciences, *Ph.D. Thesis*, University of Oviedo, Spain, 235 p.

Gao J., 1995, Comparison of sampling schemes in constructing DTMs from topographic maps. *ITC Journal*, 1: 18-22.

Gao J., 1997, Impact Resolution and accuracy of terrain representation by grid DEMs at a micro-scale, *International Journal of Geographical Information Science*, 11(2): 199-212.

Gruen A. and Akca D., 2005, Least squares 3D surface and curve matching. *ISPRS Journal of Photogrammetry and Remote Sensing*, 59(3):151–174.

Haralick R.M., Shanmugam K., and Dinstein I., 1973, Textural features for image classification. *IEEE Transactions on Systems, Man and Cybernetics*, 3(6):610–621.

Li Z., 1992, Variation of the accuracy of digital terrain models with sampling interval. *Photogrammetric Record*, 14(79):113-128.

Pegase, 2009, http://dassault.ddo.net/pegase. Accessed, June 2009.

Toutin T., 2002, Impact of terrain slope and aspect on radargrammetric DEM accuracy. *ISPRS Journal of Photogrammetry and Remote Sensing*, 57(3): 228-240.

Weng Q., 2002, Quantifying uncertainty of digital elevation models derived from topographic maps, Advances in Spatial Data Handling (D. Richardson and P. van Oosterom, editors), Springer-Verlag, New York, pp. 403–418.

Spatial Variability in Channel and Slope Morphology within the Ardennes Massif, and its Link with Tectonics

N. Sougnez[1], V. Vanacker[1]

[1]University of Louvain (UCL), Place Louis Pasteur 3 1348 Louvain-la-Neuve Belgium
Telephone: +32 10 47 91 82
Fax: +32 10 47 28 77
Email: nicolas.sougnez@uclouvain.be

1. Introduction

There is great interest across a broad spectrum of geoscience disciplines in unravelling the role of tectonic activity in accelerating erosion processes and landscape evolution (Burbank et al. 1996, Maddy 1997, Vanacker et al. 2007). Surface processes that produce and transport sediment, and incise river valleys are complex; and difficult to quantify at longer timescales of 10^3 to 10^5 years. In this research, we analyze spatial variation in channel and slope morphology for low relief terrain with differential uplift rates. We specifically test if we can deduce the landscape response to tectonic activity based on the present-day channel and slope morphology. For these transient landscapes, we hypothesize that the channel morphology is a better indicator of landscape response than the hillslope form and relief.

The Ardennes Massif is an excellent field site for studying these processes. The area has been subject to differential tectonic movement: the Northeastern part of the Massif is characterized by moderate uplift and seismic activities, whereas the western and southern parts are undergoing only slight epeirogenic upheaval (Pissart 1974, Demoulin 1995, Meyer and Stets 1998, Garcia-Castellanos et al. 2000, van Balen et al. 2000). Various morphometric indices were used and developed to capture the specific slope and channel morphology of the basins. We then analysed possible correlation between these indices, lithology, and tectonic activity.

2. Material and Methods

We selected 10 catchments of about 150 to 250 km^2 across the Ardennes Massif (Fig. 1: Aisne, Bocq, Hermeton, Hoegne, Hoyoux, Molignée, Salm, Vierre, Wamme and Warche rivers). Most catchments are third order basins belonging to the Meuse River Basin. They cover various tectonic domains with uplift rates ranging from about 15 to 200 mm/kyr since mid-pleistocene times according to van Balen et al. (2000).

Our morphometric study is based on the Digital Elevation Model (DEM) produced by the Belgian National Geographical Institute (IGN/NGI). We used the DTM-1:10.000 product that is developed from photogrammetric derived levelling curves. This product is a regular grid of data points at 20 m resolution, and is reported to have RMS errors between 0.5 and 1.25 m horizontally and 1 and 1.6 m vertically. Due to interpolation artefacts in the original dataset, we were obliged to reconstruct the initial levelling curves (5 m equidistance) from the digital elevation data. We interpolated these contourlines using the “Topo to Raster” ArcGis function to obtain a continuously varying 3D surface. The DEM was then hydrologically corrected using the sink-fill method presented in Schäuble (2000).

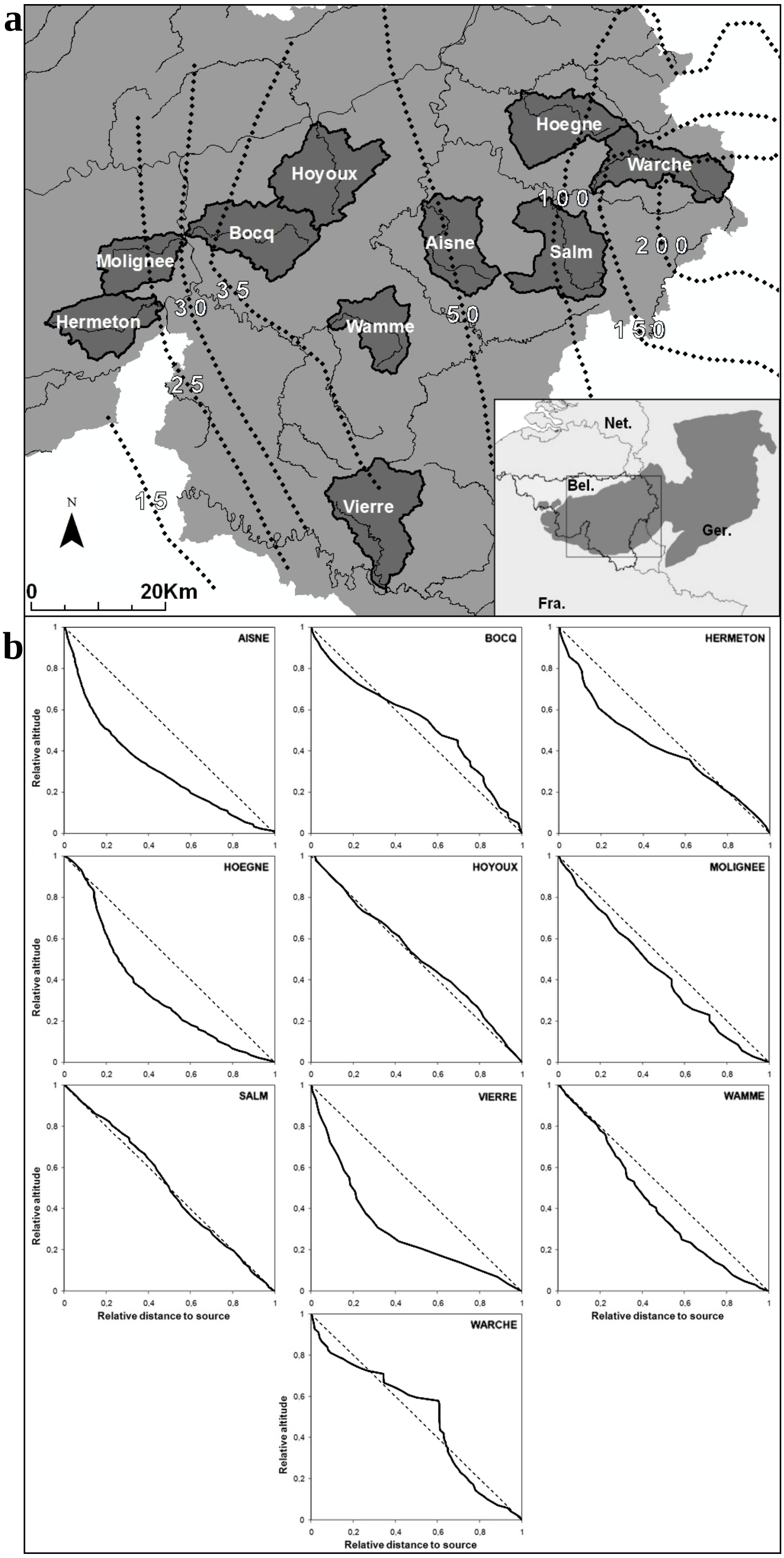

Figure 1**a.** Location of the 10 catchments in the Ardennes-Rhenish Massif (inset map). The dotted lines correspond to the uplift isolines (mm/kyr) from the studies of Meyer and Stets (1998) and van Balen et al. (2000), and were derived from terrace sequences.
b. Normalised longitudinal profiles of the selected rivers.

First, we derived simple morphometric indices that capture the overall slope morphology. Classical morphometric indexes (index of Gravelius, Shumm and Horton) were extracted to compare the overall geometrical shape between the catchments. The indexes of Schumm and Horton have the advantage of not being scale-dependent, which is not the case for the index of Gravelius that proved to be highly raster resolution dependent (Sanadeera et al. 2004). To get an insight in the spatial distribution of the slope morphology within the catchments, slope and local relief maps were made (with local relief here defined as the relief in a 100 m range moving window).

Second, we focused on the river channel morphology. For each drainage basin, we extracted the longitudinal river profiles and several transversal profiles based on the original levelling curves. The transversal profiles were measured perpendicularly to the river and between tributaries confluences to avoid the lowering of the slopes in such cases. For each river, more than 20 transversal profiles were extracted using the ArcGis 3D Analyst Function. The 8 most representative profiles with minimal effect of anthropogenic artefacts (such as roads, reservoirs, or villages) were then selected for analysis. Stream proximal slope (S_k in %) and curvature (C_k) were calculated using the following equations:

$$S_i = \frac{(y_{i-1}) - (y_{i+1})}{(x_{i-1}) - (x_{i+1})} \cdot 100 \tag{1}$$

$$C_i = \frac{\left(\frac{(y_{i+2}) - (y_i)}{(x_{i+2}) - (x_i)}\right) - \left(\frac{(y_i) - (y_{i-2})}{(x_i) - (x_{i-2})}\right)}{(x_{i+2}) - (x_{i-2})} \tag{2}$$

with x_i = distance to source (m), and y_i = altitude (m) at point i.

Slope-Area diagrams were constructed to help us to identify knick zones. For each river, we fitted an inverse power law equation (so-called Flint law) between the drainage area (A) and the channel gradient (S):

$$S = k_s A^{-\theta} \tag{3}$$

The empirically derived parameters k_s and θ are indicators of the steepness and the concavity of the longitudinal river profile (Hack 1973, Whipple 2004). A comparison of the observed Slope-Area relationships for the 10 rivers in the Ardennes Massif allows us to compare the channel morphology of rivers draining highly different tectonic regimes. As the empirically derived value of the steepness index k_s is dependent on the profile concavity, we normalised the steepness to a reference concavity, θ_r, of 0.45 following Howard (1994) and Whipple and Tucker (1999).

In addition to these parameters, we derived the Stream Concavity Index (*SCI*) of each river channel as defined by Demoulin (1998). The form of the river channels in the Ardennes Massif is highly variable, and some rivers display clear convexities (Fig. 1b). In this low-relief terrain, the stream concavity index can be used as an index of transient response to tectonic uplift. The SCI is a measure of the surface between the normalised longitudinal profile and a straight line joining the source and the outlet of the catchment (Equation. 4):

$$SCI_i = 1 - \sum_{i=0}^{1} \left((x_i - x_{i+1})(y_i + y_{i+1}) \right) \tag{4}$$

with x_i = distance to source (m), and y_i = altitude (m) at point i.

Third, we analysed the hypsometry of the catchments to get a measure of the overall slope and channel morphology. The hypsometric integral, *HI*, was calculated as follows:

$$HI_i = \sum_{i=0}^{1} \frac{1}{2} (y_{i+1} + y_i)(x_{i+1} - x_i) \tag{5}$$

where x_i = distance to source (m), and y_i = altitude (m). As our catchments have similar size, the scale-dependency of the hypsometric integral should not affect our results. The hypsometric integral is a measure of the distribution of landmass volume above a basal reference plane, and can be interpreted in terms of relative landform age (Strahler 1952). Differences in the shape of the hypsometric curve can be related to differences in erosive and tectonic processes (Luo 1998, Weissel and Pratson 1994).

3. Results and Discussion

Our morphometric analyses indicate that large differences exist in morphology both within and between the selected catchments. Based on our observations, we identified three broad ‘morphological’ groups (S1, S2, S3; in Fig. 2). The slope and channel morphology of these groups can be interpreted in terms of adjustment of the topography to relative base level change following uplift (Fig. 2).

The first slope and channel morphology group (S1) is typical for catchments that are located in the upper part of the catchments where smooth channel-to-hillslope transition could be observed. This morphology was mostly observed for plateau positions, and corresponds to alluvial stream systems where slope and channel processes are coupled.

The second and third group are transitional systems. The S2 scheme is characterized by very high constant slopes close to the rivers and by a rapid transition to flat slopes. This scheme is typical for knick zones with a decoupling of channel and slope processes. The S3 scheme (smooth S-curved slopes) can be seen as the later stage of evolution of the S2 scheme with the development of a large valley plain and with highest slope gradient located in the middle part of the slopes. We found this S3 scheme often in the downstream part of the catchments, and it corresponds to recent rejuvenated topography.

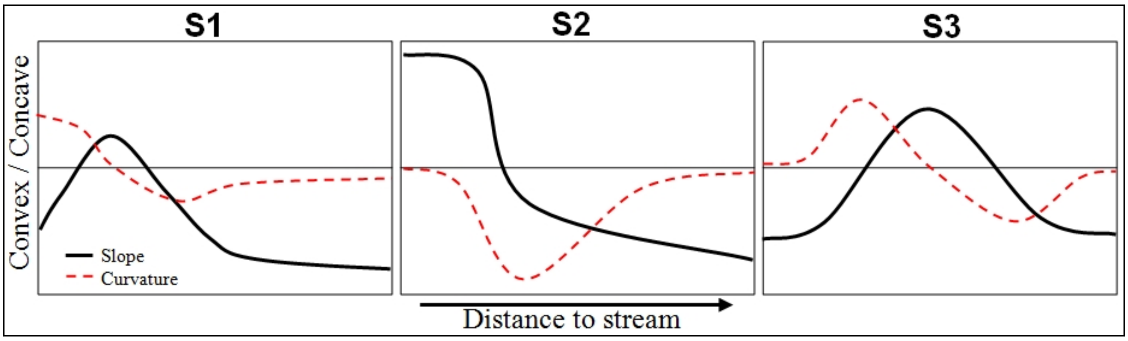

Figure 2. Schematic illustration of the Slope/Curvature evolution along the streams.

The observed variability in slope and channel morphology broadly coincides with the regional differences in tectonic and seismic activity that were reported by Meyer and Stets (1998) and van Balen et al. (2000). The catchments in the western and southern part of the Ardennes Massif are more prone to have relatively smooth river and channel profiles, although various exceptions exists. In the Northeastern part of the Ardennes Massif, we observed various catchments with irregular 'non-equilibrium' slope and channel profiles, and the presence of clear knickzones.

We specifically tested the correlation between the slope and channel morphology and the regional tectonic differentiation patterns. The Mean Uplift Rate (*MUR*) for each catchment was derived from van Balen et al. (2000). In addition to the morphometric indices that are described above, we calculated two parameters that are linked to the position of the knickzone: *Cha* and *Chr*, respectively the absolute and relative position of the principal stream convexity (above sea level or above catchment outlet). Table 1 summarizes the morphometric parameters for each river catchment.

Rivers	*S* (*km²*)	*P* (*km*)	*MUR* (*mm/kyr*)	*Cha* (*m a.s.l.*)	*Chr* (*m*)	*ho* (*m a.s.l.*)	*Gr* (*-*)	*Ho* (*-*)	*Sc* (*-*)	*θ* (*-*)	*Ksn* (*-*)	*HI* (*-*)	*SCI* (*-*)
Aisne	190,6	71,0	70	450	315	135	1,439	0,441	0,750	0,478	44,45	0,251	0,379
Bocq	235,4	89,0	40	195	100	95	1,624	0,341	0,659	0,478	11,87	0,523	-0,055
Hermeton	169,3	69,6	22,5	150	50	100	1,498	0,316	0,635	0,323	13,25	0,442	0,165
Hoegne	208,6	75,1	120	510	375	135	1,456	0,356	0,673	0,552	72,19	0,221	0,316
Hoyoux	255,7	94,6	45	200	125	75	1,656	0,570	0,852	0,017	26,15	0,481	0,002
Molignée	139,3	58,5	30	150	60	90	1,388	0,384	0,699	0,138	18,77	0,376	0,145
Salm	238,0	90,3	162,5	460	210	250	1,640	0,423	0,734	0,052	24,39	0,422	-0,002
Vierre	259,1	89,2	42,5	330	10	320	1,551	0,374	0,690	0,519	13,62	0,263	0,408
Wamme	140,2	68,8	45	430	245	185	1,627	0,440	0,748	0,196	38,93	0,308	0,178
Warche	191,2	94,7	180	522,5	222,5	300	1,918	0,245	0,558	0,513	11,12	0,484	0,011

Table 1. Computed rivers parameters: *S* = Surface; *P* = Perimeter; *MUR* = Mean Uplift Rate; *Cha* and *Chr* = the absolute and relative height of the convexities (in meters); *ho* = the altitude of outlet; *Gr*, *Ho* and *Sc* = the classical morphometric indexes (Gravelius, Horton and Shumm); *θ* and *Ksn* = the Convexity and Normalised Steepness indexes (Flint law); *HI* = the hypsometry integral; and *SCI* = the Stream Convexity Index.

Our data show some correlation between the overall catchment morphology and tectonic activity. First, a nonlinear relation was observed between the hypsometric integral, *HI*, and the relative position of the stream convexity, *Chr* (Fig. 3). This observation is related to the upward migration of knick zones in the catchments. We broadly identified three types of catchments (Fig. 3). The first channel morphological type (low *HI*, and low position of the convexity) broadly corresponds to river basins with equilibrium long profiles. Three river basins (Vierre, Hermeton, and Molignée) in the upper part of the Meuse catchment have such a channel morphology, and seem not yet affected by the base level changes following the uplift of the Ardennes Massif. The second type (high *HI*, medium relative height of convexity) contains catchments that were subject to recent tectonic activity (Bocq and Hoyoux) or that had higher tectonic uplift rates (Warche and Salm). The rivers that are draining regions with weak lithologies and/or long incision history appear in the third group.

This theoretical model indicates that the hypsometric integral (HI) is not adequate to determine the adaptation stage of a river profile. A river with a low hypsometric integral may either have been formerly crossed by a tectonically-driven knickpoint, or have not yet been affected by the uplift and thus remained in equilibrium state.

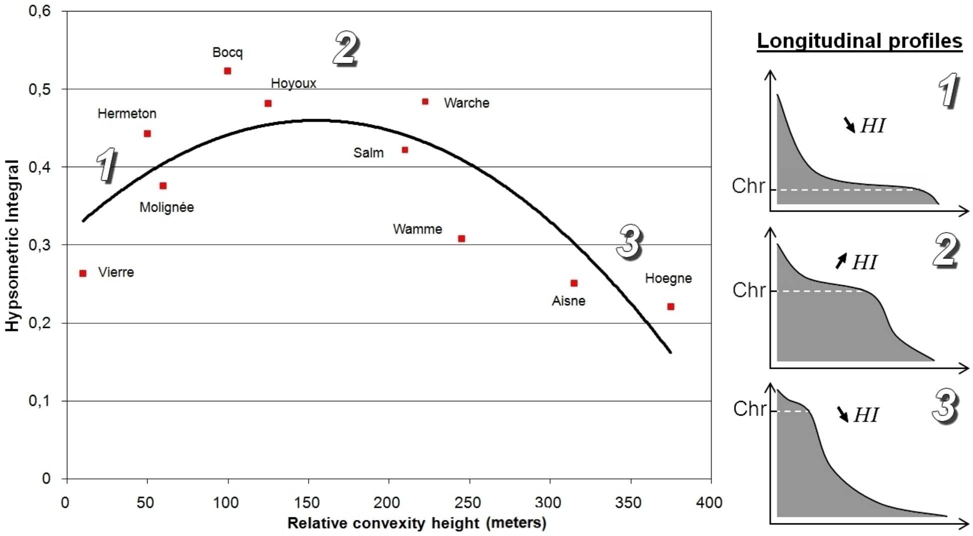

Figure 3. Nonlinear relation between the relative convexity height (*Chr*) and the hypsometric integral (*HI*).

Second, we observe that the absolute height of the river channel convexity is related to the mean uplift rate: catchments that are located in regions with higher uplift rates generally have knickzones at higher altitude (Fig. 4). This relationship may seem self-evident, as the mean elevation in the catchment can be expected to be directly related to the total uplift. However, this observation also shows that knickpoints do not dissipate rapidly in low relief terrain with low to moderate uplift rates.

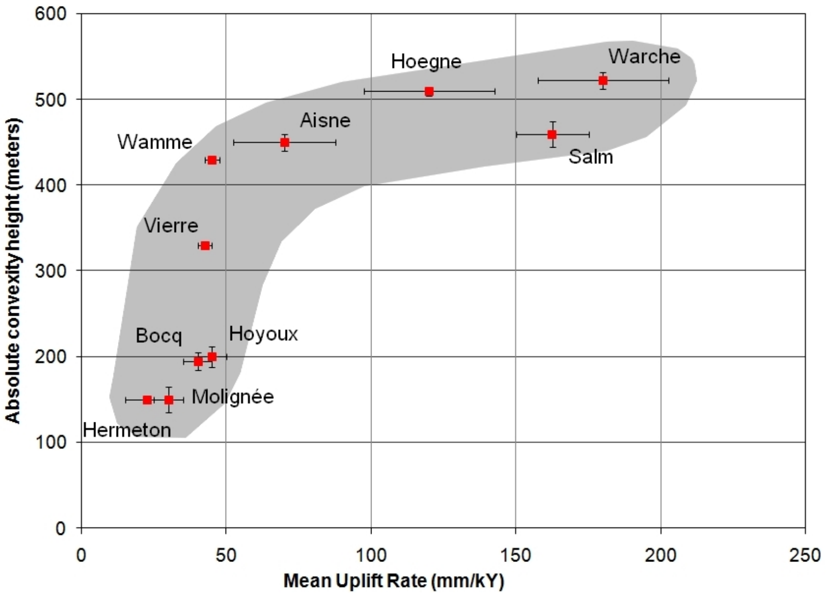

Figure 4. Relation between the *MUR* and the *Cha* parameters for the selected catchments. Errors bars are represented according to the position of the uplift isolines inside the catchment and to the position of the knickpoint into the longitudinal profile.

We observed some correlation between the Mean Uplift Rate of the catchments and the Stream Concavity Index (Equation. 4): catchments with concave upward river profiles are generally located in zones with low uplift rates (Fig. 5). However, convex reaches are not necessarily associated with zones with high uplift rates. This might partially be explained by the presence of local lithological contrasts, but might also be associated with local tectonic activity (Bocq and Hoyoux catchments, located close to centre of subsidence of Namur). The latter is currently under study, and is known as being poorly represented in the data of van Balen et al. (2000).

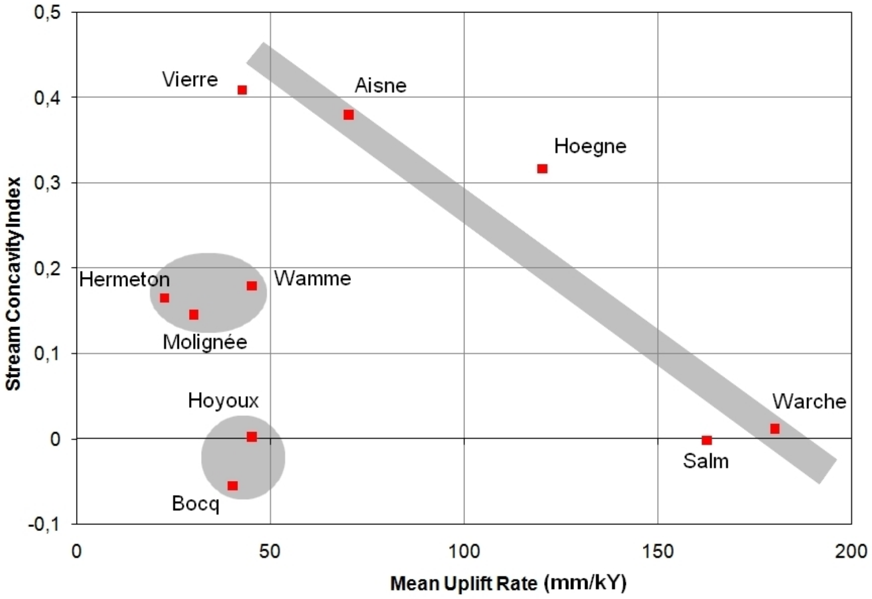

Figure 5. Stream Concavity Index (*SCI*) vs. Mean Uplift Rate (*MUR*).

Finally a *K*-means cluster analysis was performed on several variables to catch the spatial pattern in slope and channel morphology and see the relations with the differential tectonic activity. A reduced number of variables were selected to avoid redundancy in the analysis: *Chr*, *Gr*, *Ho*, *Sc*, θ, *HI*, *ksn* and *SCI*. Table 2 shows the main characteristic of the three clusters that were recognized by the statistical procedure:

	Rivers	*Mean Chr*	*Mean Gr*	*Mean HI*
Cluster 1	Salm, Wamme and Warche	255.83	1.72	0.40
Cluster 2	Aisne and Hoegne	345	1.44	0.23
Cluster 3	Bocq, Hermeton, Hoyoux, Molignée and Vierre	69	1.54	0.42

Table 2. Results of the clustering analysis and mean values of the three main parameters.

The clusters cover different tectonic domains in the Ardennes Massif (Fig. 1a). The first and second cluster contain rivers that are draining the most uplifted part of the Ardennes Massif, while the third cluster contains all Condruzian Rivers and the Vierre which is located in the Semois system. In a slope-area diagram (Fig. 6), the three clusters cover different domains. The first cluster is characterized by a low concavity index (θ = 0.34) opposed to reference concavities of θ = 0.43 and 0.45 for the 2nd and 3rd cluster resp. The two clusters (cluster 2 and 3) are clearly different in steepness value.

This observation clearly shows that variations in channel and slope morphology between the basins are not only reflecting differential uplift rates, but also the transient response of the basins to relatively base level lowering following uplift. Our data seem to suggest that relative base level lowering of the Meuse River is the driving force of river incision in the Ardennes Massif, and that a transient signal of adjustment is migrating through the Meuse basin. This hypothesis is conform with recent measurement of terraces by Rixhon et al. (2009). Rivers that are hydrologically more distant from the Meuse River are more likely to be in transient state, as the knickzones have not yet propagated to the upper parts of the river network.

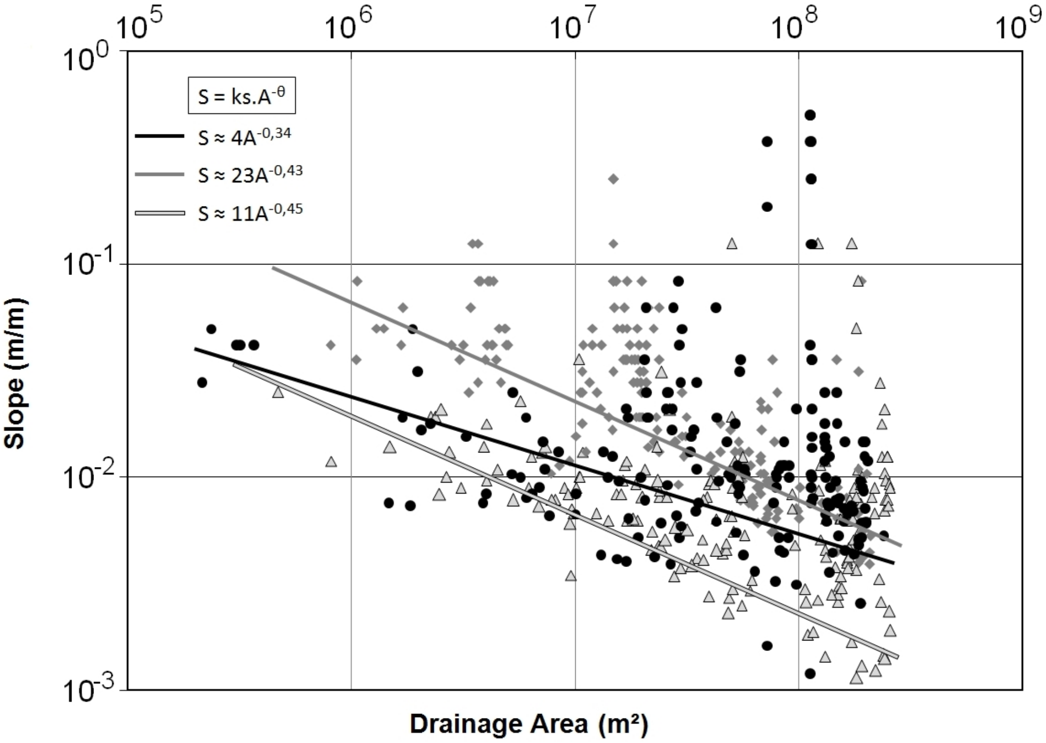

Figure 6. Illustration of the three Cluster groups within the Slope-Area space. The black dots represent the first cluster (Salm, Wamme and Warche Rivers), the grey diamonds represents the second cluster (Aisne and Hoegne), and the white triangles the last cluster (Bocq, Hermeton, Hoyoux, Molignée and Vierre Rivers).

4. Conclusion

Our morphometric analysis of 10 catchments in the Ardennes Massif indicates that slope and channel morphology is often an indicator of transient adjustment of rivers to tectonic uplift. Whereas there is some general agreement between some of the overall morphometric parameters and the mean uplift rates for the Ardennes Massif, the detailed picture is far more complex and some metrics appear to be insensitive to differential tectonic uplift.

It is clear that further research is needed both on the rates and patterns of tectonic evolution of the Ardennes Massif and on improved morphometric indices of local slope and channel morphology to fully elucidate the tectonic imprint on the landscape.

Acknowledgments

This study is part of a PhD research project that deals with the link between topography, tectonics and erosion in the Ardennes Massif. This project is financed by a FSR grant to VV.

References

Burbank DW, Leland J, Fielding E, Anderson RS, Brozovic N, Reid MR and Duncan C, 1996, Bedrock incision, rock uplift and threshold hillslopes in the northwestern Himalayas. Nature, 379 : 505-510.

Demoulin A, 1995, L'Ardenne des Plataux, heritage des temps anciens-surfaces d'érosion en Ardennes. In: Demoulin A (Ed.), *L'Ardenne, essai de géographie physique*. Dep. Géogr. Phys. Quat., Univ. Liège, pp110-135

Demoulin A, 1998, Testing the tectonic significance of some parameters of longitudinal river profiles: the case of the Ardenne (Belgium, NW Europe). *Geomorphology*, 24:189-208.

Demoulin A, Bovy B, Rixhon G and Cornet Y, 2007, An automated method to extract fluvial terraces from digital elevation models: The Vesdre valley, a case study in eastern Belgium. *Geomorphology*, 91:51-64.

Garcia-Castellanos D, Cloetingh S, van Balen R, 2000, Modelling the Middle Pleistocene uplift in the Ardennes-Rhenish Massif: thermo-mechanical weakening under the Eifel?. *Global and Planetary Change*, 27:39-52.

Hack J, 1973, Stream-profile analysis and stream-gradient index. *U. S. Geological Survey Journal of Research*, 1:421-429.

Howard A, Dietrich W and Seidl M, 1994, Modeling fluvial erosion on regional to continental scales. *Journal of Geophysical Research*, 99(B7):13,971–13,986.

Luo W, 1998, Hypsometric analysis with a Geographic Information System. *Computers & Geosciences*, 24(8):815-821.

Maddy D, 1997, Uplift-driven valley incision and river terrace formation in southern England. Journal of quaternary science, 12: 539-545.

Meyer W and Stets J, 1998, Junge Tektonik im Rheinischen Schiefergebirge und ihre Quantifizierung. *Zeitschrift der Deutschen Geologischen Gesellschaft*, 149:359–379.

Norton K, von Blanckenburg F, Schlunegger F, Schwab M, Kubik P, 2008, Cosmogenic nuclide-based investigation of spatial erosion and hillslope channel coupling in the transient foreland of the Swiss Alps. *Geomorphology*, 95(3-4)474-486

Pissart A, 1974, La Meuse en France et en Belgique. Formation du basin hydrographique. Les terraces et leurs enseignements. In: Macar P (Ed.), *Centenaire de la Soc. Géol. De Belg. L'évolution quaternaire des basins fluviaux de la mer du Nord méridionale*. Liège, pp. 105-131.

Rixhon G, Braucher R, Siame L, Bourlès D, Demoulin A, 2009, 10Be and 26Al dating of river terraces and quaternary incision rates in the Ardenne massif (eastern Belgium). *Geophysical Research Abstracts*, EGU General Assembly 2009, Vol. 11 - EGU2009-9419.

Schäuble H, 2000, Erosionsmodellierungen mit GIS. Probleme und Lösungen zur exakten Prognose von Erosion und Akkumulation. II. *Ergebnisse der Jahrestagung des Arbeitskreises GIS 25/26.* Tübingen, 51-62.

Senadeera K, Piyasiri S and Nandalal K, 2004, The evaluation of Morphmetric Characteristics of Kotmale Reservoir catchment using GIS as a tool, Sri Lanka. *The International Archives of the Photogrammetry, Remote Sensing and Spatial Information Sciences*, 34(XXX).

Strahler AN, 1952, Hypsometric (area-altitude) analysis of erosional topology. *Geological Society of America Bulletin*, 63:1,117-1,142.

Van Balen R, Houtgast R, Van der Wateren F, Vandenberghe J, Bogaart P, 2000, Sediment budget and tectonic evolution of the Meuse catchment in the Ardennes and the Roer Valley Rift System. *Global and Planetary Change*, 27(1-4):113-129.

Vanacker V, von Blanckenburg F, Hewawasam T, Kubik PW, 2007, Geomorphic development of the Sri Lanka Central Highlands. *Earth and Planetary Science Letters*, 253: 402-414.

Weissel J and Pratson L, 1994, The length-scaling properties of topography. *Journal of Geophysical Research*, 99:13,997-14,012.

Whipple K and Tucker G, 1999, Dynamics of the Stream Power River Incision Model: Implications for Height Limits of Mountain Ranges, Landscape Response Timescales and Research Needs. *Journal of Geophysical Research*, 104:17,661-17,674.

Whipple K, 2004, Bedrock rivers and the geomorphology of active orogens. *Annual review of earth and planetary sciences*, 32:151-185.

Proceedings of Geomorphometry 2009. Zurich, Switzerland, 31 August - 2 September, 2009

A Parameterisation Attempt of Scoria Cones of the San Francisco Volcanic Field (Arizona, USA) by Conical Fitting

B. Székely[1,2], E. Király[2], D. Karátson[3,4], T. Bata[3]

[1]Institute of Photogrammetry and Remote Sensing, Vienna University of
Technology, Vienna, Gusshausstr. 27-29, A-1040 Wien, Austria
Telephone: (43) 1 58801-12251
Fax: (43) 1 58801-12299
Email: balazs.szekely@ipf.tuwien.ac.at

[2]Department of Geophysics and Space Science, Eötvös Loránd University, Budapest, H-1117 Budapest Pázmány P. sétány 1/c.
Telephone: (36) 1 209-0555/6651
Fax: (36) 1 372-2927
Email: kiralye@gmail.com

[3]Department of Physical Geography, Eötvös Loránd University, Budapest, H-1117 Budapest Pázmány P. sétány 1/c.
Telephone: (36) 1 381-2111
Fax: (36) 1 381-2112
Email: dkarat@ludens.elte.hu

[4]Geoscience Centre, Georg-August University of Göttingen, Goldschmidtstr. 1-3,
D-37077 Göttingen, Germany

1. Introduction

The availability of the Shuttle Radar Topography Mission (SRTM) Digital Terrain Model (DTMs) paved the way of new approaches in volcanic geomorphology. Because of their relatively well definable geometric form, the gradually degrading volcanic edifices shaped by the surface processes are suitable targets for morphometric studies. After the cessation of the volcanic activity the relatively steep slopes are gradually changing together with the height of the form. This process can be studied by the categorisation of the volcanic cones and parameter estimation on the different group members. During the degradation of volcanic edifices the characteristic properties of the cones change, so the geometric modelling of their surface may result in parameters that are meaningful in the understanding of these processes.

Our study area, the San Francisco Volcanic Field (SFVF), is a ca. 4500 km^2-large volcanic region situated around the San Francisco stratovolcano in Arizona near Flagstaff (USA; Fig. 1).

The SFVF hosts some 600 scoria and lava domes, numerous lava flows with extensive volcanic ash deposits. Because of the wide range in size and age, as well as contrasting degradation of these volcanic features, several authors have analysed them in order to derive general rules of their lowering. Morphometric parameters were determined that were expected to be suitable to fulfil this requirement. In his pioneering work, Wood (1980a,b) considered 40 scoria cones, while almost two decades later Hooper and Sheridan (1998) included 237 features in their study. Their manual morphometric analyses were based on topographic maps that are time consuming, therefore their limited scope can now be extended with the availability of digital data.

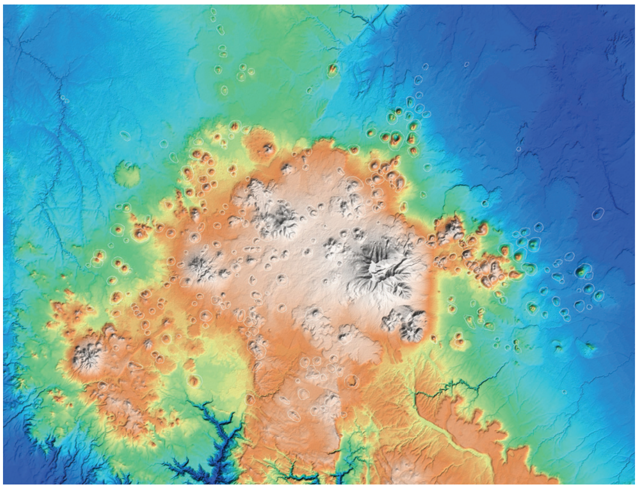

Figure 1. An overview shaded relief map of the San Francisco Volcanic Field area.

2. Conceptual Considerations

The classic approach of the aforementioned authors focus on some parameters that can be estimated manually relatively easily from the topographic data. The height of the cone (H_{co}), the width of the cone (W_{co}), the width of the crater (W_{cr}, if applicable) are the most important ones that were used in these seminal papers.

The application of digital data allows somewhat more complex approach: the fitting of the 3-dimensional conical shape is also possible. However, the larger number of parameters increase the complexity of finding the best fitting model. In the case of five parameters, each point of the resulting five dimensional parameter space is a potentially fitting cone, while most of these models represented by the appropriate parameter values are far from being close to the shape to be modelled. On the other hand, the algorithms that are used to find the best fit models, tend to get stranded at local minima, failing to reveal the optimal solution.

An applicable general technique to help the algorithms to succeed is to figure out some parameters independently, that are later feed in the 3D processing. In our case the 2D profiles and planar (map view) contours were used for this purpose.

In order to facilitate further the minimization, the number of parameters has been reduced via the simplification of the model (e.g., the with the manual removal of the crater area) and replacement of the aforementioned classic parameters with simplistic ones.

3. Data Processing

In the initial phase of our project more than 300 cones were analysed using the classic approach (height of the cone, width of the cone and crater, etc.). Additionally the slope histogram were analysed in order to classify the cones into different evolutionary categories.

These analyses led to the selection of a few volcanoes, that entered in the next processing phase. We selected scoria cones according to their morphology: the basic requirement was to have a conical shape. We analysed the groups of cones with closed vent, cones with open vent and cones without vent. Initially a five-parameter 3D model was conceptualised and the optimization is carried out using the simplex method (Nelder and Mead 1965):

$$Q_{cone} = \sum_{i=0}^{N} \left[\left(z_0 - \frac{H}{R}\sqrt{(x_i - x_0)^2 + (y_j - y_0)^2} + H \right)^T - h_{ij}^{M} \right]^2 \qquad (1)$$

where Q_{cone}: value of the residual
z_0: elevation of the base plate level,
R: radius of the base of the cone,
x_0, y_0: coordinates of the centre,
x_i, y_j: coordinates of the pixels,
h_{ij}^{M}: elevation data of the DTM.
N: number of the pixels
H: height of the cone,

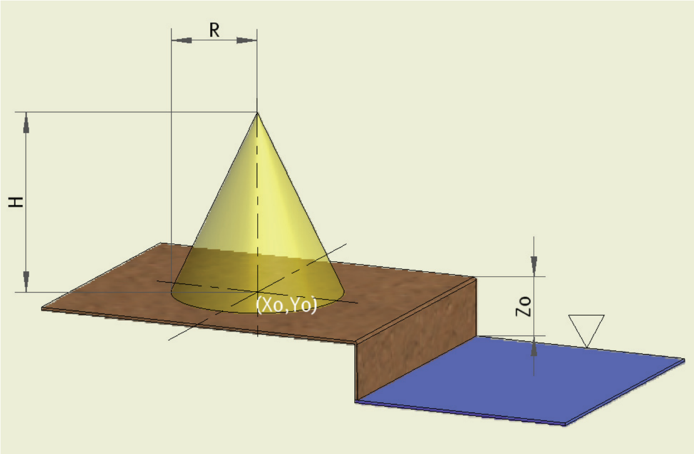

Figure 2. Parameters of the fitted upright cone.

Because of the aforementioned complexity of the parameter estimation we reduced the number of the parameters to four (Fig. 2) using some simple geometrical considerations:

$$Q_{cone} = \sum_{i=0}^{N} \left[\left(c + a\sqrt{(x_i - x_0)^2 + (y_j - y_0)^2} \right)^T - h_{ij}^{M} \right]^2 \qquad (2)$$

where $c = z_0 + H$, $a = -\frac{H}{R}$, consequently $\alpha = -\arctan a$

and α is the elevation angle of cone (i.e., the slope angle of the volcanic edifice).

In order to achieve a better fit, some filtering of the DTM based on the slope distribution was carried out: we removed those points that were considered to be off from the *sensu stricto* volcanic cone (typically the products of the erosional processes at the hillfoot). Likewise we removed the crater area as well to avoid the bias introduced by this part of the volcanic feature.

4. Results

Most of the processed cones give a reasonably good fit, the residuals usually remain below +/- 30m. Residual maps (difference of the original DTM and the fitted cone) shows more or less the local roughness of the surface. An example for the residuals, the results for the SP Crater (Arizona, USA) is shown in Fig. 3.

Slope angles (values of α) were calculated using the parameters of the fitted cones. These values were correlated with the age group of the volcanoes. In accordance with the expectations the slopes angles are ranging between 6°and 30°, however most of the values are scattering in the lower angle ranges. Only those scoria cones of the Late Pleistocene and the Holocene give slopes above 24° which are known to be the most recent edifices in this field while many of the cones are characterised by typical angles of 10°, 12°, 14° and 19-20° (Fig. 4). The results are in good congruence with the morphological and age groups and their evolution, however the quantization error in the slope angle histograms should also be considered in the case of underpopulated groups.

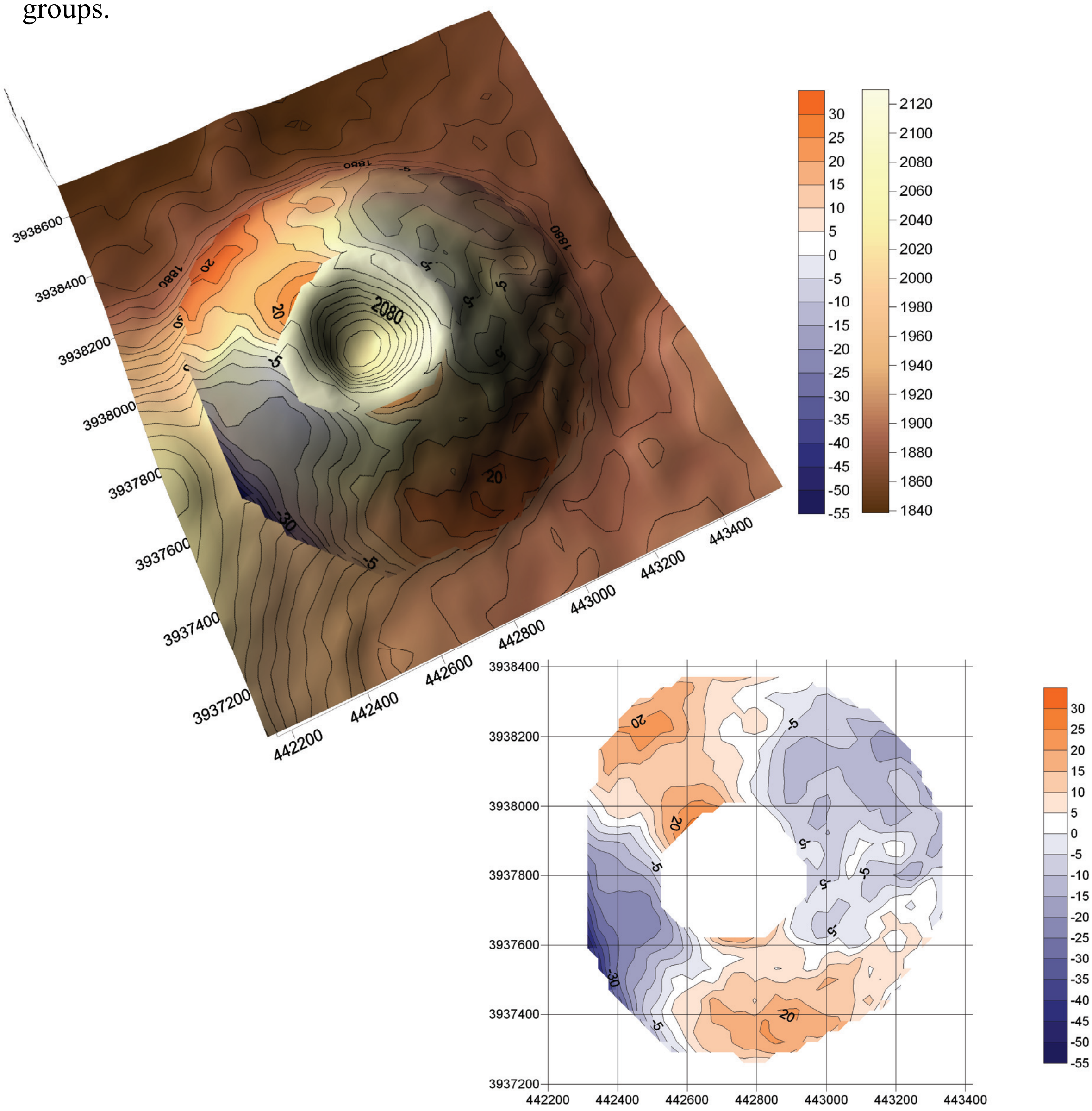

Figure 3. The residual map overlain on the DTM of the original volcanic cone of SP Crater, Arizona. Note the residual pattern (see also in map view as inset in the bottom right) that implies a somewhat elliptical shape of the volcanic form). In the crater area the original elevation contours are drawn (all elevation values are in m).

The results show that for a successful fit, only the most regular volcanoes are suitable. If the cone to be processed is well described by the 2D fit results in the preprocessing steps (this defines the initial simplex), in most of the cases a very good fit is achievable. In this case, the residuals often remain below +/-20 m, while the standard deviation of the residuals is ca. 10 m. In comparison with the accuracy of the SRTM DTM this is very promising.

If the volcano is less regular, or the scoria cone is situated on a larger stratovolcano, there is necessary a break in the slope angle at the lower elevation parts, the fit is not so successful, giving residuals reaching 50 m. The parameters sometimes are tending to give a more general, average solution if there is some irregularity left in the data.

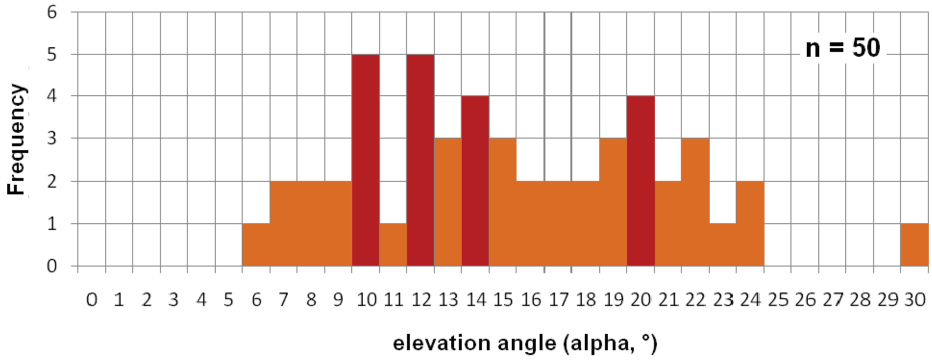

Figure 4. The elevation angle/slope angle histogram of the 50 processed SFVF scoria cones using 1°-wide bins. The highlighted bars indicate the angles where some tendency to clustering can be observed.

5. Conclusions

In the San Francisco Volcanic Field a number of scoria cones can be modelled by 3D cone fitting with acceptable accuracy. These cones are the youngest ones, characterised by regular shapes, but may also have craters that is not considered by our processing. However, even in these cases sometimes the parameter estimation method cannot find the optimal solution. Therefore the preprocessing step that preselects some parameters, may turn to be crucial in achieving a good fit. A typical good fit is characterised by maximal residual of +/– 20 m, while the standard deviation of the residuals is in the order of magnitude of the accuracy of the elevation data. Elongated forms may also be modelled, but they result in larger residuals.

Acknowledgements

A part of these studies were carried out during the Békésy György Postdoctoral Fellowship to BSz. DK is currently is a fellow of Alexander von Humboldt Fellowship in Göttingen, Germany. Á. Graf, L. Lócsi and F. Schell are thanked for the close cooperation.

References

Hooper, DM, Sheridan MF, 1998, Computer-simulation models of scoria cone degradation. *Journal of Volcanology and Geothermal Research*, 83:241-267.

Nelder JA, Mead, R, 1965, A simplex method for function minimization. *Computer Journal*, 7:308-313.

Wood, CA, 1980a, Morphometric evolution of cinder cones. *Journal of Volcanology and Geothermal Research*, 7(3-4):387-413.

Wood, CA, 1980b, Morphometric analysis of cinder cone degradation. *Journal of Volcanology and Geothermal Research*, 8(2-4):137-160.

Influence of DEM and Soil Property Uncertainty on an Infinite Slope Stability Model

M. Ulmer[1], P. Molnar[2] and R. Purves[3]

[1]WSL Institute for Snow and Avalanche Research SLF
Flueelastrasse 11
7260 Davos Platz
Switzerland
Telephone: +41 81 417 0243
Fax: +41 81 417 0110
Email: ulmer@slf.ch

[2]Institute of Environmental Engineering, Swiss Federal Institute of Technology Zurich
Wolfgang-Pauli-Str. 15
8093 Zurich
Switzerland
Telephone: +41 44 633 2958
Email: peter.molnar@ifu.baug.ethz.ch

[3]Department of Geography, University of Zurich
Winterthurerstrasse 190
8057 Zurich
Switzerland
Telephone: +41 44 635 6531
Fax: +41 44 635 6848
Email: ross.purves@geo.uzh.ch

1. Introduction

Landslides pose a worldwide threat to humans, infrastructure and agricultural land, with around 1800 people dying in landslides annually (Alexander, 1995). GIS-based slope stability models are widely used to identify areas prone to landsliding, however the predictions of these models, and indeed any models, are susceptible to a range of uncertainties, including that resulting from uncertainty or error in input data and error propagation within models (Heuvelink, 1998). Furthermore, model evaluation typically explores either a single set of parameters, or extremes in individual parameters through sensitivity analysis (e.g. soil parameters (Guzzetti, 2005)), but neglects a holistic characterisation of the nature and form of uncertainty of parameters on model results.

In this paper, we illustrate the importance of digital elevation model (DEM) uncertainty in landslide modelling, and compare it with the uncertainty in other model parameters. We also explore the relation between DEM resolution and prediction performance and methods to evaluate model results using ground truth. The analysis is based on a standard slope stability model using the 'infinite slope approximation', similar to SINMAP (Pack et al., 2005). The model produces a spatially distributed factor of safety (FS) which is the ratio of stabilizing and destabilizing forces on a hillslope. The model is best suited to shallow rainfall-triggered landslides and in our study incorporates two parameters derived from a DEM: slope gradient and the topographic wetness index. Soil properties are represented by four parameters: soil thickness, cohesion, hydraulic conductivity and friction angle. The analysis focuses on a research area in the region of Napf, Switzerland, where a storm in July 2002 led to widespread landsliding (Rickli and Bucher, 2002).

2. Materials and Methods

Modelling was carried out using two DEMs: a LIDAR-derived DEM at a 2 m resolution (DTM-AV produced by Swisstopo) and a DEM of 25m resolution (DHM25 produced by Swisstopo). Soil properties were from a combination of the small-scale Digital Soil Map of Switzerland (BFS, 2000), and more detailed point measurements of soil thickness and friction angle within the study area (Rickli and Bucher, 2002). Finally, high-resolution (20cm) post-event orthophotos were used to locate the initiation zones of 29 landslides which occurred during the July 2002 event and to digitise areas of forest/ non-forest.

Since the aim of the study was to explore the influence of uncertainty in input parameters on slope stability, we first characterised these uncertainties before carrying out Monte Carlo Simulations (MCS) to explore the influence of uncertainty across the study area. DEM uncertainty depended on two surface properties - slope angle through the geometric relation between the LIDAR instrument and the surface, and forest coverage which results in lower densities of raw LIDAR data points under the canopy. Uncertainty in elevation was simulated from normal distributions, with a mean of 0 and the standard deviation dependent on slope angle and forest coverage, with an average of 0.5 m, in accordance with the information given by the DEM producer (Swisstopo, 2005). Furthermore, process convolution (Oksanen and Sarjakoski, 2005) was applied to the uncertainty field added to the DEM to generate spatial autocorrelation in this field. The range of this spatial autocorrelation was difficult to estimate, since no information on this subject is given by the DEM producer, nor could any sensible statement concerning this issue with respect to LIDAR-produced DEMs be found in the literature. The simulation was therefore carried out with two ranges representing optimistic and pessimistic assumptions about DEM quality: 80m and 8m respectively. A larger range implies a more strongly spatially autocorrelated uncertainty field, and thus a smoother variation in the uncertainty in space. Assumptions on variation in soil properties were based on measurements (soil depth and friction angle) and a combination of values from the Digital Soil Map of Switzerland and considerations by the authors of SINMAP (Pack et al., 2005) (hydraulic conductivity and cohesion). Soil depth was assumed to be normally distributed, with a mean of 0.8 m and a standard deviation of 0.27 m. Values for the other three parameters were drawn from a uniform distribution, with rather small ranges to account for the limited information on possible values of these parameters

MCS was then carried out to determine the number of simulations necessary to achieve convergence of the MCS results. In our case we tested for convergence by comparing the results of two MCS after 500 iterations and made sure that, in all cases, the difference between broad spatial patterns and global means in simulations appeared qualitatively small enough not to be relevant for the conclusions drawn.

Having explored uncertainty in input parameters, we carried out modelling runs at a variety of resolutions (2, 4, 8 and 25m), where the 4 and 8m DEMs were bilinearly-interpolated from the 2m LIDAR-derived DEM, and the 25m DEM was the standard Swisstopo DEM. The 2 and 4m results factor of safety values were aggregated to a resolution of 8m by retaining only the lowest (least stable) factor of safety.

For the evaluation the initiation zones of 29 visible landslides on the 20cm orthophoto in the study area were digitized as polygons. The mapped slides were all located outside of the forest and consequently, the evaluation reference surface was also limited to open land. The polygons were used to compare model predictions and slide activity. The model prediction for a given landslide was classified as correct if the maximum factor of safety FS inside the slide boundaries was smaller than a chosen threshold. The reasoning behind this rule was that a slide was not considered as having been predicted if only a part of its release area was identified as unstable. Though from a physical viewpoint, one could argue that a single unstable cell is sufficient to trigger a landslide, using only the lowest value inside the slide would favour noisy model results of little practical use.

Finally, the proportion of predicted landslides was combined with the portion of the area classified as unstable to create the Prediction Rate Curve (PRC) (Chung and Fabbri, 2003). The PRC serves as a means to measure prediction performance independently of FS threshold values.

3. Results

Fig. 1 shows an example of the spatial pattern of variability in the factor of safety, where uncertainty was applied to all parameters (soil and topographic). It is clear that uncertainty is higher in flatter areas and areas where the fluvial relief is less pronounced.

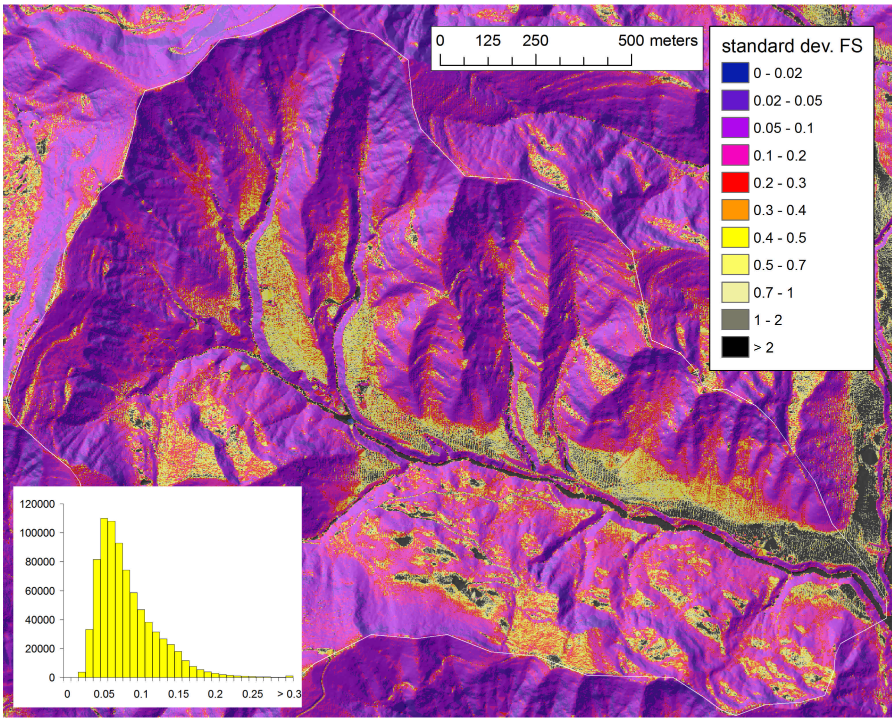

Figure 1. Standard deviation of the factor of safety after 500 Monte Carlo runs. The relevant range of factor of safety values is about 1.5. The histogram shows the distribution of the standard deviations of all cells.

Prediction Rate Curves for 4 resolutions of DEM are shown in Fig. 2. Best performance is achieved when the PRC is furthest removed from the 1:1 line which represents a random model. This means that well-performing models maximise the fraction of cells correctly classified as landslides and at the same time destabilize the smallest area of the basin. The results of the run using the 8m-DEM showed the best performance, while the two finer scale DEMs (2 and 4m) yielded very similar results. The DHM25 did considerably worse, but mainly at the conservative end of the model results. This means that the DHM25 was successful in predicting a certain amount of slides (in this case 70%) while missing a number of events. However to predict all slides correctly at this resolution almost the whole area has to be considered slide-prone. The finer scale DTMs perform better at the conservative (upper) end of the PRC but 40 to 50% of the entire area is still considered unstable before all slides are predicted, in comparison with a total area of 0.2% of the area where slides are actually found.

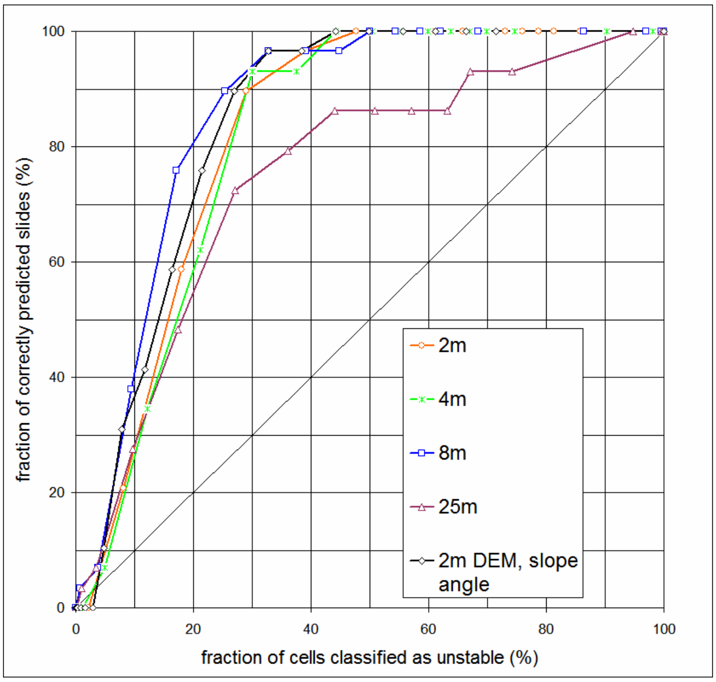

Figure 2. Prediction rate curves of slope stability model results using DEMs with four different resolutions and prediction rate curve of a slope angle map.

The model performance can thus not be seen as very satisfactory. This reflects the remarks of the authors of SINMAP who state that the model’s purpose is to produce and map broad stability classes to identify regions where more detailed assessments are warranted (Pack et al., 2005). A further indication that model performance is generally quite poor is the fact that predicting slides simply from the slope inclination map by slopes larger than a threshold yields results that are as good as the slope stability model. The slope map used was derived from the 2m DEM and aggregated to a resolution of 8m using a method equivalent to the slope stability model results. Its results can therefore be compared to those of the slope stability model results also using the 2m DEM. The PRC of the slope map is shown in Fig. 2. We interpret these results to imply that, firstly slope steepness is a primary factor for landslide susceptibility in this area, and secondly, that the wetness of the shallow soils in the study area has a less significant effect on landslide susceptibility, or that the model fails to predict wetness correctly.

4. Implications of Uncertainty for Prediction Performance

The results of the uncertainty analysis and the evaluation were combined to assess the influence of model uncertainty on model performance. The standard deviation of the factor of safety for each cell, as determined by Monte Carlo Simulation, was added as a range to the deterministic factor of safety computed with mean parameters and no

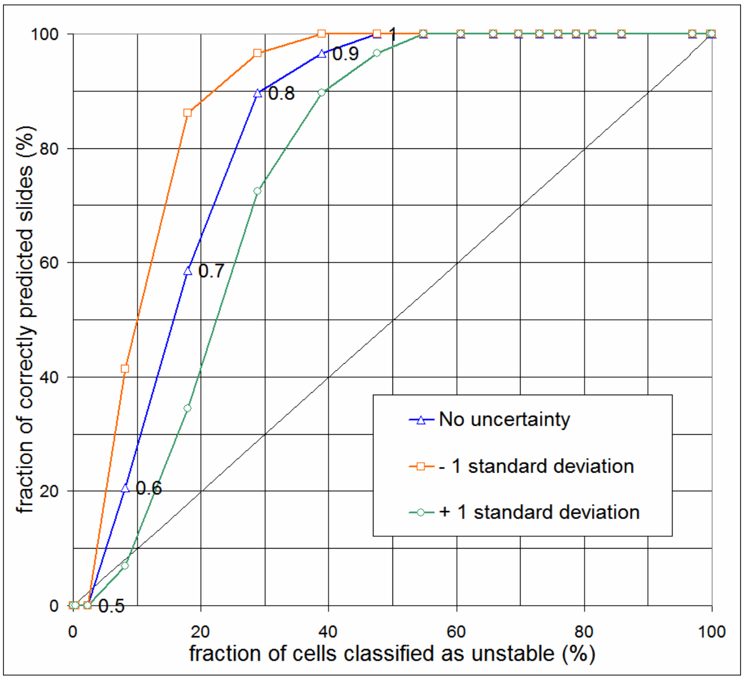

Figure 3. Prediction rate curves of the factor of safety and a range of one standard deviation from the factor of safety. The vertical distance between the curves represents the range of uncertainty. Labels on the graph indicate factor of safety classification thresholds.

uncertainty. The result is shown in the PRC in Fig. 3. The vertical distance between the two PRC incorporating the uncertainty analysis represents the range of uncertainty.

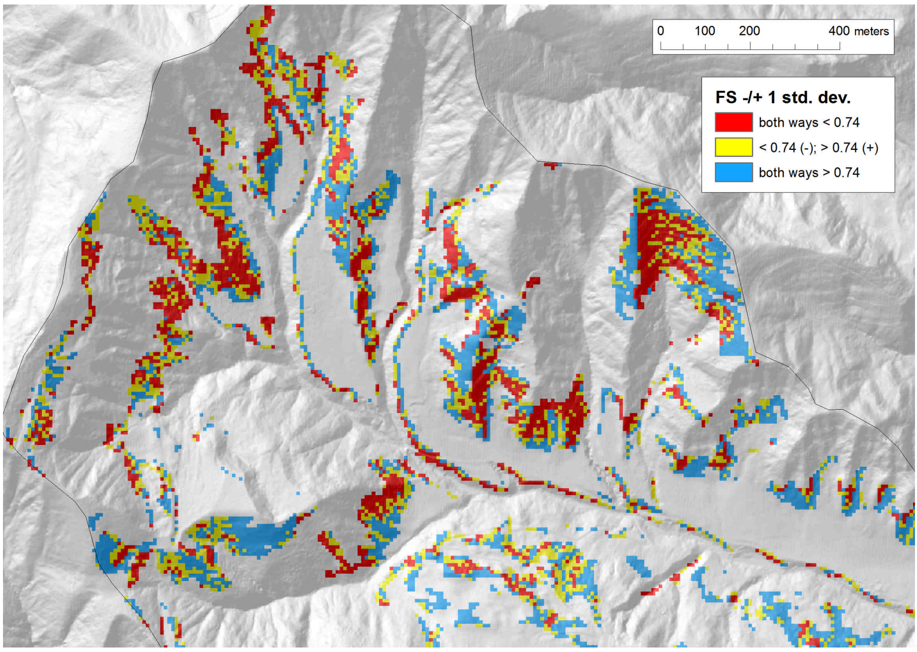

Figure 4: Sensitivity of stability values to uncertainty. Red cells are classified as "unconditionally" unstable (FS < 0.74), blue cells are classified as "unconditionally" stable (FS > 0.74). Yellow cells switch class when one standard deviation is added or subtracted.

To explore sensitivity of slide prediction to uncertainty in soil and DEM parameters, for a given classification threshold (FS = 0.74, at which about 72% of all slides are predicted correctly), cells were grouped in three classes: The first two are those classified as "unconditionally" stable or unstable, respectively, even when a standard deviation is added or subtracted. The third class contains the cells that change from stable to unstable or vice versa when a standard deviation is added or subtracted. These cells represent the areas where the uncertainty affects the prediction performance. They cover 28% of the study areas that is both unforested and steeper than 20° (in other words the areas where slides might occur and where ground truth data were available) (Fig. 4.). This helps to put the MCR results into context, and it demonstrates that model uncertainty affects the results significantly.

An equivalent analysis was made with the instability model based only on slope. The cells switching between unstable and stable when adding uncertainty account in this case for only 9% of the potentially unstable area, as opposed to 28% when using the slope stability model. This suggests that a further advantage of simply using topographic slope as a predictive model in areas where slope dominates landsliding is its increased robustness with respect to uncertainty.

5. Conclusions

Uncertainty of the analysed slope stability model is clearly important, and given the mediocre prediction performance, a simple slope map much less prone to uncertainty might do a better job. Indeed, this study suggests that the main source of uncertainty in this case is not input parameters, but rather the choice of model itself.

In general, when evaluating models of natural hazards, their practical use should be considered, especially as the increasing availability of high resolution DEMs, creates a need to generalise results. In this case high DEM resolution also violates the main assumption behind the slope stability model, i.e. that the slope is "infinite" in that its width is much larger than the soil depth. Another conclusion of this work is that understanding of the spatial structure of soil properties and DEM-error is poor and that to perform uncertainty studies there is a general need for better models of the spatial structure of DEM uncertainty.

References

Alexander DE, 1995: Survey of the field of natural hazards and disaster studies. In: Carrara A and Guzzetti F, (eds), *Geographical information systems in assessing natural hazards,* Kluwer Academic Publisher, Dordrecht, Netherlands, 1-19.

Chung C-JF and Fabbri AG, 2003: Validation of spatial prediction models for landslide hazard mapping. *Natural Hazards*, 30: 835-844.

BFS, 2000: *Digitale Bodeneignungskarte der Schweiz*. Bundesamt für Statistik, Servicestelle Geostat.

Guzzetti F, 2005: *Landslide hazard and risk assessment*. Dissertation, Rheinische Friedrich-Wilhelms-Universität Bonn.

Heuvelink GB, 1998: *Error Propagation in Environmental Modelling with GIS*. Taylor & Francis, London, UK.

Pack RT, Tarboton DG, Goodwin CN and Prasad A, 2005: *SINMAP 2. A Stability Index Approach to Terrain Stability Hazard Mapping, technical description and users guide for version 2.0*. Technical report, Utah State University.

Oksanen J and Sarjakoski T, 2005: Error propagation analysis of DEM-based drainage basin delineation. *International Journal of Remote Sensing*, 26: 3085-3102.

Rickli C and Bucher H, 2002: *Shallow landslides in Napf and Appenzell areas in the 2002 storms*, WSL report for BAFU.

Swisstopo, 2005: *Flyer DTM-AV*. http://www.swisstopo.ch/pub/down/products/digital/height/dtm_av_flyer_de-fr.pdf. Access: 2. 4. 2007.

A Two-Stage Classification Approach for Effective Geomorphic Mapping of Planetary Surfaces

Tomasz F. Stepinski[1], Chaitanya Bagaria[2]

[1]Lunar and Planetary Institute, Houston, TX 77058, USA
Telephone: (+1-281-486-2170)
Fax: (+1-281-4862162)
Email: tom@lpi.usra.edu

[2]Dept. of Computer Science, University of Houston, 4800 Calhoun Rd., Houston, TX 77204
Email: chaitanya.bagaria@gmail.com

1. Introduction

Advances in remote sensing from spacecrafts have produced a large amount of data on topography of planetary surfaces. In particular, the entire surface of planet Mars is covered by a digital elevation model (DEM) with a resolution of ~500 m derived from laser altimeter measurements. In addition, an increasing number of sites on Mars are covered by higher resolution DEMs derived from stereo images. The high resolution global DEMs of planet Mercury and the Moon will be available in the near future. Last but not least, most landmasses on Earth are covered by the 30-90 m/pixel DEM produced from data collected by the Shuttle Radar Topography Mission (SRTM). The major tools for understanding the origin and evolution of planetary surfaces are geomorphic and geologic maps that are traditionally created manually on the basis of photo-geologic interpretation. The slowness and expense of manual methods severely limits the area that can be mapped at the level of detail corresponding to the resolution of available elevation data. For example, 1:500,000 geomorphic maps of Mars exist only for a tiny percentage of its surface. Thus, there is a critical need to develop an effective method for automating the process of geomorphic mapping. In this paper we describe a framework for auto-generation of such maps. The resultant maps have information esthetics similar to manually drawn maps and they can be stored in a standard GIS shapefile format. We assert that our method has a combination of features that makes it likely to become a useful exploratory tool for planetary scientists.

2. Mapping Framework

In the context of this paper a geomorphic map is defined as a thematic map of terrain types or regions, patches of topography having similar terrain attributes. A challenge is to design an efficient algorithm that generates maps which are perceived as useful by the community of end users. Most previously developed mapping methods are pixel-based (for example: Irvin et al. 1997, Hengl and Rossiter 2003, Ehsani and Quiel 2008); an algorithm assigns a terrain type label for each pixel in a DEM separately. Our experience shows that pixel-based maps are not readily accepted by the planetary community which is used to the maps in the vector data format (for example, ESRI shapefile format). Some previously developed mapping methods are segment-based (for example: Dragut and Blaschke 2006, Stepinski et al. 2006); an algorithm assigns terrain type labels for multi-pixel but attribute-homogeneous segments of the landscape. The appearance and format of the resultant maps are acceptable for planetary analysts but segment classification is usually achieved via supervised learning – a technique ill suited for purpose of data exploration.

Our new unsupervised method combines the best aspects of pixel-based and segment-based mapping approaches. The core idea is to design a two-stage classifier consisting of a pixel-based *base* classifier and a segment-based *meta* classifier. A base classifier is applied to multiple pixels in a neighborhood of a focus pixel resulting in an ensemble of terrain type predictions. A meta classifier is an unsupervised segmentation/classification algorithm that combines these predictions and outputs a segment-based map of emergent terrain regions or classes. Hereafter we will refer to labels derived by a base classifier as “terrain types” and to labels derived by a meta classifier as “terrain classes.”

2.1 Base Classifier

Our method constitutes a “framework” inasmuch as it works with any base classifier. From a practical point of view a rule-based classifier is probably the best choice for this stage of the method. The rule-based classifier uses empirical knowledge to construct a decision tree; submitting a set of terrain attributes to a trunk of the tree results in a terrain type label at the leave of the tree. A number of such classifiers (for example, Wood 1996, Gallant et al. 2005, Iwahashi and Pike 2007) have been developed, and all of them could be used as the base classifier in our method. From planetary perspective a classifier proposed by Iwahashi and Pike (2007) is attractive because, using only three terrain attributes (slope, convexity, and texture), it assigns one of possible 16 terrain types to each pixel in a DEM. Because it uses the nested means technique to construct a decision tree, the meanings of the terrain types do not correspond directly to named terrestrial formations, thus, they won’t lose their relevance in application to non-terrestrial surfaces.

2.2 Meta Classifier

For a neighborhood of a focus pixel we use an N x N square window. The value of N controls the level of generalization from terrain types to terrain classes; N=11 is used in present calculations. The labels of terrain types from this neighbourhood form an ensemble used by the meta classifier to assign a terrain class to the focus pixel. A 19-features vector is calculated from the ensemble. The first 16 features are normalized frequencies of terrain types in the ensemble. The last three features measure pattern of terrain types in a neighborhood and are based on a modification of Multi-Scale Local Binary Pattern (LBP) concept (Ojala et al. 2002). The 19-features vector is used by the meta classifier to generate a final map. We use the Recursive Hierarchical Segmentation (RHSEG) algorithm (Tilton, 2000) that *simultaneously* segments the DEM and cluster the segments into terrain classes. The RHSEG is an iterative algorithm that produces hierarchies of both, segmentation levels, and clustering levels. Stopping the RHSEG at a given iteration level yields a map of a certain geographical and feature-space resolutions.

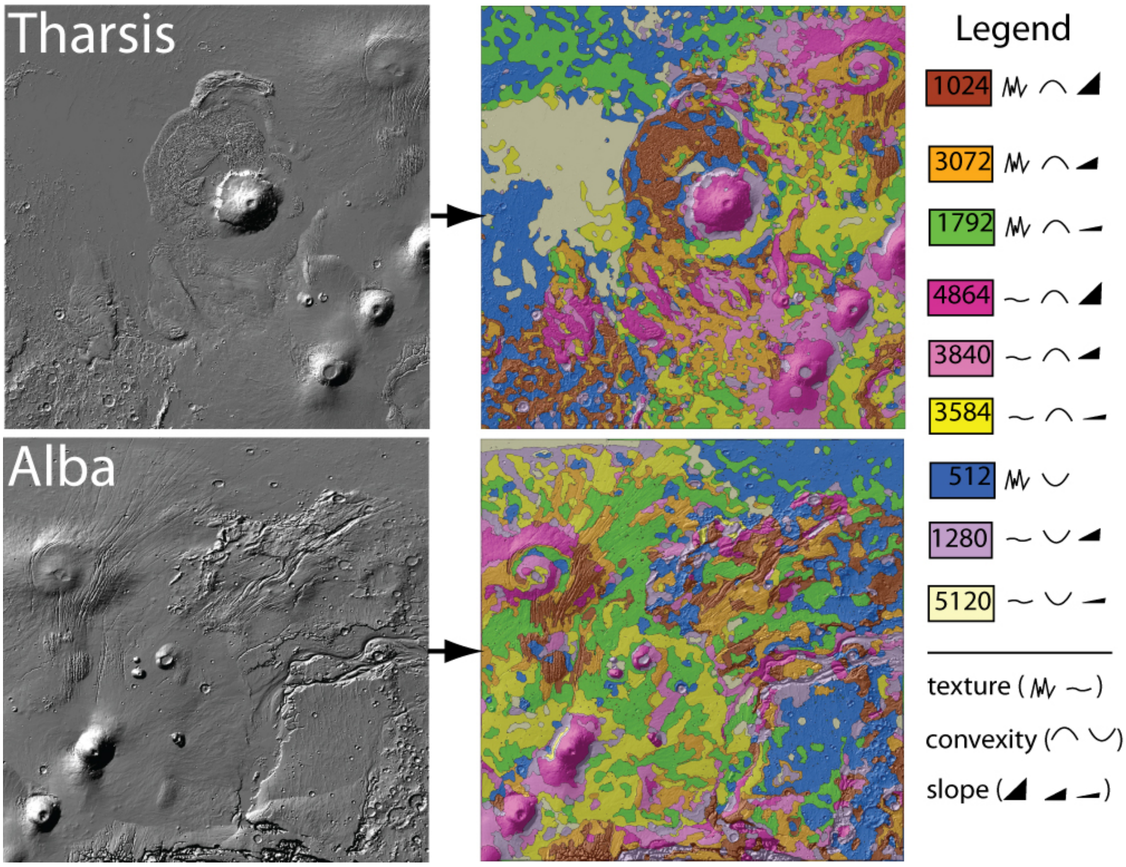

Figure 1. Auto-generated geomorphic maps of Tharsis and Alba regions on Mars.

3. Applications

In order to illustrate our method we have applied it to two large, partially overlapping regions on Mars referred to as Tharsis (centered on -137°E and 13°N) and Alba (centered on -85°E and 25°N), after prominent features in each site. In order to efficiently demonstrate an application of our mapping technique to large sites the global DEM was resampled to 4 km/pixel and the 1024 x 1024 pixels clips were taken to represent the two sites. The base classification was calculated using an AML script, and 19-features vectors were calculated using a Matlab code. Final map was obtained using the RHSEG software. Figure 1 shows the maps of the two sites obtained by stopping the RHSEG at level 11 of the hierarchy when segments are clustered into just 9 generic terrain classes. The classes are post-interpreted (see the legend) on the basis of frequencies of terrain types contributing to the classes.

The map generated by our method have higher visual appeal than pixel-based (or even segment-based) maps of homogenous terrain types because they partition sites in a fashion similar to what an analyst would do manually – into fewer larger, more heterogeneous areas corresponding to terrain classes. Existing, manually drawn geomorphic maps of planetary surfaces concentrate on few selected landforms and cannot facilitate validation of our auto-mapping. Geologic maps provide exhaustive mapping of a site and are formally comparable to our maps, however a geologic map uses many additional criteria besides surface morphology to define units so only a qualitative validation is possible. Figure 2 shows a comparison between the auto-generated and geologic maps of the Tharsis region. There is a rough correspondence between spatial distribution of terrain classes and geologic units. Thus, the immediate application of our technique is as an *exploratory* tool to offer a quick first draft of geologic map that needs to be further revised and elaborated by an analyst.

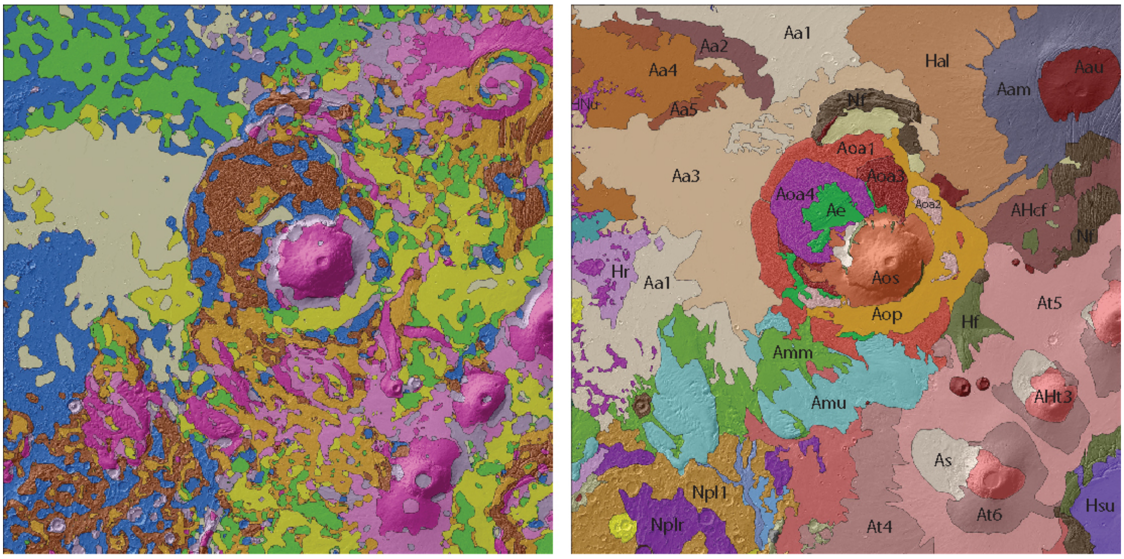

Figure 2. Tharsis region: comparison of auto-generated geomorphic map (left) and manually drawn geologic map (right) with prominent units indicated by labels.

Because we have used a base classifier that assigns terrain types on the basis of statistics of site's terrain, the precise physical meanings of terrain classes change from site to site. For example, there are some small differences in the meaning of classes in the maps of Tharsis and Alba; a full narrative of the classes would reflect these differences. This is why there are small differences in mapping an overlapping part of Tharsis and Alba sites. In order to map a series of sites with classes of exactly the same meaning, a base classifier needs to be used on a concatenation of pixels from all the sites. Moreover, the segments in a selected site should be treated as a training set, and the segments in all other sites should be labeled using a supervised classification technique. However, in most planetary geomorphology applications an analyst focuses on a single site.

4. Discussion

Exhaustive auto-mapping of landscape elements is a challenging problem. Our two-stage classification method yields a map of terrain classes that is an improvement over maps generated by a single-stage classification algorithm. The improved appearance and utility of our map is achieved by a meta classifier that generalizes numerous homogenous terrain types into fewer more heterogeneous terrain classes. This improvement comes at a computational cost; each site shown in this paper required 7 hours of processing time using a 2.0 GHz Intel processor with only a fraction of that time needed for an execution of the base classifier, and the bulk of the time needed for an execution of the meta classifier. The method is robust; we have utilized it, without any modification, to generate a map of the continent of Africa using the SRTM data. For mapping terrestrial sites it may be more advantageous to use a base classifier described by Gallant et al. (2005) which is modeled after a manual method developed by Hammond (1964) – a standard in terrestrial landform mapping. However, an exhaustive auto-mapping of landform types (as opposed to terrain classes) may not be feasible using our technique because such landforms are recognized by a combination of DEM-derivable terrain attributes and morphogenetic criteria that cannot be derived from the DEM.

Acknowledgements

This work was supported by the National Science Foundation under Grants IIS-0812271 and by NASA under grant NNG06GE57G. A portion of this research was conducted at the Lunar and Planetary Institute, which is operated by the USRA under contract CAN-NCC5-679 with NASA. This is LPI Contribution No. 1480.

References

Dragut L and Blaschke T, 2006, Automated classification of landform elements using object-based image analysis. *Geomorphology*, 81:330–344.

Ehsani AH and Quiel F, 2008, Geomorphometric feature analysis using morphometric parameterization and artificial neural networks. *Geomorphology*, 99:1–12.

Gallant AL, Brown DD and Hoffer RM, 2005, Automated mapping of Hammond's landforms. *IEEE Geoscience and Remote Sensing Letters*, 2(4):384–288.

Hammond EH, 1964, Analysis of properties in land form geography: An application to broad-scale land form mapping, *Ann. Assoc. Amer. Geogr.*, 54:11–19.

Hengl T and Rossiter DG, 2003, Supervised landform classification to enhance and replace photointerpretation in semi-detailed soil survey. *Soil Science Society of America Journal*, 67:1810—1822.

Irvin BJ, Ventura SJ and Slater BK, 1997, Fuzzy and isodata classification of landform elements from digital terrain data in Pleasant Valley, Wisconsin. *Geoderma*, 77:137–154.

Iwahashi J and Pike RJ, 2007,. Automated classifications of topography from DEMs by an unsupervised nested-means algorithm and a three-part geometric signature. *Geomorphology*, 86:409-440.

Ojala T, Pietikainen M and Maenpaa T, 2002, Multiresolution gray-scale and rotation invariant texture classification with local binary patterns. *IEEE Trans. Pattern Analysis and Machine Intelligence*, 24 (7):971–987.

Stepinski TF, Ghosh S and Vilalta R, 2006, Automatic recognition of landforms on Mars using terrain segmentation and classification *Lecture Notes in Computer Science* # 4265: 255–266.

Tilton JC, 2000, Method for recursive hierarchical segmentation by region growing and spectral clustering with a natural convergence criterion. In *Disclosure of Invention and New Technology: NASA Case Number GSC 14,328-1*.

Wood, J, 1996, The geomorphological characterization of digital elevation models. *Ph.D. Thesis*, Department of Geography, University of Leicester, UK.

Automated Classification of Martian Morphology Using a Terrain Fingerprinting Method

R. Koenders[1], R. C. Lindenbergh[1], T. E. Zegers[2]

[1]Delft University of Technology, P.O.Box 5058, 2600 GB Delft, The Netherlands
Telephone: (+31)610383808
Email: roderikk@gmail.com

[2]Utrecht University, P.O Box 80125, 3508 TC Utrecht, The Netherlands

1. Introduction

The planet Mars has a relatively short human exploration history, while the size of the scientific community studying Mars is also smaller than its Earth equivalent. On the other hand the interest in Mars is large, basically because it is the planet in the solar system most similar to Earth. Several satellites are currently orbiting Mars, and transmit data back in unprecedented detail. In fact, the Martian surface is mapped at up to 5 times higher resolution than the bottom of the ocean here on Earth.

The scientific community studying Mars has already made great discoveries concerning, for example, the variability of the surface (Bibring, 2005), and the presence of water. To learn more about the history of the surface and about the planet as a whole, data generated by different satellite missions will have to be combined. Processing such large, multi-attribute datasets at a global Martian scale requires efficient automated classification methods.

The use of automated classification in combination with geomorphometric data has only recently been possible on Mars with the creation of the global Mars Orbiter Laser Altimeter (MOLA) digital elevation model (DEM) (Smith et al. 2003), as obtained between 1997-2001 by the Mars Global Surveyor. (Bue and Stepinski, 2006) demonstrated the potential of classifying global MOLA DEM data and concluded that similar methodology could be applied on other data sets like the ~60m spatial resolution DEM, as currently under construction from High Resolution Stereo Camera (HRSC) images collected by ESA's Mars Express (Gwinner, 2007).

On Earth, morphological classification has been used for numerous specific applications (Guzetti and Reichenbach, 1994; Hosokawa and Hoshi, 2001). Also only relatively recent it was demonstrated that attributes like gradient and roughness, as derived from elevation data, can be used to construct a multi-attribute feature vector, that, possibly in combination with other data, like intensity or multi-spectral data, can be consecutively applied in land surface and vegetation classification procedures (e.g. Antonorakis et al., 2008; Bork and Su, 2007; Chust et al., 2008).

Even though the use of automated classification on Martian datasets has great potential, it is not yet being used as intensively by the scientific community studying Mars. The research presented in this abstract therefore formalises the methodology presented by Bue and Stepinski (2006) as the Terrain Fingerprinting Method (TFM) in Section 2. We have applied the TFM to several areas on Mars based on the MOLA DEM, which has a maximum spatial resolution of 400 meters per pixel; HRSC DEM, which has a maximum resolution of 50 meters per pixel; and a combination of the MOLA DEM with data from the Mars Express mineralogical spectrometer (OMEGA). The present abstract focuses on an analysis of the combination of OMEGA and MOLA DEM data as presented in Section 3.

2. The Terrain Fingerprinting Method

The Terrain Fingerprinting Method consists of 5 steps that closely follow the steps a geoscientist takes when he or she analyses a terrain.

Step 1: Defining the research question

The first step requires the scientist to define the research area and the type of terrain to be analysed. This is exactly how a scientist starts researching a terrain on Earth; first selects a region to analyse and then he decides what research questions need to be answered about that region – or vice versa.

Step 2: Choosing the attributes

The next step requires the expert to describe how the terrain would be analysed if it was analysed by hand. For example, to categorise a certain region into different geological units a geoscientist would look at terrain attributes including slope, elevation, terrain roughness, and rock colour to determine where the geological units' boundaries lie.

Step 3: Converting unprocessed data

The next step is to translate the attributes found in the previous step into a computer readable format. This involves converting unprocessed satellite data of the region to be studied to data read by GIS software, and finally deriving the required attributes; for example creating slopes from elevation data.

Step 4: Clustering data

In the supervised terrain classification, this step would involve manually classifying the terrain with GIS software. This step is replaced by an automated classification method. This research uses a combination of a partitive clustering technique (Self-organising Maps, Kohonen, 2001) and a hierarchical clustering technique (Ward clustering, Ward, 1963) to create a fingerprint of the terrain analysed automatically, see section 2.1.

Step 5: Analysing and validating results

The final step in the TFM is also very similar to the final step in the manual process. It includes validating, analysing, and interpreting the classification made by the automated classification.

2.1. Automated Classification of Landforms

Classification schemes can generally be divided into two categories: hierarchical and partitive clustering. In hierarchical clustering, each data point can be seen as being on the end of a twig on a tree, which is part of a branch, which connects to the tree. The more two twigs are set apart, the more dissimilar the two points of data are.

This way of classifying is very useful for smaller datasets. However, as each data point corresponds to a twig, the classification tree, and therefore the storage and processing power, grows with every point of data.

On the other hand, partitive clustering does not look at each individual data point; it tries instead to look at the dataset as a whole to find clusters. To continue the analogy, partitive clustering tends to ignore the twigs of the tree and only look at the branches. One of the disadvantages of this approach is that it is more difficult to distinguish between clusters that are closer together.

When classifying large areas of terrain and/or terrain at a high resolution, the number of data points grows very fast. To still be able to classify these terrains, while avoiding the disadvantages of the single methods, a combination of the partitive and hierarchical clustering techniques can be applied. Vesanto (2001) has shown the feasibility of this technique.

The present research uses self-organising maps (Kohonen, 2001) to create an initial mapping of the original data to a lower number of proto-vectors. These proto-vectors are then clustered using so-called Ward clustering (Ward, 1963) to bring them down to 20 classes.

3. Results

To design and validate the Terrain Fingerprinting Method we have applied it to several different use-cases. This section describes each of the TFM steps for one of the use-cases.

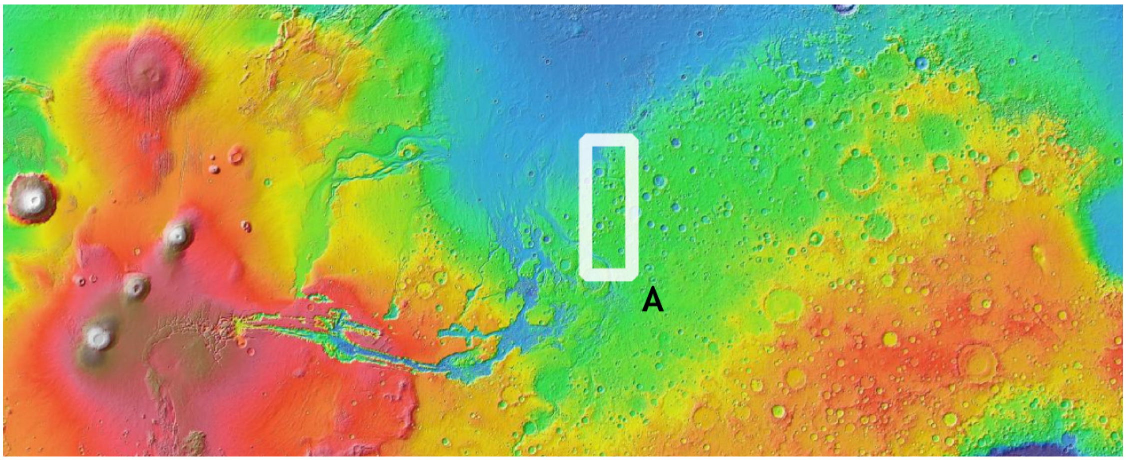

Figure 1. The area analysed in this research.

R*esearch question*: The research question for area A is whether the area contains terrain that is on one hand safe to land on for a rover such as ExoMars, whilst on the other hand the terrain is also interesting from a scientific point of view. In this case safe is defined using the characteristics given in Table 1; and being interesting is based solely on whether there are indicators for phyllosilicates[1] in the OMEGA data.

This particular area—around the Mawrth Vallis—was chosen because it is known for its high phyllosilicates content and its possible suitability as a landing site for NASA's Mars Science Laboratory (Michalski, 2008).

Characteristic	Lower Bound	Upper Bound
Elevation [m]	-	-1000
Slope [°]	0	2

Table 1. Primary safety characteristics for ExoMars.

A*ttributes*: To classify the terrain by hand into safe, unsafe, and interesting units, it was agreed that there were 5 relevant attributes:

---

[1] Phyllosilicates are considered to be an indicator of the past presence of liquid water; ExoMars scientific and exploration goals are to find traces of past and/or present life; since life as we know it requires, among other things, the presence of liquid water, we assume that evidence of phyllosilicates will indicate an interesting region.

1. Elevation: to distinguish between low and high;
2. Slope: to identify crater walls and cliffs;
3. Filled Difference[2]: to identify craters;
4. Filled Slope[3]: to distinguish crater walls and cliffs elsewhere; and
5. Phyllosilicates: to identify interesting terrain, based on Pelkey (2007).

U*nprocessed data*: The classification is based on a set of OMEGA images that covered the region, all of which had approximately the same resolution of 1000 meters per pixel.

The file was read into `GRASS` (GRASS Development Team, 2008) and the attributes were generated using the following `GRASS` routines:

1. Elevation: -
2. Slopes: `r.slope.aspect`
3. Filled Difference: `r.terraflow` and `r.math`
4. Filled Slope: `r.terraflow` and `r.slope.aspect`
5. Accumulation: `r.terraflow`

C*lustering data*: Figure 2a shows a close up of part of the elevation data on which the previously discussed attributes were based. The final classification result is shown in Figure 2b. At the bottom, each colour can be seen to correspond with a class, and the classes are grouped according to their relative distances and the clustering algorithm.

A*nalysis*: The groups indicated in the legend of Figure 2b can also be visually identified in the mapping of the classification: group 1 can be identified on the higher, southern terrain; group 2 fills up the spaces between group 1 and the craters of the said highlands; group 3 can be identified as craters; group 4 is located in the northern lowlands; and group 5 is found in the area between the lowlands and the highlands.

In order to verify these claims, Table 2 summarises the attribute means for each group. The first row shows the means for the attributes over the entire area of study, this can be used to compare the values of the other groupings.

The final column in this table shows the amount of phyllosilicates in the group. According to Pelkey (2007) only levels above 0.02 indicate the presence of this mineral group on that location. None of the groups in Table 2 show this level, though the values in the table represent a mean over an area. When compared to the mean of all groupings, groups 4 and 5 show above average phyllosilicate levels.

It can be concluded from the data given in Table 2 that groups 4 and groups 5 potentially identify terrain types that are both safe and interesting; with the latter being more interesting as it has a higher phyllosilicates content.

---

[2] Filled difference is an attribute generated by using a fill algorithm to make lakes out of all the craters and blocked channels, finally the `filled difference' attribute is the difference between this map of lakes and the real elevation map; thus generating domes where craters are located.

[3] The filled slope attribute is generated by creating a slope map from the `map of lakes' created in the filled difference attribute procedure.

Groups	Area [%]	Elevation [m]	Fill. Diff. [m]	Fill. Slope [°]	Slope [°]	Phyllo. [-]
All	100	-2507	233	0.83	2.08	0.00383
1	24	-2008	21	2.52	3.43	0.00368
2	38	-2058	135	0.14	1.21	0.00127
3	13	-3216	1221	0	3.42	0.00193
4	12	-3736	94	0.2	1.01	0.00775
5	8	-2727	19	0.73	1.25	0.00871

Table 2. Attribute means for different groups in area A.

4. Conclusions

Bue and Stepinski (2006) used MOLA data to create an automated classification of Martian terrain. The present research has looked at how their methodology can be formalised to appeal to the broader planetary science community, and how it can be applied to other types of data.

As can be deduced from the process description above, the steps taken for the TFM are almost identical to those taken for a terrain classification done by hand. The fingerprint produced in step 4 of the TFM is the key difference. The terrain fingerprint produced can for instance be used to:

- perform an initial terrain classification on an area to quickly identify the primary terrain classes, which can be used as input for a manual classification;
- locate terrains elsewhere on the surface that have the same fingerprint and could therefore be similar terrains;
- use a classification made for one area and apply it to a different area to quickly, and consistently classify this new area with the same classes as the original area; and
- translate a classification made manually by an expert to a computer readable terrain fingerprint and apply it consistently to other areas.

The most challenging TFM step is the one where the list of attributes is created. During manual terrain classification a geoscientist combines many attributes, including interpretations from previous terrains. More research is required to turn these more `interpretive' attributes into attributes that the computer can understand.

Another property of TFM—and of analysing datasets of Mars in general—is that combining the different datasets into a single frame of reference requires many processing tools and steps. Scaling the analysis to cover larger swathes of terrain will therefore require investigations on how to optimally load the unprocessed data.

Another often-heard criticism about the automated classification method is that the results are not similar enough to how a geoscientist would interpret the terrain. One way to circumvent this criticism is to use a manual terrain classification as the basis for the fingerprint.

In the course of the present research we have identified several items for further research. Due to the lack of ground-truth on Mars it will be important to validate TFM on Earth with terrestrial geoscientists.

It is expected that using geostatistical methods considering both cross-correlation between attributes, and spatial correlation within one attribute, will further optimise the distinction between different terrain types. Moreover the use of geostatistical methods provides a framework to combine datasets with different spatial point densities and/or individual point qualities.

Figure 2. *a)* MOLA elevation data of area A; *b)* Classification made with TFM.

References

Antonarakis, A.S. and Richards, K.S. and Brasington, J.,2008. *Object-based land cover classification using airborne LiDAR,* Remote Sensing of Environment, 112(6), pp. 2988-2998.

Bibring, J.P. and Langevin, Y. and Gendrin, A. and Gondet, B. and Poulet, F. and Berthe, M. and Soufflot, A. and Arvidson, R. and Mangold, N. and Mustard, J. et al, 2005. *Mars Surface Diversity as Revealed by the OMEGA/Mars Express Observations*, Science, Vol 307, 1576-1581.

Bork, E.W. and Su, J.G.,2007. *Integrating LIDAR data and multispectral imagery for enhanced classification of rangeland vegetation: A meta analysis,* Remote Sensing of Environment, 111(1), pp. 11-24.

Bue, B.D. and Stepinski, T.F., 2006. *Automated classification of landforms on Mars*, Computers and Geosciences, Vol 32.

Chust G, Galparsoro I, Borja A, Franco J, Uriarte A (2008) *Coastal and estuarine habitat mapping, using LIDAR height and intensity and multi-spectral imagery*. Estuarine Coastal and Shelf Science 78:633–643.

GRASS Development Team, 2008. *Geographic Resources Analysis Support System (GRASS) Software*, Version 6.3.0. http://grass.osgeo.org .

Guzetti, F. and Reichenbach, P., 1994. *Towards a definition of topographic regions for Italy*, Geomorphology, Vol. 11.

Gwinner, K. et al., 2007. *Global mapping of Mars by systematic derivation of Mars Express HRSC high-resolution digital elevation models and orthoimages*, ISPRS WG IV/7 Extraterrestrial Mapping Workshop, Houston, Texas.

Hosokawa, M. and Hoshi, T., 2001. *Landform classification method using self-organizing map and its application to earthquake damage evaluation*, IEEE 2001 International Geoscience and Remote Sensing Symposium, IGARSS'01.

Kohonen, T., 2001. *Self-organizing Maps*, Springer.

Michalski, J. and Bibring, J. et al, 2008. *Mineral Mapping of High Priority Landing Sites for MSL and Beyond Using Mars Express OMEGA and HRSC Data*. American Geophysical Union, Fall Meeting 2008, abstract P33B-1463

Pelkey, SM and Mustard, JF et al, 2007. *CRISM multispectral summary products: Parameterizing mineral diversity on Mars from reflectance*. J. Geophys. Res, Vol 112.

Smith, D.E., M.T. Zuber, G.A. Neumann, E.A. Guinness, and S. Slavney, 2003. *Mars Global Surveyor Laser Altimeter Mission Experiment Gridded Data Record*, MGS-M-MOLA-5-MEGDR-L3-V1.0, NASA Planetary Data System.

Vesanto, J. and Alhoniemi, E., 200. *Clustering of the self-organizing map*, IEEE Transactions on Neural Networks, Vol. 11.

Ward Jr, J.H., 1963. *Hierarchical grouping to optimize an objective function*, Journal of the American Statistical Association.

A Method for Automated Extraction of Martian Talus Slopes – Case Studies of Nanedi Valles and West Candor Chasma, Mars

B. Székely[1,2], T. Podobnikar[1,3]

[1]Institute of Photogrammetry and Remote Sensing, Vienna University of Technology, Gusshausstr. 27-29, A-1040 Vienna, Austria
Telephone: (43) 1 58801-12251
Fax: (43) 1 58801-12299
Email: balazs.szekely@ipf.tuwien.ac.at

[2]Department of Geophysics and Space Science, Eötvös University, Budapest, H-1117 Budapest, Pázmány P. sétány 1/C, Hungary
Telephone: (36) 1 209-0555/6651
Fax: (36) 1 372-2927
Email:balazs.szekely@elte.hu

[3]Scientific Research Centre of the Slovenian Academy of Sciences and Arts, Novi trg 2, SI-1000 Ljubljana, Slovenia
Telephone: (386) 1-470-6493
Fax: (386) 1-425-7795
Email: tp@zrc-sazu.si

1. Introduction

Terrestrial talus (or scree) slopes are common features in mountainous environments. Their geomorphic form is determined by their constituting material, scree or similar loose, often poorly sorted material. The angle of repose of this type of material defines more or less the surface slope of these forms. On Earth they are sometimes slightly vegetated, therefore they might become slightly oversteepened and metastable.

Martian talus slopes are governed by differing environmental conditions: lower gravity (ca. 38% of the terrestrial), largely available loose material (often windblown), the lack of (present) fluvial erosion and typical large escarpments make the talus slopes more important areomorphic feature on Mars than on Earth.

Our previous approach to outline terrestrial talus surfaces in the Eastern Alps in an automated way (Székely and Podobnikar 2008) has been successful in finding certain types of talus surfaces. On the other hand the method has been found to be somewhat sensitive to the resolution of the applied DTM. Here we apply a similar technique to two Martian DTMs derived from High Resolution Stereo Camera (HRSC) imagery on board of ESA Mars Express (Jaumann et al. 2007).

Our main aim is to separate and outline the talus surface areas from other slopes (like escarpments, impact rims, etc.) in the study areas of Nanedi Valles and West Candor Chasma in order to analyse the spatial distribution of this phenomenon, in craters, along escarpments, and, especially, in the area of vallis sides.

2. Data and Methods

The 50 m resolution DTMs (Heipke et al. 2007) of the two test areas of Nanedi Valles (ca. 4.9°N, 49°W; orbit No. 1235) and West Candor Chasma (6.6°S, 70.9°W; orbits No. 805, 902, 927) derived from HRSC images have been used for the morphometric analysis. Since the DTMs have limited accuracy due to the automated matching procedure of relatively featureless plateau areas, Context Camera (CTX; on board of Mars Reconnaissance Orbiter, MRO), HiRISE (High Resolution Imaging Science Experiment, also on board of MRO) and anaglyph HRSC images were used for visual control. The HRSC SRC (Super Resolution Channel) data provide unique details of the

Martian surface like dunes in the bottom of valles, terraces and spurs of former thalwegs, that were necessary for the visual classification of areomorphic features.

The concept of the recognition is based on the idea that a talus slope has a certain slope angle, but also ends on a low-lying, typically horizontal, subhorizontal surface. So if we calculate the local relief on a basis of local moving window analysis, the talus slopes can be characterised by the property that there is much relief area above them and not much relief are below them. On the other hand, the talus itself may cover some relief as well.

For the automated recognition of talus surfaces development of significant and, as much as possible independent, DTM-derivative spatial variables are necessary, that are converted to indicator variables by applying threshold values. Beside of the independence of the variables the idea on improvement of the initial approximation of the talus slopes step-by-step is important (Podobnikar 2005). The modelling starts with the most coarse estimations and continue using increasingly finer variables that improve the quality of the modelling until the changes are within the certain threshold.

A two-phase data processing has been carried out. The slope distribution was analysed first in order to find appropriate threshold values for the second phase. Then, the indicator variables have been computed and, finally, the indicator variables are integrated to one category by simple summation. If the sum reaches a preset number (on a pixel by pixel basis), the pixel in question will be categorized as classified to the respective group.

In the latter phase a novel visibility simulation technique has been applied. Here the pixels of the DTM are considered successively as central points of a sequence of visibility test as follows:

1. Calculate visibility (visible: 1, not visible: 0) from a central point of the particular grid cell in the DTM using a specific zenith angle θ (Fig. 1).

2. Repeat the visibility calculation for every grid-point of the DTM to produce a derivative binary grid B_φ applying certain parameters.

3. To certify the isotropic processing continue calculation of the derivative binary grids B_φ by a sequence of azimuths φ (applying an appropriate azimuth interval δ), sum up B_φ to produce continuous grids according to upper views U_θ, and lower views L_θ as $\Sigma(B_\varphi)$, where $\varphi = \{0°, \delta, 2\delta, 3\delta, \ldots, 360° - \delta\}$, $n = 360/i$ times and where θ is carefully chosen.

4. Calculate continuous derivative grids that simulate a sort of relative relief: $RR_\theta = U_\theta - L_\theta$

These channels serve then as input for the summation.

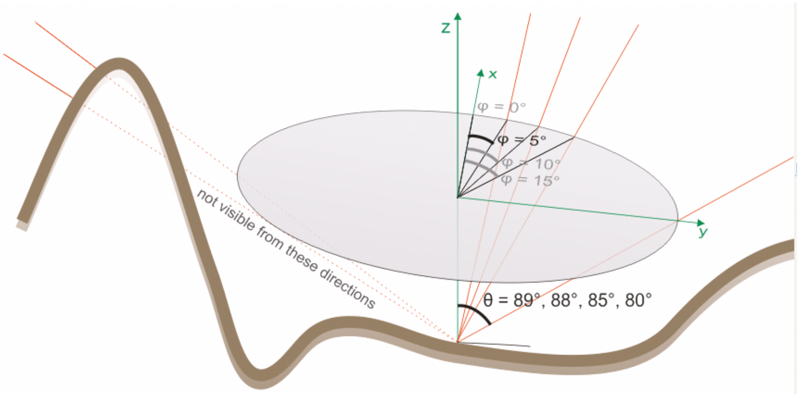

Figure 1. Principle of visibility simulation with definitions of φ (azimuths) and θ (zenith angles).

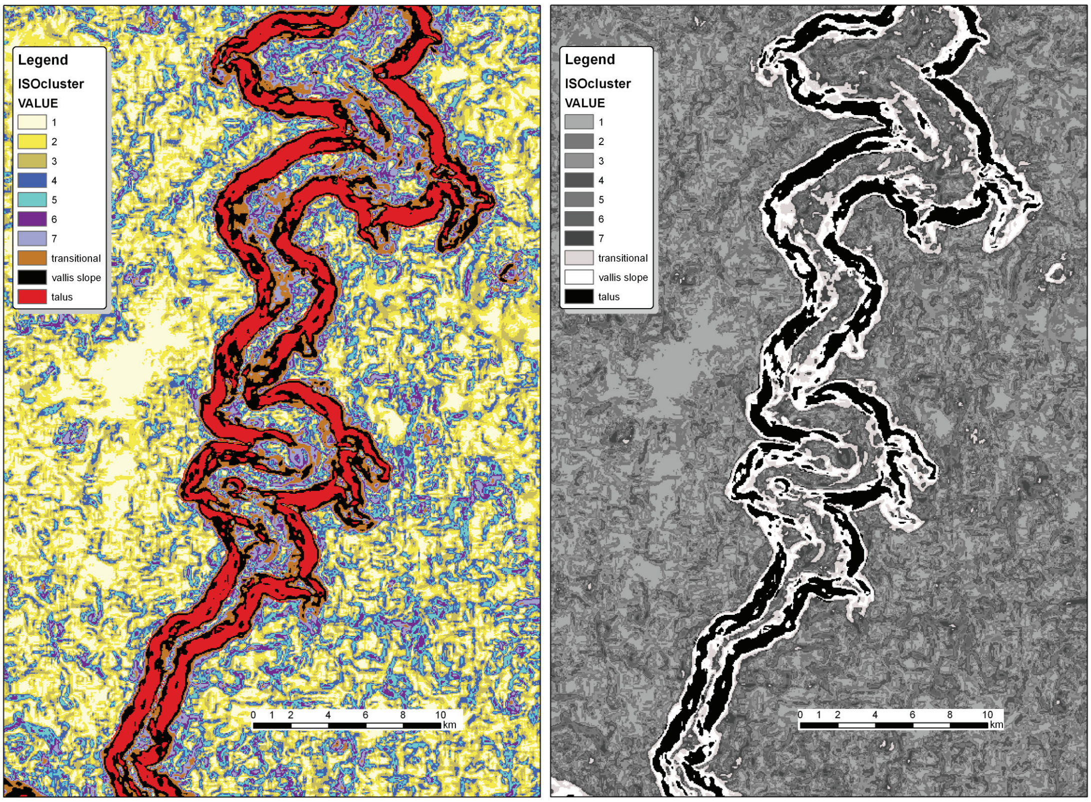

Figure 2. Result of the pre-processing step outlining the candidate pixels of talus (left: in colour). Clusters 1-3 are characteristic for the planation surface, clusters 4-7 representing the smaller dissecting forms, while the transitional cluster is situated mostly in the valley bottom but also forms a band at the rim of the vallis. The vallis sides are mostly falling into the cluster that is expected to represent the talus surface.

3. Data Processing

In order to analyze the slope distribution, a preprocessing step has been carried out to outline the potential areas for talus slopes (Fig. 2). The slope angle and the standard deviation of the slope angle (as a measure for the variability) have been used as input. This two-channel data set has been processed by ISOcluster classification. (ISOcluster was used here to keep the possibility of extension. In case of a more complex slope distribution other derivatives can be integrated as third, fourth, etc. channel in the same scheme.) The number of target clusters has been defined to be 10, because of the expected classes: Beside of the plateau and terrace areas (#1-#3) and the incision(?) features (#4-#7) the internal slopes of craters and valles may need to be separated. The “bedrock” areas (scarp surface) are expected to fall in an individual category. Toe areas of mass movements can also be present.

The resulting clusters showed promising separation (Fig. 2). The classified variable should cover the talus surfaces in their entirety, e.g. an interval between the minimum and maximum of the values characteristic for fans was defined, and the area encompassed thus represent an area that is likely can be identified as talus.

A number of variables have been tested to provide similar results as the ISOcluster output. The most successful (estimated as the most significant) variables were those that are based on the relative relief based on innovative visibility simulation technique discussed above. A further group of potentially useful variables are based on the relief above function by applying focal operations with annular window. These masks combined with the restrictions on slope angles (derived from the ISOcluster procedure) effectively separated the horizontal, subhorizontal areas, as well as terraces (that can be found in Nanedi Valles) and the rock escarpments as well. The latter features may remain in the selection under certain conditions.

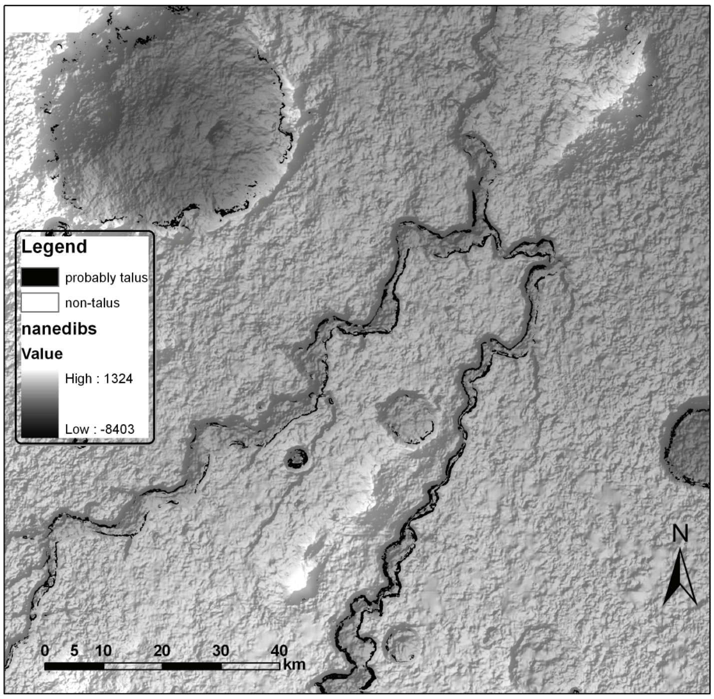

Figure 3. Example of Nanedi Valles area, the result of the processing (probably talus category) is depicted in black. Note the spatial distribution of the talus pixels also around the rims of craters.

4. Results and Discussion

Fig. 3. shows a larger area outlining the results of masking. It is important to note that for both areas of Nanedi Valles and West Candor Chasma (Fig. 4) the same processing has been applied (including all parameter selections). Although the relief that is partly covered in the two test areas are rather different, the success of recognition of the appropriate pixel groups is the same.

The vallis sides of Nanedi Valles are often comparable with the sides of larger craters where talus slopes are also occur, consequently the fluvial features are less probably present in the valles; the mass wasting processes have already reshaped these slopes. The same applies to West Candor Chasma, where larger slopes, exceeding 2 km in relief, are also showing these properties. However, in this area the remnants of larger landslides also occur, where talus is not observable.

Although the DTM has some errors that can be revealed by comparison with the SRC channel imagery, the processing remained robust and uninfluenced by some gross errors, most probably because the slope distribution of Martian surface features is persistent in this scale.

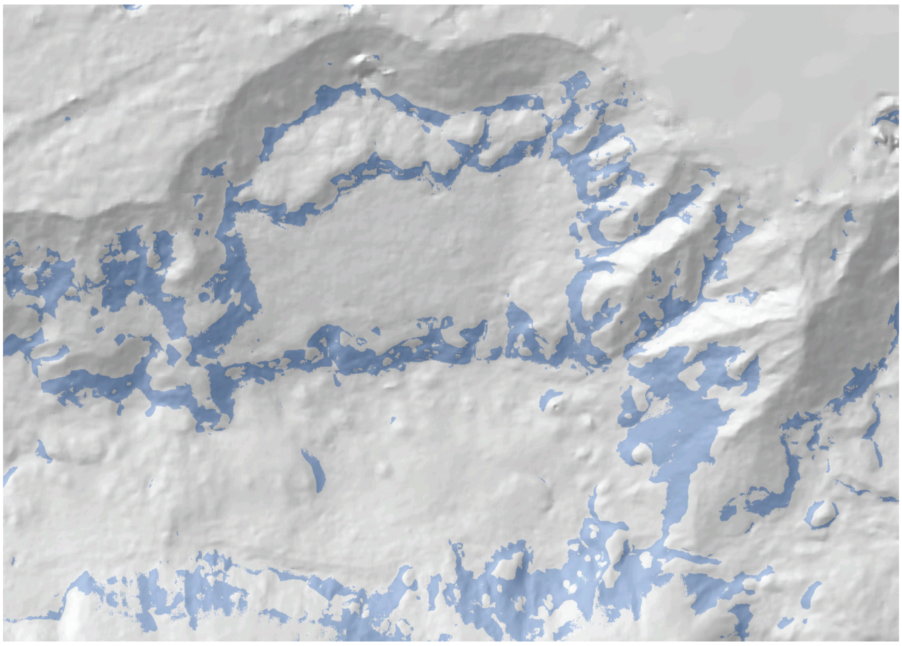

Figure 4. Example of West Candor Chasma, the result of the processing (probably talus category) is in light blue (dark grey in greyscale). The horizontal size of the image is ca. 50 km, north is to the top. Note that despite of the staircase-like setting, at the foot of each escarpment a belt of talus is recognized. This pattern is different within the incising valleys on the right.

Carrying out a thorough visual checking of the identified features, it is found that the majority of the areas that can be visually classified as talus surface are identified also by the automated processing. This result paves the way towards the analysis of multi-resolution DTMs as well in the lack of high-resolution DTM.

5. Conclusions

An automated recognition method has been developed for 50 m resolution Martian DTMs derived from HRSC imagery. The processing scheme has been found robust in two different Martian areomorphic settings, that may indicate that the technique can be applicable in generally for high-resolution Martian DTMs. The procedure is somewhat DTM-error tolerant. However, the verification of the results yet can be of qualitative nature only. Due to the known accuracy problems in the DTM generation a quantitative in-depth analysis of DTM and its derivatives is not suitable, therefore the visual checking remains as the only option for the verification: the original imagery has still somewhat better resolution and characterised by higher information content.

Acknowledgements

The study is a part of the *Areomorphological Analysis of Data from HRSC on Mars Express* (TMIS.morph) project (Austrian Space Applications Programme (ASAP); funding by the Austrian Research Promotion Agency (FFG)). Parts of the conceptual work on talus cones were developed in an Austrian Academy of Sciences (ÖAW) funded project. We are also grateful to G. Neukum (Berlin) and the Mars Express HRSC Team for the images and DTMs.

References

Heipke C, Oberst J, Albertz J, Attwenger M, Dorninger P, Dorrer E, Ewe M, Gehrke S, Gwinner K, Hirschmüller H, Kim JR, Kirk RL, Mayer H, Muller J-P, Rengarajan R, Rentsch M,Schmidt R, Scholten F, Shan J, Spiegel M, Wählisch M, Neukum G and the HRSC Co-Investigator Team, 2007, Evaluating planetary digital terrain models — The HRSC DTM test. *Planetary and Space Science* 55(14):2173-2191.

Jaumann R, Neukum G, Behnke T, Flohrer J, van Gasselt S, Giese B, Gwinner K, Hauber E, Hoffmann H, Köhler U, Matz K-D, Mertens V, Pischel R, Roatsch T, Reiss D, Scholten F, Stephan K, Oberst J, Saiger P, Schwarz G, Wählisch M, 2007, The High Resolution Stereo Camera (HRSC) experiment on Mars Express: instrument aspects from interplanetary cruise through nominal mission. *Planetary and Space Science*, 55(7-8):928-952.

Podobnikar T, 2005, Production of integrated digital terrain model from multiple datasets of different quality. *International Journal of Geographical Information Science*, 19(1):69–89.

Székely B and Podobnikar T, 2008, An attempt for automatic detection and visualization of talus cones from digital elevation data. In: Konečný M and Bandrova T (eds), *Second International Conference on Cartography & GIS, Proceedings 2,* Borovets, Bulgaria, 151-159.

Cell Size Dependence of Threshold Conditions for the Delineation of Drainage Networks from Gridded Elevation Data

P. Tarolli[1], G. Dalla Fontana[1], G. Moretti[2], S. Orlandini[2]

[1]Department of Land and Agroforest Environments, University of Padova, Agripolis,
Viale dell'Università, 16 – 35020 Legnaro (Padova), Italy
Telephone: +39 049 827 2695
Fax: +39 049 827 2686
Email: paolo.tarolli@unipd.it, giancarlo.dallafontana@unipd.it

[2]Department of Mechanical & Civil Engineering, University of Modena & Reggio Emilia,
Via Vignolese, 905 – 41100 Modena, Italy
Telephone: +39 059 205 6105
Fax: +39 059 205 6126
Email: giovanni.moretti@unimore.it, stefano.orlandini@unimore.it

1. Introduction

The drainage network is the pattern of tributaries and master streams in a drainage basin as delineated on a planimetric map. In theory, the network includes all the minor rills which are definite watercourses, even including all the ephemeral channels in the furthermost headwaters. In practice, the detail of the drainage network is dependent on the scale of the map used to trace the channels (Leopold et al. 1964, p. 131). When preparing a topographic map the headward limits of the blue lines do not reflect any statistical characteristic of streamflow occurrence, nor differences in the hydrologic response of the headwater due to the various combinations of climate, topography and geology. In actual fact, they are drawn to fit a rather personalized aesthetic (Leopold 1994, p. 228). However, in light of recent field studies on the channel head (e.g., Dietrich and Dunne 1993), of increasing availability of accurate digital elevation data due to the LiDAR (Light Detection And Ranging) technology (e.g., Tarolli and Tarboton, 2006; Carter et al. 2007; Cavalli et al. 2008; Vianello et al. 2009; Tarolli and Dalla Fontana 2009), and of recent advances in terrain analysis (e.g., Gallant and Wilson 2000; Moretti and Orlandini 2008; Orlandini and Moretti 2009), a rationale for the delineation of drainage networks can be sought.

A field definition of the channel head is provided by Dietrich and Dunne (1993) as the upstream boundary of concentrated water flow and sediment transport between definable banks. Although it is not easy to provide a globally useful criterion for a well-defined bank, it is commonly accepted that the bank is recognizable as a morphological feature independent of the flow. In this perspective, a detailed description of hydrologic flows may not be required in order to predict channel heads, and meaningful predictive models can be formulated by combining terrain analysis and generalizations from field facts. Field and theoretical studies addressing the problem of defining where channels begin have led to the definition of different threshold conditions for channel initiation. O'Callaghan and Mark (1984) and Tarboton et al. (1988) defined channel networks on a digital elevation model as those pixels that have an accumulated drainage area greater than some "threshold support area." Montgomery and Dietrich (1988) proposed to use a threshold on a power function of both drainage area and the local slope. Howard (1994) considered a threshold on the gradient divergence normalized by mean gradient. Peckham (1995) investigated a method based on Strahler's (1957) classification of drainage networks extracted from digital elevation data, and iterated pruning of exterior links.

In the present study, these criteria are evaluated by using accurate field observations of channel heads and channel network in the Rio Cordon catchment (Eastern Italian Alps, Fig. 1), gridded elevation data obtained from high-precision LiDAR surveys (Cavalli et al. 2008), and advanced methods for the delineation of drainage basins and surface flow paths from these data (Orlandini et al. 2003; Orlandini and Moretti 2009). The dependence of threshold conditions for the delineation of drainage networks on the size of grid cells involved is investigated.

2. Methods

Surface flow paths are determined by using the D8 and D8-LTD single flow direction algorithms (O'Callaghan and Mark 1984; Orlandini et al. 2003; Orlandini and Moretti 2009). In Orlandini and Moretti (2009) the D8-LTD method is found to provide a sounder description of surface flow paths than multiple flow direction algorithms. The D8-LTD method is therefore preferred in this study over other flow direction algorithms, and the capabilities of this method over the simpler and still commonly used D8 method are highlighted. The D8-LTD (eight flow directions, least transverse deviation) method performs a path-based analysis in which the deviations between steepest and possible flow directions are accumulated along the path and not just evaluated at the local scale as made by the D8 method. Transverse deviations are used to provide an accurate path-based analysis and this explains the name given to the method. A detailed description of the D8-LTD method can be found in Orlandini et al. (2003) and Orlandini and Moretti (2009).

Five criteria for the automated identification of channel heads from gridded elevation data are evaluated in this study. Each of these criteria defines a threshold condition for channel initiation and assumes that channels originate where threshold exceedences occur. Thresholds are given in terms of (1) drainage area A as proposed by O'Callaghan and Mark (1984) and Tarboton et al. (1988), (2) slope area function AS^k as proposed by Montgomery and Dietrich (1988), (3) gradient divergence normalized by mean gradient D as proposed by Howard (1994), (4) Strahler order SO of the drainage network extracted from gridded elevation data as proposed by Peckham (1995), and (5) Horton order HO of the drainage network extracted from gridded A elevation data (Horton 1945; Strahler 1957). It is specified that the drainage area A at a given cell is computed by accumulating local contributions along the upslope drainage system. The slope S at a given cell is evaluated along the flow direction towards its downslope neighbor, and it is conventionally assumed to be positive downward. The gradient divergence D is computed as the total curvature divided by mean gradient positive upward. Some details on the implementation of these criteria are provided here. A two-step procedure is used to determine the drainage network from criteria (4) and (5). In the first step, Strahler classification is applied to all the surface flow paths, including those generated at the source cells of the DTM. A surface flow path order (SFPO) is assigned to each link between a source and a junction or between junctions. In the second step, surface flow paths having order less than or equal to a given threshold (SFPO_t) are filtered. The remaining surface flow paths are assumed to provide predictions of the channels forming the drainage network. Channel orders (CO) in the obtained drainage network are computed as $\mathrm{CO} = \mathrm{SFPO} - \mathrm{SFPO}_t$.

3. Case Study

The Rio di Col Duro basin, a sub-basin of Rio Cordon, is located in the Dolomites, a mountain region in the Eastern Italian Alps (Fig. 1). The area of the Rio di Col Duro basin is about 0.5 km^2. The elevation ranges from 1935 to 2385 m above sea level (asl) with an average of 2199 m asl. The slope angle is 25° in average, and 74° at maximum. The area has a typical Alpine climate with a mean annual rainfall of about 1100 mm. Precipitation occurs mainly as snowfall from November to April. Runoff is dominated by snowmelt in May and June, but summer and early autumn floods represent an important contribution to the flow regime. During summer, storm events and long dry spells are common. During these events several shallow landslides are triggered on steep screes at the base of cliffs (Tarolli et al., 2008). Soil thickness varies between 0.2 and 0.5 m on topographic spurs to depths of up 1.5 m on topographic hollows. The vegetation covers the 97% of the area and consists in high altitude grassland (91%), and sporadic tall forest (6%). The remaining 3% of the area is unvegetated talus deposits. The geological settings of the basin are rather complex: sandstones and calcareous-marly rocks crop out; moraines, scree deposits and landslide accumulations are also widespread. Differently from many Alpine torrents, in which control works such as check dams and channel lining have extensively been built, no artificial structures are present in the headwaters of the Rio di Col Duro, where channels develop their morphology in response to loads of water and sediments imposed on them, reflecting ultimately the natural interaction between climate and geology. A picture of the study area showing the junction of Rio di Col Duro with Rio Cordon is provided in Fig. 2.

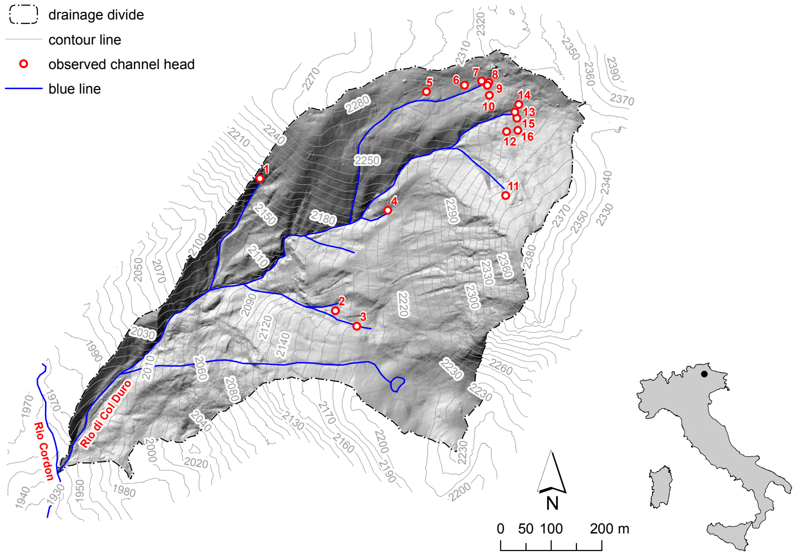

Figure 1. Topographic map of the Rio di Col Duro drainage basin showing observed channel heads, numbered progressively from left to right, and related blue lines. The location of the study area is also shown on the right hand side.

Several field surveys were conducted during the past few years including a LiDAR survey carried out during snow free conditions in October 2006. A recent campaign carried out in September–October 2008 has provided additional details on field-mapped channels and channel heads. Field surveys were carried out along the entire drainage network. The area was systematically walked along all drainage lines up to the catchment divide. Sixteen channel heads were mapped with an accuracy of a few centimetres using a differential global positioning system (DGPS). The channel head or first-order stream head was defined as the point at which non-confined divergent flows on the hillslope converge to a drainage line with a well-defined flow path, i.e., the upstream limit of concentrated flow (Dietrich and Dunne 1993). The width of surveyed channels at the bankfull stage was found to range from 1 to 5 m.

Figure 2. Picture of the study area showing the junction of Rio di Col Duro with Rio Cordon.

LiDAR data and high resolution aerial photographs were acquired from a helicopter using an airborne laser terrain mapper (ALTM) 3100 OPTECH, and Rollei H20 Digital camera flying at an average altitude of 1000 m above ground level (agl) during snow free conditions in October 2006. The flying speed was 80 knots, the scan angle 20° and the pulse rate 71 kHz. The survey design point density was approximately 7 points/m^2, recording up to 4 returns, including first and last. LiDAR point measurements were filtered into returns from vegetation and bare ground using the Terrascan™ software classification routines and algorithms. The vertical accuracy, evaluated by a direct comparison between LiDAR and ground DGPS elevation points, was estimated to be less than 0.2 m (RMSE), an acceptable value for LiDAR analyses in the field of geomorphology (Mckean and Roering 2004; Glenn et al. 2006; Frankel and Dolan 2007; Tarolli and Dalla Fontana 2009).

The LiDAR bare ground dataset was used to generate an accurate 1-m resolution digital terrain model (DTM). Among the techniques for interpolation proposed in the literature, the natural neighbour technique was selected. This technique was found to provide accurate gridded elevation data from regular, sparse, clustered or random combinations of distributions of points (Sibson 1981). In addition, such interpolator is expected to produce smaller smoothing effects than other methodologies such as spline or kriging. This is a desirable property since a rough morphology representation is able to detect small convergences/depressions that are critical for the recognition of morphological features such as channels. Natural neighbour uses the ratio between the Voronoi tassel of the point to be estimated and “borrowed” area from the other tassels from the existing points. The 1-m resolution DTM was resampled to 3, 5, 10, 20, and 30 m grid cell resolution by using the mean aggregation function in order to obtain coarser DTMs.

4. Cell Size Dependence of Threshold Conditions

Numerical experiments are carried out to investigate the dependence of threshold conditions for the delineation of the drainage network on the grid cell size of the DTMs involved. For each channel head surveyed in the field, the related values of critical variables for channel initiation such as the drainage area A_t, the slope area relation AS^k_t with k = 2, the gradient divergence normalized by mean gradient D_t, the Strahler order $\mathrm{SO_t}$, and the Horton order $\mathrm{HO_t}$ were determined by considering surface flow paths obtained from the application of the D8 and D8-LTD flow direction algorithms to DTMs of variable resolution. Mean and standard deviation of the critical variables computed over the 16 observed channel heads are shown in Fig. 3 in terms of data points and uncertainty bars, respectively, for all the considered grid cell sizes. Plots on the left hand side of Fig. 3 (a, c, e, g, and i) describe the results obtained from the D8 flow direction algorithm, while plots reported on the right hand side of Fig. 3 (b, d, f, h, and j) describe the results obtained from the D8-LTD algorithm. The method of weighted least squares described in Orlandini et al. (2006) is applied to determine predictive models of the variations of critical variables with grid cell size. Linear models are used to predict the variation of A_t, AS^k_t, and D_t with grid cell size h. Simple power function relationships are used to predict the variations of thresholds in terms of Strahler $\mathrm{SO_t}$ and Horton $\mathrm{HO_t}$ orders with h. The method of weighted least squares is applied to variable transformed logarithmically (base 10) in these cases. Predictive relationships are shown in Fig. 3 and reported in Table 1 along with the related coefficient of determination R^2.

The results shown in Fig. 3 reveal a progressive increase of values of critical A_t and AS^k_t as the grid cell size increases (plots a, b, c, and d). The linear models reported in Table 1 display satisfactory coefficients of determination R^2, especially when the D8-LTD algorithms is considered. The values of critical D_t at 1 m grid cell size displays a high uncertainty compared to the values obtained on coarser DTMs. This point does not significantly affect the predictive model obtained by weighted least square fitting and the resulting critical D_t is found to be practically constant. Under these circumstances the coefficient of determination R^2 does not provide high values as shown in Table 1. The plots related to the elaborations carried out with the critical $\mathrm{SO_t}$ and $\mathrm{HO_t}$ show a progressive decrease of thresholds order for channel initiation as the grid cell size increases. The $\mathrm{SO_t}$ is found to follow a power function relationship of grid cell size quite well, displaying a value R^2 equal to 1.00 when the D8 algorithm is applied, and equal to 0.99 when the D8-LTD algorithm is applied. This result appears noteworthy and suggests further investigations.

It is noted here that the results shown in Fig. 3 provide useful indications on the ability to identify threshold values that do not change significantly from one observed channel head to the others. These indications are provided by standard deviations used to compute uncertainty bars. In addition, these results illustrate the variations of threshold conditions as grid cell size varies. It is specified that the capability of a given criteria to identify a well defined threshold variable and the related variability with grid cell size does not necessarily ensure the ability of that criteria to predict accurately the drainage network. In fact, a well-identified criteria can provide predictions of channel heads in locations where these head does not occur and the predictive capabilities of criteria need to be evaluated separately. This evaluation is reported below.

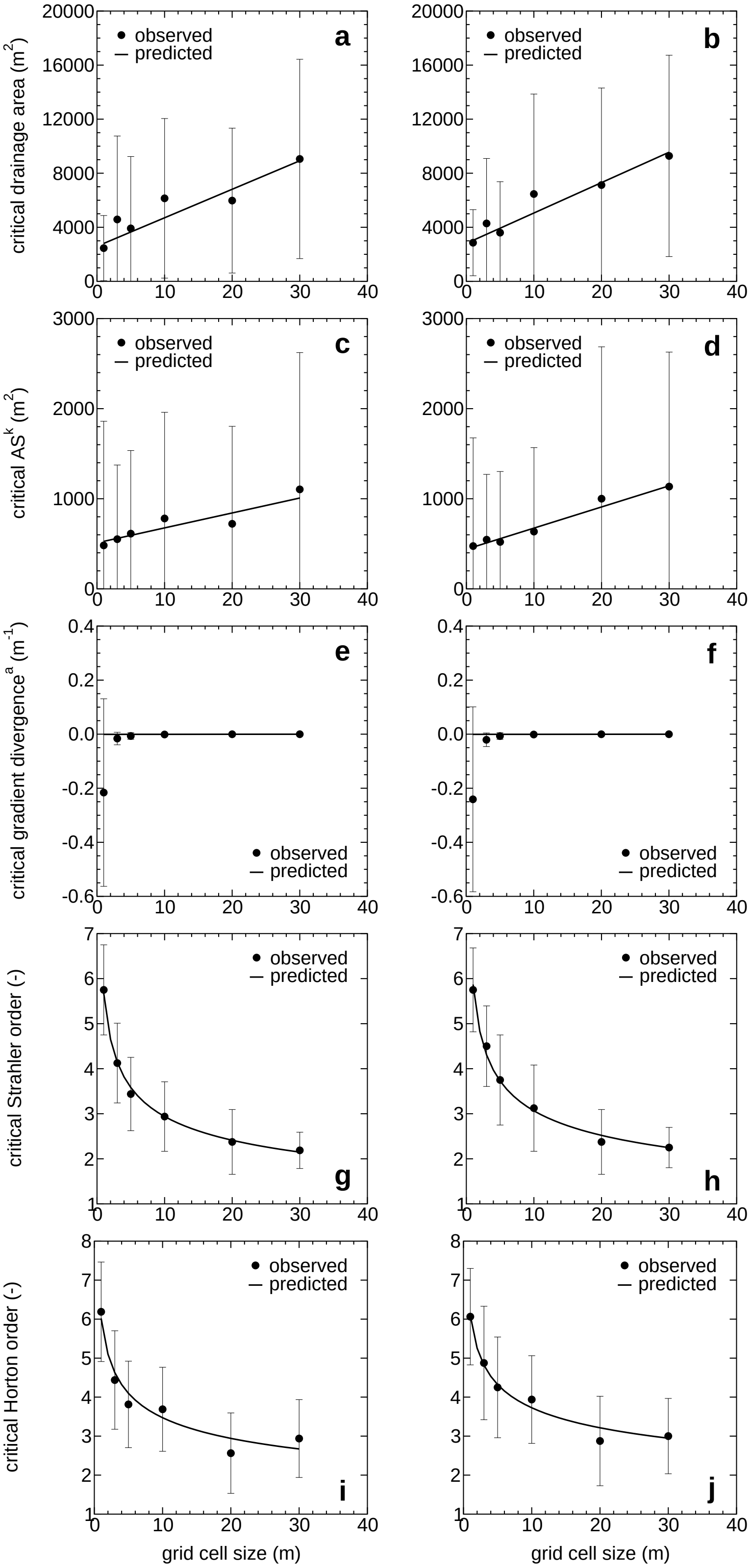

Figure 3. Observed and predicted values of critical variables for channel initiation as functions of grid cell size. Means (data points) and standard deviations (uncertainty bars) over the observed channel heads are provided for each grid cell size. Predictive relationships are obtained by weighted least squares fitting. Flow directions are determined by using the D8 (plots a, c, e, g, and i) and the D8-LTD (plots b, d, f, h, and j) flow direction algorithms.

5. Prediction of the Drainage Networks

The mean values of critical variables for channel initiation shown in the Fig. 3 have been used to extract the drainage networks from DTMs having variable resolution. In Fig. 4 the drainage networks determined using the various kind of critical variables and the D8 (maps on the left hand side) and D8-LTD (maps on the right hand side) flow direction algorithms are shown. The drainage networks extracted using the A_t (Fig. 4a and 4b) and SO_t (Fig. 4g and 4h) methods are found to reproduce satisfactorily the blue lines shown in Fig. 1. The best drainage network is obtained by considering the Strahler classification of the drainage network extracted directly from DTM data and pruning the exterior links with order less than or equal to $\mathrm{SO}_t = 4$ (Fig. 4h). One can note that the agreement between predicted and observed channels is significantly less satisfactory when the D8 flow direction algorithm is used instead of the D8-LTD flow direction algorithm. The drainage networks extracted using the D8 algorithm provide predictions of channels in places where channels are not observed in the field nor reported in terms blue lines (Fig. 1). This is likely to indicate a poor ability of the D8 flow direction algorithm to describe surface flow paths along headwaters (e.g., Orlandini et al. 2003; Orlandini and Moretti 2009).

Fig. 4i and 4j show the drainage networks predicted by using the HO_t method. In the Horton classification, a channel of any order extends headward to the place the most distant tip ends, near the basin divide. In the case of D8-LTD algorithm the main channel follows a different path (Fig. 4j, near channel head #11) respect to the main channel reported in other maps. Once again, this reflects a different pattern of surface flow paths identified by the D8-LTD method and by the D8 method.

The drainage net extracted with $AS^k{}_t$ (Fig. 4c and 4d) is well-identified along the steep valleys with all flow direction algorithms. This is not true when one looks at gently sloping areas where channel heads 5, 6, 7, 8, 9 and 10 are located. Here the channel is not recognized due to lower values of slope. It is noted that this approach strongly depends on the values of the local slope S, and in place where gentle slopes prevail seems not to be very reliable. The D_t method is found to provide a complex pattern of predicted channel heads that poorly reproduces the observed channel heads (Fig. 4e and 4f). These results suggests that this method predicts accurately the valleys but may not distinguish accurately the conditions in which channels occur.

Critical Variable for Channel Initiation	Flow Direction Method	Predictive Model as a Linear or Power Function of Grid Cell Size h (m)	R^2
Drainage area, A_t (m^2)	D8	$A_t = 2594.678 + 210.852\ h$	0.87
Drainage area, A_t (m^2)	D8-LTD	$A_t = 2806.613 + 224.895\ h$	0.92
$AS^k{}_t$ (m^2)	D8	$AS^k{}_t = 510.531 + 16.579\ h$	0.81
$AS^k{}_t$ (m^2)	D8-LTD	$AS^k{}_t = 439.712 + 23.461\ h$	0.96
Gradient divergence[a], D_t (m^{-1})	D8	$D_t = -0.001 + 0.000\ h$	0.30
Gradient divergence[a], D_t (m^{-1})	D8-LTD	$D_t = -0.001 + 0.000\ h$	0.21
Strahler order, SO_t	D8	$\mathrm{SO}_t = 5.669\ h^{-0285}$	1.00
Strahler order, SO_t	D8-LTD	$\mathrm{SO}_t = 5.869\ h^{-0282}$	0.99
Horton order, HO_t	D8	$\mathrm{HO}_t = 6.018\ h^{-0239}$	0.95
Horton order, HO_t	D8-LTD	$\mathrm{HO}_t = 6.095\ h^{-0214}$	0.98

[a] Gradient divergence normalized by mean gradient.

Table 1. Predictive models of the critical variables for channel initiation.

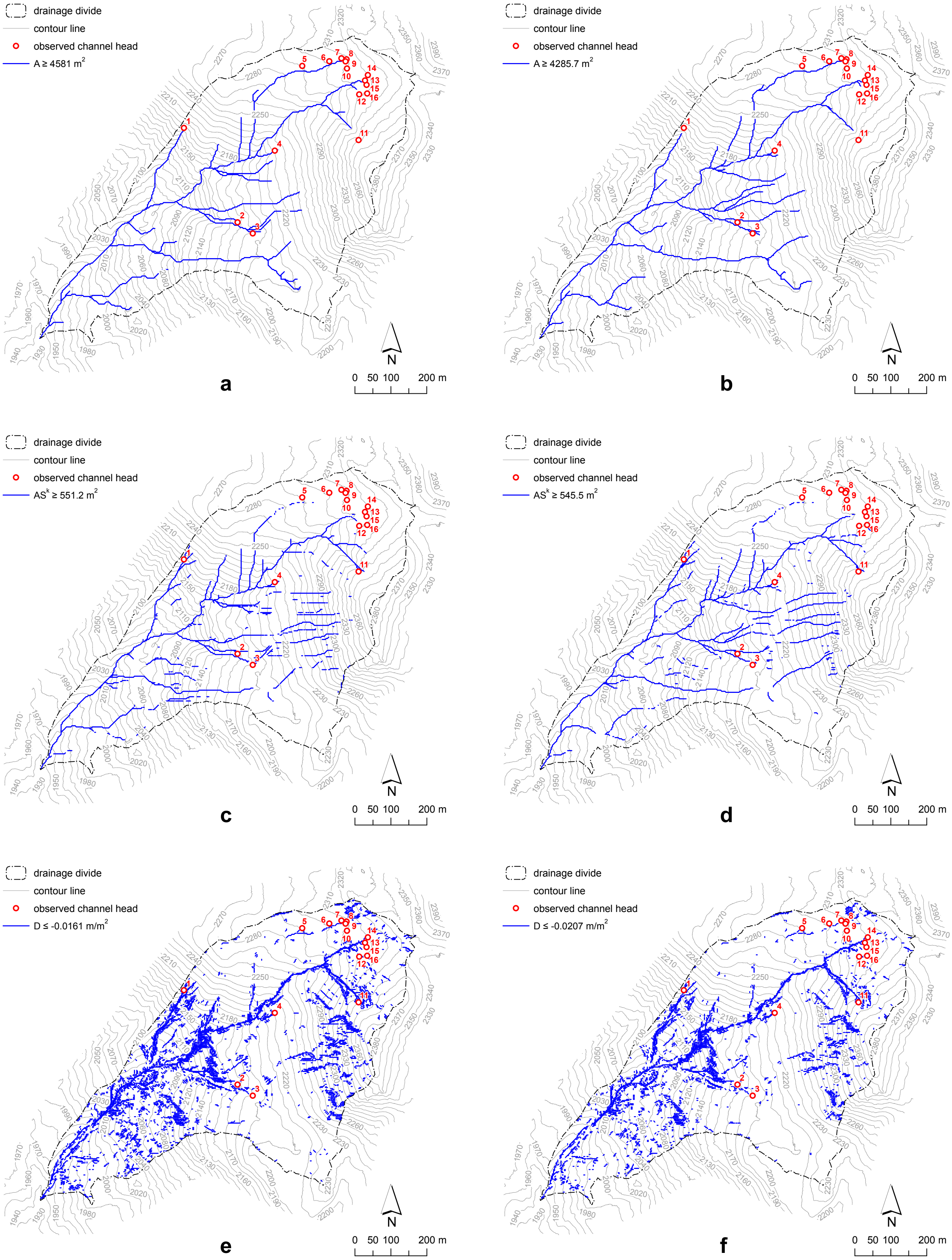

(continues)

Figure 4. Drainage networks obtained from 3-m resolution gridded elevation data by using the D8 and D8-LTD flow direction methods. The networks were extracted using the threshold for each critical variable for channel initiation (Fig. 3).

(continued)

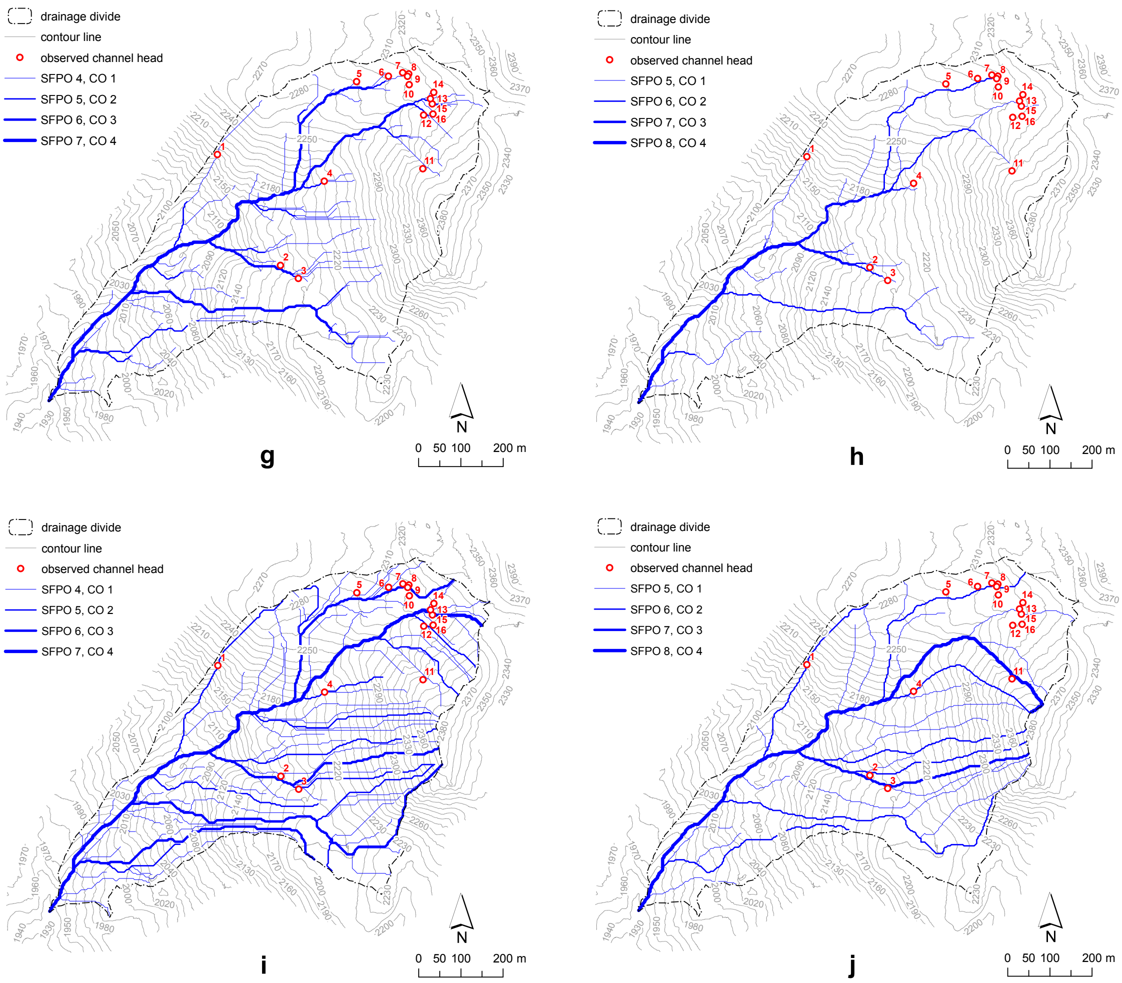

6. Summary and Conclusions

This paper presented an analysis of the dependence of threshold conditions for the delineation of drainage networks from DTM on grid cell size. Two methods for the identification of flow direction were considered: the D8 and the D8-LTD methods. Five critical variables were considered for channel initiation: A_t, AS^k, D_t, SO_t, and HO_t. The results indicated that: (i) the threshold criteria for the channel initiation are grid cell size dependent, (ii) the critical variables A_t and SO_t for channel initiation are found to provide robust predictions of drainage networks from gridded elevation data, (iii) the SO_t method is found to follow well a scaling relation of grid cell size, and it represents therefore a good option for scaling analysis (upscaling and downscaling) related to drainage network identification, (iv) in some cases the use of the D8-LTD flow direction algorithm in preference to the D8 flow direction algorithm is critical in order to adequately describe surface flow paths along headwaters and the related channel heads. Future work will be carried out to test other methodologies for drainage network extraction based on the pure and semi-automatic geomorphometric approaches (Lashermes et al., 2008; Tarolli and Dalla Fontana, 2009), in order to provide a comprehensive view on dependence of threshold conditions for the delineation of drainage networks from grid cell size.

References

Carter WE, Shrestha RL and Slatton KC, 2007, Geodetic laser scanning. *Physics Today*, 60(12): 41-47, doi:10.1063/1.2825070.

Cavalli M, Tarolli P, Marchi L and Dalla Fontana G, 2008, The effectiveness of airborne LiDAR data in the recognition of channel bed morphology. *Catena*, 73: 249-260.

Dietrich WE and Dunne T, 1993, The channel head. In: Beven K and Kirkby MJ (eds), *Channel Network Hydrology*. Wiley, New York, 175-219.

Frankel KL and Dolan JF, 2007, Characterizing arid region alluvial fan surface roughness with airborne laser swath mapping digital topographic data. *J. Geophys. Res.*, 112: F02025, doi:10.1029/2006JF000644.

Gallant JC and Wilson JP, 2000, Primary topographic attributes. In: Wilson JP and Gallant JC (eds), *Terrain Analysis: Principles and Applications*. Wiley, New York, 51-85.

Glenn NF, Streutker DR, Chadwick DJ, Tahckray GD, and Dorsch SJ, 2006, Analysis of LIDAR-derived topography information for characterizing and differentiating landslide morphology and activity. *Geomorphology*, 73: 131-148.

Horton RE, 1945, Erosional development of streams and their drainage basins: hydrophysical approach to quantitative morphology. *Bulletin of the Geological Society of America*, 56(3): 275-370.

Howard AD, 1994, A detachment-limited model of drainage basin evolution. *Water Resources Research*, 30(7): 2261-2285.

Lashermes B, Foufoula-Georgiou E and Dietrich WE, 2007, Channel network extraction from high resolution topography using wavelets. *Geophys. Res. Lett.*, 34: L23S04.

Leopold LB, 1994, *A View of the River*. Harvard University Press, Cambridge, MA, USA.

Leopold LB, Wolman MG and Miller JP, 1964, *Fluvial Processes in Geomorphology*. WH Freeman, San Francisco, CA, USA.

Mckean J and Roering J, 2004, Objective landslide detection and surface morphology mapping using high-resolution airborne laser altimetry. *Geomorphology*, 57: 331-351, doi:10.1016/S0169-555X(03)00164-8.

Montgomery DR and Dietrich WE, 1988, Where do channels begin? *Nature*, 336(6196): 232-234.

Moretti G and Orlandini S, 2008, Automatic delineation of drainage basins from contour elevation data using skeleton construction techniques. *Water Resources Research*, 44: W05403, doi: 10.1029/2007WR006309.

O’Callaghan J and Mark DM, 1984, The extraction of drainage networks from digital elevation data, *Computer Vision, Graphics, and Image Processing*, 28(3), 323-344.

Orlandini S and Moretti G, 2009, Determination of surface flow paths from gridded elevation data. *Water Resources Research*, 45, W03417, doi: 10.1029/2008WR007099.

Orlandini S, Boaretti C, Guidi V and Sfondrini G, 2006, Field determination of the spatial variation of resistance to flow along a steep Alpine stream, *Hydrol. Process.*, 20(18), 3897–3913, doi: 10.1002/hyp.6163.

Orlandini S, Moretti G, Franchini M, Aldighieri B and Testa B, 2003, Path-based methods for the determination of nondispersive drainage directions in grid-based digital elevation models. *Water Resources Research*, 39(6): 1144, doi: 10.1029/2002WR001639.

Peckham SD, 1995, Self-similarity in the three-dimensional geometry and dynamics of large river basins, PhD Thesis, University of Colorado, Boulder.

Sibson R, 1981, A brief description of natural neighbor interpolation. *Interpreting Multivariate Data*. V. Barnett (eds) John Wiley: Chichester; 21-36.

Strahler AN, 1957, Quantitative analysis of watershed geomorphology. *Transactions of the American Geophysical Union*, 38(6): 913-920.

Tarboton G, Bras RL and Rodriguez-Iturbe I, 1988, The fractal nature of river networks. *Water Resources Research*, 24(8): 1317-1322.

Tarolli P, Borga M and Dalla Fontana G, 2008, Analyzing the influence of upslope bedrock outcrops on shallow landsliding. *Geomorphology*, 93: 186-200, doi:10.1016/j.geomorph.2007.02.017.

Tarolli P and Dalla Fontana G, 2009, Hillslope-to-valley transition morphology: new opportunities from high resolution DTMs. *Geomorphology*, doi:10.1016/j.geomorph.2009.02.006.

Tarolli P and Tarboton DG, 2006, A new method for determination of most likely landslide initiation points and the evaluation of digital terrain model scale in terrain stability mapping. *Hydrol. Earth Syst. Sci.*, 10: 663-677.

Vianello A, Cavalli M and Tarolli P, 2009, LiDAR-derived slopes for headwater channel network analysis. *Catena*, 76, 97-106, doi:10.1016/j.catena.2008.09.012.

Robust Extraction of Thalwegs Networks from DTMs for Topological Characterisation: A Case Study on Badlands

N. Thommeret[1], J.S. Bailly[2], C. Puech[2]

[1]UMR 8591- CNRS, Laboratoire de Géographie Physique,
1 place Aristide Briand, 92195 Meudon Cedex
Telephone: +33145075583
Email: nathalie.thommeret@cnrs-bellevue.fr

[2]UMR TETIS – AgroParisTech-Cemagref-Cirad, Maison de la Télédétection,
500 rue JF Breton, 34093 Montpellier Cedex 5
Telephone: +33467548720
Email: bailly, puech@teledetection.fr

1. Introduction

To study the link between thalweg networks in badlands and hydrological functioning over eroded areas, digital indices describing the 3D network geometry and topology must be computed for different extents and resolutions. Thalwegs correspond to the line connecting the lowest points of the gully. In badlands, these networks are characterised by tree structure topologies. In case of large extents, grid DTM acquired by airborne or high resolution satellite sensors seem to be the most appropriate source of data for thalweg network extraction.

To extract and characterise thalweg networks from a grid DTM, various drainage algorithms (O'Callaghan and Mark 1984, Fairfield and Leymarie 1991, Lea 1992, Tarboton 1997) offer possibilities of computing drainage networks all over the grid surface. However, the transition from one drainage flow path to a vector thalweg network is not obvious (Martz and Garbrecht 1995, Tarboton 2001, Turcotte et al. 2001). Most of the time, the process uses a unique and arbitrary drainage surface threshold beyond which thalwegs, valleys or hydrographic networks are depicted. Since this criterion has no physical significance, where to start thalwegs upstream? How to get thalweg networks fitting to the amount of information really contained in a DTM? How to limit drainage algorithm artefacts in wide valleys disrupting the resulting network topology? In other words, how to compute robust thalweg network from a grid DTM?

This paper presents a method that combines existing drainage algorithm and a morphological index, first, to map gully floor pixels and then to define a continuous and tree-structured thalweg network. To run the method on a given DTM, only the spatial and statistical distribution of altimetrical error data is needed. This method aims to extract thalweg network objectively considering the significant landforms included in a DTM.

This method has been applied on two DTMs simulating virtual landscapes and on an LiDAR DTM acquired on the Draix badlands catchments (French Alps). Results are visually compared to those obtained with the usual drainage area threshold criteria. On the Draix test site, network topological index distributions are computed and compared together.

2. Method

The method runs in three steps. In a first step using a convergence index defined by Kiss (2004), discontinuous terrain cells with significant curvature, where flow converges, are derived from the DTM. We assume that these cells reflect gully floors. In a second step, these cells are connected using an accumulated flow algorithm (Lea 1992) weighted by the results of the first step. A connected and tree-structured scheme is obtained at the end of this second step. The third step is a vectorisation and cleaning step to obtain a refined vector thalwegs network (Fig.1).

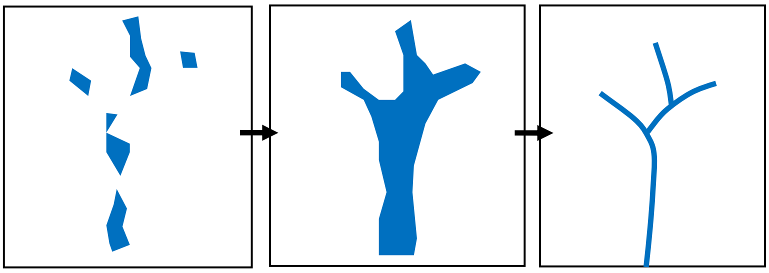

1. Flow convergent areas detected

2. Gully floors connected

3. Vector thalwegs network extracted

Figure 1. A three-step method.

2.1 Significant Flow Convergence Areas Detection

The convergence index (CI) is used to distinguish flow convergent areas from divergent ones in the DTM at initial spatial resolution. It is based on the aspect, which corresponds to the slope direction. Considering a 3*3 cells window (Fig. 2), for each external cell i, θ_i is the angle between the aspect of cell i and the direction to the centre i.e. the direction of the vector joining the centre of cell i and the centre of the 3*3 window. The convergence index is the average of the θ_i minus 90°. CI ranges from $-90°$ to $90°$.

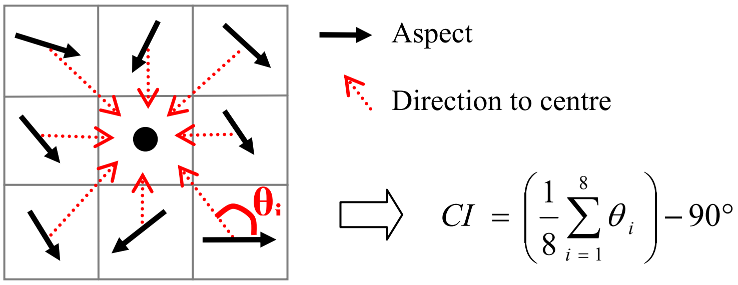

$$CI = \left(\frac{1}{8}\sum_{i=1}^{8}\theta_i\right) - 90°$$

Figure 2. Convergence Index calculation.

In the resulting grid, positive values represent divergent areas and negative values represent convergence areas. Null values relate to areas without curvature. To highlight the significant convergent cells, which should correspond to gully floors, a threshold is applied on these values. The DTM altimetrical error spatial distribution helps to objectively determine this threshold. The computation of CI from simulation of numerous tilted planes DTM, with a noise respecting the spatial altimetrical error distribution, provides a threshold beyond which CI values can be considered as significantly different from a plane landform. At the end of this step, disconnected convergence areas are identified and considered as gully floor features.

2.2 Tree-structured Gully Floors Connection

The cells obtained previously are connected to create a continuous area. The use of drainage algorithms appears to be a good way to reach this goal. Indeed, these algorithms are usually based on the idea of flow accumulation and thus generate continuous drainage areas. Also, the choice of a unidirectional flow ensures the tree structure (each cell has a unique output).

Among the many drainage algorithms, we choose the kinematic routing algorithm (Lea 1992). The flow is compared to a rolling ball moving in the direction of the steepest slope on a plane surface. Then the flow accumulation for a given cell is calculated as the number of flow paths passing through that cell multiplied by the grid cell area (Wilson et al. 2008). We propose to weight the accumulation computation by the thresholded convergence grid in order to keep only the gully floors identified as draining cell. As a result, we obtain a continuous and tree-structured area corresponding to the gully floors.

2.3 Thalweg Network Extraction and Topological Analysis

The last step aims at doing a topological analysis of the network extracted. The network is settled from raster gully floors. It must be a vector object, corresponding to directed tree vector network. It also has to be as refined as possible (without artefacts) through a cleaning-up step. We successively use a vectorisation process based on skeletonisation and a vector filtering process. Finally, we compute topological indices on the resulting directed tree thalweg network.

We use the most known topological indices, the Horton-Strahler order and ratios (Strahler 1957). To add a third dimensional analysis, two slope indices are computed: a simple slope index and a developed slope index. The use of such indices allows description and comparison of 3D planar thalweg network structures. Consequently, comparison between different methods of thalweg network extraction is possible.

3. Material

The method was applied to both virtual and actual terrain cases. Virtual terrain catchments models were built as tilted plane in which simple shapes are embedded. The actual terrain model is a one-meter resolution DTM of the Moulin catchment produced by an airborne LiDAR. The Moulin (8 ha) is one of Draix experimental catchments that are labelled “Draix Observatory for Research on the Environment (ORE), a field laboratory for mountains erosion studies”.

4. Results

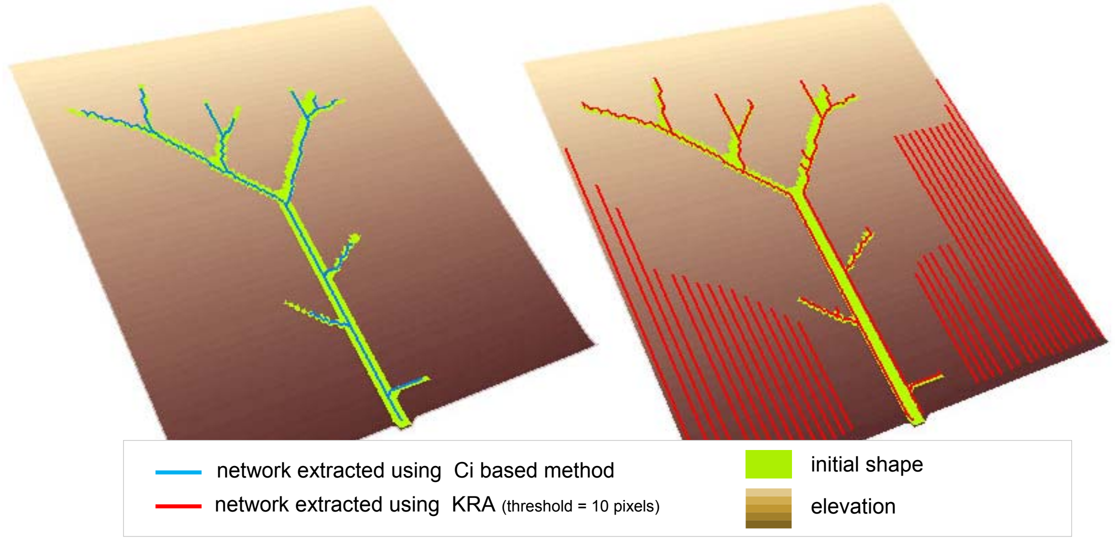

Figure 3. An example of networks extracted from a virtual catchment DTM: 1- the proposed method; 2- usual drainage area criteria.

The use of virtual catchment DTM permits representation and comparison of networks extracted using different methods while the initial shape of the valley is totally controlled (Fig. 3). Two major observations are made: 1) all existing drains are extracted and no more; 2) upstream limits appear to fit the valley heads (solving the problem of an arbitrary threshold).

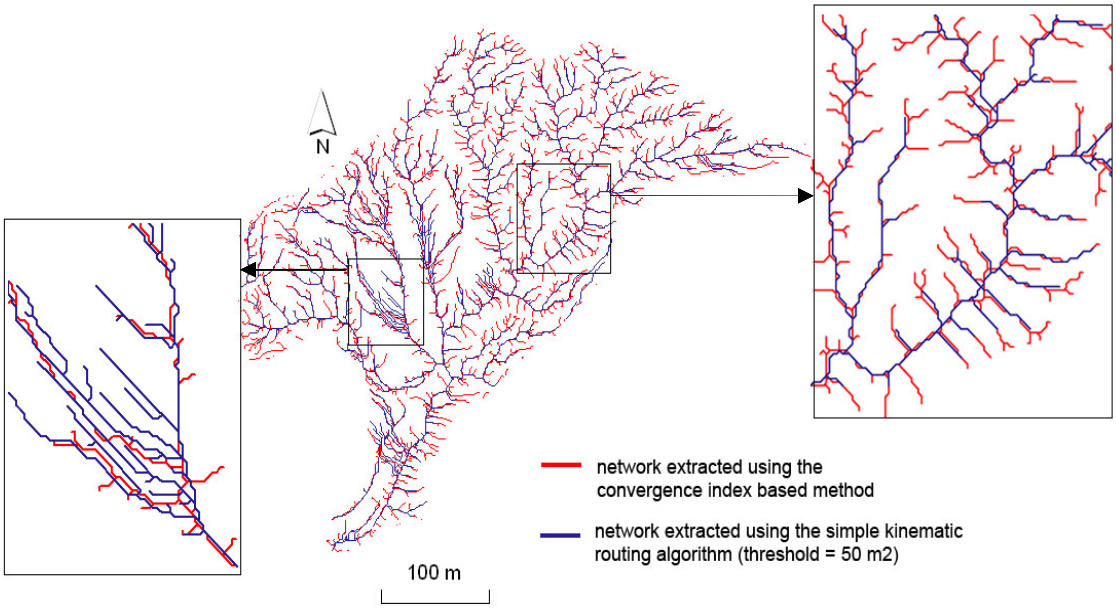

Figure 4. Comparison of networks extracted using the CI based method and the kinematic routing algorithm with an arbitrary drainage area threshold.

We also compare the networks extracted on the actual catchment using the proposed method (CI based) and an unique area threshold criterion on kinematic routing algorithm (KRA) drainage areas (Fig. 4). The use of a unique area threshold (here 50 m^2) has resulted in both the presence of numerous drains disrupting the network topology (left of Fig. 4) and the absence of drains that should be represented (right of Fig. 4). The result would be equivalent for any threshold value. This means that not all the information of the DTM is used unlike with the CI based method.

The network topology is described with Horton-Strahler stream orders and slope ratios. With classical methods of extraction, the number of drains, especially those of first orders, increases as the threshold area decreases (Table 1). The ratio between the first and second order underlines the perturbation and the instability of the extracted network. With the CI based methods, the number of first-order drains is drastically lower but the ones extracted correspond to the DTM information. So, the CI based method provides a stabilisation of the tree network topology.

Method	Number of drain for each order						Ratio N1 / N2
	N1	N2	N3	N4	N5	N6	
KRA T = 100 m^2	184	39	7	2	1		4.72
KRA T = 50 m^2	375	72	14	4	2	1	5.21
KRA T = 25 m^2	797	136	69	6	2	1	5.86
CI based before cleaning step	1432	246	44	9	2	1	5.82
CI based after cleaning step	912	246	44	9	2	1	3.71

Table 1. Networks comparison using digital indices.

5. Discussion and Conclusion

In this paper, we proposed a method aiming at extracting tree-structured gully floors and corresponding continuous thalweg networks. Whereas classical methods of extraction are based on an arbitrary threshold, the presented method extracts thalwegs only where the DTM expresses a landform. Thus, this method allows a more robust computation of topological indices of thalweg networks that can otherwise be highly disrupted in geometry and topology.

This method is data dependent and data-driven. Results are available for a given spatial resolution of DTM. Moreover, the main parameter used in the method is the spatial distribution of the altimetrical error of DTM data, giving an objective threshold for the delineation of significant flow convergence areas. This means that some initial work on DTM quality evaluation has to be handled first.

Regarding the use of convergence index to decide the more upstream part of thalwegs, other curvature morphological indices could have been used. For instance, it would be interesting to test the use of plan curvature. In other contexts and for other resolutions, convergence indices performed on local neighbourhood can limit and be unsuitable to show wide and rough valleys. In that case, a multi-resolution approach based on the same principles would be interesting to develop.

The proposed method is suitable for badlands areas or any other with bare soils. In other areas, like forested ones, results may be less effective but this would probably be due to the DTM quality rather than any method deficiency.

Acknowledgements

The authors would like to thank the Draix ORE and INSU that made this work possible.

References

Chorley RJ, 1971, *Introduction to fluvial processes*. Methuen & co, London.

Fairfield J., Leymarie P, 1991, Drainage network from grid digital elevation models, *Water Resources Research*, 27(5): 709-717.

Kiss R, 2004, Determination of drainage network in digital elevation model, utilities and limitations, *Journal of Hungarian Geomathematics*, 2:16-29.

Lea NJ, 1992, An aspect-driven kinematic algorithm. In: Parson AJ and Abrahams AD (eds), *Overland flow: hydraulics and erosion mechanics*, UCL Press, London, 393-407.

O'Callaghan J, Mark D, 1984, The extraction of drainage networks from digital elevation data, *Computer vision, graphics and image processing*, 28: 323-344.

Strahler AN, 1957, Quantitative analysis of watershed geomorphology, *American Geophysical Union*, 38: 913-920.

Tarboton, DG, Ames DP, 2001, Advances in the mapping of flow networks from digital elevation data. In: *World Water and Environmental Resources Congress*, Orlando, Florida.

Traboton DG, 1997, A new method for the determination of flow directions and contributing areas in grid digital elevation models, *Water Resources Research*, 33(2): 309-319.

Wilson JP, Aggett G, Deng Y, Lam CS, 2008, Water in the landscape: a review of contemporary flow routing algorithms. In: Zhou Q, Lees B, Tang G (eds), *Adances in digital terrain analysis*, LNG&C, Springer, 213-236.

Turcotte R, Fortin JP, Rousseau AN, Massicotte S, Villeneuve JP, 2001, Determination of the drainage structure of a watershed using a digital elevation model and a digital river and lake network, *Journal of Hydrology*, 240: 225-242.

Martz LW, Garbrecht J, 1995, Automated recognition of valley lines and drainage networks from grid digital elevation models: a review and a new method – Comment, *Journal of Hydrology*, 167: 393-396.

An Adaptive Approach for Channel Network Delineation from Digital Elevation Models

A. Afana[1], G. del Barrio[2]

[1]Desertification and Geo-Ecology Department, Arid Zones Research Station (CSIC),
C/ General Segura, 1, 04001, Almeria, Spain.
Tel. +34 950 281045
Fax. +34 950 277100
E-mail: ashraf@eeza.csic.es

[2]Desertification and Geo-Ecology, Arid Zones Research Station (CSIC),
C/ General Segura, 1, 04001, Almeria, Spain.
Tel. +34 950 281045
Fax. +34 950 277100
E-mail: gabriel@eeza.csic.es

1. Introduction

The quantitative description of land surface parameters is one of the essential tasks in hydrologic and geomorphologic studies, mainly river system structure and its related geomorphometric properties (Hancock 2005). Digital Elevation Models (DEMs) are generally used to delineate basin's limits and to extract its corresponding channel networks, using either automatic or semi-automatic approaches for such depiction. In many cases, methods for stream-limits delineation are broadly based on a constant threshold area that defines channel initiation in relation to upslope contributing area. However, the majority of these approaches fail to detect an appropriate threshold value, mainly when the basin is made up of heterogeneous sub-zones, as they only work lumped. In this work, a new approach is proposed to define an optimum threshold value (A_S) based on the intrinsic properties of the drainage network structure. Such technique provides various critical thresholds in relation to DEM-data resolution and to the heterogeneity of the dominant landform structures.

1.1 Manual and Automatic Approaches

The majority of the existing techniques assume A_S as a constant value, and evaluate its validity in a qualitative and quantitative form in judgment to the blue lines (*BLs*) generated from topographic maps (Band 1986). However the drawing of *BLs* on maps usually involve subjective decision by the topographer (Tarboton et al., 1991). On the other hand, DEM-use in stream network generation may incorporate local factors, and hence a priori information is needed, or alternatively DEM-data would be directly used without any reference to auxiliary data, and hence DEMs will be the solely available information under such approach.

Several algorithms have been proposed for automatic drainage network delineation, from which the slope-area relationship is the most underlined

$$S = cA^{-\theta} \tag{1}$$

where S is the local slope, A is the contributing area, c is a constant and θ is a scaling coefficient.

Researchers (e.g. Montgomery and Dietrich, 1989) underlined that Equation 1 reflects the transition from convex hillslopes to concave valleys, which is expressed by a characteristic change from a positive to negative trend. Tarboton et al., (1991, 1992) proposed to use the value of A at this breaking point as the critical contributing area (A_S). Throughout this work, results of an accepted slope-area relationship (*SAR*) model are directly compared with the results of the new approach in order to check the model performance of the latter.

1.2 Single versus Multiple Approach

In general, using a single A_S value over extended area of heterogeneous landforms is usually applied due to the lack of necessary information (Hutchinson and Dowling 1991). Theoretically, the use of a single A_S is applicable only under homogeneous-landscape conditions (Vogt et al., 2003), which is often limited to small-scale size catchments. It has been argued (Rodriguez-Iturbe and Rinaldo 1997) that a monofractal dimension (i.e. a unique A_S value) does not seem entirely consistent with the properties of measured field data. So, whatever approach used it should best describe existing landforms irrespectively of the terrain heterogeneity. Thus, an adequate solution, according to our judgment, could be achieved by using algorithms that best simulate landscape spatial heterogeneity, represent landscape dominant processes, and make use of available data.

Hence, the general aim of this work is to define the optimal channel network that best describe landscape dissection at a given resolution. Another associated objective is the generalized analysis of channel network complexity to other areas of complex heterogeneity under distinct scales and resolutions in order to obtain the best approach for channel networks description. In order to achieve these objectives, the proposed procedure is based on the analysis of intrinsic properties of channel network structure provided by the information extracted directly from DEM-data.

2. Methodology

The basic assumption is that DEMs are self-contained structures to detect drainage networks, and that channel complexity is best reflected by its corresponding intrinsic properties. Basically, the model combines exterior and interior link lengths ratio (R_A) (Schumm 1956) with length and bifurcation properties described in terms of structure regularity framework (Horton 1945) and topological random approach (Shreve 1966), in order to produce a varying ratio in relation to changeable threshold values.

$$R_A = \bar{l}_i / \bar{l}_e \tag{2}$$

where $\bar{l}_i$ is the average length of interior links and $\bar{l}_e$ is the average length of exterior links.

The structure regularity framework of Horton consists of bifurcation ratio (R_B) and length ratio (R_L), defined as

$$N_{\omega-1}/N_\omega \approx R_B \qquad \omega = 2, 3, \ldots, \Omega \tag{3}$$

$$\bar{L}_\omega/\bar{L}_{\omega-1} \approx R_L \qquad \omega = 2, 3, \ldots, \Omega \tag{4}$$

where N_ω is the number of streams of order ω, $\bar{L}_\omega$ is the arithmetic average of the length of streams of order ω and Ω is the total network order. Equations 3 and 4 have been expressed by Smart (1968, 1972) in a topological form by:

$$\bar{L}_\omega = \bar{l}_i \prod_{a=2}^{\omega} (N_{a-1} - 1)/(2N_a - 1) \qquad \omega = 2, 3, ..., \Omega \tag{5}$$

where N_a is the number of streams of order a, and Ω is the network order. Individual stream length ratios are given by:

$$\lambda_2 = \bar{L}_\omega / \bar{L}_1 = R_A (N_1 - 1)/(2N_2 - 1) \tag{6}$$

$$\lambda_3 = \bar{L}_\omega / \bar{L}_{\omega-1} = (N_{\omega-1} - 1)/(2N_\omega - 1) \qquad \omega = 3, 4, ..., \Omega \tag{7}$$

If we assume that channel networks are space-filling with a fractal dimension of 2 in the plane, where Hortonian's laws holds exactly at all scales in the network, we can accept the assumption of Smart, in the case of moderately large N_{ω}, that

$$\lambda_{\omega} \sim R_B / 2 \;\approx\; R_B = 2\lambda_{\omega} \tag{8}$$

Reorganizing equations 6 and 7 in 3 and 4, and substituting in 8 we can get a modified value of R_A given by:

$$R'_A = \left[2 * (\Delta + (\Lambda * R_A))\right] / \Gamma \tag{9}$$

where $\Delta = (N_1 - 1)/(2N_2 - 1)$, $\Lambda = \sum_{\omega=3}^{\Omega} (N_{\omega-1} - 1)/(2N_{\omega} - 1) = \lambda_3$, and $\Gamma = \sum_{\omega=2}^{\Omega} (N_{\omega-1} / N_{\omega})$

The resulted ratio of Equation 9 describes well natural channel networks since R'_A integrates structure-regularity and random topology model approaches, both are widely confirmed by observations in real landscapes (Jarvis, 1977). Accordingly, a changeable relationship is constructed between growing thresholds and its corresponding R'_A values, in which each R'_A is plotted against its related threshold and the optimum A_S is defined by the maximum rate of change (*MRC*) produced by the varying-tendency curve relationship (Fig. 1). The *MRC* bears a range of thresholds, from which the local minima (i.e. minimum rate of change) and local maxima (i.e. maximum change of rate) are detached. These locals are connected, in one way or another to catchment complexity. In this context, we believe that local minima represents the maximum complexity of the generated drainage network with the minimum possible feathering in a heterogeneous complex landscape, whereas the local maxima represents the minimum complexity with the minimum possible feathering in a homogeneous simple landscape. The resulting rate of change is steady in homogenous landforms, simulating experimental models for stream initiation (Schumm 1977), and unsteady in heterogeneous relief leading to variable rates of change depending on DEM capacity to convey the finest terrain forms at the working resolution (Fig. 2). Such oscillations are attributed to a varying change in R'_A value associated to the transformation of exterior links into interior ones as A_S increases. In order to verify landscape units of similar characteristic properties, a hierarchical classification procedure (*HCP*) has been integrated in the above approach, which allows for a simple reclassification of the generated sub-catchments of decreasing orders. Such classification provides as much as A_S values in relation to the classified sub-basins, which usually approximates to homogenous relief forms. Hereafter, the combination of R'_A and *HCP* procedures will be designated as the $R'_A t$ approach.

2.1 Validation Procedure

The validation procedure has been realized in the badlands of the Cautivo catchment following two approaches. The first one employs a 1 m DEM resolution and uses the *BLs* as a reference to compare with either models (*SAR* and R'_A) for validation. The comparison procedure is based on a collection of about 27 geomorphometrical indices that cover a vast range of river system properties. Redundancy and correlation are widely dominant between geomorphometric parameters, since various indices measure the same element but in different ways or contain common dimensions. Such problem was tackled through the combination of a multivariate statistical technique that verifies the degree of redundancy and structure detection between variables, and a regression measure in order to quantify the amount of correlation between parameters. Later on, a one-to-one comparison test was applied between the parameters derived from both automatic channel network detection approaches and those from the reference ones (i.e. *BLs*) using the *"Gower Metric (GM)"* measure of dissimilarity (Gower 1971). The second approach utilizes real topographic data obtained by a Laser Scanner device to detect the topographic landforms at 6 cm grid resolution for a small sub-catchment of about 13 m^2. A spatial dependence analysis was then made along stream and hillslope profiles (Fig. 3) to verify directional effect in the field sampled data, in which range values were determined in semivariograms to check for isotropy in the topographic structure. Moreover, a 3D-terrain reconstruction enabled a meticulous inspection of the finest stream limits in the constructed basin.

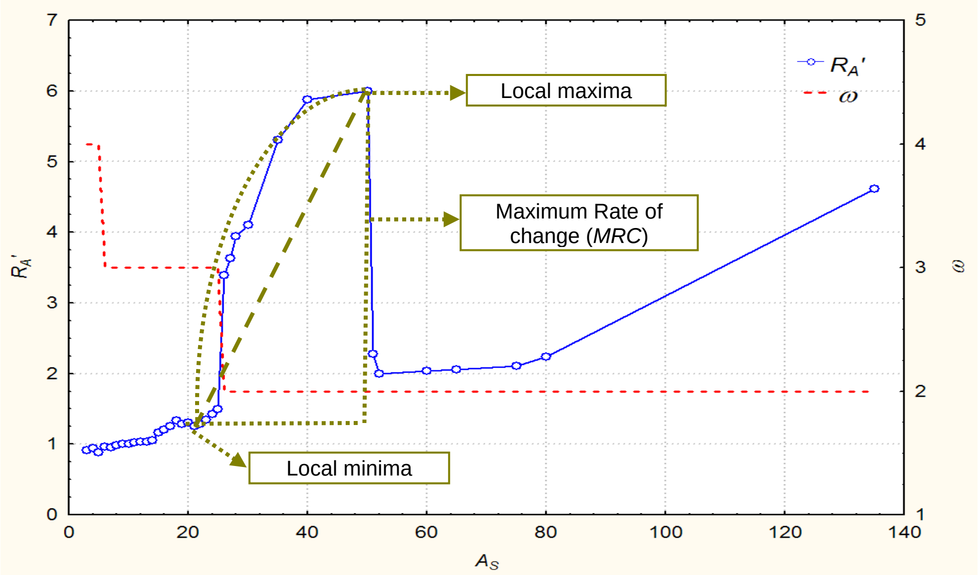

Figure 1. Curve relationship between R_A' and A_S for Tabernas Basin at 30m resolution.

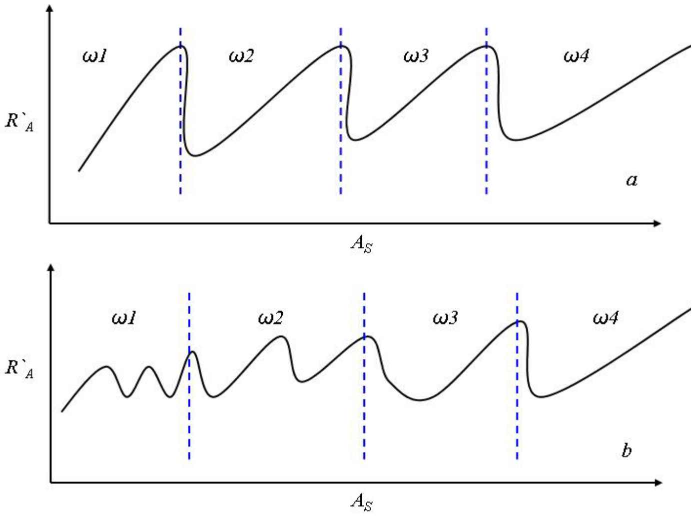

Figure 2. A conceptual framework for R_A' behaviour in, a) a hypothetical homogeneous landscape, and b) a hypothetical heterogeneous landscape

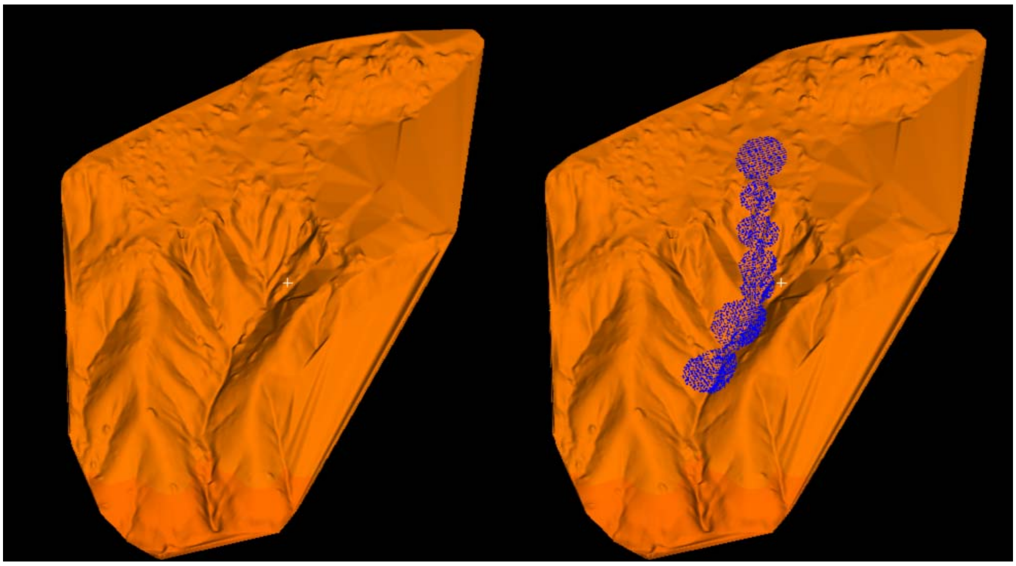

Figure 3. DEM of a small sub-catchment at 6 cm resolution built using data from a Laser-scanner device. Blue plots indicate the sampling network for the spatial analysis along a hillslope to stream profile

3. Results and Discussions

The visual comparison reveals a clear feathering for the *SAR* approach, mainly in the upper part of the catchment, and moderately reliable similarity between R'_At and *BLs* streams (Fig. 4). In the direct comparison using the geomorphometric indices, again the *GM* test confirms that stream network defined by the R'_At approach simulates better digitized *BLs* than the *SAR* does (Table 1). Finally, the spatial analysis of semi-variograms along the main stream profile shows anisotropic effect in the hillslope and isotropic variation on the stream profile (Fig. 5). Such tendency has been confirmed in all initiation areas of first order streams of the R'_At approach, whereas in the *SAR* approach limits of exterior streams were observed in hillslope sectors.

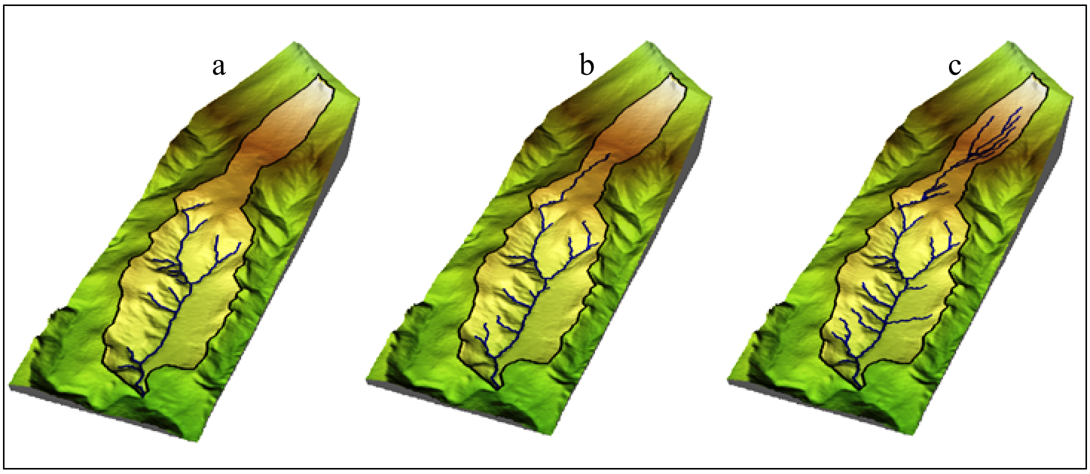

Figure 4. Channel network limits in the Cautivo Catchment at 1 m DEM resolution. a) Digitized *BLs*. b) Stream network with R'_At approach. c) Stream network with *SAR* approach.

Index	*BLs*	*SAR*	$R'_A t$	*GM*	
				BLs-SAR	*BLs-* $R'_A t$
Ω	3	3	3	0	0
La	235.4	377.9	312.9	0.41666	0.22661
Dd	0.0261	0.0568	0.0291	$8.9*10^{-05}$	$8.6*10^{-06}$
μ	13	35	13	0.06432	0
ε	1.847	1.8922	1.8707	0.00013	$6.9*10^{-05}$

Table 1. Gower Metrics dissimilarity index values for some geomorphometric parameters. *Ω*: order, La: longest stream, *Dd*: drainage density, *μ*: magnitude, *ε*: fractal dimension.

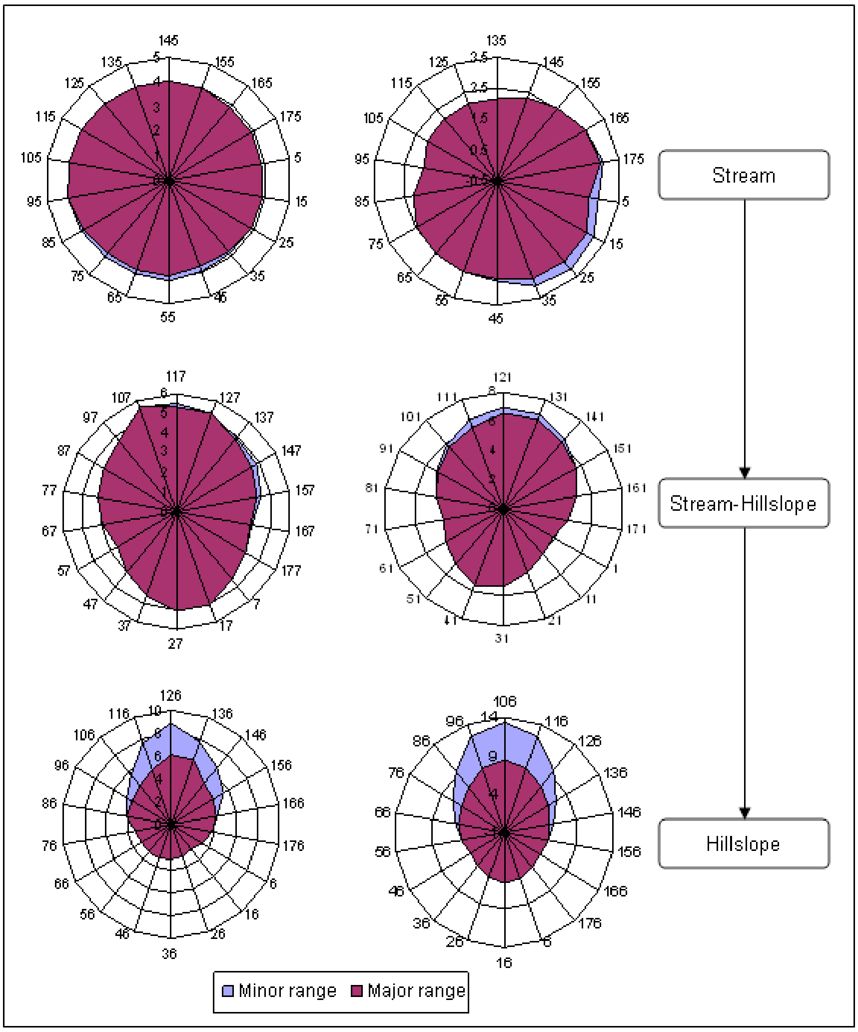

Figure 5. Change in range values of the generated semivarigrams from the red plots in Fig 3. Major ranges indicate hillslope formations whereas minor ones point out to a stream profile section.

3. Conclusions

Results underline the following conclusions: *i*) the $R'_{A}t$ approach has improved channel networks delineation over the *SAR* approach, since its function depends on intrinsic properties of the drainage network, being at the same time objective and easy to implement; *ii*) each geomorphometric index has variable dimensions, and their geomorphic and hydrologic importance are varied in relation to the parameters included in each index; *iii*) the spatial analysis is a useful tool for hillslope and stream-pattern detection; and, i*v*) morphometric properties vary considerably with A_S, and thus values reported without their associated A_S are meaningless and should be used in hydrological analysis with caution.

References

Band L, 1986, Topographic partition of watersheds with digital elevation models. *Water Resources Research*, 22(1):15-24.

Gower JC, 1971, A general coefficient of similarity and some of its properties. *Biometrics*, 27(4): 857-871.

Hancock GR, 2005, The use of DEMs in the identification and characterization of catchments over different grid scales. *Hydrological Processes*, 19(19):1727-1749.

Horton RE, 1945, Erosional development of streams and their drainage basins: hydrophysical approach to quantitative morphology. *Bull. Geol. Soc. Am.,* 56:275-370.

Hutchinson MF, and Dowling TI, 1991, A continental hydrological assessment of a new grid-based digital elevation model of Australia. *Hydrological Processes*, 5(1):45-58.

Jarvis RS, 1977, Drainage network analysis. *Progress In Physical Geography*, 1(2): 271-295.

Montgomery DR, and Dietrich WE, 1989, Source Areas, Drainage Density, and Channel Initiation. *Water Resources Research*, 25 (8): 1907-1918.

Rodriguez-Iturbe I, and Rinaldo A, 1997, Fractal river basins: chance and self-organization. Cambridge University Press, U.K.

Schumm SA, 1977, The Fluvial System: John Wiley, N.Y., 338 p.

Schumm SA, 1956, Evolution of drainage systems and slopes in badlands at Perth Amboy, New Jersey, *GSA Bulletin*, 67(5): 597-646

Shreve RL, 1966, Statistical law of stream numbers. *J. Geol.,* 74:17-37.

Smart JS, 1968, Statistical properties of stream lengths. *Water Resources Research*, 4 (5): 1001-1014.

Smart JS, 1972, Quantitative characterization of channel network structure. *Water Resources Research*, 8 (6): 1487-1496.

Tarboton DG, Bras RL, and Rodriguez-Iturbe I, 1991, On the extraction of channel networks from digital elevation data. *Hydrological Processes*, 5(1):81-100.

Tarboton DG, Bras RL, and Rodriguez-Iturbe I, 1992, A physical basis for drainage density. *Geomorphology*, 5(1/2): 59-76.

Vogt JV, Colombo R, and Bertolo F, 2003, Deriving drainage network and catchment boundaries: a new methodology combining DEM data and environmental characteristics. *Geomorphology*, 53(3/4):281-298.

Influence of Spurious Pit Removal Methods from SRTM on River Network Positioning

Laura Poggio[1], Pierre Soille[2]

[1] The Macaulay Institute Aberdeen AB158QH (UK)
email: l.poggio@macaulay.ac.uk

[2] Joint Research Centre, European Commission, Ispra (Italy)
email: pierre.soille@jrc.it

1. Introduction

Digital elevation models (DEMs) provide us with a digital representation of the continuous land surface. DEMs often contain depressions that result in areas described as having no drainage, referred to as sinks or pits. These depressions disrupt the drainage surface, which preclude routing of flow over the surface. Sinks arise when a connected component of pixels occurring at the same elevation level is surrounded by pixels of higher elevation, or when two cells flow into each other resulting in a flow loop, or the inability for flow to exit a cell and be routed through the grid. Hydrologic parameters derived from DEMs, such as flow accumulation, flow direction, upslope contributing area and river network detection require sinks to be removed (Maune, 2001). Naturally occurring sinks in elevation data with a grid cell size of $100m^2$ or larger are rare in terrains modelled by fluvial erosion processes. They could occur more frequently in glaciated or karst topographies. Various algorithms have been proposed to detect and remove surface depressions, such as elevation-smoothing method (Mark 1984), depression-filling algorithms (Jenson and Domingue, 1988; Soille and Ansoult, 1990; Tarboton et al., 1991), breaching (Martz and Garbrecht, 1998) carving method (Soille et al., 2003) or hybrid method combining carving and depression filling (Soille, 2004). For a detailed review it is possible to refer to e.g. Reuter et al. (2008) or Wang and Liu (2006). Lindsay and Creed (2005) compared the performance of different algorithms on various slope classes and landforms using a very high resolution dataset. However there is few information on the influence of the various algorithms on the accuracy of the positioning of the extracted networks. The aim of this study was to assess the effects of three pit removal methods on the position of river networks extracted from the SRTM dataset.

2. Test Area and DEM Processing

The area used for the test is situated in the Rhine basin with a size of approximately 120 km^2, with a variety of land uses and morphological characteristics (Fig. 1). It is a subcatchment of river Ruwer with very limited artificial channels, counting for less then 1% of the whole network.

The considered SRTM dataset (Jarvis et al., 2006) has an original resolution of 3 arc-seconds. The SRTM digital elevation data were originally produced by NASA. The dataset used was further processed from the original NASA DEMs to fill in no-data voids (Jarvis et al., 2006). The processing included: (i) the support for auxiliary information, (ii) the use of a void region specific processing over a tile based processing, and (iii) use

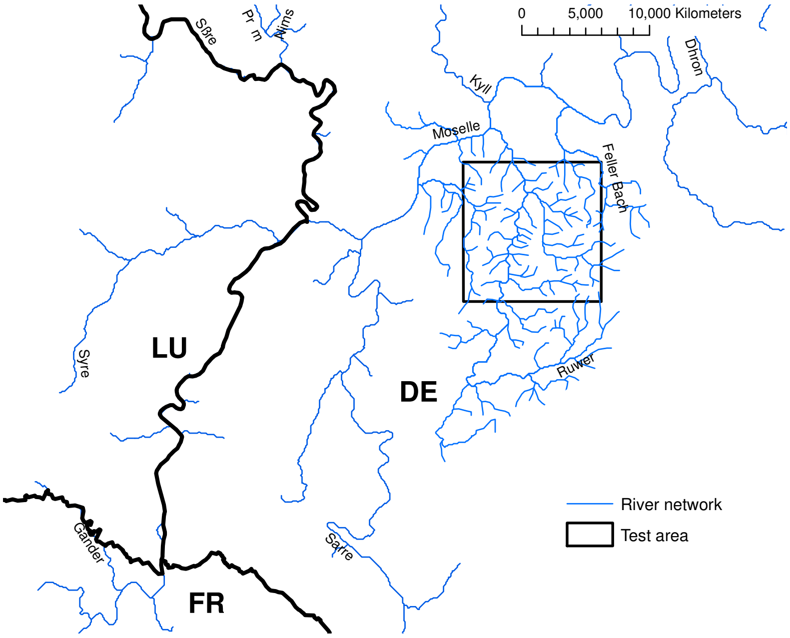

Figure 1: Test area. DE for Germany, FR for France and LU for Luxembourg

of SWDB V2 water body database. The dataset was mosaicked for the available scenes, and projected to the ETRS89-LAEA projection (Annoni et al., 2003). The methods used for pit filling and generating flowing surfaces were:

1. **Filling algorithm (F1)**. A sink is filled in an iterative two steps procedure: (i) to identify local minima, and (ii) to fill them from the bottom to the top by exploring the neighbourhood to find the pour points (Jenson and Domingue, 1988; Tarboton et al., 1991). Mathematical morphology offers a suitable framework for the development of efficient pit filling procedures even in the presence of composite pits and natural depressions (Soille and Ansoult, 1990).
2. **Carving (F2)**. The carving method (Soille et al., 2003) relies on a flooding simulation. The sinks are not filled, but the terrain is carved to make pits flowing further down, i.e. carving decreases the elevation of pixels occurring along a path starting from lower elevation pixels. All spurious minima of the input DEM are identified. If the terrain does not contain any significant natural depression all minima connected to the image border are used as outlets.
3. **Optimal hybrid (F3)**. The optimal approach combines morphological pit filling and carving (Soille, 2004) in order to reduce the sum of the differences in elevation between the original DEM and the elaborated one. In the combined approach sinks are filled up to a certain level and then carving proceeds from that level. The level is set to: i) minimise the sum of the heights differences between the input and the output depressionless DEM; or ii) minimise the number of modified pixels.

The number of pixels modified by each considered method is summarised in Table 1. Carving (F2) and optimal hybrid (F3) modified less pixels than the plain filling method. These results are reflected also in the sum of the elevation differences between the in-

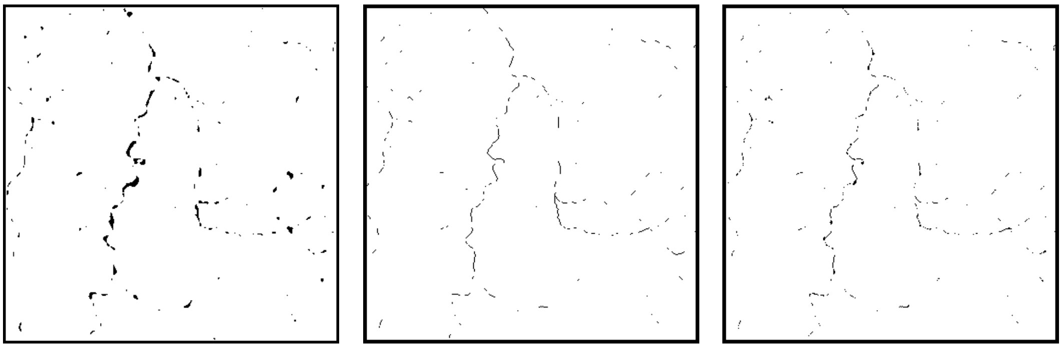

(a) F1 (b) F2 (c) F3

Figure 2: Spurious pit removal methods: mask of the modified pixels.

	Number pixels	% modified pixels	Sum of elevation differences (m)
F1	3303	2.52	712400
F2	2023	1.54	592809
F3	2025	1.54	564015

Table 1: Spurious pit removal methods: summary statistics.

put and the modified dataset when suppressing all pits, minimised by the optimal hybrid method (Soille, 2004). Most of the spurious pits were located at the bottom of the valleys, where the main sections of the rivers network are to be located (Fig. 2).

The river network used as reference was extracted from the German digital topographic maps (DTK5) for the Rheinland-Pfalz region, an independent dataset at very high resolution. The widest stream section is 20 metres large, below the pixel size of the SRTM dataset. Several buffer areas were created around the river network at distance multiple of 15m (Fig. 3).

The SRTM river networks were defined as all cells with a flow accumulation value higher then a certain threshold. Flow direction and flow accumulation values were calculated using the D8 (Fairfield and Leymarie, 1991).The spatial positioning of the extracted river networks was assessed by calculating the number of pixels of the networks falling in the different buffer areas normalised by the total number of pixels for each network.

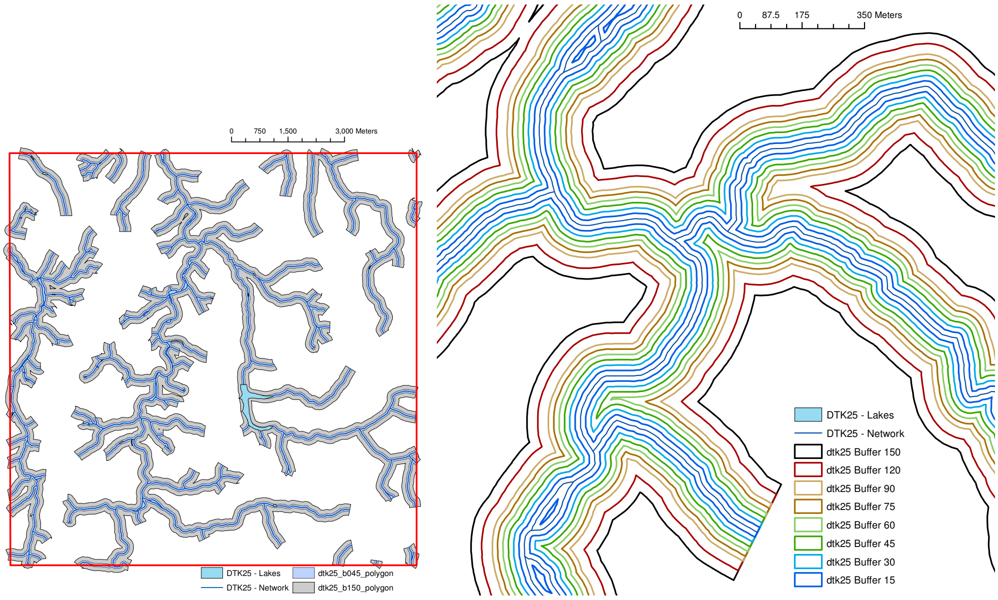

(a) Buffered reference river network (b) Zoom on buffered network

Figure 3: Buffering in the test area

3. Preliminary Results

The preliminary results for SRTM are presented in Fig. 4. Only less then 20% of the pixels of the extracted river networks are contained on the smallest buffer size. The values are then regularly growing up to a maximum of 75%. The river network extracted form the dataset filled with optimal carving (F3) is the closest to the ground truth network.

In Fig. 5 are presented some preliminary results for the Strahler order level obtained from networks extracted with D8 method. The curves have similar trends with F3 method reaching higher results. The figures underline the higher uncertainty in the position of network segments with lower Strahler order. Further analysis and computations are envisaged for breaking the results for slope classes and other land parameters, such as land use or morphological features. The comparison of different datasets in the same area would be carried out in order to highlight possible difference due to resolution, DEM preparation and error structure of the dataset.

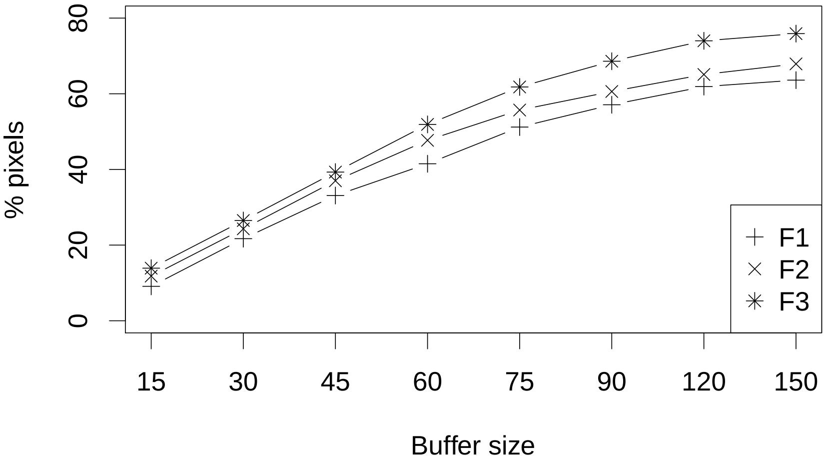

Figure 4: Filling algorithms and percent of pixels in the different buffer areas. The size of buffers are in meters for each side of the reference network.

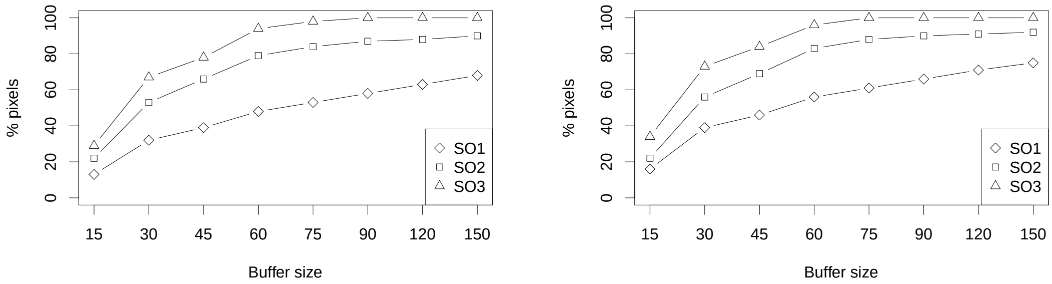

(a) F1

(b) F2

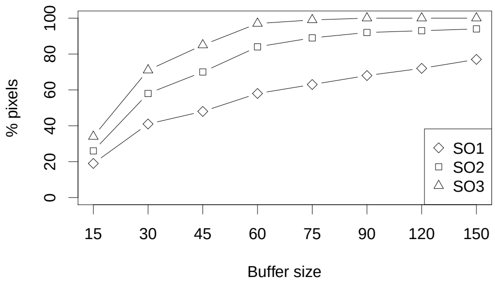

(c) F3

Figure 5: Filling algorithms and percent of pixels in the different buffer areas for Strahler orders.

References

Annoni A, Luzet C, Gubler E and Ihde J (eds) , 2003, *Map Projections for Europe*, Vol. EUR20120EN, European Commission, DG Joint Research Centre. http://www.ec-gis.org/sdi/publist/pdfs/annoni-etal2003eur.pdf

Fairfield J and Leymarie P, 1991, Drainage networks from grid digital elevations models. *Water Resources Research*, 27(5): 709–717.

Jarvis A, Reuter H, Nelson A and Guevara E, 2006, *Hole-filled seamless SRTM data V3*, Technical report, International Centre for Tropical Agriculture (CIAT).

Jenson SK and Domingue JO, 1988, Extracting topographic structure from digital elevation data for Geographic Information System analysis. *Photogrammetric Engineering and Remote Sensing*, 54(11): 1593–1600.

Lindsay J and Creed I, 2005, Removal of artifact depressions from digital elevation models: towards a minimum impact approach. *Hydrological Processes*, 19: 3113–3126.

Martz L and Garbrecht J, 1998, The treatment of flat areas and depressions in automated drainage analysis of raster digital elevation models. *Hydrological Processes*, 12: 843–855.

Maune D (ed.), 2001, *Digital Elevation Model Technologies and Applications: The DEM Users Manual*. American Society for Photogrammetry and Remote Sensing.

Reuter H, Hengl T, Gessler P and Soille P, 2008, Preparation of DEMs for geomorphometric analysis. In: Hengl T and Reuter H (eds), *Geomorphometry: Concepts, Software, and Applications*, Vol. 33 of Developments in Soil Science, Elsevier, chapter 4, 87–120.

Soille P, 2004, Optimal removal of spurious pits in grid digital elevation models. *Water Resources Research*, 40(12): W12509.

Soille P and Ansoult M, 1990, Automated basin delineation from digital elevation models using mathematical morphology. *Signal Processing*, 20: 171–182.

Soille P, Vogt J and Colombo R, 2003, Carving and adaptative drainage enforcement of grid digital elevation models. *Water Resources Research*, 39(12): 1366.

Tarboton DG, Bras RL and Rodriguez-Iturbe I, 1991, On the extraction of channel networks from digital elevation data. *Hydrological Processes*, 5: 81–100.

Wang L and Liu H, 2006, An efficient method for identifying and filling surface depressions in digital elevation models for hydrologic analysis and modelling. *International Journal of Geographical Information Science*, 20(2): 193–213.

Fast Stream Extraction from Large, Radar-Based Elevation Models with Variable Level of Detail

M. Metz[1], H. Mitasova[2], R.S. Harmon[3]

[1]Research Group Cognitive Ethology , German Primate Center
Kellnerweg 4, 37077 Goettingen, Germany
Telephone: +49-(0)921-2614299
Email:markus_metz@gmx.de

[1]Department of Marine, Earth and Atmospheric Sciences, North Carolina State University
Campus Box 8208, Raleigh, North Carolina 27695, USA
Telephone:001- 919-513-1327
Fax:001-919-515-7802
Email:hmitaso@unity.ncsu.edu

[3]Environmental Sciences Division, Army Research Office, U.S. Army Research Laboratory,
4300 South Miami Boulevard, Durham, North Carolina, 27703-9142, USA
Telephone:001-919-549-4326
Email:russell.harmon@us.army.mil

1. Introduction

Interferometric Synthetic Aperture Radar for Elevation (IFSARE) and Shuttle Radar Topographic Mission (SRTM) surveys provide a new generation of digital surface models (DSM) in regions that have had only limited elevation data coverage. These new topographic data sets are increasingly used to improve mapping of geomorphic and hydrologic features in remote, hard to reach areas and at regional to global scales (e.g. Kinner et al. 2005, Lehner and Döll 2004, World Wildlife Fund 2009). Extraction of hydrologic features from radar-based elevation data poses several challenges: (a) elevation surfaces include tree canopy that often requires depression filling of large areas (Figures 1, 2); (b) depending on the size of the study region and resolution, data sets can be massive and require extensive processing time. Significant effort has been devoted to development of new flow tracing and watershed analysis algorithms that support efficient processing of large DSMs and address the issue of depression filling (e.g., Arge et al. 2003; Danner et al. 2007).

We present a new implementation of method for flow routing, flow accumulation, and watershed analysis based on a least-cost path search algorithm (A* Search, Hart et al. 1968; module *r.watershed* in GRASS GIS, Ehlschlaeger 1989). This implementation dramatically improves computational efficiency while preserving its high accuracy routing capabilities through nested depressions, even for a challenging triple-canopy tropical rainforest environment with tree heights of more than 30m above the land surface. The new implementation that includes both single (SFD) and multiple flow direction (MFD) routing is compared with previously developed methods in terms of performance and accuracy. The impact of mapping technology (IFSARE, SRTM) and resolution on the extracted stream networks is also analyzed.

2. Methods

2.1 Fast Least Cost Flow Routing with SFD and MFD Support

Traditional flow routing algorithms that rely on depression filling are not suitable for data that include large numbers of nested pits due to natural topography, vegetation cover (Figure 2), or man-made structures like bridges. Alternative approaches that rely on digital elevation model (DEM) carving or combined depression-filling and carving were not designed for DSMs and may require significant modifications in elevation surface in regions with variable canopy height. Therefore, this work focuses on an algorithm that does not require depression filling or DEM carving and uses the *A** least-cost search method (Ehlschlaeger 1989).

The original implementation of the *A* Search* algorithm was optimized for large datasets by both increasing the processing speed and decreasing memory consumption. The core *A* Search* algorithm was not changed. Intermediate results of the *A* Search* process are now stored in a heap data structure (Atkinson et al. 1986) instead of a linked list. The speed gain in the time required to process a given grid is not fixed but increases with the number of grid cells to be processed and thus becomes more prominent for larger datasets.

Additionally, a multiple flow direction (MFD) algorithm has been implemented in *r.watershed* that makes use of the path determined by the *A* Search* and is based on Holmgren (1994), with an option to control the strength of flow convergence. Multiple flow direction provides more realistic results for flow accumulation in terrain with low slope and when using higher resolution (<= 10m) DEMs as input. Improvement in computational performance was evaluated by comparing the efficiency and accuracy with the old version of *r.watershed,* the GRASS module *r.terraflow* (Arge et al. 2003) designed for massive data sets, and flow routing modules from SAGA and TAS, with focus on treatment of depressions.

2.2 Data

The improved flow routing and watershed analysis algorithm was evaluated by performing stream extraction for the entire country of Panama using a combination of IFSARE and SRTM data.

Countrywide elevation coverage of Panama was available as 90m resolution SRTM DSM. We selected SRTM version 2 for our study as the most reliable in terms of accuracy and minimal artifacts, after evaluating properties of the currently available SRTM products (v1, v2, v3, v4.1). SRTM v2 tiles covering all of Panama were combined and gaps in the dataset filled using the regularized spline with tension (RST) interpolation method (GRASS module *r.fillnulls*; Mitasova and Mitas 1993). The seamless SRTM coverage was then reprojected from geographic to UTM zone 17N coordinate system with 90m resolution to keep resampling modifications to a minimum. For testing purposes, the DSM was then reinterpolated to 30m resolution using the RST method. A recent IFSARE survey has provided new, more detailed information about the topography in central Panama. The original IFSARE data were collected at 2.5m resolution and processed by standard procedures into 10m resolution DSM (Kinner et al. 2005). Stream extraction was performed on each of the DSMs separately at their original resolutions and then on a seamless 30m resolution DSM. Two levels of detail were created by merging the IFSARE and SRTM DSMs and re-interpolating to 30m resolution using RST, to ensure adequate routing for rivers flowing along the borders of the two DSMs (Figure 3).

Streams digitized from LANDSAT imagery (Earthsat dataset GLS2000, year 2000 with improved orthorectification, provided by the United States Geological Survey (USGS)) and field measurements were used for accuracy assessment. Georeferenced stream data were collected in the field during the years 2002-07 at sites in the Chagres river watershed (Figure 1) and during 2005-09 at lower reaches of most major rivers across Panama.

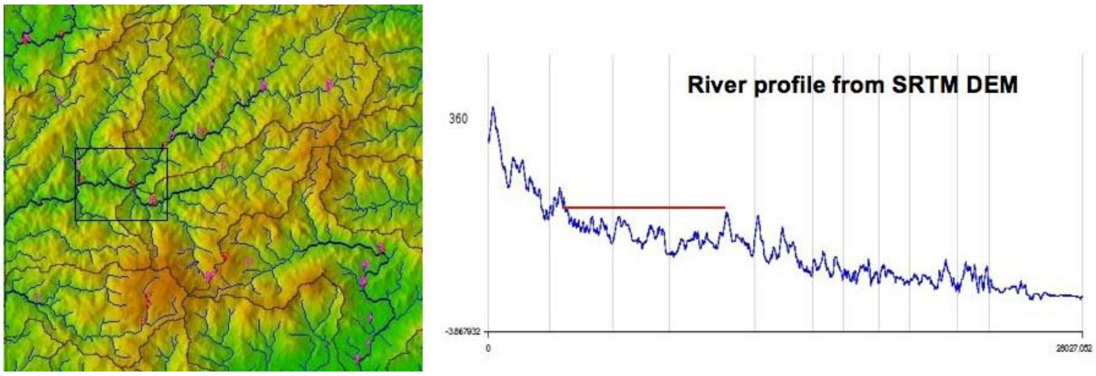

Figure 1. Left: Shaded SRTM relief with extracted streams (blue) and measured points (magenta). Right: Sample river profile, with local peaks and nested depressions.

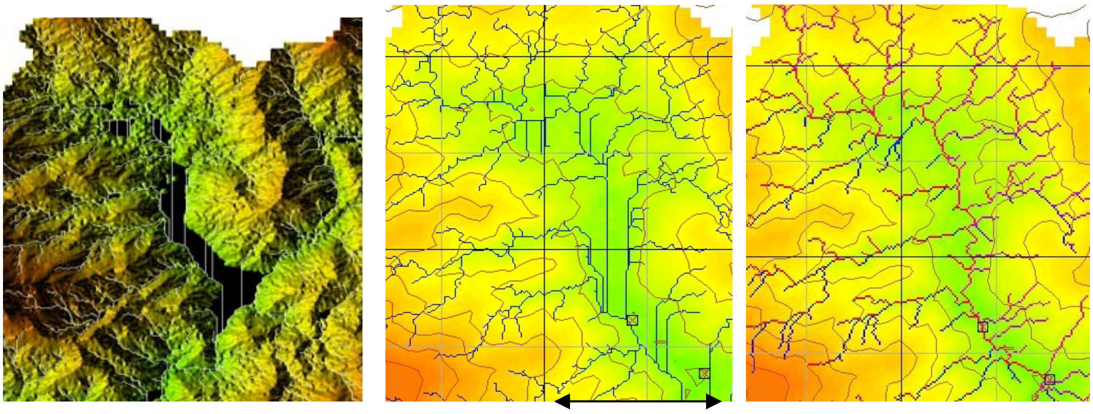

a b 1km c

Figure 2. Impact of depression filling on stream extraction from IFSARE-based DSM in tropical forest environment: (a) extent of depression filling (black area), (b) artificial stream geometry extends over 1.5 km, (c) improved result - least cost path algorithm.

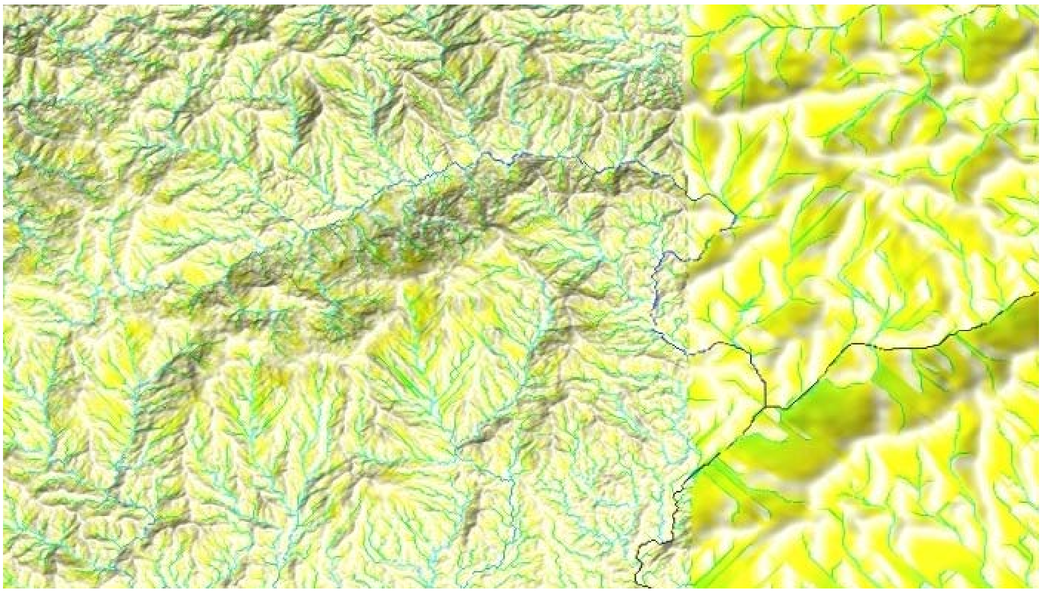

Figure 2. Seamless extraction of flow accumulation at 30m resolution with two levels of detail from merged IFSARE and SRTM DSMs.

2.3 Evaluation of Performance and Accuracy

Assessment of stream extraction accuracy was performed by computing distances between the extracted stream segments and (a) on-ground GPS measurements, (b) points digitized on rivers that could be clearly identified on LANDSAT imagery. The extracted streams were vectorized using the threshold of a minimum upstream catchment area of 100,000 square meters. General statistics of the measured distances was used to assess the accuracy of a particular method, dataset and spatial resolution. Deviations of derived streams from rivers visible on LANDSAT could be the result of either errors in the DSM or failure of the algorithm in difficult terrain, e.g. low topography or flow blocked by dams or bridges.

3. Results

Stream and watershed boundaries extraction was done individually at the original resolutions of 10m for IFSARE (156 million cells) and 90m for SRTM (27 million cells) and on the seamless 30m DSM (241 million cells) for the entire country of Panama.

To illustrate the improvement in computational performance of the new implementation of the *A* Search* method, a comparison was made between the processing time needed by the new and old version of *r.watershed* for flow accumulation computation at 90m resolution for all of Panama and for the central Panama subregion (IFSARE spatial extent). The new version was 350 times faster than the old version for central Panama represented by a relatively small DSM with 2 million grid cells at 90m resolution. The improvement was even more dramatic for the countrywide application with 27 million grid cells: the new version was 1940 times faster. The resulting flow accumulation raster maps from the old and the new version are identical for SFD; MFD is supported in the new version only.

For large regions represented by DSMs that fit into memory, the processing time of the new *r.watershed* in ram mode (all in memory) is shorter than that of *r.terraflow*. If data do not fit into memory, *r.watershed* uses segmented processing with intermediate data stored on disk, leading to longer processing time than for *r.terraflow* which uses I/O efficient algorithm specially designed for this case (Arge et al. 2003). The size of intermediate data created by *r.watershed* is about 16% of the size of intermediate data created by *r.terraflow*. Apparently, the segmented mode of r.*watershed* needs further optimization.

Accuracy assessment based on ground control points was done for 10m IFSARE, 30m IFSARE, 30m SRTM, and 90m SRTM, processed with *r.watershed* once in SFD and once in MFD mode, and processed with *r.terraflow* in MFD mode only. The 10m IFSARE DEM processed with the *A* Search* method and MFD provided the most accurate results and ground control points were closest to extracted streams.

Accuracy assessment based on rivers digitized from LANDSAT imagery revealed the known problems of the depression-filling method. Multiple flow direction produced more accurate results in areas with low topography. These areas are often also areas where depression-filling would be necessary, and where the combination of *A* Search* and MFD delivered the best results. Figure 4 shows LANDSAT GLS2000 imagery as backdrop and streams extracted once with *A* Search* and MFD and once with depression-filling and MFD. Additional comparisons will be performed using methods in SAGA and TAS.

4. Conclusion

We have presented a method for fast hydrological analysis specially designed for DSMs with large, nested depressions and evaluated it against other commonly used methods. We also provided insight into accuracy of stream extraction from widely available SRTM data using IFSARE data, ground control points and LANDSAT satellite imagery in a triple canopy tropical forest environment and coastal plain setting.

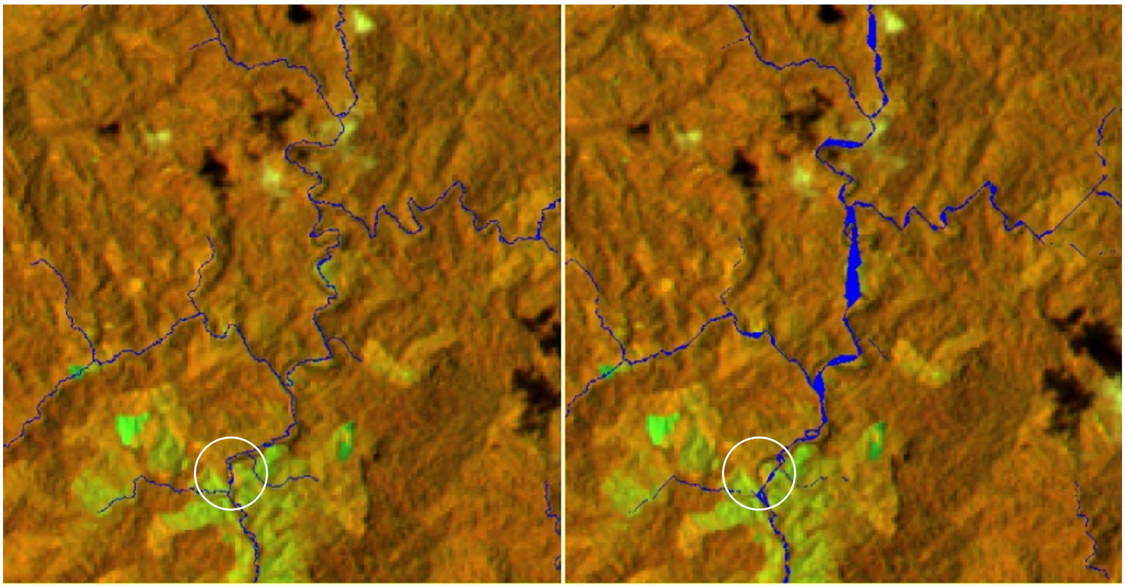

Figure 4. LANDSAT with bands 453 as RGB overlaid with A: River streams extracted with A * *Search* and MFD, and B: River streams extracted with depression-filling and MFD. Dense green vegetation appears dark orange, water bodies and cloud shadows appear dark, extracted streams are blue.

Acknowledgements

U.S. Army Research Office support for this research is gratefully acknowledged.

References

Arge L, Chase JS, Halpin PN, Toma L, Vitter JS, Urban D and Wickremesinghe R, 2003, Flow computation on massive grid terrains. *GeoInformatica* 7(4):283-313.

Atkinson MD, Sack J-R, Santoro N and Strothotte T, 1986, Min-max heaps and generalized priority queues. *Programming techniques and Data structures, Comm. ACM*, 29(10): 996-1000.

Danner A, Yi K, Moelhave T, Agarwal PK, Arge L and Mitasova H, 2007, TerraStream: From Elevation Data to Watershed Hierarchies, *Proc. ACM GIS 2007*

Ehlschlaeger C, 1989, Using the A* Search Algorithm to Develop Hydrologic Models from Digital Elevation Data. *Proceedings of International Geographic Information Systems (IGIS) Symposium*, Baltimore, MD, USA, 275-281.

Hart P E, Nilsson N J, Raphael B, 1968, A Formal Basis for the Heuristic Determination of Minimum Cost Paths, *IEEE Transactions on Systems Science and Cybernetics* 4 (2):100-107.

Hofierka J, Mitasova H, Neteler M, 2008, Geomorphometry in GRASS GIS. In: Hengl T and Reuter HI (eds), *Geomorphometry: Concepts, Software, Applications. Developments in Soil Science*, Elsevier, 33:387-410.

Holmgren P, 1994, Multiple flow direction algorithms for runoff modeling in grid based elevation models: An empirical evaluation. *Hydrological Processes,* 8(4):327-334.

Kinner D, Mitasova H, Harmon R, Toma L, Stallard R, 2005, GIS-based Stream Network Analysis for The Chagres River Basin, Republic of Panama. In: Harmon R (ed) *The Rio Chagres: A Multidisciplinary Profile of a Tropical Watershed*, Springer/Kluwer, 83-95.

Lehner B and Döll P, 2004, Development and validation of a global database of lakes, reservoirs and wetlands. *Journal of Hydrology* 296(1-4): 1-22.

Mitasova H and Mitas L, 1993, Interpolation by Regularized Spline with Tension: I. Theory and Implementation. *Mathematical Geology,* 25:641-655.

Neteler M and Mitasova H, 2008, *Open Source GIS: A GRASS GIS Approach*. Third Edition. Springer New York.

World Wildlife Fund, 2009, HydroSHEDS, http://hydrosheds.cr.usgs.gov/index.php

The Swiss Alps Without Glaciers – A GIS-based Modelling Approach for Reconstruction of Glacier Beds

A. Linsbauer[1], F. Paul[1], M. Hoelzle[2], H. Frey[1], W. Haeberli[1]

[1]Glaciology, Geomorphodynamics and Geochronology
Department of Geography, University of Zurich
Winterthurerstrasse 190
CH-8057 Zurich, Switzerland
Telephone: +41 44 635 51 57
Fax: +41-44-635 68 41
Email: andreas.linsbauer@geo.uzh.ch

[2]Department of Geosciences, University of Fribourg
Chemin du Musée 4
CH-1700 Fribourg, Switzerland

1. Introduction

Due to the ongoing and expected future increase in global mean temperature, the Alpine environment will continue to depart from equilibrium (Watson and Haeberli 2004). As glaciers form a significant part of the mountain cryosphere and their changes are considered to be the best natural indicators of climatic change (IPCC 2007), they constitute a key indicator within global climate related observing programs (Haeberli 2004). The already observed as well as the expected changes in glacier geometry and volume could have large impacts on global (sea level rise), regional (water supplies) and local scales (natural hazards, hydropower). The calculation and visualization of future glacier development thus plays a vital role in communicating climate change effects to a wider public (Paul et al. 2007).

Of particular interest regarding hydrological aspects is the water volume that is stored in the glaciers (Jansson et al. 2002). This requires information on the glacier bed which is only accessible after the glacier has disappeared (e.g. Maisch and Haeberli 1982). Otherwise, glacier thickness has to be obtained in the field at discrete points or profiles using a range of techniques (e.g. GPR, seismic or drilling). The spatial extra- and interpolation of this local thickness information for reconstruction of the entire glacier bed is again based on a wide range of methods and assumptions with related uncertainties, but at least mean glacier thickness values can be derived. In order to overcome the scarcity of available measurements, a set of empirical (e.g. Chen and Ohmura 1990, Maisch and Haeberli 1982) or more physically based (Driedger and Kennard 1986, Haeberli and Hoelzle 1995) relationships have been proposed to obtain glacier volume for large samples of glaciers.

Apart from the amount of available water stored in glaciers, there is also an urgent need to have topographic information on the glacier bed itself. Anticipation and quantitative modelling of changes in surface topography and characteristics in large regions related to future climate change, and corresponding developments (landscape evolution, water cycle modifications, natural hazard potentials, tourism, hydropower, etc.) in cold mountain regions has become an important task. In this respect, an estimated topography of the glacier bed would facilitate a large number of applications including the visualization of future ice-free ground. Using examples from the Swiss Alps, this contribution presents a fast and robust GIS-based approach to construct digital elevation models (DEMs) "without glaciers" in currently glacierized mountain chains from a minimum set of input data (DEM, glacier outlines and flowlines).

2. Method

The glacier surface reflects a smoothed image of the underlying bed. One basic parameter that influences glacier thickness is mean slope: the steeper the glacier, the thinner the ice and vice versa. This relation is also given from the so-called shallow ice approximation (SIA) which is a theoretical concept for highly idealized glacier geometries (Paterson 1994), but has been shown to reveal good results compared to more comprehensive approaches (Leysinger Vieli and Gudmundsson 2004). The required calculation of the mean basal shear stress in our approach is based on data from late glacial glacier geometries (Maisch and Haeberli 1982) and a concept that calculates average shear stress as a function of mass turnover determined by vertical extent (Haeberli and Hoelzle 1995). This concept was applied to large glacier ensembles, using numerical information as available in detailed glacier inventories (Haeberli and Hoelzle 1995). Corresponding thickness and volume estimates for individual glaciers thereby became much more realistic as glaciers are 3-dimensional rather than planar bodies, and flow-related glacier thickness is primarily slope rather than area dependent. A decisive further step is introduced by combining this approach with geomorphometric analysis of DEMs and automated GIS-based data processing, which now make ice-depth estimates possible for individual parts of glaciers (Linsbauer 2008).

The method requires only the DEM, glacier outlines and a set of flowlines for individual glacier branches. For each glacier, an average basal shear stress is then estimated as a function of vertical extent, and ice depth is calculated along selected points of the flowlines as a function of surface slope (Fig. 1). The subsequent spatial interpolation of the thickness values is performed with the topogrid interpolation as implemented in the GIS software Arc/Info from ESRI. Topogrid has been designed to generate hydrologically consistent DEMs from elevation contours/points and other vector data (Hutchinson 1989), resulting in preferably concave-shaped landforms. It is thus well suited to mimic the typical parabolic shape of glacier beds without explicitly considering mass fluxes as applied in the approach by Farinotti et al. (in press). The most time consuming part of the work is the determination of flowlines on the individual glacier branches. For various reasons, this digitizing is still best and most reliably made by hand, starting at the lower end of the glacier tongue and cutting at a right angle through the elevation contour lines of the glacier surface.

The developed method is a raster-based GIS-tool, which is implemented in a short Arc Macro Language (AML) script. The basic steps of modelling are illustrated in Fig. 1 along with a schematic diagram of the modelled parameters. The steps are: (a) data preparation, (b) calculation of glacier thickness for base points of the flowlines from the SIA using mean slope for 50 m elevation bands, (c) spatial densification of base points along the flow lines using an IDW interpolation, and (d) the interpolation of the bed with topogrid and addition of the bed elevations to the DEM. When all input data (DEM, glacier outlines, flowlines) are prepared, a few hundred glacier beds are automatically calculated in a short time (minutes).

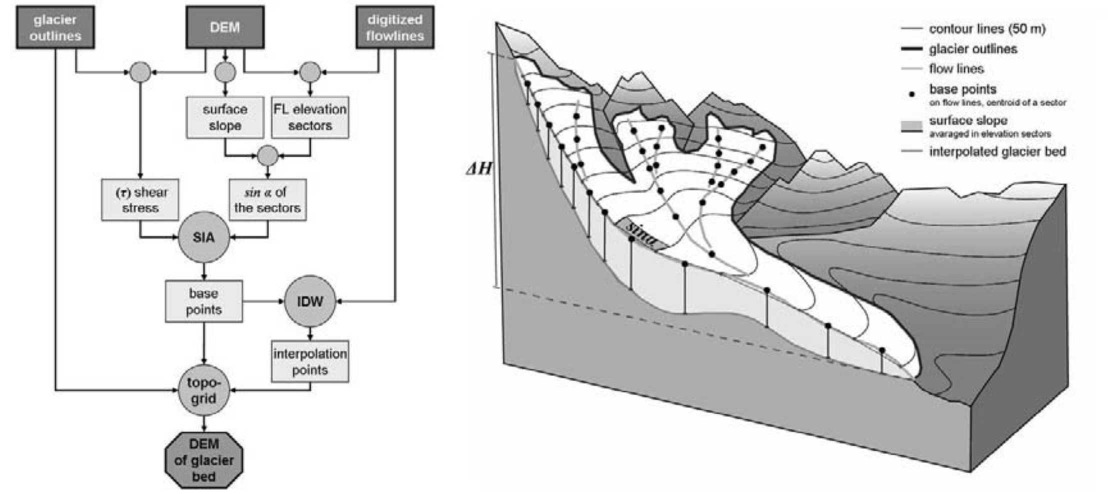

Figure 1. Flowchart of the method and schematic diagram of the modelled parameters.

3. Fields of Application

As mentioned above, the basic intention behind the development of this approach lies in the reconstruction of glacier beds over large regions, e.g. the entire Swiss Alps. The direct result is (1) an ice thickness distribution of all glaciers (Fig. 2) and (2) a DEM without glaciers (Fig. 3). From these data sets a number of further products and applications can be derived. At first, (3) mean thickness and (4) total volumes can be derived for each glacier in the sample. A comparison of (1) and (3) with direct measurements or results from other (more generalized/sophisticated) approaches can be performed, while (4) yields improved estimates of available water resources in the respective region.

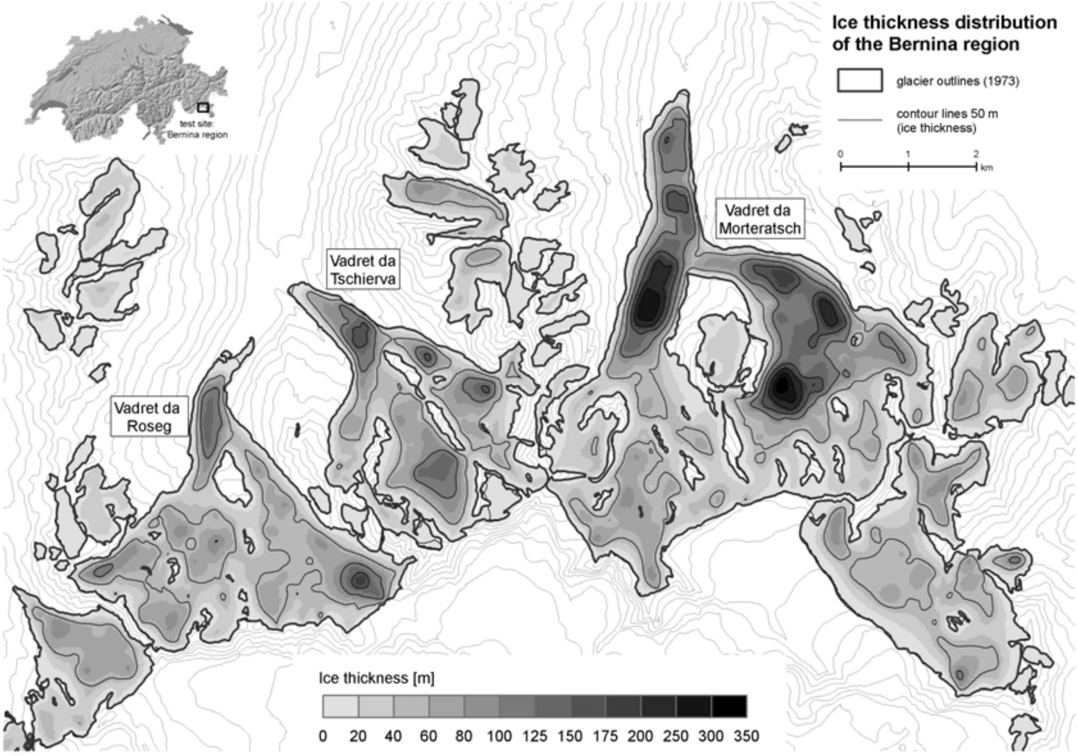

Figure 2. Modelled ice thickness distribution of the entire Bernina region, Switzerland. Reproduced by permission of swisstopo (BA091300).

A direct application of (2) is (5) the detection of overdeepenings in the glacier bed which can be easily visualized in the GIS by filling-up the depressions (Fig. 3). Dependent on the sedimentary nature of the glacier bed (Maisch et al., 1999), the depressions can fill with water and form lakes in the glacier forefield after the glacier has disappeared. These potential future lake formation sites can pose a hazard to downstream communities when the lake is located underneath steep rock walls or hanging glaciers (e.g. Haeberli and Hohman 2008). The glacier bed topography will also (6) facilitate the modelling of flow paths of potential outburst floods, which might help for the planning of mitigation measures (Rothenbühler 2006).

Furthermore, (7) a more realistic visualization of future glacier change than in Paul et al. (2007) can be achieved when the lost volume is eroded from the DEM and the bedrock becomes visible. Combined with a mass balance and hydrological model, the glacier beds can also be used for (8) improved modelling of changes in run-off from glacierized catchments (Huss et al. 2008). Finally, the bedrock can also serve as (9) an input for glacier flow models.

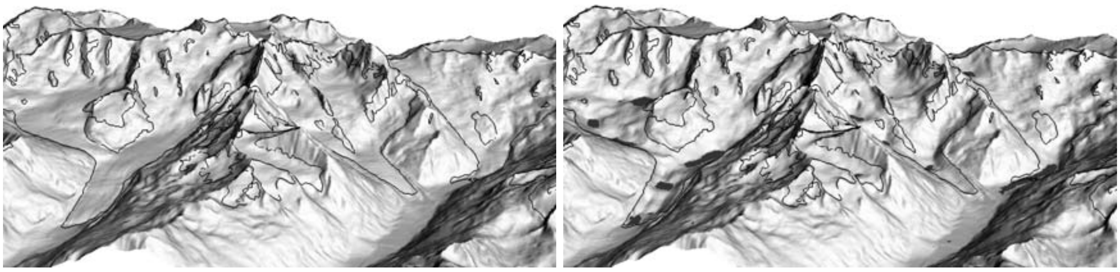

Figure 3. Input data and modelled glacier bed topographies with detected overdeepenings (potential lake formation sites) in the Bernina region, Switzerland. Reproduced by permission of swisstopo (BA091300).

4. Discussion and Conclusion

This simple approach of calculating glacier beds from geomorphometric properties of the glacier surface alone has of course several shortcomings. However, the modelled glacier beds were in a good agreement with field measurements (GPR profiles) and results from more complex approaches as described by Farinotti et al. (in press). Our approach is independent of glacier size and can be adjusted to different glacier types or climatic settings by considering glacier specific values of the form factor or a different calculation of the basal shear stress (τ) from the elevation range, respectively. It is also possible to incorporate a more localized (slope-dependent) calculation of τ for each glacier (e.g. Driedger and Kennard 1986) to consider the effect of higher shear stresses in steep ice falls than in flat glacier parts (Haeberli and Schweizer 1988). However, these modifications only change the estimated ice thickness of a glacier without influencing the general shape of the modelled glacier bed. Changing of the latter can only be achieved by digitizing new flowlines.

Apart from the required further validation of our approach with independent field data and more specific calculation of some parameters, we see a large potential for Alpine-wide application of the approach in the context of forthcoming climate change impact studies and hydrological assessments.

References

Chen J and Ohmura A, 1990, Estimation of Alpine glacier water resources and their change since the 1870s. *IAHS* 193:127-135.

Driedger C and Kennard P, 1986, Glacier volume estimation on cascade volcanos: an analysis and comparison with other methods. *Annals of Glaciology* 8:59-64.

Farinotti D, Huss M, Bauder A, Funk M and Truffer M, 2009, A method to estimate ice volume and ice thickness distribution of alpine glaciers. *Journal of Glaciology* 55(191):422-430.

Haeberli W, 2004, Glaciers and ice caps: historical background and strategies of world-wide monitoring. In: Bamber JL and Payne AJ (eds), *Mass Balance of the Cryosphere*, Cambridge University Press, Cambridge, 559-578.

Haeberli W and Hoelzle M, 1995, Application of inventory data for estimating characteristics of and regional climate-change effects on mountain glaciers: a pilot study with the European Alps. *Annals of Glaciology* 21:206-212.

Haeberli W and Hohmann R, 2008, Climate, Glaciers and Permafrost in the Swiss Alps 2050: Scenarios, Consequences and Recommendations. In: *Proceeding of the 9th International Conference on Permafrost*, Fairbanks, Alaska, USA.

Haeberli W and Schweizer J, 1988, Rhonegletscher 1850: Eismechanische Überlegungen zu einem historischen Gletscherstand. *Mitteilung VAW/ETHZ* 94:59-70.

Huss M, Farinotti D, Bauder A and Funk M, 2008, Modelling runoff from highly glacierized alpine drainage basins in a changing climate. *Hydrological Processes* 22(19):3888-3902.

Hutchinson M, 1989, A new procedure for gridding elevation and stream line data with automatic removal of spurious pits. *Journal of Hydrology* 106(3-4):211-232.

IPCC, 2007, *Climate Change 2007. The scientific basis*. Technical report, WMO/UNEP. Cambridge University Press, New York.

Jansson P, Hock R and Schneider T, 2003, The concept of glacier storage: a review. *Journal of Hydrology* 282(1-4):116-129.

Leysinger Vieli GJMC and Gudmundsson GH, 2004, On estimating length fluctuations of glaciers caused by changes in climatic forcing, *Journal of Geophysical Research – Earth Surface* 109:F01007.

Linsbauer A, 2008, *Modellierung von Gletscherbetten mit GIS*. Diploma thesis, Geographisches Institut, Universität Zürich.

Maisch M and Haeberli W, 1982, *Interpretation geometrischer Parameter von Spätglazialgletschern im Gebiet Mittelbünden, Schweizer Alpen*. Schriftenreihe Physische Geographie, Universität Zürich 1:111-126.

Maisch M, Haeberli W, Hoelzle M and Wenzel J, 1999, Occurrence of rocky and sedimentary glacier beds in the Swiss Alps as estimated from glacier-inventory data, *Annals of Glaciology* 28:231-235.

Paterson W, 1994, *The physics of glaciers*, Pergamon-Press, Oxford.

Paul F, Maisch M, Rothenbuehler C, Hoelzle M and Haeberli W, 2007, Calculation and visualisation of future glacier extent in the Swiss Alps by means of hypsographic modelling. *Global and Planetary Change* 55(4):343-357.

Rothenbühler C, 2006, *GISALP - Räumlich-zeitliche Modellierung der klimasensitiven Hochgebirgslandschaft des Oberengadins*. Schriftenreihe Physische Geographie, Universität Zürich 50.

Watson R and Haeberli W, 2004, Environmental threats, mitigation strategies and high-mountain areas. *Ambio Special Report* 13:2-10.

Allometric Development of Glacial Cirques: An Application of Specific Geomorphometry

I. S. Evans,
Department of Geography,
Durham University,
South Road,
Durham City
DH1 3LE
England, U.K.
Telephone : 0044 191 334 1877
Fax : 0044 191 334 1801
Email : i.s.evans@durham.ac.uk

1. Introduction

In geomorphometry many of the variables we measure describe size or shape of landforms. Taking the further step of analysis, a central question is whether shape varies with size. Here the hypothesis that larger cirques differ in shape from smaller ones is tested. First some general considerations about specific geomorphometry and allometry are outlined. Implications for cirque development and mountain glaciation are considered and, finally, the possibility that allometric development applies more generally to landforms is considered.

2. Specific Geomorphometry

Often we view the land surface as a continuous rough surface and analyse distributions of, for example, altitude derivatives: this is g**eneral geomorphometry**. On the other hand, we may recognize **discontinuities**. These relate to breaks in the continuity of form and process, and typically arise because of rock contrasts or events in the historical development of the landscape. These discontinuities can be joined up to outline **Elementary Forms** (segments, units, facets) of the land surface. Currently, this is a subjective, manual process: formulating a satisfactory automated routine is a continuing research challenge (Minar and Evans 2008).

Elementary forms in turn can be associated with neighbours, with which their development is related, to define **specific landforms** such as cirques, drumlins, dunes, landslides, and valley-sides. When completely delimited, landforms can be measured and their position, size and shape (including gradient) can be analysed. This is **specific geomorphometry**, of which a large part involves relating the shape and size of delimited forms – the study of **allometry** or isometry.

Evans (1987) recognized nine stages in a specific geomorphometric analysis. Techniques have changed, but all nine stages are still applicable:

1. **Conceptualisation** of landform types
2. Precise operational **definition**
3. Complete **delimitation** from surrounding land
4. **Measurement** of position, direction, size, gradient, shape and context
5. **Calculation** of derived indices, ratios
6. Assessment of **frequency distributions**; transformation - check effects
7. **Mapping** and spatial distributional analyses
8. **Interrelation** of attributes, e.g. shape v. size or position
9. **Interpretation** cf. genesis and chronology

3. Allometry

Many landforms develop **allometrically**, that is they change shape as size increases. In all but the most dynamic situations this can be tested only by considering variation with size at a given time, i.e. static allometry, as was proposed for **cirques** originally for a small population (15) in Colorado. It is now possible to test this for several cirque populations, each much bigger than in Olyphant's (1981) original study. This use of static allometry implies acceptance of the ergodic principle, substituting space for time.

First, several measures of cirque dimensions (components of overall size) are defined (Evans 2006); each is in units of length (metres):

Length = Horizontal distance from top to bottom of the median axis, which divides the cirque into two equal map areas and starts from the middle of the threshold, the division between the cirque floor and the valley below. Note that this definition is specific to this landform, and differs from the commonly used 'greatest separation between any two points'; thus length may be less than width;

Width = maximum map length of any line at right angles to the median axis;

Amplitude = vertical fall from top of median axis to lowest point on threshold;

Height range = overall, from highest altitude on crest to lowest (on threshold);

Wall height = maximum fall along a single slope line, from headwall crest to start of floor below.

Size (overall) = cube root of (length x width x amplitude).

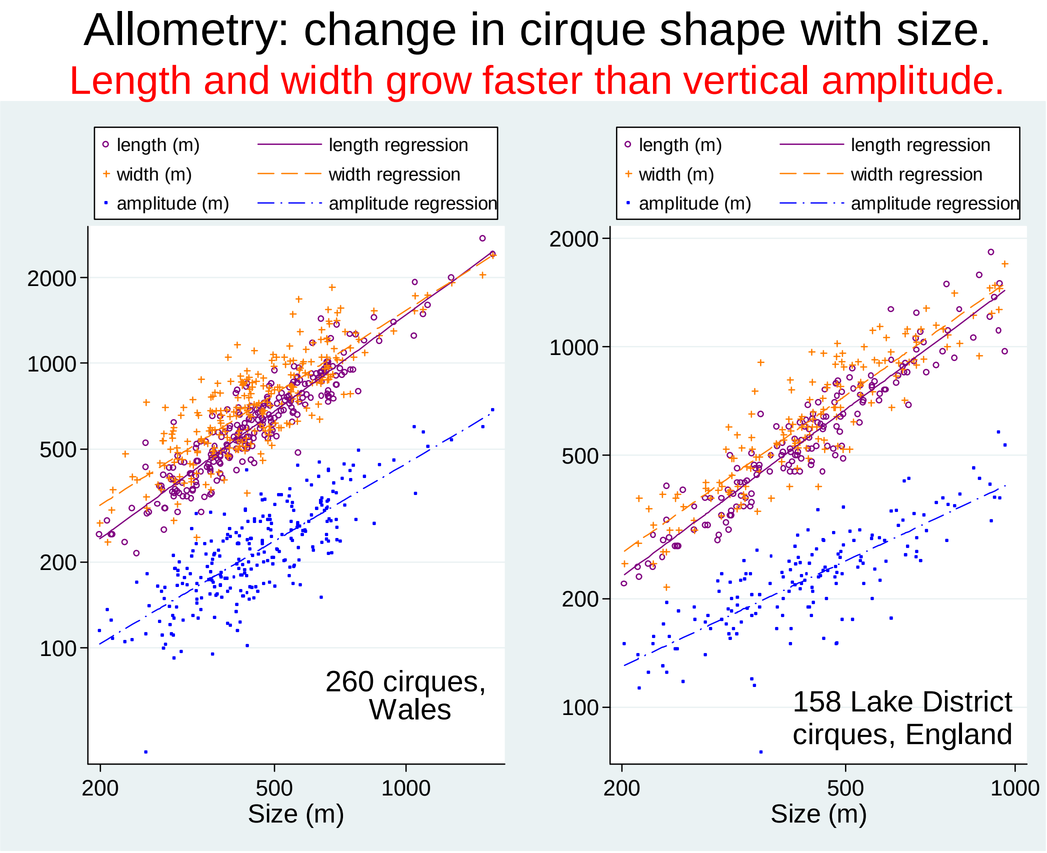

Figure 1. Allometric plots for Wales and the English Lake District.

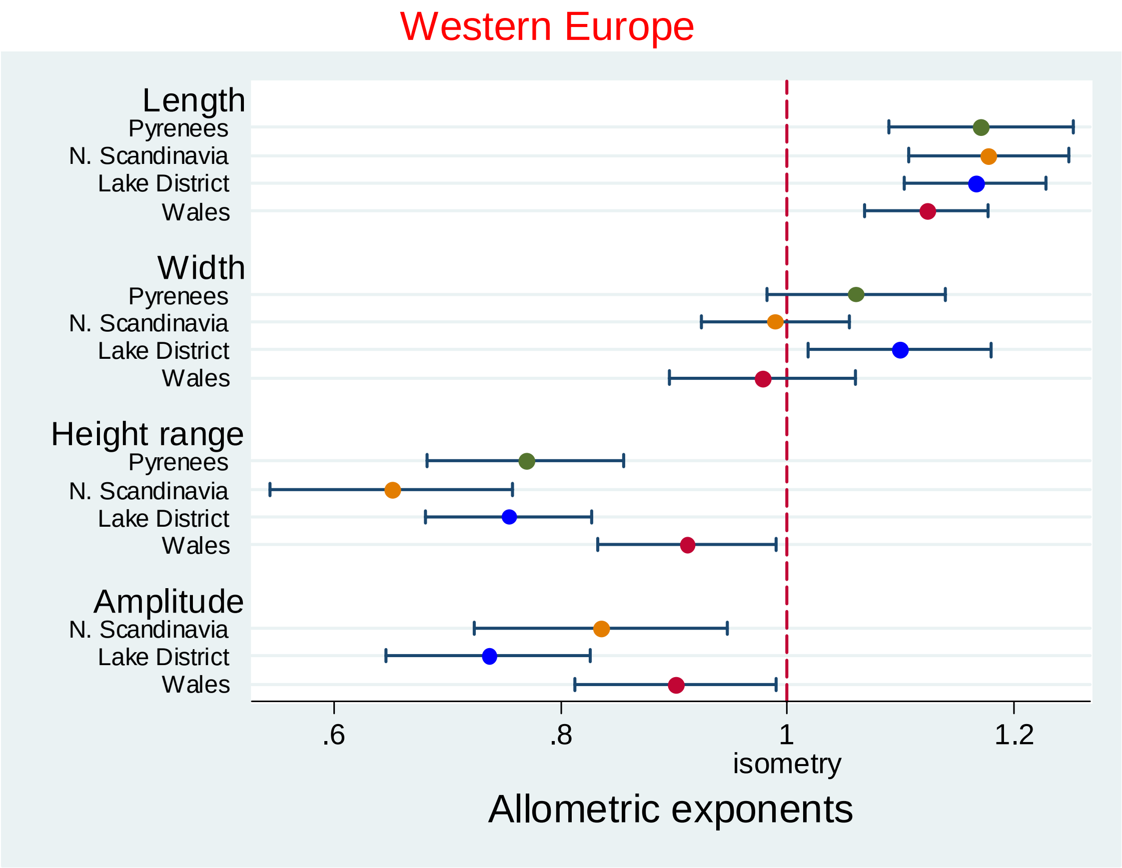

Figure 2. 95% Confidence limits on exponents for Western Europe.
Data as for Table 1.

4. Results

Exponents are fitted as the gradients of ordinary least squares regressions of size variables against overall size. This ensures that exponents for the three components of overall size sum to 3.0. Logarithmic plots of horizontal and vertical dimensions against overall size (e.g. Fig. 1) show that, as size increases, cirque length increases at a greater rate than vertical dimensions. This is confirmed wherever the 95% confidence intervals on exponents do not overlap – which is consistent across regions (Fig. 2 and Table 1). For isometry, all **power coefficients** (exponents) must be statistically indistinguishable from 1.0.

Exponents for-	**Exponent**	**95% Confidence limits**		R^2
Length				
Pyrenees	1.170	1.089	1.251	.798
N. Scandinavia	1.177	1.106	1.248	.662
Lake D.	1.166	1.103	1.228	.897
Wales	1.122	1.067	1.176	.863
Width				
Pyrenees	1.060	0.982	1.139	.774
N. Scandinavia	0.988	0.923	1.054	.619
Lake D.	1.099	1.018	1.179	.823
Wales	0.977	0.895	1.060	.678
Height range				
Pyrenees	0.769	0.682	0.856	.597
N. Scandinavia	0.650	0.543	0.757	.208
Lake D.	0.754	0.680	0.827	.721
Wales	0.911	0.832	0.990	.667
Amplitude				
N. Scandinavia	0.835	0.723	0.947	.285
Lake D.	0.736	0.646	0.825	.625
Wales	0.901	0.812	0.990	.605

Table 1. Size exponents (power coefficients) for four regions in Western Europe [Pyrenees (C. Spanish) 206 cirques *(data: J.M. Garcia-Ruiz et al. 2000)*; Northern. Scandinavia 541 *(a transect through Narvik; data: S. Hassinen 1998)*; Lake District 158; Wales 260].

Results for different regions of **British Columbia, Britain, Romania, Scandinavia, and Spain** are consistent in confirming the static allometry of glacial cirques: larger cirques are relatively longer and broader, more than they are deeper. Observed exponents include: length 0.99, 1.08, 1.08, 1.10, 1.10, 1.12, 1.17 and 1.18 ; width 0.98, 0.99, 1.00, 1.01, 1.04, 1.05, 1.08 and 1.10; and depth 0.74, 0.84, 0.85, 0.86, 0.90 and 0.91. Coefficients for length and width are generally **above 1.0**, while those for depth are significantly below. In most regions the length exponent exceeds the width exponent: hence the allometry cannot be explained by lateral coalescence of cirques. All length exponents are significantly above 1.0, and **all depth exponents** are significantly **below,** whether vertical dimension is expressed as height range or axial amplitude (Table 1), or headwall height. Isometry is observed only in one region (out of 14): the Ben Ohau Range in New Zealand (Brook et al. 2006).

These results are robust in that they are found for different grades and types of cirque (Table 2). The length exponent is significantly greater than amplitude and height range exponents, but the width exponent for Wales (unusually) is not. The results on the right show consistency for different grades and types of cirque. Relations between length and width, however, vary between ranges.

Variable	*expon.*	*95% conf.*	R^2	*better*	*no outer*	*v-side*	*v-head*
Length	1.12	1.07-1.18	.86	1.10	1.12	1.13	1.01
Width	0.98	0.89-1.06	.68	0.98	0.99	0.97	0.94
Amplitude	0.90	0.81-0.99	.61	0.91	0.89	0.90	1.05
Height range	0.91	0.83-0.99	.67	0.89	0.90	0.90	0.93
Wall height	0.97	0.86-1.09	.52	0.85	0.97	1.02	0.99

Table 2. Exponents for logarithmic (power) regressions of size variables on overall size for Wales. 95% **confidence intervals** and $\boldsymbol{R}^2$ measures of fit for all 260 cirques in Wales are given on the left. These are followed by exponents for 142 **better** cirques (graded **definite, well-defined or classic**), for the 249 cirques **excluding 'outer'** cirques, for 157 **valley-side** and for 75 valley-head cirques.

This study shows the importance of considering **confidence intervals** when making conclusions about relative rates of change. This permits size of data set to be given due weight, and prevents conclusions based on random variations. Detailed subdivision is seen to be counter-productive, as results become insignificant. Confidence intervals are also an aid in checking consistency of results between regions and between types of landform.

5. Cirque Development and the 'Buzzsaw'

It is inferred that cirque **headwall retreat is faster** than cirque deepening. Yet many cirques have **deep lakes** that attest to considerable cirque deepening (Lewis, 1960); this means that cirque development in all three dimensions is considerable (Evans 2007). Faster headwall recession implies support for the 'buzzsaw hypothesis' (Mitchell and Montgomery 2006) of rapid glacial erosion limiting the height of many mountain ranges. Instances of complete range truncation are, however, hard to find: coalescent and back-to-back cirques are common, but only occasionally do intervening ridges seem to have been removed. Cirques are rarely more than 2 km long or wide. It is interesting that cirques in plateau areas, where range truncation has clearly not occurred, are not dissimilar in size to those in more dissected mountains with back-to-back cirques, where the buzzsaw hypothesis might be applicable.

6. Conclusions

a: cirque allometry –

- Taking larger cirques as having developed further, each dimension can be plotted against an overall size measure to express static **allometry** or **isometry**.
- Large cirques differ in shape and gradient from small ones.
- Vertical dimensions increase more slowly than do horizontal.
- The allometric nature of cirque development is thus confirmed on the basis of a set of large inventories of cirques.
- Length usually increases faster than width, but length – width relations vary between areas. (*Exponents: length > width > height.*)

b: broader context: scaling -

- Many **fluvial** features scale over many orders of magnitude. Scaling (e.g. with a fractal model) is more important for hydrology and fluvial landforms, but always has limits (if only grain size, and size of Earth!)
- **Cirques** are scale-specific (Evans 2003) but also scale allometrically within one decimal order of magnitude.
- **Bedforms** (dunes, drumlins…) are also scale-specific. Whether allometry is general also for them has yet to be established.
- Scale specificity is important because it relates either to **process thresholds** or to the scale of controlling **frameworks** (e.g. whole valley-side, for mass movements)
- I hypothesize that all landforms show some scale-specificity: there are good process reasons for limits to their scaling behaviour.

Acknowledgements

I am grateful to Marcel Mindrescu, J.M. Garcia-Ruiz, S. Hassinen and M.S. Brook for providing data sets, and to Nick Cox and Marcel Mindrescu for useful discussions.

References

Brook, M.S., Kirkbride, M.P., and Brock, B.W., 2006, Cirque development in a steadily uplifting range: rates of erosion and long-term morphometric change in alpine cirques in the Ben Ohau Range, New Zealand. *Earth Surface Processes and Landforms,* 31 (9): 1167-75.

Evans, I.S., 1987, The morphometry of specific landforms. In Gardiner, V. (Ed.) *International Geomorphology 1986* Part II, J. Wiley, Chichester: 105-124.

Evans, I. S., 2006, Allometric development of glacial cirque form: geological, relief and regional effects on the cirques of Wales. *Geomorphology* 80 (3-4): 245-266.

Evans, I. S., 2007, Glacial landforms, erosional features: major scale forms. In Elias, S.A. (Ed.) *Encyclopedia of Quaternary Science.* Elsevier, Amsterdam, v.1: 838-852. [Evans, D.J.A. (Sub- Ed.) Glacial landforms] [ISBN-10: 0-444-51919-X]

Evans, I. S., 2003, Scale-specific landforms and aspects of the land surface. In I.S. Evans, R. Dikau, E. Tokunaga, H. Ohmori and M. Hirano (eds.) '*Concepts and modelling in Geomorphology: International Perspectives'*. Tokyo: Terrapub: 61-84. http://www.terrapub.co.jp/e-library/ohmori/index.html

García-Ruiz, J.M., Gómez-Villar, A., Ortigosa, L. and Martí-Bono, C., 2000, Morphometry of glacial cirques in the C. Spanish Pyrenees. *Geografiska Annaler* 82A: 433-442.

Hassinen, S., 1998, A morpho-statistical study of cirques and cirque glaciers in the Senja – Kilpisjärvi area, northern Scandinavia. *Norsk geografisk Tidsskrift* 52: 27-36.

Lewis, W.V. (ed.), 1960, *Norwegian cirque glaciers*. *R.G.S. Research Serie*s, 4, London: Royal Geographical Society, 104 pp.

Minár, J. and Evans, I. S., 2008, Elementary forms for land surface segmentation: The theoretical basis of terrain analysis and geomorphological mapping. *Geomorphology* 95 (3-4): 236-259. *doi:10.1016/j.geomorph.2007.06.003.*

Mitchell, S.G. and Montgomery, D.R., 2006, Influence of a glacial buzzsaw on the height and morphology of the Cascade Range in central Washington State, USA . *Quaternary Research* 65: 96-107.

Olyphant, G.A., 1981, Allometry and cirque evolution. *Bull. Geol. Soc. Amer.* 92, Part I: 679-685.

Morphometric Modelling of Rockglaciers – An Exploratory Case Study from the Alps

R. Frauenfelder[1]*, B. Schneider[2]**, B. Etzelmüller[3]

[1]Department of Geography, University of Zurich, Switzerland

* now at: Norwegian Geotechnical Institute, Postboks 3930 Ullevaal Stadion, 0806 Oslo, Norway
Telephone: +47 22 02 19 87
Fax: +47 22 23 04 48
Email: rf@ngi.no

[2]Department of Earth Sciences, University of Basel, Switzerland

** now at: ilu AG, Zentralstrasse 2a, 0610 Uster, Switzerland
Telephone: +41 (0)44 944 55 54
Fax: +41 (0)44 944 55 66
Email: bernhard.schneider@ilu.ch

[3]Department of Geocsiences, University of Oslo, Blindern, 0316 Oslo, Norway

Telephone: +47 22 85 72 29
Fax: +47 22 85 72 30
Email: bernd.etzelmuller@geo.uio.no

1. Introduction

Rockglaciers are landforms originating from periglacial talus (‘talus-derived’ rockglaciers) and/or glacier-transported debris, mostly from lateral and terminal moraines (‘moraine-derived’ rockglaciers). The occurrence of talus-derived rockglaciers (Fig.1) is influenced primarily by climatic and topographic preconditions (cf., e.g., Barsch 1996). They are found in areas characterized by specific topographic attributes; they occur, for example, within a certain altitudinal band, favour certain slope aspects, require a particular slope, and need a rock-contributing headwall above them (cf., e.g., Frauenfelder et al. 2003, Janke and Frauenfelder 2007).

Figure 1. Oblique photograph of an active talus-derived rockglacier in the eastern Swiss Alps. The rockglacier root zone (= *RRZ*, see explanations in the text below) is partly visible in the snow-covered upper right of the picture.

Modelling of the entire rockglacier bodies applying simple geomorphometric approaches is difficult as these landforms vary considerably in form and size. There are, however, areas within each talus-derived rockglacier that possess specific characteristics similar to all these forms: in the so-called *rockglacier root zone (RRZ)* the accumulated debris is triggered to creep (cf. Barsch 1996). This zone is located within or at the end of a concave landform where debris can accumulate (see Fig. 1, area in the upper right corner).

Recent advances in statistical modelling triggered a considerable amount of studies to model periglacial features (e.g., Brenning 2009, Etzelmüller et al. 2001, Etzelmüller and Sulebak 2003, Hjort et al. 2007, Hjort and Luoto 2008, Hjort and Marmion 2009, Luoto and Hjort 2004, 2006, Marmion et al. 2009, to name just a few). While some of these studies apply sophisticated statistical modelling schemes, for example, generalized additive models, support vector machines, boosting, etc., our contribution reports about the application of a simpler approach. We present an exploratory approach to the analysis of relationships between multiple explanatory variables and a presence/absence response variable for the modelling of *RRZ* distribution. Our approach essentially consists of the study of histograms and descriptive statistics, and the construction of heuristic probabilistic and deterministic classification rules.

The focus in this contribution is on the distribution of talus-derived rockglaciers (i.e. *RRZs* of talus-derived rockglaciers), and the explanations in the following text refer, by implication, to these forms only.

2 Geographical Settings and Data Sources

The study is carried out in the Upper Engadine, eastern Swiss Alps (Fig. 2). The area covers approximately 530 km^2, stretching from 46°22’N to 46°35’N, and 9°39’E to 9°59’E. The study area is characterized by a high-situated valley floor with an average altitude of 1700 m a.s.l.

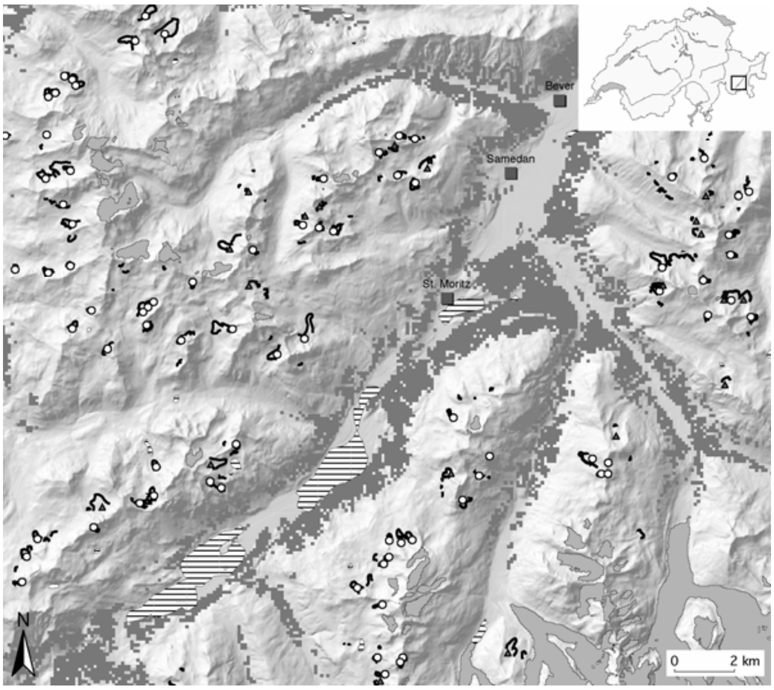

Figure 2. Shaded DEM25 of the study region. Size of original DEM (25 m resolution): 2201 x 1781 Pixels (ca. 55 x 44.5 km). Rockglacier outlines are represented by black lines, circles mark empirically derived talus-derived *RRZs*. Glaciers are depicted with light grey, lakes are striped, dark grey pixelated zones represent forested areas. Data sources: glacier extent from Paul (2003), rockglacier distribution from Hoelzle (1989, 1998), forest areas extracted from the data base of the Swiss Land Use Statistics (BFS 1992), DEM25 © 2004 *swisstopo* (BA046054).

Hoelzle (1989, 1998) identified 84 active rockglaciers in the study area by means of field investigation and analyses of aerial photography; 64 of these rockglaciers were identified as (periglacial) talus-derived forms. Together with 22 additionally mapped rockglaciers, a total of 86 rockglaciers was analysed.

To map potential *RRZs*, topographic attributes need to be identified that correlate well with their occurrence. The surface parameterization must be carried out at an appropriate scale, determined by the considered process. Potential *RRZs* are influenced by landforms in the range of decametres to hectometres. Therefore, the reference scale for the modelling is several tens of metres to hundreds of metres. For this purpose, the use of a raster-based digital elevation model (DEM) with a resolution in the range of decametres seemed adequate. A DEM with 50 metres or 100 metres cell size would be too coarse to allow *RRZ* detection, as they do not capture all topographic features relevant for the development and occurrence of rockglaciers. Hence, primary and secondary topographic attributes are extracted from a DEM with a 25 m cell size from *swisstopo* (the former Swiss Federal Office of Topography).

2. Methods and Results

2.1 Derivation of Topographic Attributes

Comprehensive compilations of topographic attributes to be computed from DEM data are given, for example, in Moore et al. (1990) and Wilson and Gallant (2000). We selected attributes with close relationships to gravity-driven slope processes, namely:

- *primary* topographic attributes:
  altitude, aspect, slope (for scale levels equivalent to 25 m and 50 m resolution), total curvature, plan curvature and profile curvature,
- *secondary* topographic attributes (i.e. statistical, mathematical or logical combinations of primary attributes):
  local relief, elevation-relief ratio, skewness of altitude, distance to nearest ridge (slope length), topographic wetness index, roughness index, radiation balance.

These topographic attributes were calculated for all *RRZs* using standard routines within GIS and were stored as individual grids. Together with the DEM these new grids represented a multidimensional geometric description of the *RRZs*. A thoughtful choice of selected topographic attributes from this geometric description should result in a set of measures that describe the *RRZs* well enough to distinguish them from other different landforms.

The distributions of the *RRZ*s were derived with respect to the selected topographic attributes. Firstly, the statistical values (min, max, mean, and standard deviation) of each of the topographic attributes were derived. The values obtained were then used to classify each topographic attribute into six classes of equal size with class borders at μ, $\mu \pm 0.5\sigma$, and $\mu \pm \sigma$, where μ is the mean of the attribute values and σ the relevant standard deviation. These results were plotted as histograms, which allowed for the qualitative distinction between attributes for which the *RRZs* are evenly distributed, i.e. attributes that are ineffective for modelling, and attributes showing clear accumulations of *RRZs* in distinct classes, in other words, attributes suitable for the modelling. Based on the results of the histogram analyses, topographic attributes which seemed to be representative of the sought *RRZs* were chosen for the modelling procedure. Three different terrain classification methods were applied (see sections 2.2, 2.3, and 2.4).

2.2 (A) Probabilistic Approach

The quantitative information of the frequency distribution histograms was interpreted as an indication of probability where higher occurrence of *RRZs* in individual attribute value classes indicates higher probability, and vice versa, i.e. lower occurrence of *RRZs* in individual attribute value classes indicates lower probability. An example of this procedure is given in Table 1 for the topographic attribute ‘slope’. The same procedure was applied for all topographic attributes which were found suitable for the modelling, i.e. which were inhomogeneously distributed between the classes (see above).

The following topographic attributes were used: altitude, aspect, slope, curvature (plan, profile), local relief, elevation-relief ratio, skewness of altitude, wetness index and roughness index.

The probabilities for these topographic attributes were multiplied in order to obtain combined probabilities of rockglacier occurrence for all locations in the test area. This was done for different combinations of topographic attributes.

Class	Relative boundaries	Absolute boundaries	Number of *RRZs*	Percent	Prob.
1	< m-s	< 12.1°	9	8.3	0.083
2	m-s to m-0.5s	12.1°–18.9°	16	14.7	0.147
3	m-0.5s to m	18.9°–25.7°	34	31.2	0.312
4	m to m+0.5s	25.7°–32.5°	23	21.1	0.211
5	m+0.5s to m+s	32.5°–39.3°	14	12.8	0.128
6	> m+s	> 39.3	13	11.9	0.119

Table 1. Absolute and percent distribution of the *RRZs* relative to the topographic attribute ‘slope’(Prob. = Probability; m: mean; s: standard deviation)

With a probabilistic approach the regions classified as potential *RRZs* were (a) too large, and (b) had a significant number of *RRZs* located in areas that were assigned low probabilities of rockglacier occurrence.

The modelling results can neither be improved by removing a topographic attribute from the criteria list, nor by adding a new one. Removing would enlarge the area with high probability, while adding would result in even more rockglaciers being located in areas with low probability for rockglacier occurrence.

2.3 (B) Deterministic Approach

In this approach, the range of occurring values for the significant topographic attributes (again altitude, aspect, slope, curvature (plan, profile), local relief, elevation-relief ratio, skewness of altitude, wetness index and roughness index) is used and values outside these ranges ruled out. For example, active rockglaciers in the study area are found at elevations between 2230 m a.s.l. and 3500 m a.s.l., in areas with medium wetness index, and on slopes with a steepness between 7° and 52°. In a boolean procedure, values outside the defined ranges (between the minimum and maximum values for all attributes) are marked as ‘no *RRZs* possible’.

Compared to the results of approach (A), two main differences become obvious when modelling the *RRZs* with a deterministic approach: (a) the problem of rockglaciers occurring outside the modelled zones could be solved, i.e. all *RRZs* lie within the modelled potential *RRZ* areas, and (b) the zones modelled as potential *RRZs* (depicted in red) are, however, much too large. This results from the very conservative procedure that is applied. Additionally, there is no weighting of the modelled zones included. A specification of the probability of occurrence within the modelled zones as in approach (A) is, therefore, not possible.

2.4 (C) Inclusion of Rockfall Accumulation Areas

The third approach broadens the *deterministic approach (B)* to include rockfall accumulation areas, which can be modelled using a (semi-)geomorphometrical approach. The expansion is based on the (rather banal) observation that rockglaciers can only develop where rock debris is available. As mentioned above, does the rock debris incorporated in talus-derived rockglaciers originate from contributing headwalls. Hence, if it were possible to locate these debris-supplying headwalls geomorphometrically and to estimate the extent of the relevant rockfall, the number of potential *RRZs* (cells) would get significantly reduced.

The so-called 'overall-slope' or 'reach-angle' approach (also known as 'Fahrböschung', Heim 1932) was used to compute rockfall and rockfall accumulation (Brändli 2001). Assuming that a rockglacier can only emerge where rock accumulation takes place, the potential *RRZ* occurrence areas resulting from approach (B) were intersected with the rock accumulation areas. With the inclusion of rockfall accumulation areas in the modelling, the number of falsely modelled potential *RRZs* was significantly decreased compared to the results from Approach (A) and (B); however, overestimations still occurred (see Fig. 3).

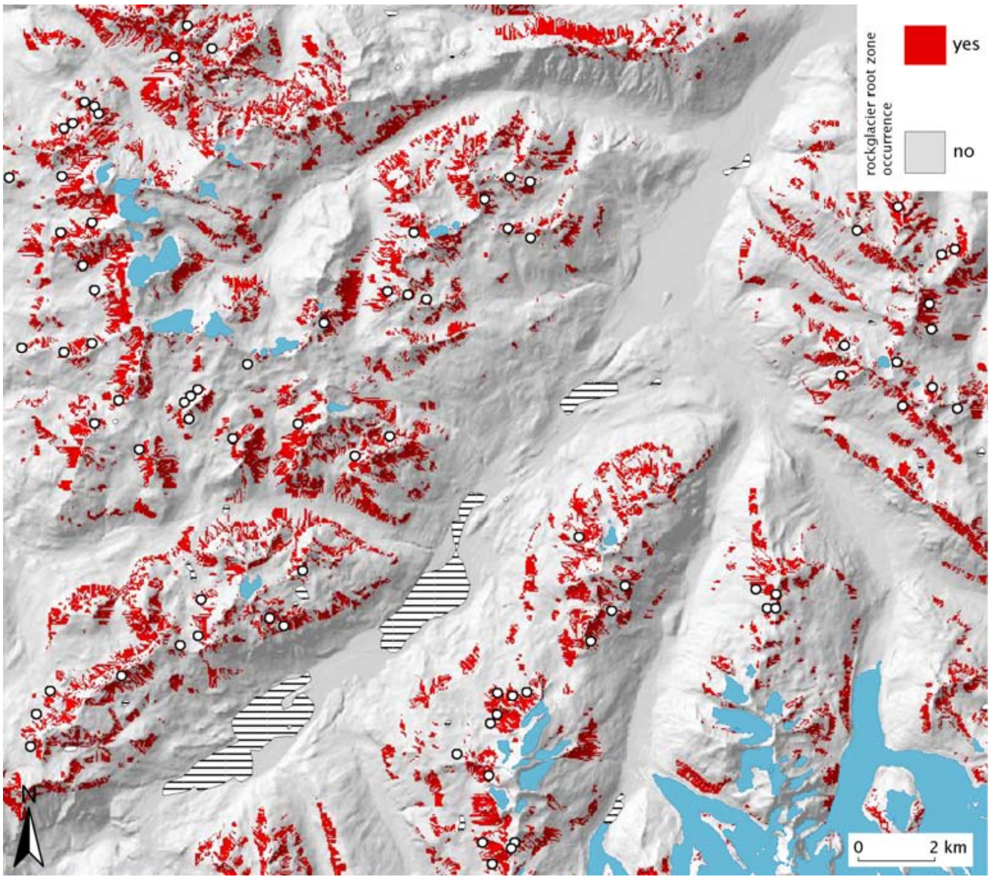

Figure 3. Approach (C): approach (B) with inclusion of the modelled rockfall accumulation areas, representing zones where debris is available. *RRZs* of active talus-derived rockglaciers are depicted with circles, glaciers are coloured light-blue and lakes are striped, data sources as in Fig. 2.

One explanation for this comes from the fact that rockfall accumulations were modelled by calculating a random number of rockfall trajectories. Due to undesired side-effects caused by the raster data model of the DEM, rockfall accumulation patterns tend to exhibit 'holes' between the individual trajectories. *RRZs* that are located in such 'holes', which presumably do not exist as frequently in nature as implied by the model results, are considered as 'falsely' modelled. Upon analyzing the individual cases it can be argued with reasonable certainty, however, that *RRZ*s modelled ≤ 25 m away (which corresponds to 1 grid-cell), can be considered as 'correctly' modelled as well (Table 2).

Distance to mapped *RZZ*s (in m)					
0	≤ 25	≤ 50	≤ 75	≤ 125	>150
67	7	5	5	2	0

Table 2. Amount of correctly and falsely modelled *RRZs* with approach (C).

3. Discussion and Conclusions

In approach (A), the size of the areas that are classified as potential *RRZs*, without actually having any rockglaciers in reality, is considerably large. At the same time, some rockglaciers that actually do exist lie in areas with low probabilities ($p \leq 0.7$) for the occurrence of *RRZs*. As the results of this approach indicate, a model based only on an univariate consideration of topographic attributes seems inadequate. Hence, simply multiplying the probabilities of the individual attributes is not a suitable approach for the detection of rockglaciers *RRZs*. This is partly caused by the implicitly underlying assumption that the conditional probability distributions of rockglacier occurrence on individual explanatory variables are independent, which is a rather strong assumption. Logistic regression would help to reveal individual attribute values only occurring in specific combinations. Such multivariate classification schemes have been successfully applied in geomorphological studies (e.g., Brenning and Trombotto 2006, Hjort et al. 2007, Sulebak et al. 1997, Wood-Smith and Buffington 1996) but were not carried out in this study.

Modelling with the deterministic approach (B) enables the inclusion of the *RRZs* of all talus-derived rockglaciers which occur. However, due to the very conservative procedure, the number of areas that are falsely modelled as potential *RRZ* areas unsurprisingly increases significantly compared to approach (A).

In contrast to this, the inclusion of rockfall accumulation areas in approach (C) leads to a distinct decrease in falsely modelled areas. A certain number of problematic cases remain even with this approach, however. They are basically of three kinds: (a) for very small (and often steep) rockglaciers the contributing headwall is not represented in a DEM with 25 m resolution. Therefore, rockfall is not modelled in these areas, and consequently, the root zones lie outside the modelled potential *RRZ* areas. (b) Some rockglaciers do not (any longer) have a contributing headwall in nature. It is likely that their activity will decrease in the near future, due to a lack of debris supply. (c) The main difficulty, however, is the modelling of rockfall accumulation areas itself. Both the localization of contributing headwalls and the estimation of the rockfall extent are calculated with very simple models, partly because topographic information alone is employed.

In summary, we could show that the inclusion of rockfall accumulation areas, even if based on simple modelling schemes, allows a much better estimate of *potential RRZ* areas than mere univariate probabilistic or deterministic classification rules (Table 3).

	Approach		
No. of *RRZs*	A [1)]	B	C
within modelled area	49 (57 %)	86 (100 %) [2)]	74 (86 %)
outside modelled area	37 (43 %)	0 (0 %)	12 (14 %)
Total	86 (100 %)	86 (100 %)	86 (100 %)

Table 3. Summary table. [1)] Fulfilment criteria: $p > 0.7$ (see section 2.2). [2)] Seemingly good result, however, zones modelled as potential *RRZs* are much too large.

However, as mentioned initially, a number of more sophisticated statistical methods exist today; their application would help to overcome the deficiencies we met with our approach. Hjort et al. 2007, for example, used logistic regression and hierarchical partitioning for the modelling of the distributions of periglacial forms such as palsas and earth hummocks. Hjort and Marmion (2009) successfully applied the boosting method in periglacial distribution modelling of, amongst other things, sorted solifluction. Brenning (2009) compared the performance of eleven statistical and machine-learning techniques including logistic regression, generalized additive models, linear discriminant techniques, and the support vector machine for automatic rockglacier detection. Future efforts to model *RRZs* or entire rockglaciers in the Swiss Alps should certainly focus on such refined statistical methodology.

Acknowledgements

This contribution is based on an earlier, unpublished, manuscript reproduced within the first author’s PhD-thesis. The underlying study was supported by an international scholarship of the Research Council of Norway, Oslo and a research grant of the ‘Stiftung zur Förderung der wissenschaftlichen Forschung’ at the University of Zurich, Switzerland. This funding is gratefully acknowledged. We are indebted to Martin Hoelzle for compiling the rockglacier inventory on which this study is based on. We would also like to thank two anonymous reviewers for their important comments.

References

Barsch D. 1996. *Rockglaciers. Indicators for the present and former geoecology in high mountain environments*. Springer: Berlin.

BFS. 1992. Die Bodennutzung der Schweiz – Arealstatistik 1979/85, Kategorienkatalog. Bundesamt für Statistik: Bern.

Brändli M. 2001. Steinschlagmodellierung. HTML-page: http://www.geo.unizh.ch/~gis2/pro/stein-schlag/ helps/ pg/ c-prog-new.html. Edition: 26.6.2001.

Brenning A, Trombotto D. 2006. Logistic regression modeling of rock glacier and glacier distribution: topographic and climatic controls in the semi-arid Andes. *Geomorphology* **81**(1–2): 141–154.

Brenning A. 2009. Benchmarking classifiers to optimally integrate terrain analysis and multispectral remote sensing in automatic rock glacier detection. *Remote Sensing of Environment* **113** (1): 239–247.

Etzelmüller B, Sulebak JR. 2003. Developments in the use of digital elevation models in periglacial geomorphology and glaciology. In *Entwicklungstendenzen und Zukunftsperspektiven in der Geomorphologie. Publikation zur Jahrestagung der Schweizerischen Geomorphologischen Gesellschaft (SGmG) anlässlich des 180. Jahreskongress der Schweizerischen Akademie der Naturwissenschaften (SANW) in Winterthur (11.-13. Oktober 2000)*, Maisch M, Vonder Mühll D, Monbaron M (eds.). Department of Geography, University of Zurich: 35–58.

Etzelmüller B, Ødegård RS, Berthling I, Sollid JL. 2001. Terrain parameters and remote sensing data in the analysis of permafrost distribution and periglacial processes: principles and examples from Southern Norway. *Permafrost and Periglacial Processes* **12** (1): 79–92.

Frauenfelder R, Haeberli W, Hoelzle M. 2003. Rockglacier occurrence and related terrain parameters in a study area of the Eastern Swiss Alps. In: M. Phillips, S. Springman and L. Arenson (Editors), *8th International Conference on Permafrost, Proceedings*. Swets & Zeitlinger, Lisse, Zürich: 253–258.

Heim A. 1932. Bergsturz und Menschenleben. *Beiblatt zur Vierteljahresschrift der Naturforschenden Gesellschaft in Zürich* **20**: 217.

Hjort J, Luoto M. 2008. Can abundance of geomorphological features be predicted using presence–absence data? *Earth Surf. Process. Landforms* **33**, 741–750.

Hjort J, Marmion M. 2009. Periglacial Distribution Modelling with a Boosting Method. *Permafrost and Periglacial Processes* **20**: 15–25.

Hjort J, Luoto M, Seppälä M. 2007. Landscape Scale Determinants of Periglacial Features in Subarctic Finland: A Grid-based Modelling Approach. *Permafrost and Periglacial Processes* **18**: 115–127.

Hoelzle M. 1989. Untersuchungen zur Permafrostverbreitung im Oberengadin. Abteilung für Naturwissenschaften, ETH Zürich, Unpublished MSc-thesis.

Hoelzle M. 1998. Rock Glaciers, Upper Engadin, Switzerland. International Permafrost Association, Data and Information Working Group, NSIDC, University of Colorado at Boulder. CD-ROM: version 1.0.

Janke J, Frauenfelder R. 2007. The relationship between rock glacier and contributing area parameters in the Front Range of Colorado. *Journal of Quaternary Science* **23** (2): 153–163.

Luoto M, Hjort J. 2004. Generalized Linear Modelling in Periglacial Studies: Terrain Parameters and Patterned Ground. *Permafrost and Periglacial Processes* **15**: 327–338.

Luoto M, Hjort J. 2006. Scale matters - a multi-resolution study of the determinants of patterned ground activity in subarctic Finland. *Geomorphology* **80**: 282–294.

Marmion M, Hjort J, Thuiller W, Luoto M. 2008. A comparison of predictive methods in modelling the distribution of periglacial landforms in Finnish Lapland. *Earth Surf. Process. Landforms* 33, 2241–2254.

Moore ID, Grayson RB, Ladson AR. 1990. Digital terrain modelling: a review of hydrological, geomorphological and biological applications. *Hydrological processes* **5**: 3–30.

Paul F. 2003. The new Swiss Glacier Inventory 2000. Application of Remote Sensing and GIS. Department of Geography, University of Zurich, PhD-thesis.

Sulebak JR, Etzelmüller B, Sollid JL. 1997. Landscape regionalisation by automatic classification of terrain elements. *Norwegian Journal of Geography* **51**: 35–45.

Weibel R, DeLotto JL. 1988. Automated terrain classification for GIS modelling. *GIS/LIS 88, Proceedings*. Virginia, **2**: 618–627.

Wilson JP, Gallant JC. 2000. *Terrain analysis – principles and applications*. John Wiley & Sons: New York.

Wood-Smith RD, Buffington JM. 1996. Multivariate geomorphic analysis of forest streams: implications for assessment of land use impacts on channel condition. *Earth Surface Processes and Landforms* **21** (4): 377–393.

Authors Index